Molecular Functions of ArfGAP3 during Autophagy and Ageing in *Drosophila*

A thesis submitted for the degree of
Doctor of Philosophy in Life Sciences

By

Bhavini Patel MSc

Supervisor:
Professor Ioannis Nezis

University of Warwick, School of Life Sciences
October 2020

Thesis dedication

This PhD thesis is dedicated to the loving memory of my late paternal grandfather, Balubhai Kanjibbhai Patel (Dada). He had powerful visions for all his grandchildren. Even though we were so young, he always emphasised to us how bright our futures would be. His words still echo in my ears to this day when he once told me "Someday you will be Dr Bhavini Patel". His words gave me purpose in life and his vision for me became **our** vision. My grandfather has been my number one inspiration and motivation to pursue my doctoral degree. Although, he left for heaven early in my life and he did not get the chance to see me pursue this PhD and graduate, I know his spiritual guidance and blessings have always been with me. I hope that I have made you proud Dada. This is for you.

I also dedicate this PhD to my support systems. I want to take this opportunity to say a huge thank you to my father Kirit, my mother Sejal, my husband Pranav, my sister Nalini, my brother-in-law Sanjay and my brother Dhruv for always being there for me throughout this PhD career, sharing with me all the highs and lows that came along on this journey and never letting me feel alone in any of it. Thank you to my puppy Mila, her love has been so therapeutic during PhD stress. I am so grateful to have the most loving and supportive family and I couldn't have got through this PhD without them. I am grateful to my paternal grandmother (Ba) and maternal grandparents (Aajadada and Aajiba) for their unconditional love and blessings throughout my PhD, especially Aajiba for always sharing her wisdom with me. I want to say a huge thank you to my father-in-law Dinesh, my mother-in-law Yamini and little sister-in-law Diya for their continuous support throughout my PhD, especially during my thesis write up as I was living with them during this time. They all provided me with so much love and care and made sure I was well looked after through the

write-up process. A special thank you to my sister Manisha for always having the right words at the right time to keep my spirit up high. A heartful thank you to Anisha, Mansi, Varsha, Hirva, Sameer, Heta, Bhavna, Shahaan, Davina, Jacqueline, Marisa and Lauren for being the most amazing friends and family, always cheering me on with their positivity. To everyone mentioned above, your love, support and encouragement is deeply appreciated.

I would like to give a special thank you to the few people who positively inspired me throughout academia and helped me in some way during my journey to now. Thank you to my aunt Sheetal (Muni masi) for being the first person in my life to introduce me to a career in science. Seeing my uncle, Suraj (Suraj mama), achieve his PhD whilst juggling his family life was incredible and I am thankful for all his help during my A levels. I would like to thank my family friend Kalpesh (Kalpesh bhai), who tutored me during my A levels. I cannot express just how much I loved my lessons with him, he taught me how to enjoy studying science and his teaching concepts were remarkable. A heartful thank you to my undergraduate personal tutor and supervisor Professor Christopher Exley, who told me I had it in me to pursue a PhD. My research interests in neurodegenerative diseases originated from working on a research project with Prof. Exley's postdoc Matthew, who also inspired me to pursue a PhD. Prof. Exley's positive encouragement and support will always be remembered. To everyone mentioned above, seeing you all grow in your careers and research has been a true inspiration to follow my dreams and pursue a PhD.

Lastly and most importantly, I dedicate this PhD thesis to my incredible husband, Pranav. An incredibly special heartful thank you to him. Words just cannot express how grateful I am of all the love, support, and encouragement he has given me throughout my PhD journey. It is what kept me going until the end and I couldn't have done this all without him. Although we were in a long-distance

relationship/married life for the most part of it, he has always been and is my pillar of strength, my major support system, my go-to person to share my achievements and setbacks with and has always been there for me without fail. He has been with me through every stage of this PhD and had committed himself fully in this journey with me, from late nights to early mornings, making sure I was always well looked after and always encouraged me to look after my mental health in this process too. Beyond grateful for his positivity and wisdom that always motivated and inspired me to keep my spirit up high, stay positive and have faith in myself. Pranav has always encouraged me to pursue my PhD dream from the beginning and he was always by my side, even at times when I felt like giving up. Pranav- I thank you deeply for never giving up on me and always pushing me to reach my potential. I hope that I have made you proud my love.

-Thank you all for believing in me.

Bhavini

Contents

Page

List of figures……..vii
List of tables……ix
Acknowledgements……x
Declaration……..xi
Abstract……...xiv
Abbreviations……..xv

Chapter 1 Introduction - Selective autophagy and endosomal trafficking in Ageing……1

1.1 Introduction into ageing……2
1.1.1 The nine hallmarks of ageing……..3
1.1.2 Degradation pathways for protein homeostasis……..3
1.2 Autophagy……5
1.2.1 Selective autophagy……6
1.2.2 *Drosophila melanogaster* as a model organism for autophagy……..9
1.2.3 The discovery of autophagy – historical overview……12
1.2.4 Classification of autophagy……15
1.2.4.1 Chaperone-mediated autophagy……15
1.2.4.2 Microautophagy……...17
1.2.4.3 Macroautophagy……..20
1.2.5 Regulation of autophagy and key proteins……21
1.2.5.1 Autophagy initiation and nucleation……...25
1.2.5.2 Autophagosomal membrane protein - Atg8……28
1.2.5.3 Autophagosome expansion, maturation and fusion……30
1.2.5.4 Nitrogen-dependent regulation……...32
1.2.5.5 Energy/glucose-dependent regulation……33
1.2.6 Selective autophagy receptors……..34
1.2.6.1 Lipophagy……...39
1.2.7 LIR motif……..40
1.2.8 Autophagy in ageing and age-related diseases……44

1.3 Interplay between autophagy and endosomal trafficking……52
1.4 ADP-ribosylation factor (Arf) GTPase activating protein 3 (ArfGAP3) in membrane trafficking…….54
1.4.1 ArfGAP3 in protein transport from Golgi to endosomes……..56
1.5 Arfs and Rabs in the regulation of lipid droplet development and lipolysis……59

Chapter 2 Thesis aims & hypothesis……...61

2.1 Thesis aims ……..61
2.2 Hypothesis…….....61

Chapter 3 Material and methods……64

3.1 Chemicals and reagents…….64
3.2 *Drosophila melanogaster* husbandry and genetic principles……65
3.2.*1 Fly stocks*……65
3.2.2 Ectopic gene expression…….67
3.2.3 Fly maintaining conditions…….68
3.2.4 Fly food recipe……69
3.3 Fluorescence and Immunofluorescence……69
3.3.1 Buffers and reagents for IF…….69
3.3.2 Antibodies and dyes for IF…….70
3.3.3 Dissections……..71
3.3.4 Summary of IF experiments ……...71
3.3.5 Co-localisation studies……73
3.3.6 Clonal analysis……74
3.3.7 Garland nephrocyte staining……...74
3.3.8 Confocal microscopy acquisition……75
3.3.9 Image analysis…….75
3.4 Western blotting……76
3.4.1 Buffers for lysate extraction……76
3.4.2 Buffers for western blotting……76
3.4.3 Antibodies for WB……..77
3.4.5 Lysate extraction…….78
3.4.6 Determining protein concentration…….78

3.4.7 Preparation of loading samples……...79
3.4.7.1 Laemmli Buffer…….....79
3.4.8 Gel casting……..79
3.4.9 SDS-PAGE and transfer to membrane……...81
3.4.10 Immunoblotting…….....81
3.5 Molecular genetics……...82
3.5.1 Cloning of N-terminus HIS-tagged ArfGAP3……...82
3.5.2 Site directed mutagenesis……...85
3.5.3 Cloning of FLAG-tagged wildtype ArfGAP3 and LIR mutant ……....88
3.5.4 Primers……...89
3.6 GST pulldown……..91
3.6.1 Buffers for GST pulldown…….....91
3.6.2 Protein expression in E. coli……..91
3.6.3 Lysate preparation…….....92
3.6.4 Protein purification……....93
3.6.4.1 Preparation of Glutathione Sepharose beads……...93
3.6.4.2 Purification of bait and prey proteins…….....93
3.6.5 Protein-Protein interaction assay (In vitro pulldown)……94
3.6.6 SDS-PAGE and immunoblotting for pulldown…….94
3.7 Immunoprecipitation……....95
3.7.1 Buffers for IP…….95
3.7.2 Preparation of Protein G Sepharose beads…….95
3.7.3 Lysate preparation……..95
3.7.4 Removal of non-specific binding proteins…….96
3.7.5 Immunoprecipitation……..96
3.7.6 SDS-PAGE and immunoblotting for IP…….96
3.8 Mass spectrometry……...97
3.8.1 Proteomics and data analysis of mass spectrometry……..97
3.9 PCR and Real time-qPCR……98
3.9.1 RNA extraction……..98
3.9.2 Reverse transcription……99
3.9.2.1 DNA removal……..99
3.9.2.2 cDNA synthesis……..100
3.9.3 PCR……...100
3.9.4 Gel electrophoresis……101

3.9.5 RT-qPCR…….....101
3.10 Transmission Electron Microscopy……..102
3.11 Lifespan assay……...102
3.12 Climbing assay……..103
3.13 Statistical analysis……103

Chapter 4 Results - ArfGAP3 is a novel Atg8a-interacting protein……..105

4.1 Chapter introduction: Yeast-two hybrid reveals ArfGAP3 as Atg8a-interacting protein……...105
4.2 ArfGAP3 co-localises with Atg8a in *Drosophila melanogaster*……107
4.3 Exploring the LIR motifs in ArfGAP3 protein sequence……111
4.4 ArfGAP3 interacts with Atg8a in a LIR dependent manner……..112
4.4.1 ArfGAP3 interacts with Atg8a via LGYETI LIR motif……114
4.4.2 ArfGAP3 has a second functional LIR motif……118
4.5 Generating wildtype ArfGAP3 and LIR mutant ArfGAP3 transgenic flies…...122
4.5.1 ArfGAP3 colocalises with Atg8a in new transgenic flies……124

Chapter 5 Results – Deciphering the role of ArfGAP3 in the interplay between selective autophagy and endosomal trafficking……127

5.1 Chapter introduction: ArfGAP3 in membrane trafficking……127
5.2 ArfGAP3 is selectively degraded by autophagy……....128
5.3 Testing the efficiency of ArfGAP3 knockdown transgenic flies……...129
5.4 The effect of ArfGAP3 on the autophagic flux……..133
5.4.1 Knockdown of ArfGAP3 affects autophagosome number……..….....133
5.4.2 Knockdown of ArfGAP3 affects lysosomal size (diameter)…….....136
5.4.3 Knockdown of ArfGAP3 affects autophagosome-lysosome fusion…….138
5.5 The effect of ArfGAP3 on the endocytic flux……142
5.5.1 ArfGAP3 co-localises with Rab5 and Rab7 in *Drosophila* ……..……..142
5.5.2 Knockdown of ArfGAP3 affects endosome trafficking……...143
5.5.3 Knockdown of ArfGAP3 disrupts endosome-lysosome fusion……...150
5.6 Knockdown of ArfGAP3 does not affect endosome-autophagosome fusion…152
5.6.1 Knockdown of ArfGAP3 does not disrupt autophagosome- endosome fusion……154

5.7 ArfGAP3 in the interplay between autophagy and lipophagy……157
5.7.1 The effect of ArfGAP3 in lipid droplet development……..158

Chapter 6 Results - Investigating the physiological relevance of ArfGAP3 during ageing…….161

6.1 Chapter introduction: Autophagy and endolysosomal system in ageing……..161
6.2 Lifespan of ArfGAP3 knockdown transgenic flies is reduced…….162
6.3 Knockdown of ArfGAP3 does not affect climbing ability of *Drosophila* flies ……164
6.4 Expression of ArfGAP3 in the brain……166
6.4.1 ArfGAP3 is expressed in larval brain…….166
6.5 Knockdown of ArfGAP3 results in accumulation of Ref(2)P in aged flies ……173

Chapter 7 Discussion and conclusions……177

7.1 ArfGAP3 is an Atg8a-interacting protein and a positive regulator of the endocytic flux ……177
7.2 ArfGAP3 in the interplay between autophagy and lipophagy……..189
7.3 Possible implications of ArfGAP3 in age-related diseases……..191
7.4 Concluding remarks…….196

Bibliography…….199

List of Figures

	Page
Chapter 1 Introduction figures	
1.1 Schematic overview illustrating loss of proteostasis	5
1.2 Selective autophagy publication dynamics	13
1.3 Chaperone-mediated autophagy (CMA) mechanism	17
1.4 Microautophagy and endosomal microautophagy mechanism	19
1.5 Macroautophagy mechanism	20
1.6 Core autophagic mechanism components	30
1.7 LIR-LDS interaction	43
1.8 Endocytosis and autophagy	53
1.9 ARF GDP/GTP cycle	56
1.10 ArfGAP3 in protein transport from trans-Golgi network to endosomes	58
Chapter 2 Thesis aims and hypothesis figures	
2.1 Schematic diagram illustrating hypothesis of this PhD project	62
Chapter 3 Materials and methods figures	
3.1 Ectopic gene expression using UAS/GAL4 system	68
3.2 Location of garland nephrocytes	75
3.3 Cloning of FLAG-tagged ArfGAP3 wildtype and LIR mutant	89
Chapter 4 Results figures	
4.1 ArfGAP3 is an Atg8a-interacting protein	106
4.2 ArfGAP3 co-localises to Atg8a in *Drosophila*	110
4.3 Exploring the LIR motifs in *Drosophila* ArfGAP3 sequence	112
4.4 ArfGAP3 interacts with Atg8a in a LIR dependent manner	115
4.5 ArfGAP3 interacts with Atg8a via a 392 LGYETI 397 LIR motif	116
4.6 ArfGAP3 has a second functional LIR motif 37 PTWSSV 42	117
4.7 Cloning of WT and LM1 ArfGAP3 gene into UAS FLAG plasmid.	123

4.8 ArfGAP3 co-localises with Atg8a in new UAS FLAG ArfGAP3 transgenic flies 125

Chapter 5 Results figures
5.1 ArfGAP3 is selectively degraded by autophagy 129
5.2 ArfGAP3 RNAi fly line efficiency 132
5.3 Knockdown of ArfGAP3 affects autophagosome number 134
5.4 Knockdown of ArfGAP3 affects lysosomal size (diameter) 138
5.5 Knockdown of ArfGAP3 affects autophagosome-lysosome fusion 141
5.6 ArfGAP3 co-localises to Rab5 and Rab7 in *Drosophila* 143
5.7 Knockdown of ArfGA3 affects endosomal trafficking 145
5.8 Knockdown of ArfGAP3 affects endosomal trafficking continued 149
5.9 Knockdown of ArfGAP3 affects endosomal trafficking continued 150
5.10 Knockdown of ArfGAP3 disrupts endosome-lysosome fusion 153
5.11 Knockdown of ArfGAP3 does not disrupt autophagosome-endosome fusion 157
5.12 Knockdown of ArfGAP3 causes enlargement of lipid droplets 159

Chapter 6 Results figures
6.1 Longevity of ArfGAP3 knockdown transgenic flies is reduced 165
6.2 Knockdown of ArfGAP3 does not affect climbing ability of Drosophila flies 167
6.3 ArfGAP3 is expressed predominantly in larval brain optic lobes 172
6.4 Ref(2)P accumulates in 4 weeks old aged flies lacking ArfGAP3 expression. 174

Chapter 7 Discussion and conclusions figures
7.1 Key proteins and components of autolysosome and endolysosome system. 184
7.2 Interplay between autophagy and endolysosomal pathway and the related neurological disorders 195
7.3 *Drosophila* ArfGAP3 is a positive regulator of the endocytic flux 198

List of Tables

Page

Chapter 1 Introduction tables

1.1 Types of selective autophagy processes 8

1.2 *Drosophila* autophagy related proteins 22

1.3 Selective autophagy receptors 36

Chapter 3 Materials and methods tables

3.1 Chemicals and reagents 64

3.2 *Drosophila* fly stocks 65

3.3 Antibodies and dyes for immunofluorescence 70

3.4 Immunofluorescence experiments 71

3.5 Antibodies for western blotting. 77

3.6 Primers for cloning 90

Chapter 6 Results tables

6.1 Climbing ability significantly reduced in aged control and ArfGAP3 RNAi flies 168

6.2 Climbing ability significantly reduced in aged control and ArfGAP3 RNAi flies continued 169

6.3 Knockdown of ArfGAP3 does not affect climbing ability of *Drosophila* flies 170

6.4 Knockdown of ArfGAP3 does not affect climbing ability of *Drosophila* flies continued 171

Acknowledgements

Declaration: This thesis is submitted by the University of Warwick in support of my application for the degree of Doctor of Philosophy in Life Sciences. I declare that all the work presented in this thesis has been composed by myself and has not been submitted in any previous application for any degree. I would like to thank the following colleagues who contributed to the work presented in the below figures:

Figure 4.2 – Dr Stavroula Petridi trained and supervised me for laboratory experiments at the start of my PhD – Thank you Stavroula, you have been an amazing supervisor and friend.

Figure 5.7B/C – Dr Saskia Bakker carried out TEM experiment and acquisition in the School of Life Science imaging suite with *Drosophila* tissue samples that I prepared for the experiment – Thank you!

I would like to thank Dr Ruth Johnson from Wesleyan University, US, for providing us with the ArfGAP3 antibodies and plasmids and Panos Tsapras for the UAS FLAG TAK1 plasmid. I would like to thank Dr Anne-Claire Jacomin for providing me us with bacterial cultured plates for GST, GST-Atg8 and GST-Atg8 LDS.

I would like to thank SLS GATC sequencing team for sequencing services throughout my PhD and Dr Cleidiane Zampronio at SLS proteomics for all her help and guidance in the proteomics laboratory. I would like to thank BestGene Inc, US for generating the ArfGAP3 WT and LM1 transgenic flies.

I would also like thank my advisory panel, Dr Andre Pires da Silva and Dr Emma Anderson, for all their advice during my advisory panel meetings, they have been a very supportive panel.

I would like to thank my PhD supervisor Prof Ioannis Nezis for his advice and guidance throughout my PhD. I would like to thank my lab colleagues Marisa, Panos,

Stavroula, Anne, Laura, Ash, for all the support throughout my PhD and helping me out in the lab with any experimental related questions I had.

THESIS SUBMISSION DECLARATION FORM

Candidate's Name: .....Bhavini Patel..... Student ID: …u1660610……

Degree: Doctor of Philosophy in Life Sciences

Please ensure that you record any changes in your contact details via Start.Warwick. If the Doctoral College are required to contact you regarding your examination, they will do so via your Warwick email address, so please ensure that you check this on a regular basis.

Early submission If submitting my thesis more than one month before the end of my fee-paying registration, I have completed an early submission form. More information in part I, section 1.2 of the Guide to Examinations for Higher Degrees by Research	N/A
Late submission If submitting after the end of my registration period, I have submitted a leave to submit request. More information in part I, section 1.4 of the Guide to Examinations for Higher Degrees by Research	No
Nomination of examiners I have completed part 1 of the Nomination of Examiners form and have passed it onto my supervisor for completion.	Yes
Word count I declare my word count to be. 54073 The word count of my thesis, excluding appendices, footnotes, tables and bibliography, is within the maximum limit for my degree as set out in part I, section 3 of the Guide to Examinations for Higher Degrees by Research *If no, please ensure that prior approval from the Chair of the Board of Graduate Studies is requested.*	Yes
Proofreading I have used a proofreader, paid or unpaid, to support the submission of this thesis The University expects all proofreaders to comply with its policy in this area. By ticking 'yes', I confirm that the proofreader was made aware of and has complied with the University's proofreading policy	No

Presentation I confirm the presentation of my thesis is in line with the requirements (if applicable) set out in part I, section 4 of the Guide to Examinations for Higher Degrees by Research, with reference to: • Typing of thesis • Title and title page • Table of contents • Acknowledgements • Declaration and inclusion of material from a prior thesis • Declaration of collaborative work • Inclusion of published work • Summary or abstract • Abbreviations • Tables and illustrated material • List of tables and illustrations • Research training • Bibliography and references	Yes
PhD by Published Work If submitting for the degree of PhD by Published Work I have completed and enclose the PhD by Published Work – Submission Checklist	N/A
Resubmission of thesis I have provided two copies of a memo detailing how the revisions required by the examiners have been addressed and payment for the re-submission fee	N/A

I acknowledge awareness of any outstanding payments due to the University in respect of my studies and that my degree will not be awarded until such time as any study-related debts have been settled. Outstanding payments can be checked on your Student eVision.

Signature: Bhavini Patel Date: 17/05/21

Abstract

Loss of proteostasis is one of the key hallmarks of ageing. Autophagy is one of the two key mechanisms that regulates protein homeostasis by intracellularly degrading cellular components. Functional dysfunctions in autophagy is a mechanistic feature xiv neurodegeneration. Macroautophagy is closely related to the endosomal trafficking as both have converging steps and common participating molecules. Atg8/LC3, is a key autophagy protein embedded within the autophagosomal membrane. In order to find Atg8a-interacting proteins in *Drosophila*, a yeast-two hybrid screening was performed, in which ArfGAP3, an endosomal trafficking associated protein, was found to be a novel Atg8a interactor. ArfGAP3 belongs to the ArfGAP sub-family of multi domain proteins with a primary function to hydrolyse GTP-bound Arf proteins. Co-localisation experiments in Drosophila fat body in this study further supports this interaction as strong co-localisation of ArfGAP3 and Atg8a to autophagosomes was observed when cells were subjected to starvation to initiate autophagy. Biochemical analysis also confirmed that endogenous ArfGAP3 is selectively degraded by autophagy as accumulation of endogenous ArfGAP3 was observed in Atg8a mutant flies compared to wild-type. Herein, we show that knockdown of ArfGAP3 seems to disrupt the autophagic flux. We also show that ArfGAP3 co-localises to Rab5 and Rab7, and knockdown disrupts endo-lysosome fusion. Additionally, we show low levels of ArfGAP3 disrupts functional lysosomal degradation and lipid droplet maturation. Moreover, knockdown of ArfGAP3 resulted in an accumulation of Ref(2)P in aged flies. Our study for the first time provides convincing evidence of the interaction between ArfGAP3 and Atg8a suggesting ArfGAP3 potentially plays a key role in the relationship between endosomal trafficking and selective autophagy. Furthermore, our study also suggests possible implications of ArfGPA3 in age-related diseases.

Abbreviations

AD Alzheimer's Disease

ALS Amyotrophic Lateral Sclerosis

ArfGAP3 ADP-ribosylation factor (Arf) GTPase activating protein 3

ARFRP1 Arf-like GTPase

Atg Autophagy related genes

Atg8 Autophagy related 8

CMA Chaperone-mediated autophagy

eMI Endosomal microautophagy

ER Endoplasmic reticulum

ESCRT Endosomal sorting complexes required for transport

FFAs Free fatty acids

GABARAP γ-amino-butyric acid receptor associated protein

GATE16 Golgi associated ATPase enhancer of 16kDa

GTPases GTP-binding proteins

GGAs Golgi-localized γ-ear-containing ADP-ribosylation factor binding proteins

HD Huntington's Disease

HOPS homotypic fusion and vacuole protein sorting

Hsc70 Heat shock cognate 70

LAMP2A Lysosomal-associated membrane protein

LD lipid droplet

LDS LIR docking site

LIR LC3-interacting region

LIRCPs LIR containing proteins

LMPs Lysosomal membrane proteins

LSD Lysosomal Storage Diseases

MAP1LC3 Microtubule associated protein 1 light chain 3

MTORC1 Mammalian target of rapamycin

PAS Phagophore assembly site

PD Parkinson's Disease

PLINs perilipins

SARs Selective autophagy receptors

SNARE Soluble N-ethylmaleimide-sensitive factor attachment protein receptor

TEM Transmission electron microscopy

TGN trans-Golgi network

UBL Ubiquitin-like

ULK1 Unc-51-like kinase 1

UPS Ubiquitin proteasome system

Part I

Introduction & methods

Chapter 1

Selective autophagy and endosomal trafficking in ageing

1.1 Introduction into ageing

Ageing, which occurs naturally in all living organisms, is the process by which functioning cells deteriorates due to accumulation of molecular damage over time, resulting to disease and death (Lindner and Demarez, 2009; Barbosa, Grosso and Fader, 2019). Extensive research has been undertaken into studying ageing as it is the leading risk factor for many chronic diseases such as cancer, neurodegenerative diseases, cardiovascular diseases (Niccoli and Partridge, 2012). Ageing is a fundamental biological, demographic and socio-economic issue in the world. Neurodegenerative diseases are giving rise to significant socio-economic issues in the coming decades as disease demographics predicts by 2050 a three-to four fold increase in Alzheimer's disease cases (Brehme and Voisine, 2016). Biomedical scientists are under increased pressure to discover avenues that will extend healthspan and lifespan (Goldman *et al*, 2013; Maruzs *et al*, 2019). Studying ageing and longevity at a molecular level can aid to manipulate ageing in the future and help elucidate the mechanisms responsible for ageing (Barja, 2017; Barbosa, Grosso and Fader, 2019; Maruzs *et al*, 2019).

1.1.1 The nine hallmarks of ageing

Ageing is a multifactorial process. There are a number of features of ageing and these have been summarised as the nine hallmarks of ageing (López-Otín *et al.*, 2013; Maruzs *et al.*, 2019). The first four hallmarks are categorised as the primary hallmarks of ageing which affect normal cellular function in a negative manner thus considered as the main causes of cellular damage. These four hallmarks are genetic instability, telomere erosion, epigenetic alterations and loss of proteostasis. The next category of hallmarks is known as antagonistic hallmarks, which respond to mitigate damage. These hallmarks are deregulated nutrient sensing, mitochondrial dysfunction and cellular senescence. However, these three hallmarks over time become chronic or exacerbated and can become toxic. The end results of the primary and antagonistic hallmarks consequently lead to the final two hallmarks, stem cell exhaustion and altered intercellular communication, which are categorised as integrative hallmarks. These two hallmarks are the culprits of decline in function associated with ageing (López-Otín *et al.*, 2013; Maruzs *et al.*, 2019).

1.1.2 Degradation pathways for protein homeostasis

Protein homeostasis is controlled by two cellular mechanisms; ubiquitin proteasome system (UPS) and autophagy (Lindner and Demarez, 2009; López-Otín *et al.*, 2013). When cells age, protein homeostasis is dysregulated due to endogenous stress (e.g. rapid increase in temperature (Wallace *et al.*, 2015), transcription factors and damaged organelles (Khandia *et al.*, 2019)) and exogenous stress (e.g. pathogens and exogenous

ROS (Khandia *et al.*, 2019)) causing proteins to unfold. These unfolded proteins are targeted for degradation by the proteasome and autophagy (Kawasaki *et al.*, 2016). The UPS is a highly regulated machinery consisting of a number of components. Degradation via this system involves a chain of events leading to substrate ubiquitination and degradation (Cohen-Kaplan *et al.*, 2016). There are three types of enzymes involved in substrate ubiquitination: 1) the ubiquitin-activating enzyme, E1, 2) a ubiquitin-conjugating enzyme, E2, and 3) a ubiquitin ligase, E3. These three enzymes work to link chains of ubiquitin onto proteins targeted for degradation. The ubiquitin tagged protein is then recognised by the multi-catalytic protease complex, 26S proteasome, where it undergoes degradation into small peptides via catalytic enzymes (Lecker, Goldberg and Mitch, 2006).

However, when the UPS fails and the misfolded proteins accumulate to form ubiquitinated aggregates, the degradation of these aggregates are mediated primarily by the autophagic pathway (figure 1.1) (Kawasaki *et al.*, 2016) via specific autophagic receptors such as Ref(2)P, which is *Drosophila melanogaster* homolog of mammalian sequestosome 1 (SQSTM1), also known as p62 (Kwon and Ciechanover, 2017). When autophagy is compromised resulting in loss of function of the mechanism, this results in protein aggregation which is a key hallmark in age related conditions such as Alzheimer's disease (aggregated amyloid β and tau), Parkinson's Disease (accumulated α- synuclein) etc (López-Otín *et al.*, 2013) (figure 1.1). Many other neurodegenerative diseases also possess abnormal protein aggregation as a characteristic, such as Huntington's disease (Huntingtin) and amyotrophic lateral sclerosis (TARDBP) (Knowles, Vendruscolo and Dobson, 2014; Brehme and Voisine, 2016). Multiple studies have provided evidence to show that changes in normal function of autophagy can play a vital role in the aging process (Maruzs *et al.*, 2019).

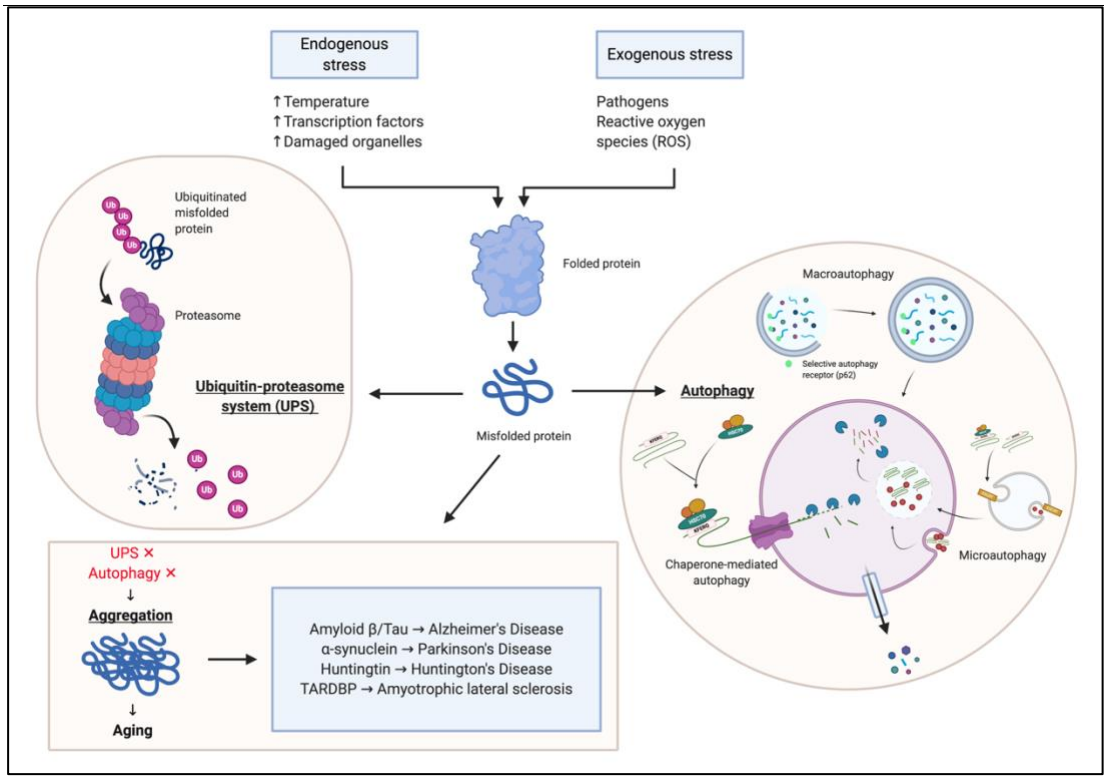

Figure 1.1. Schematic overview illustrating loss of proteostasis. Endogenous or exogenous stress to the cell can cause folded proteins to misfold in structure. These misfolded proteins are targeted for degradation by either autophagy or ubiquitin-proteasome system (UPS). When the degradation pathways are compromised in function, these misfolded proteins accumulate resulting in downstream proteotoxic effects due to protein aggregation and in turn resulting in aging and age related diseases (Created with BioRender.com).

1.2 Autophagy

The term autophagy is derived from the ancient Greek translation "self-eating" and is defined as the evolutionarily conserved cellular process by which cellular components, such as cytoplasmic proteins and organelles, are intracellularly degraded (He and Klionsky, 2009). Autophagy is a key mechanism for cell homeostasis and is initiated as a cellular response to infection (invading bacteria and viruses), nutrient starvation, and proteotoxic and oxidative stress (removal of damaged organelles and aggregated proteins/lipids) (Rubinsztein *et al.*, 2011; Lamb *et al.*, 2013; Randow & Youle, 2014; Youle & Narendra, 2011; Lamark and Johansen, 2012).

Over the past several decades, there has been a significant increase and progress in autophagy research, having its greatest impact on understanding human health and disease (Kirkin, 2020). Only in the last 20 years, the autophagic mechanism has been studied extensively due to advances in molecular and cell biology, allowing the significant discovery that degradation of material can be selective via specific receptor proteins (Kirkin, 2020). Hence, the use of model organisms to illuminate the role of selective autophagy in both normal and pathological conditions is fundamental (Nezis, 2012). Autophagy consists of three processes, all of which can be selective; 1) macroautophagy, 2) microautophagy and 3) chaperone-mediated autophagy (Kirkin, 2020). These subtypes will be outlined in detail in a later chapter.

1.2.1 Selective autophagy

Autophagy is a tightly regulated process in which cytoplasmic proteins and organelles tagged for degradation are sequestered into double membrane vesicles called autophagosomes which then delivers the cargo to lysosomes (Johansen and Lamark, 2011). Autophagosomes are key components of the autophagic machinery as it safeguards the physical sequestration of cargo tagged for lysosomal degradation from the cytoplasm and ensures the delivery of the cargo to the lysosome (Kirkin, 2020).

Following autophagosome initiation (nucleation step) by the ULK1 (unc-51-like kinase 1) complex and the class III phosphatidylinositol (PtdIns) 3-kinase complex, the bow-shaped membrane named phagophore is formed and undergoes elongation via specific autophagy related proteins. The cargo tagged for degradation is delivered to the phagophore by selective receptors that bind to the inner membrane of the phagophore. The expansion and subsequent closure of the membrane generates

the double-membrane vesicle, autophagosome, that eventually fuses when matured with the lysosome to form autolysosomes. The formation of the autolysosomes leads to the degradation of cellular cargo via acidic hydrolases. The degraded material is then recycled for other cellular processes (Johansen and Lamark, 2011; Nezis, 2012; Rubinsztein *et al.*, 2012).

As selective autophagy cargo is newly identified, this gives rise to a new pathway within the autophagy field (Kirkin, 2020). The first substrates that were discovered to be selectively degraded by autophagy were mitochondria and peroxisomes, and hence the terms ‘mitophagy’ and ‘pexophagy’ were used to describe these autophagic degradation processes (Hutchins *et al.*, 1999; Kim *et al.*, 2007). The different types of selective autophagic pathways are summarised in table 1.1. Lipophagy will be discussed in detail later in this chapter.

Table 1.1. Types of selective autophagy processes. List of selective autophagic processes with its respective substrate. (Kirkin, 2020).

Type of selective autophagy	Selective substrates for degradation	Year identified	Reference
Aggrephagy	Protein aggregates	2007	(Overbye *et al*., 2007; Lamark and Johansen, 2012)
Chlorophagy	Chloroplasts	2009	(Seay *et al*., 2009; Zhuang and Jiang, 2019)
ER-phagy	Fragments of ER	2007	(Bernales, Schuck and Walter, 2007)
Ferritinophagy	Ferritin	2014	(Mancias *et al*., 2014; Masaldan *et al*., 2018)
Glycophagy	Glycogen	2011	(Jiang, Wells and Roach, 2011; Zhao *et al*., 2018)
Granulophagy	Stress granules	2013	(Buchan *et al.*, 2013)
Lipophagy	Lipid droplets	2009	(Singh *et al.*, 2009)
Lysophagy	Lysosomes	2013	(Hung, Chen and Yang, 2013; Papadopoulos, Kravic and Meyer, 2020)
Mitophagy	Mitochondria	1998	(Scott and Klionsky, 1998; Youle and Narendra, 2011)
Myelinophagy	Myelin	2015	(Gomez-Sanchez *et al*., 2015; Thumm and Simons, 2015)
Nucleophagy	Nucleus	2009	(Park *et al*., 2009; Papandreou and Tavernarakis, 2019)
Pexophagy	Peroxisomes	1998	(Scott and Klionsky, 1998; Cho *et al.*, 2018)
Proteaphagy	Proteasome	2015	(Bartel, 2015; Marshall *et al*., 2015)
Ribophagy	Ribosomes	2008	(Kraft *et al*., 2008; Denton and Kumar, 2018)

Virophagy	Viruses	2016	(Dong and Levine, 2013; Sumpter Jr *et al.*, 2016)
Xenophagy	Bacteria/pathogens	2004	(Nakagawa *et al.*, 2004; Sharma *et al.*, 2018)
Zymophagy	Zymogen granules	2011	(Grasso *et al.*, 2011)

During *Drosophila* development, there is evidence of cross talk between selective autophagy and cell death, as it is seen to regulate cell death while eliminating obsolete tissue. This proposes a dual role for selective autophagy in physiological conditions (Yin, Pascual and Klionsky, 2016). Selective autophagy diminishes the occurrence of apoptosis by switching on mitophagy and targeting pro-apoptotic proteins for degradation. On the other hand, apoptosis activation impedes autophagy due to the cleavage and subsequent inactivation of essential autophagy proteins by caspases (Mariño *et al.*, 2014; Yin, Pascual and Klionsky, 2016). All in all, autophagy precedes apoptosis as it is classed as the primary response to cellular damage. If autophagy is unsuccessful in removing the unwanted damage cellular components, it is blocked and apoptosis is induced (Yin, Pascual and Klionsky, 2016).

1.2.2 *Drosophila melanogaster* as a model organism for autophagy

The 'father' of *Drosophila* research, Thomas Hunt Morgan, identified the white eye pigment mutation (Bier, 2005) and clarified Gregor Mendel's theory of inheritance by using *Drosophila* as a model organism to define genes and show that it is located within chromosomes. Morgan's theory was highly recognised in 1933 and he was awarded a Nobel Prize in Physiology or Medicine *"for his discoveries concerning the*

role played by the chromosome in heredity". Following this, there were many other Nobel Prizes awarded to scientists that advanced *Drosophila* research in biology and biomedical research. Studies showed genes that were associated with fly development were also crucial for all mammalian development suggesting that many underlying building blocks and processes have been conserved through evolution. This led to the famous 2000 study by Craig Venter and colleagues, in which they sequenced the entire *Drosophila* genome by the "shot-gun" approach. When the sequenced *Drosophila* genome was compared with the sequenced human genome (eleven months later), there was a 75% sequence match of known human disease genes in the *Drosophila* genome. This finding was pivotal evidence confirming *Drosophila* as the leading model organism for biological and biomedical research (Jennings, 2011).

Published in 1963 was the first study of autophagy in *Drosophila melanogaster*. The study highlighted TEM images of large structures representing autolysosomes in larval fat body cells which contained ER and mitochondria (von Gaudecker, 1963; Maruzs *et al*., 2019).

There are several practical and ethical obstacles that limit the use of humans in experiments for research in biomedical and biological sciences. Hence, using model organisms such as mice and the holometabolous insect *Drosophila melanogaster* have been the primary focus to study the underlying biology of cells and tissues (Jennings, 2011). For over a century now, *Drosophila* studies has given rise to better understanding of the evolutionary relationship between vertebrate and invertebrate organisms (Reiter *et al.*, 2001) and has been extensively used to study various biological processes such as; embryonic development, genetics and inheritance, learning, behaviour and aging because the fundamental mechanisms of these processes are conserved between these species through evolution (Jennings, 2011). A number

of traits makes the *Drosophila melanogaster* an excellent model organism to study autophagy as well as many other biological processes. The advantages of using *Drosophila* are that they have a rapid life cycle, can produce a large number of individuals, they are much easier and inexpensive to maintain in laboratory conditions and can be genetically modified for research purposes (Bier, 2005; Jennings, 2011). In addition, the *Drosophila* fat body has multiple features that can consider it as a liver-like organ; it is able to store fat in a similar manner to human adipose tissue, it allows nutrient storage and utilization and possesses major metabolic functions. Since the fat body in *Drosophila* is the major tissue for storage of lipids, glycogen and proteins, its response to nutrient starvation is fast and efficient (Arrese and Soulages, 2010; Lőrincz, Mauvezin and Juhász, 2017).

The developmental stages of *Drosophila* life cycle consist of three larval stages (L1, L2 and L3). In laboratory experiments, the L3 larval stage is mostly used to study autophagy in larvae since the developmental stage after L3 is the wandering phase, where the larvae exit the food, and this is when developmental autophagy is induced for metamorphosis. The L3 larvae are subjected to 20% sucrose solution for approximately four hours to induce autophagy in fat body cells via amino-acid starvation. This is because it takes 60 to 90 minutes to induce autophagy, however, around three to five hours is when maximum number of autophagic structures are observed in the fat body (Scott, Schuldiner and Neufeld, 2004; Lőrincz, Mauvezin and Juhász, 2017).

1.2.3 The discovery of autophagy – historical overview

Christian de Duve, who discovered lysosomes and peroxisomes, coined the term "autophagy" at the *Ciba Foundation Symposium on Lysosomes* in London 1963 (Klionsky, 2008). However, autophagy was first discovered by Thomas Ashford and Keith Porter in 1962 in a study where it was revealed that lysosomes had considerably increased in number following the addition of glucagon in rat liver cells. They found these lysosomes had translocated to the centre of the cell and consisted of cytoplasmic material including mitochondria which were deteriorated, indicating these organelles most likely were autophagosomes rather than lysosomes (Ashford and Porter, 1962).

Autophagy research has augmented drastically in the past 15 years, where a number of key discoveries in autophagy were made to better understand the mechanism at a cell and molecular level (figure 1.2).

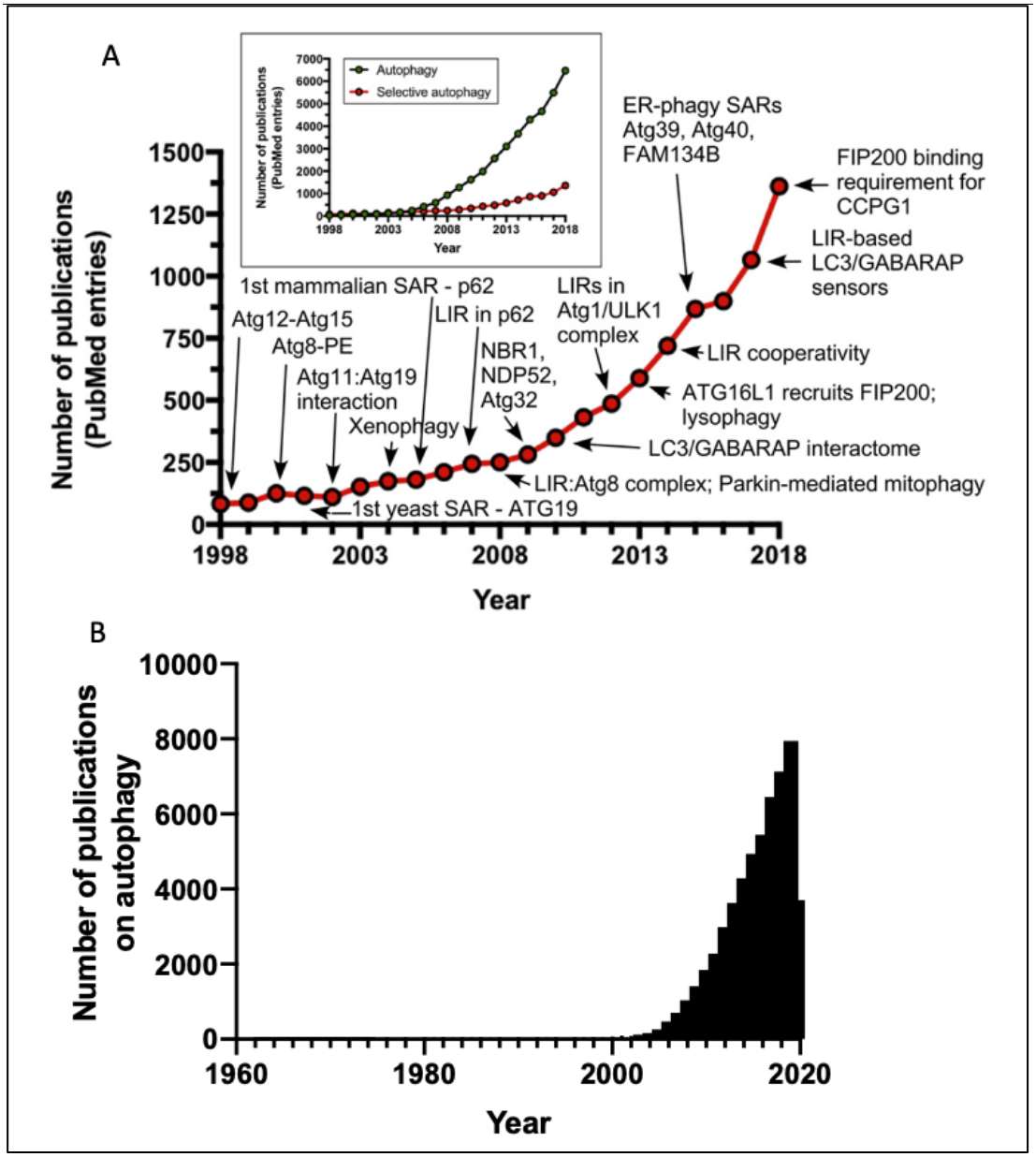

Figure 1.2. Selective autophagy publication dynamics. A) Number of publications sourced from PubMed showing key discoveries in selective autophagy research from 1998 to 2018 (Kirkin, 2020). B) Updated number of publications on selective autophagy since 1960 (Sourced from PubMed on 21/05/20).

In 1993, the first genetical study carried out in yeast on autophagy by Yoshinori Ohsumi identified fifteen autophagy related genes (Tsukada and Ohsumi, 1993). Dr Yoshinori started studying yeast biology as a postdoctoral scientist in the mid 1970's at The Rockefeller University in New York after acquiring his PhD from the University of Tokyo. In the late 1970's, for approximately a decade, his research focussed on functions of yeast vacuoles. Yeast vacuoles are equivalent to lysosomes

in mammalian cells. Ohsumi continued studying yeast vacuoles into the early 1990's when he published in 1992 that the autophagic mechanism in yeast *Saccharomyces cerevisiae* is similar to the autophagic process in mammalian cells. Dr Yoshinori Ohsumi and colleagues discovered, in nutrient-deficient media conditions, an accumulation of autophagic bodies in yeast cells vacuoles lacking vacuolar proteinases compared to normal nutrient medium conditions. Further investigations, via electron microscopy and biochemical analysis, revealed that the autophagic bodies non-selectively engulfed cytosolic components in the yeast vacuoles (Takeshige *et al.*, 1992).

Since autophagosomes have a transitory nature, remaining stable in the cytoplasm for around fifteen minutes compared to the more stable lysosomes (Tsukada and Ohsumi, 1993; Mijaljica *et al*., 2012), Ohsumi grew yeast mutants on a nutrient-deprived medium lacking vacuolar proteases. This resulted in an increase in the number of autophagosomes, however due to the lack of vacuolar proteases it's subsequent degradation would be prevented. Random mutations were induced in the yeast via ethyl methanesulfonate (EMS) treatment. The strains that did not display accumulation of autophagosomes were selected (apg mutants). Dr Yoshinori Ohsumi identified and isolated 15 mutants which displayed defective accumulation of autophagic bodies (autophagosomes) in the yeast vacuoles. Each of the 15 apg mutant strains were found to be defective in protein degradation in the yeast vacuoles which suggested that autophagosomes are crucial machinery to the autophagic mechanism for protein degradation in yeast vacuoles. In addition, it also suggested that these 15 Apg genes, also now known as "autophagy-related genes" (Atg genes), are fundamental for activating autophagy in yeast. All 15 genes were conserved within the animal kingdom (Tsukada and Ohsumi, 1993).

From the point of this landmark study published in 1993 by Ohsumi and colleague, all autophagy research subsequently involved Atg genes. Dr Yoshinori Ohsumi's work in autophagy was universally recognised as he was awarded the Nobel Prize in Physiology or Medicine in 2016 *"for his discoveries of mechanisms for autophagy"*.

1.2.4 Classification of autophagy

As mentioned previously, there are three sub-types of autophagy; 1) macroautophagy, 2) microautophagy and 3) chaperone-mediated autophagy (CMA). Each type of autophagy differs in the nature of the cargo and in the mechanism in which the cargo tagged for degradation enters the lysosome.

1.2.4.1 Chaperone-mediated autophagy

Chaperone-mediated autophagy (CMA) is the process in which protein substrates from the cytosol are directly translocated into the lysosome. CMA substrates are mostly cellular proteins. This process is mediated by lysosome-associated membrane protein type 2A (LAMP2A). A cytosolic chaperone, in mammals heat shock protein family A (Hsp70) member 8 (HSPA 8) and in *Drosophila* heat shock cognate 70 (Hsc70), is responsible for delivering CMA substrates to the lysosome. The CMA substrates have a characteristic penta-peptide motif, KFERQ, to which Hsc70 binds and brings the substrates to the LAMP2A protein on the lysosome membrane. After binding of substrates to LAMP2A, the substrates undergo unfolding, which also involves Hsc70. Translocation of the CMA substrates into the lysosomal lumen for

degradation is executed by Hsc70. Lysosomal acidic hydrolases degrade the CMA substrates (figure 1.3). The activity of CMA is directly proportional to the amount of LAMP2A, as the rate limiting step is substrate binding to LAMP2A. Therefore, LAMP2A is the major factor of CMA. By measuring the amount of LAMP2A, the activity of CMA can be measured. Although levels of LAMP2A regulates the rate of CMA, upstream events of this process is still unclear (Bandyopadhyay *et al.*, 2008; Ghosh and Pattison, 2018; Yim and Mizushima, 2020).

CMA is activated primarily in response to nutrient starvation, after four to six hours of macroautophagy activity gradually decreases, when cells are persistently starved for more than ten hours. CMA activity is peak at around twenty hours into fasting and activity can last for up to three days (Massey *et al.*, 2006; Ghosh and Pattison, 2018). It has been revealed that LAMP2A is conserved between birds and mammals, however there has been no such discovery yet of LAMP2A gene in *Drosophila*, hence it is still unsure if CMA occurs in the fruit fly. However, in *Drosophila*, selective endosomal microautophagy (described below) shares with CMA the essential KFERQ-like motif and the Hsc70 protein for substrate targeting. This possibly suggests an alternative process to CMA in *Drosophila* (Lescat *et al.*, 2018).

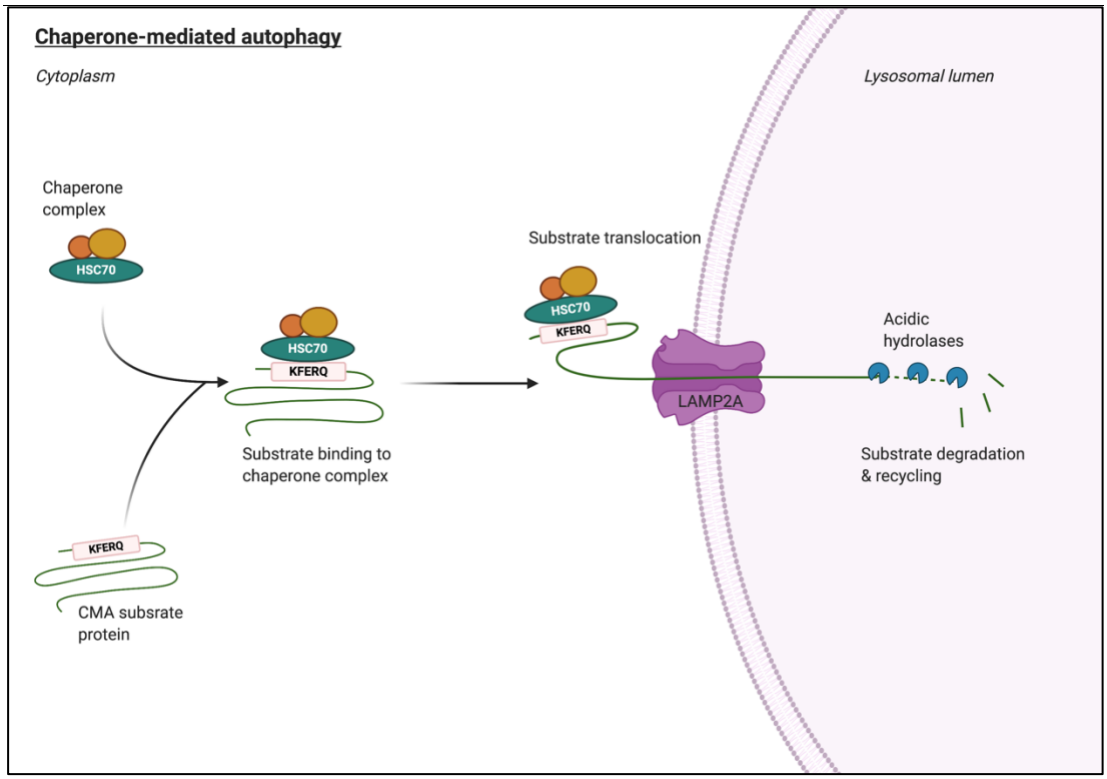

Figure 1.3. Chaperone-mediated autophagy (CMA) mechanism. HSC70 chaperone complex selectively recognises proteins with the KFERQ (-like) motif. This allows the direct uptake of the selective protein into the lysosome lumen via the translocation complex LAMP2A embedded in the lysosomal membrane. Acidic hydrolases located within the lysosomal lumen are responsible for substrate degradation (Created with BioRender.com adapted from Ghosh and Pattison, 2018).

1.2.4.2 Microautophagy

Microautophagy is mostly a non-selective process, with a few exceptions. The process is defined by the direct engulfment of cytosolic material by lysosomes via membrane invaginations. The lysosomes then breakdown these intra-luminal vesicles (figure 1.4) (Yim and Mizushima, 2020).

Microautophagy was first discovered in lysosomes over 50 years ago by de Duve and Wattiaux but details of this mechanism and its regulation is still not well known (de Duve and Wattiaux, 1966; Mijaljica *et al*., 2011). Limitations of studying microautophagy include the small size of lysosomes in mammalian cells, which makes

it difficult to observe membrane invaginations, and the lack of assays to measure the rate of microautophagy. On the contrary, studying microautophagy in yeast cells has been much easier due to having one large vacuole (lysosome), making it easier to observe the mechanism in detail. Studies of microautophagy in yeast cells have led to critical discoveries in this field of research (Yim and Mizushima, 2020).

Research in mammalian cells have revealed that microautophagy can also occur on endosomes and is termed endosomal microautophagy (eMI). The mechanism of eMI is slightly better understood than non-selective microautophagy, and hence has been suggested as the primary microautophagy pathway for now. Substrates for eMI contain KFERQ (-like) motifs, which are recognised by cytosolic HSC70. The substrates are delivered to the endosomes by the HSC70, where the HSC70 binds to phosphatidylserine. This binding causes the membrane to deform and the ESCRT machinery executes the scission of the intralumenal vesicle from the endosomal membrane. The process ends with the subsequent degradation of eMI substrates within the endosomes or lysosomes (figure 1.4) (Sahu *et al.*, 2011; Yim and Mizushima, 2020).

Some studies in microautophagy have been carried out in *Drosophila melanogaster* to better understand the process of mammalian eMI. Starvation via the inactivation of TOR (homologous to mTOR) induces eMI in *Drosophila*. Investigations in *Drosophila* eMI have suggested a cross-link between eMI and macroautophagy as it was found that components of the initiation complex in macroautophagy, Atg1 and Atg13, are also vital for eMI in *Drosophila*. This indicated the same upstream factors regulates both eMI and macroautophagy (Mukherjee *et al.*, 2016). In addition, there is also evidence of the rapid degradation of macroautophagy receptors by eMI in mammalian cells in the first few hours of starvation, indicating a

stronger cross-link between the two processes (Mejlvang *et al.*, 2018; Yim and Mizushima, 2020).

The microautophagy process can be non-selective or selective. Examples of selective microautophagy include micropexophagy, piecemeal microautophagy (PMN) and micromitophagy. In selective microautophagy, specific organelles are sequestered with arm-like protrusions. Micropexophagy is the selective autophagic process that engulfs damaged peroxisomes, PMN selectively degrades unwanted nuclear portions and micromitophagy is the direct sequestration of damaged mitochondrion by the lysosome (vacuole in yeast) (Li, Li and Bao, 2012).

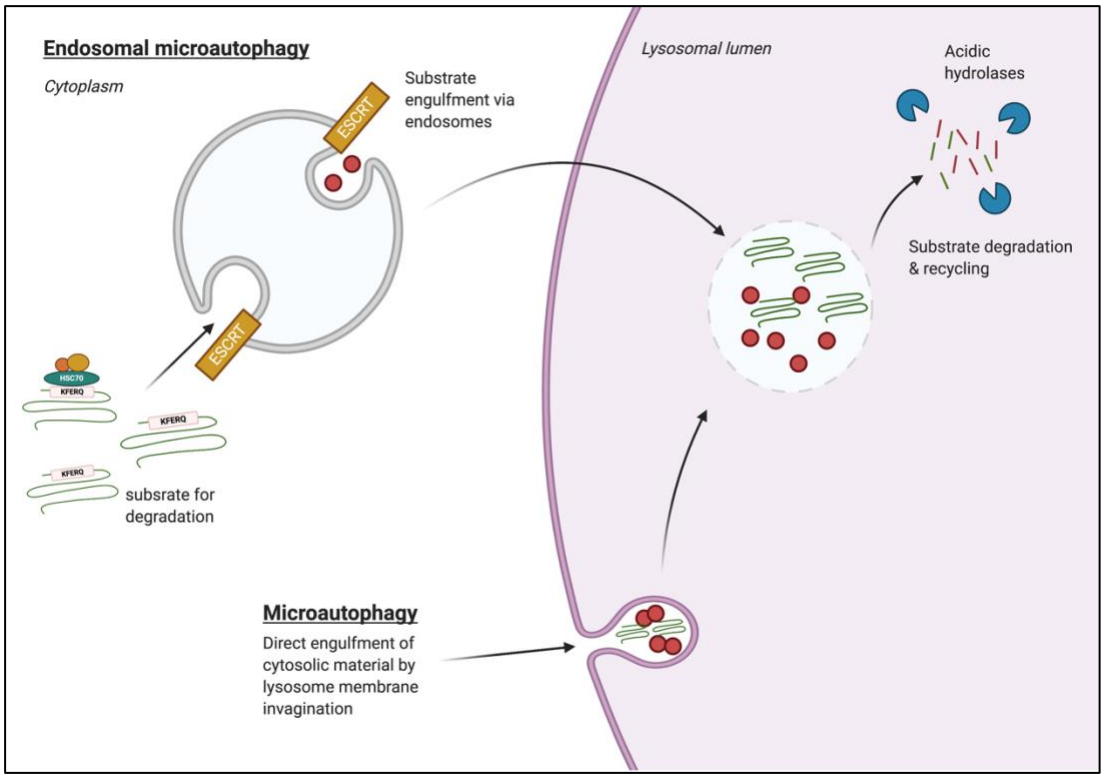

Figure 1.4. Microautophagy and endosomal microautophagy mechanism. Microautophagy involves the direct engulfment of cytosolic material by the lysosomes (membrane invagination). Endosomal microautophagy involves engulfment of cytosolic material via endosomal invaginations. The ESCRT system aids endosomal invagination. Proteins possessing the KFERQ motif can also be selectively degraded by microautophagy via HSC70 targeting. The cytosolic material targeted for microautophagy is then degraded within the lysosomal lumen. (Created with BioRender.com adapted from Zheng *et al.*, 2019).

1.2.4.3 Macroautophagy

As mentioned previously, macroautophagy (autophagy) is the process in which cytosolic cargo tagged for degradation are sequestered into a double-membrane autophagosome. The mature autophagosome fuses with lysosomes forming autolysosomes in which the acidic hydrolases degrade the cytosolic cargo (figure 1.5). Macroautophagy is the most well studied and understood subtype of autophagy, it was the first of the three subtypes to be discovered (Kirkin, 2020). The mechanistic detail of macroautophagy is outlined in the following subchapters and will be referred to as 'autophagy' from this point onwards.

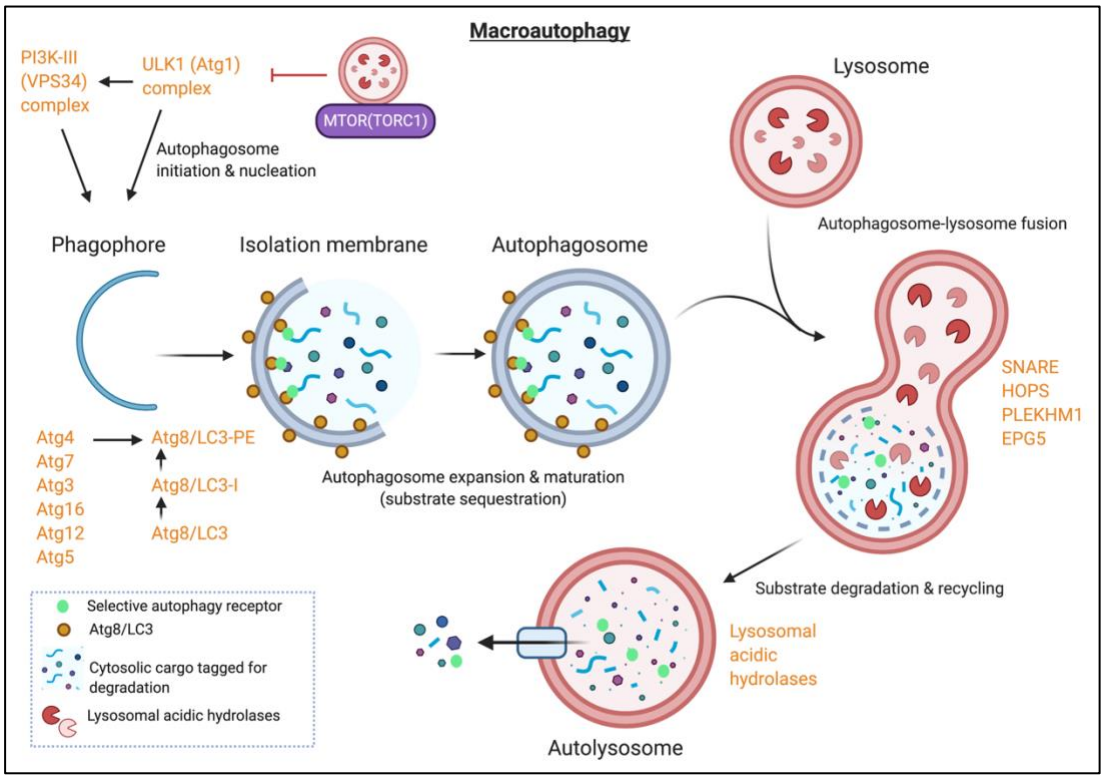

Figure 1.5. Macroautophagy mechanism. Under nutrient starvation conditions, mTORC1 (Drosophila TORC1) stimulation is discontinued, activating autophagosome initiation by activating the ULK1 (Atg1) kinase complex. Autophagosome nucleation involves the recruitment of the PI3K-III (VPS34) complex which in turn recruits ATG proteins, Atg4, Atg7, Atg3 and the Atg16, Atg12 and Atg5 complex, responsible for the Atg8/LC3 lipidation. Selective autophagy receptors bind to cytosolic cargos tagged for autophagic degradation and delivers to the growing phagophore. The autophagosome closes, matures and fuses with the lysosome. A number of docking proteins regulate the autophagosome-lysosome fusion. The resulting autolysosome degrades the cytosolic cargo via lysosomal acidic hydrolases. The resulting building blocks are recycled back into the cytoplasm. (Created with BioRender.com)

1.2.5 Regulation of autophagy and key proteins

Since autophagy plays an essential role in the maintenance of cell homeostasis and cell survival, and its involvement is crucial for animal development and pathophysiology, the process needs to be highly regulated. Excessive or insufficient activity can be deleterious to the cell. Studies in yeast have provided better understanding of the networks that regulate autophagy, and it has been discovered to be common across many organisms from yeast to mammals. The two main types of regulations are; 1) nitrogen-dependent regulation and 2) energy/glucose-dependent regulation (Yin *et al.*, 2016), which will be discussed later in this chapter.

As first mentioned in chapter *1.2.3 The discovery of autophagy – historical overview*, autophagy (Atg) genes were first identified in yeast, these Atg proteins are key regulators of autophagy. Since the discovery of the first fifteen Atg genes, multiple genetic screens have revealed more Atg genes, many of which are conserved between yeast, mammals and *Drosophila*. Table 1.2, categorised into different stages of the autophagic process, summarises a list of *Drosophila* autophagy related proteins with its function and the corresponding mammalian homologue. Mechanistic details of the autophagy process and functional details of the autophagy related proteins are discussed in the following sub-chapters.

Table 1.2. *Drosophila* autophagy related proteins. List of *Drosophila* autophagy related proteins (Atg). Atg proteins were first identified in yeast by Yoshinori Ohsumi. These proteins are well conserved throughout the animal kingdom. The proteins involved in the core autophagic process are listed below with its function and corresponding mammalian homologue (Adapted from Chang and Neufeld, 2010).

Drosophila protein	Mammalian homologue	Function	Reference
		Autophagosome initiation	
Atg1	ULK1/2	Serine/threonine protein kinase involved in initiation of isolation membrane	(Matsuura *et al.*, 1997; Kamada *et al.*, 2010; Das, Shravage and Baehrecke, 2012)
Atg13	Atg13	Regulatory subunit of Atg1 kinase complex	(Weidberg, Shvets and Elazar, 2011; Das, Shravage and Baehrecke, 2012)
Atg17	FIP200	Regulatory subunit of Atg1 kinase complex	(Weidberg, Shvets and Elazar, 2011; Das, Shravage and Baehrecke, 2012)
Atg101	Atg101	Regulatory subunit of Atg1 kinase complex	(Das, Shravage and Baehrecke, 2012; Mulakkal *et al.*, 2014)
		Autophagosome nucleation	
Vps34	Vps34	Lipid kinase, also known as class III PtdIns3K, subunit of Vps34 regulatory complex. Responsible for initiation of phagophore.	(Das, Shravage and Baehrecke, 2012; Yin, Pascual and Klionsky, 2016)
Vps15	Vps15/p150	Regulatory kinase. Subunit of Vps34 regulatory complex.	(Simonsen and Tooze, 2009; Das, Shravage and Baehrecke, 2012)
Atg6	Beclin1	Subunit of Vps34 regulatory complex	(Das, Shravage and Baehrecke, 2012; Yin, Pascual and Klionsky, 2016)
Atg14	Atg14L	Subunit of Vps34 regulatory complex	(Chang and Neufeld, 2010; Das, Shravage and Baehrecke,

			2012; Melani *et al.*, 2017)
Uvrag	Uvrag	Subunit of Vps34 regulatory complex	(Chang and Neufeld, 2010; Das, Shravage and Baehrecke, 2012; Melani *et al.*, 2017)
Rubicon	Rubicon	Subunit of Vps34 regulatory complex	(Chang and Neufeld, 2010; Das, Shravage and Baehrecke, 2012; Melani *et al.*, 2017)
	Autophagosome expansion		
Atg8a/Atg8b	GABARAP, GATE-16 and LC3	Ubiquitin-like (Ubl) protein, also known as Atg8/LC3. Atg8 conjugates to PE, regulating formation of autophagosome. Localised to autophagosomal membrane, acts as a scaffold protein for selective autophagy receptors.	(Das, Shravage and Baehrecke, 2012; Yin, Pascual and Klionsky, 2016)
Atg7	Atg7	E1-like activating enzyme which conjugates Atg12 to Atg5 and conjugates Atg8a to PE.	(Das, Shravage and Baehrecke, 2012; Yin, Pascual and Klionsky, 2016)
Atg3	Atg3	E2-like conjugating enzyme for Atg8	(Das, Shravage and Baehrecke, 2012; Yin, Pascual and Klionsky, 2016)
Atg10	Atg10	E2-like enzyme that conjugates Atg12 to Atg5	(Das, Shravage and Baehrecke, 2012; Yin, Pascual and Klionsky, 2016)
Atg4a, Atg4b	Atg4A, Atg4B, Atg4C, Atg4D	Cysteine protease that cleaves the c-terminal of Atg8	(Das, Shravage and Baehrecke, 2012; Yin,

			Pascual and Klionsky, 2016)
Atg12	Atg12	Ubiquitin-like (Ubl) protein responsible for autophagosome expansion. Conjugates to Atg5. Subunit of the Atg12-Atg5-Atg16 complex involved in Atg8 lipidation.	(Das, Shravage and Baehrecke, 2012; Yin, Pascual and Klionsky, 2016)
Atg5	Atg5	Conjugates to Atg12. Subunit of Atg12-Atg5-Atg16 complex	(Das, Shravage and Baehrecke, 2012; Yin, Pascual and Klionsky, 2016)
Atg16	Atg16L1, Atg16L2	Subunit of Atg12-Atg5-Atg16 complex	(Das, Shravage and Baehrecke, 2012; Yin, Pascual and Klionsky, 2016)
		Recycling	
Atg9	Atg9A, Atg9B	Transmembrane protein that functions as a membrane transporter to growing phagophore. Subunit of Atg9-Atg2-Atg18 complex.	(Das, Shravage and Baehrecke, 2012; Yin, Pascual and Klionsky, 2016)
Atg2	Atg2	Subunit of Atg9-Atg2-Atg18 complex.	(Das, Shravage and Baehrecke, 2012; Yin, Pascual and Klionsky, 2016)
Atg18a, Atg18b	WIPI-1, WIPI-2	PI3P binding protein. Subunit of Atg9-Atg2-Atg18 complex.	(Das, Shravage and Baehrecke, 2012; Yin, Pascual and Klionsky, 2016)

1.2.5.1 Autophagy initiation and nucleation

Changes in extracellular environment can initiate autophagy. A shift in nutrient levels is recognised by the TOR signalling pathway. Under conditions where nitrogen and/or amino acids are limited, i.e. nutrient starvation, an intracellular signalling cascade is activated in which the mammalian target of rapamycin MTORC1 (*Drosophila* TORC1) stimulation is discontinued. The downstream effect of this is the activation of the Atg1 kinase complex. In *Drosophila*, this complex consists of the serine/threonine protein kinase Atg1 (ULK1/2 in mammals), the regulatory protein Atg13 and Atg17 (FAK family-interacting protein of 200kD (FIP200) in mammals, also called retinoblastoma 1-inducible coiled-coil 1 (RB1CC1)) (Kamada *et al.*, 2000; Yin, Pascual and Klionsky, 2016). Assembly of the Atg1 kinase complex is vital for autophagy since the complex enables the recruitment of other Atg proteins to the phagophore assembly site (PAS) (figure 1.5). Additionally, the complex also activates downstream targets by phosphorylation (Suzuki *et al.*, 2007; Papinski *et al.*, 2014; Yin, Pascual and Klionsky, 2016).

Autophagy is regulated by Atg1 since it has been shown that the depletion of Atg1 prevents autophagosome formation (Scott, Schuldiner and Neufeld, 2004; Yang and Klionsky, 2009b; Chang and Neufeld, 2010). In *Drosophila*, the co-expression of both Atg1 and Atg13 proteins results in an increase in phosphorylation of both Atg1 and Atg13 in a TOR- and Atg1 kinase-dependent manner, signifying both proteins are substrates of the Atg1 kinase (Chang and Neufeld, 2009). This TOR- and Atg1 mediated hyper-phosphorylation of Atg13 and Atg1 is also observed in mammals *in vivo* and *in vitro* (Hosokawa *et al.*, 2009; Chang and Neufeld, 2010). In yeast cells, Atg1 and Atg13 interaction is limited to starved cells, however in *Drosophila*, regardless of the nutrient level, Atg1 and Atg13 interact constitutively (Chang and

Neufeld, 2010). It has been displayed, through biochemical studies in flies and mammals, the direct binding of Atg13 to all three subunits of the Atg1 kinase complex (Chang and Neufeld, 2009; Mizushima, 2010; Nagy *et al.*, 2014). There are 3 scenarios which suggests Atg1 catalytic activity is seen to be vital for induction of autophagy; 1) Kinase dead Atg1 expression inhibits, in a dominant-negative manner, autophagy (Scott, Juhász and Neufeld, 2007), 2) autophagy is strongly induced via Atg1 overexpression (Scott, Juhász and Neufeld, 2007) and 3) during starvation, Atg1 is subjected to limited autophosphorylation resulting in an increase in its activity (Mizushima, 2010; Mulakkal *et al.*, 2014). In *Drosophila*, overexpression of Atg1 is adequate to autophagy initiation, on the other hand in mammalian cells, overexpression of ULK1 impedes starvation-induced autophagy (Scott, Juhász and Neufeld, 2007; Chang and Neufeld, 2010). Furthermore, Atg13 overexpression in *Drosophila* also inhibits autophagy induction (Chang and Neufeld, 2009). Both of these observations propose that the Atg1-Atg13 complex can regulate autophagy in a positive and negative manner.

Autophagosome nucleation is the stage when a small group of molecules, responsible for synthesis of the phagophore membrane, are assembled. In essence, it is an amplification event resulting in further recruitment of proteins crucial for phagophore expansion to form the autophagosome (Yin, Pascual and Klionsky, 2016). In yeast and *Drosophila*, the phagophore is assembled at the phagophore assembly site (PAS), in mammals the phagophore is assembled at multiple sites (Johansen and Lamark, 2020). The origins of autophagosomal membrane has been a great debatable question. It has been suggested that the origins of the vesicle's double-membrane could be the endoplasmic reticulum (ER) (Zoppino *et al.*, 2010; Graef *et al.*, 2013), Golgi network (van der Vaart, Griffith and Reggiori, 2010; Ge *et al.*, 2013),

mitochondria (Hailey *et al.*, 2010), plasma membrane (Ravikumar *et al.*, 2010) and recycling endosomes (Longatti *et al.*, 2012; Puri *et al.*, 2013; Carlsson and Simonsen, 2015).

One of the key complexes recruited to PAS for autophagy induction is the Vps34 regulatory complex (also known as class III PtdIns3K complex I), consisting of the lipid kinase Vps34 (class III PI3K), the regulatory kinase Vps15 (p150 in mammals) and Atg6 (Beclin1 in mammals) (Juhász *et al.*, 2008; Simonsen and Tooze, 2009; Das, Shravage and Baehrecke, 2012; Yin, Pascual and Klionsky, 2016). From phosphatidylinositol, Vps34/class III PI3K produces phosphatidylinositol-3-phosphate (PtdIns3P) which is responsible for correct localization of some Atg proteins, including Atg18 and Atg2. The downstream effect of the correct localisation of Atg18 and Atg2 is the recruitment of Atg proteins, Atg8, Atg9 and Atg12 to the PAS (figure 1.5) (Obara *et al.*, 2008; Yin, Pascual and Klionsky, 2016). Studies in mammals have shown that PI3K inhibitors (3-methyladenine) inhibits autophagy, in addition to inhibition of autophagosome formation via mutations in Vps34, emphasising the importance of PI3P involvement in autophagy (Juhász *et al.*, 2008; Simonsen and Tooze, 2009; Wu *et al.*, 2010).

The multi-spanning membrane transporter protein, Atg9, is less well understood however evidence suggests Atg9 plays a role in transporting membrane material to the PAS for the growing phagophore by shuttling, in a Atg1- and Vps34-dependent manner, between early/recycling endosomes and the PAS (Rogov *et al.*, 2014). Studies have revealed that mice lacking Atg9 possess an identical phenotype to mice lacking Atg7, Atg5 or Atg3 (Tooze and Yoshimori, 2010).

1.2.5.2 Autophagosomal membrane protein - Atg8

The autophagy-related 8 (Atg8) protein is an autophagosomal membrane protein. The Atg8 proteins are highly conserved protein families in eukaryotes. There are several Atg8 genes in multicellular mammals, green plants and protists, in contrast to the single Atg8 gene in yeast and other fungal species. In animals, there are three sub-families of Atg8 proteins; 1) microtubule-associated protein 1 light chain 3 (MAP1LC3 or also referred as LC3), 2) γ-amino-butyric acid receptor-associated protein (GABARAP) and 3) Golgi-associated ATPase enhancer of 16 kDa (GATE-16). Mammals have multiple paralogues within the Atg8 family. Specifically, in humans, there are two GABARAP genes (GABARAP and GABARAPL1), four LC3 genes (LC3A, LC3B, LC3B2, LC3C) and a single GATE-16 gene. In *Drosophila melanogaster*, there are two Atg8 genes, ATG8A and ATG8B (Shpilka *et al.*, 2011).

The first molecule found to be necessary for autophagosome formation and discovered to be localised to the autophagosome was Atg8 and since has been the most used marker for autophagy studies. This protein has a unique ubiquitin-like fold and a lipid moiety allowing it to embed itself on both the inner and outer membranes of the autophagosome (Ichimura *et al.*, 2000). The process of Atg8 lipidation is described in the chapter below.

The lipidated Atg8 proteins have a number of functions. The Atg8 proteins in autophagy are involved in regulating the formation and maturation of autophagosomes by membrane scaffolding core autophagy components such as ULK1/2 (Atg1), Atg13, FIP200 (Atg17), Vps34, Beclin1 (Atg6), Atg14 and Atg12-Atg5 to the outer phagophore surface. Secondly, it acts as a scaffold protein for selective autophagy receptors to bind to the inner surface of the growing phagophore (autophagosomal membrane), which carry cellular cargo tagged for autophagosomal degradation

(Johansen and Lamark, 2020). This interaction between Atg8 and selective autophagy receptors is mediated by a short motif called LC3-interacting region (LIR) motif (Birgisdottir, Lamark and Johansen, 2013; Rogov *et al.*, 2014), described in detail later in this chapter. The recruitment of cargo itself is thought to contribute to phagophore expansion by increasing the number of Atg8 proteins at the assembly site. A study in 2008 verified the quantitative correlation between Atg8 protein levels and size of the sequestering autophagosome (Xie, Nair and Klionsky, 2008; Yang and Klionsky, 2009). Additionally, Atg8-PE (lipidated Atg8)(detailed below in sub-chapter 1.2.5.3) also drives the expansion of the autophagosomal membrane and autophagosome completion (Nakatogawa, Ichimura and Ohsumi, 2007; Yang and Klionsky, 2009). Lastly, Atg8 proteins are also fundamental to the autophagosome-lysosome fusion process by recruiting core fusion machinery and auxiliary fusion factors. It also promotes autophagosome trafficking by facilitating autophagosome-microtubule association in order to position the autophagosome in close vicinity to lysosomes. Atg8 proteins also have the ability to tether and deform membranes (figure 1.6). (Kriegenburg, Ungermann and Reggiori, 2018; Johansen and Lamark, 2020).

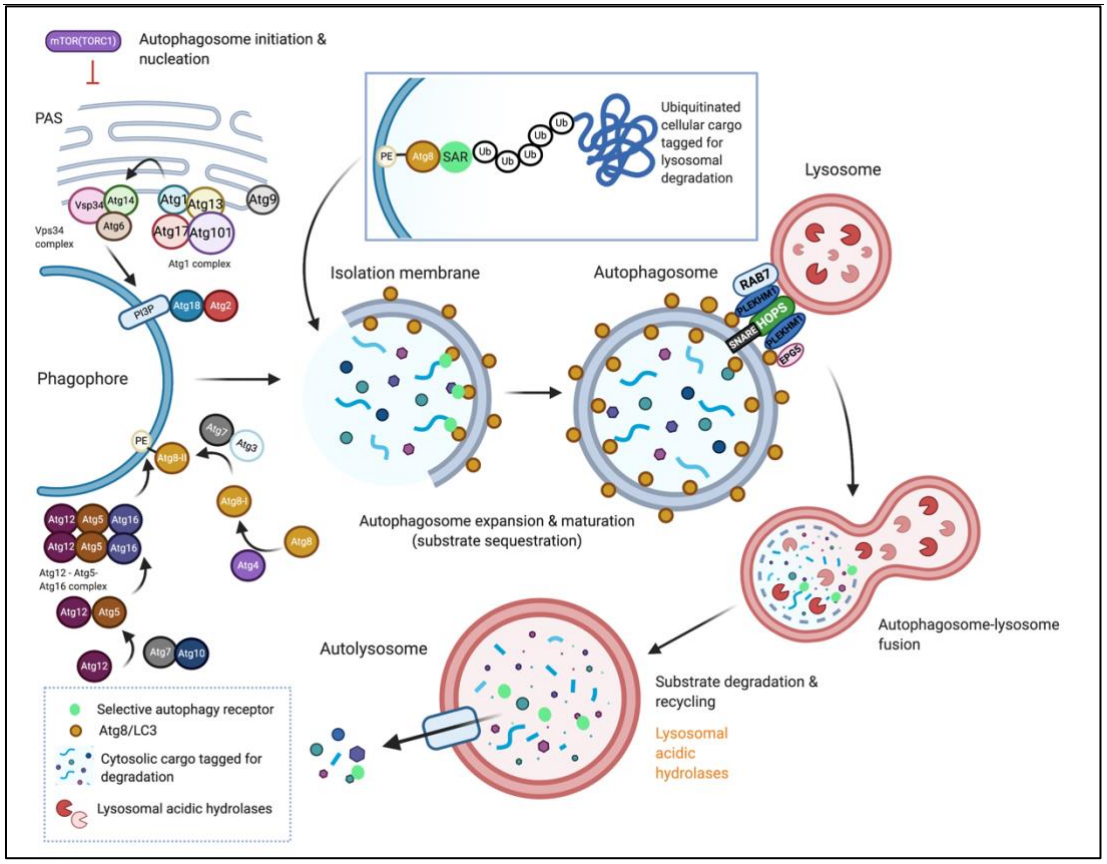

Figure 1.6. Core autophagic mechanism components. Upon mTOR inactivation, Atg1 (ULK1) complex (Atg1, Atg13, Atg17 and Atg101) is activated at the phagophore assembly site. The activated Atg1 complex recruits the class III PI3K (Vsp34, Atg14 and Atg6). The cycling of Atg9 delivers membrane material which in turn causes the Vsp34 complex to initiate PI3P production for the generation of the phagophore, Atg18 and Atg2 forms a complex. Atg8a lipidation process involves cysteine proteases, Atg4, that cleaves Atg8 protein followed by the action of Atg7 (E1) and Atg3 (E2). The final step of the conjugation of Atg8 to PE is mediated by the Atg5:Atg12:Atg16 complex (E3). This complex is formed by action of Atg7 (E1) and Atg10 (E2). The lipidated Atg8 (Atg8-PE) is then localised to the isolation membrane. Selective autophagy receptors, tagged to ubiquitinated cellular cargo destined for degradation, traffic the cargo to the phagophore where it binds to Atg8a-PE. The phagophore membrane elongates and the double membrane autophagosome matures. The autophagosome recruits tethering & docking proteins, HOPS, PLEKM1 etc for fusion with the lysosome to form autolysosomes in which degradation of the cargo occurs. The broken-down cellular components are then recycled back into the cytosol (Created by BioRender.com).

1.2.5.3 Autophagosome expansion, maturation and fusion

The expansion of the phagophore and the subsequent formation of the double-membraned vesicle autophagosome is a characteristic feature of autophagy. There are two ubiquitin-like (Ubl) conjugation systems which are fundamental to phagophore expansion; Ubl proteins Atg12 and Atg8. These two Atg proteins are known as ubiquitin-like proteins because they are structurally similar to ubiquitin, however they

are not homologs (Yin, Pascual and Klionsky, 2016). Atg12 is associated with Atg5 and Atg16, where it conjugates to Atg5 via E1 enzyme Atg7 and E2 enzyme Atg10. The Atg12:Atg5 then binds to Atg16 forming the dimeric Atg12:Atg5:Atg16 complex (Ohsumi, 2001; Kuma *et al.*, 2002). Atg8 covalently conjugates to lipid phosphatidylethanolamine (PE) and is mediated by Atg4, a cysteine protease that cleaves the c-terminal arginine of Atg8 leaving the glycine residue at the c-terminus. The conjugation of Atg8 to PE is then mediated via an amide bond linking the c-terminal glycine and an amino group of PE (Ichimura *et al.*, 2000). This lipidation of Atg8 is facilitated by a ubiquitination-like system in which Atg7 acts as an E1 enzyme and Atg3 acts as an E2 enzyme. In addition, the Atg12-Atg5-Atg16 complex participates as an E3 enzyme (Ichimura *et al.*, 2000; Das, Shravage and Baehrecke, 2012). The Atg8-PE is key for both the phagophore and the autophagosome, however, the Atg12-Atg5-Atg16 complex is solely associated with the phagophore and detaches on autophagosome formation (Das, Shravage and Baehrecke, 2012).

The completing step of the autophagic pathway, upon completion of the autophagosome, is the fusion of the autophagosome with the lysosome to form an autolysosome. The fusion is executed by SNARE (soluble N-ethylmaleimide-sensitive factor attachment protein receptor) proteins and a number of tethering proteins and complexes, primarily HOPS (homotypic fusion and vacuole protein sorting) complex (Jiang *et al.*, 2014), PLEKHM1 (McEwan *et al.*, 2015) and EPG5 (Wang *et al.*, 2016). In *Drosophila*, the SNARE complex, STX17-ubisnap-VAMP7/VAMP8 (STX17-SNAP29-VAMP7/VAMP8 in mammals) (Mulakkal *et al.*, 2014), is involved in the fusion and the formation of these complexes is mediated by tethering proteins that bridge the two vesicles closely. The tethering proteins, HOPS complex, PLEKHM1 and EPG5 simultaneously interact with both autophagosomal

membrane and lysosomal membrane proteins to mediate autophagosome-lysosome fusion. The HOPS complex interacts with Arl8 on the lysosomal membrane and with Qa-SNARE STX17 on the autophagosomal membrane. PLEKHM1 interacts with Arl8b GTP (small GTPase) and Rab7 GTP on the lysosomal membrane as well as Atg8 on the autophagosomal membrane. Lastly, EPG5 also binds to Rab7 GTP and Atg8 (Yim and Mizushima, 2020).

Following fusion of the autophagosome to the lysosome, the cargo is degraded within the autolysosome by the activity of acidic lysosomal hydrolases, e.g. cathepsins. The degraded material are recycled as macromolecules back into the cytosol for re-use in cellular pathways (Mulakkal *et al.*, 2014). Thus, the autophagic flux (rate of autophagy) is dependent on two events; 1) the number of formed autophagosomes, 2) the degradative capacity of lysosomes and resulting turnover of degraded cargo within the cell (Das, Shravage and Baehrecke, 2012).

1.2.5.4 Nitrogen-dependent regulation

Activation of autophagy via glucose or amino-acid deprivation was identified long before the discovery of Atg genes (Mortimore and Schworer, 1977). The conserved serine/threonine kinase, TOR or the mammalian homolog mTOR (mammalian/mechanistic target of rapamycin), is the chief sensor of nitrogen and amino acid change. TOR negatively regulates autophagy. Stimuli such as nutrient levels, energy status, growth factors and amino acids can activate TORC1. For example, in nutrient-rich conditions, Atg13, Atg1 and Atg14 can be directly phosphorylated by TORC1. As a result of the phosphorylation, the formation and/or activation of the Atg1-Atg13-Atg17-Atg31-Atg29 complex is prevented,

consequently suppressing autophagy-specific class III phosphatidylinositol 3-kinase (PtdIns3K) activity leading to autophagy induction being inhibited (Kamada *et al.*, 2010; Yuan *et al*., 2013). Moreover, in mammals, downstream effects of mTORC1 inactivation results in transcription of autophagy genes involved in degradation (Yin *et al.*, 2016).

1.2.5.5 Energy/glucose-dependent regulation

Autophagy can be regulated also by glucose metabolism and energy level, which is key for cellular homeostasis. In the presence of glucose, the activated PKA phosphorylates Atg1 and Atg13. This phosphorylation hinders Atg13 localisation to the phagophore assembly site (PAS). Furthermore, autophagy can be inhibited by PKA by the direct phosphorylation of TORC1 or by indirect activation of mTORC1 in mammals via AMPK inhibition. Moreover, just like nitrogen deprivation, Atg gene transcription by deacetylation of transcription factors can also be activated by glucose starvation (Yin *et al.*, 2016).

Other types of stimuli that are inducers of autophagy are ER stress, hypoxia, depletion of iron and absence of growth factors. To further investigate regulators of autophagy and the roles of specific Atg proteins in the regulation of autophagy, the focus has primarily diverted to screening and analysing transcription factors which are involved in autophagy regulation (Yin *et al.*, 2016).

1.2.6 Selective autophagy receptors

Selective autophagy receptors (SARs) are receptors that are able to recognise cargo tagged for autophagosomal degradation. Most SARs have two common features; 1) a ubiquitin-binding domain, allowing the receptor to bind to polyubiquitinated cargo and 2) LC3-interacting region (LIR – described below), allowing the receptor to bind to Atg8 proteins on the autophagosomal membrane.

Ubiquitin is a highly conserved precursor protein from yeast to mammals, that possess a tightly folded globular structure and is 76 amino acids long. When ubiquitin is synthesised and subjected to proteolytic maturation, its c-terminal Gly residue is exposed, allowing conjugation to a Lys of another ubiquitin molecule or substrate protein. Following a cascade of enzymatic reactions that involves E1 enzyme for activating, E2 enzyme for conjugating and E3 enzyme for ligating, ubiquitin conjugates consisting of either mono-ubiquitin or poly-ubiquitin chains that are generated. Ubiquitin is a multi-functional protein and one of its key roles involved targeting proteins for degradation (Rogov *et al.*, 2014).

The first genuine SAR to be discovered was the human p62/SQSTM1 (sequestosome-1) (Ref(2)P in *Drosophila*) (Pankiv *et al.*, 2007; Johansen and Lamark, 2020) and is one of the most common SAR involved in a number of selective autophagic pathways including aggrephagy, pexophagy, zymophagy, mitophagy and xenophagy (Rogov *et al.*, 2014). It has been highly documented that p62/SQSTM1 protein functions to recognise polyubiquitinated proteins (tagged for autophagosomal degradation) and transports these to the growing phagophore via the interaction with Atg8 proteins (Yang and Klionsky, 2009). It has been shown that p62 accumulates in multiple protein aggregation diseases such as Alzheimer's disease, Parkinson's

disease, Pick's disease and multiple system atrophy (Zatloukal *et al.*, 2002; Birgisdottir, Lamark and Johansen, 2013). Studies have revealed that as well as being a SAR for ubiquitinated protein aggregates, it is also a selective autophagy substrate (Pankiv *et al.*, 2007; Birgisdottir, Lamark and Johansen, 2013). A study in 2007 documented in knockout of autophagy in mice liver that p62 regulated protein aggregation formation and was removed by autophagy. The study revealed when autophagy was blocked, there was a failure to degrade p62 resulting in an accumulation of protein aggregates and liver dysfunction (Komatsu *et al.*, 2007; Birgisdottir, Lamark and Johansen, 2013).

As mentioned previously, the interaction between Atg8 and selective autophagy receptors is mediated by a short motif called LC3-interacting region (LIR) motif (Birgisdottir, Lamark and Johansen, 2013; Rogov *et al.*, 2014). Table 1.3 lists all the selective autophagic pathways with its respective selective autophagy receptors and substrates.

Table 1.3. Selective autophagy receptors. List of selective autophagy pathways with its respective selective autophagy receptors. Table adapted from Johansen and Lamark, 2020.

Selective autophagy	Year identified	Substrate	Selective autophagy receptor (SAR)	Reference
Aggrephagy	2007	Protein aggregates	p62 (Ref(2)P), NBR1, OPTN, Cue5, TOLLIP	(Pankiv *et al.*, 2007; Overbye *et al.*, 2007; Kirkin *et al.*, 2009; Lamark and Johansen, 2012; Korac *et al.*, 2013; Lu, Psakhye and Jentsch, 2014)
Chlorophagy	2009	Chloroplasts	ATI-1 ATI-2	(Seay *et al.*, 2009; Zhuang and Jiang, 2019; Stephani and Dagdas, 2020)
ERphagy	2007	ER	FAM134B (Atg40), SEC62, RTN3, CCPG1, ATL3, TEX264	(Bernales, Schuck and Walter, 2007; Khaminets *et al.*, 2015; Mochida *et al.*, 2015; Fumagalli *et al.*, 2016; Grumati *et al.*, 2017; Smith *et al.*, 2018; Chen *et al.*, 2019; Chino *et al.*, 2019)
Ferritinophagy	2014	Ferritin	NCO4A	(Mancias *et al.*, 2014; Masaldan *et al.*, 2018)
Glycophagy	2011	Glycogen	Stbd1	(Jiang, Wells and Roach, 2011; Zhao *et al.*, 2018)
Lipophagy	2009	Lipid droplets	ATGL, p62, NBR1	(Singh *et al.*, 2009) (Singh *et al.*, 2009;

				Schulze *et al.*, 2017)
Lysophagy	2013	Lysosome	TRIM16, NDP52, Galectin-8	(Thurston *et al.*, 2012; Hung, Chen and Yang, 2013; Maejima *et al.*, 2013; Chauhan *et al.*, 2016; Papadopoulos, Kravic and Meyer, 2020)
Midbody autophagy	2009	Midbody rings	p62, NBR1, TRIM17	(Pohl and Jentsch, 2009; Mandell *et al.*, 2017)
Myelinophagy	2015	Myelin	-	(Gomez-Sanchez *et al.*, 2015; Thumm and Simons, 2015)
Nuclear lamina autophagy		Nuclear lamina	Lamin B1	(Dou *et al.*, 2015)
Nucleophagy	2009	Nuclear envelope	Atg39	(Park *et al.*, 2009; Mochida *et al.*, 2015; Papandreou and Tavernarakis, 2019)
Proteaphagy	2015	Proteasomes	RPN10	(Bartel, 2015; Marshall *et al.*, 2015)
Ribophagy	2008	Ribosomes	NUFIP1	(Kraft *et al.*, 2008; Denton and Kumar, 2018; Wyant *et al.*, 2018)
Ub-dependent Mitophagy	1998	Mitochondria	NDP52, OPTN, p62, TAX1BP1, AMBRA1	(Scott and Klionsky, 1998; Heo *et al.*, 2015; Lazarou *et al.*, 2015; Strappazzon *et al.*, 2015)
Ub-independent Mitophagy	1998	Mitochondria	NIX, BNIP3, FUNDC1,	(Scott and Klionsky,

			BcI2L13 (Atg32), FKBP8, PHB2, NLRx1, AMBRA1, cardiolipin, ceramide	1998; Novak *et al.*, 2010; Hanna *et al.*, 2012; Liu *et al.*, 2012; Sentelle *et al.*, 2012; Chu *et al.*, 2013; Murakawa *et al.*, 2015; Strappazzon *et al.*, 2015; Bhujabal *et al.*, 2017; Wei *et al.*, 2017; Zhang *et al.*, 2019)
Pexophagy	1998	Peroxisome	NBR1, p62, Atg30, Atg36	(Scott and Klionsky, 1998; Farre *et al.*, 2008; Motley, Nuttall and Hettema, 2012; Deosaran *et al.*, 2013; Cho *et al.*, 2018)
Virophagy	2016	Viral capsids	TRIM5α, p62	(Orvedahl *et al.*, 2010; Dong and Levine, 2013; Mandell *et al.*, 2014; Sumpter Jr *et al.*, 2016)
Xenophagy	2004	Bacteria	NDP52, p62, OPTN, TAX1BP1, Galectin-8	(Nakagawa *et al.*, 2004; Thurston *et al.*, 2009; Zheng *et al.*, 2009; Dikic *et al.*, 2011; Tumbarello *et al.*, 2015; Sharma *et al.*, 2018)
Zymophagy	2011	Secretory granule	p62	(Grasso *et al.*, 2011)

1.2.6.1 Lipophagy

Lipophagy is the term used to describe lipid droplet (LD) (lipid stores) degradation via lysosomes. Lipids are stored in the form of lipid droplets in all cells under nutrient sufficient conditions. During times when nutrients are scarce, lipid droplets are rapidly depleted for cellular energy (Ward *et al.*, 2016). Lipid droplets consists of triglycerides, cholesteryl esters and LD coat proteins perilipins (PLINs) (Kimmel *et al.*, 2010).

There are also three forms of lipophagy similar to autophagy, macrolipophagy, microlipophagy and chaperone-mediated lipophagy. The exact mechanistic details of lipophagy is still yet unknown. The first stage of lipid droplet degradation involves chaperone-mediated autophagic degradation of PLINs (perilipins-LD coat proteins). The HSC70 protein recognises and binds to the LD coat proteins PLIN2 and PLIN3, directing the proteins to the LAMP-2A receptor on the lysosomal membrane. The subsequent translocation of the LD coat proteins results in the breakdown of these proteins. The removal of the LD coat proteins from the LD surface permits access of cytosolic lipases such as ATGL (which hydrolyses the LD triglycerides) for lipolysis and the autophagic machinery to proceed with macro- and macrolipophagy. The degraded building blocks are largely free fatty acids (FFAs) that are recycled towards the oxidative pathway (Ward *et al.*, 2016).

In macrolipophagy, small lipid droplets and/or small portions of lipid droplets are engulfed by the Atg8/LC3 positive phagophore. The phagophore elongates and forms the double membrane autophagosome (with the engulfed LD). The mature autophagosome then fuses with the lysosomes allowing the acidic hydrolases to break down the lipid droplets to fatty acids (Ward *et al.*, 2016). Macrolipophagy was first

studied in mouse starvation models. The studies have shown evidence of autophagosome and lysosome marker proteins to co-localise with lipid droplets under starvation conditions (Singh *et al.*, 2009; Garcia, Vevea and Pon, 2018). (Schulze, Sathyanarayan and Mashek, 2017).

Microlipophagy is the direct engulfment of portions of the lipid droplet by the lysosome via membrane invaginations. These portions of the lipid droplets are internally broken down by lysosomal acidic hydrolases (Schulze, Sathyanarayan and Mashek, 2017).

In recent years, scientific evidence has shown that lipid droplets are essential for the regulation of autophagosome biogenesis. Studies by Shpilka and Elazar in 2015 discovered that both lipid droplet biogenesis and lipolysis are vital processes for autophagosome biogenesis, and in particular suggesting the importance of membrane flow from endoplasmic reticulum (ER) to LDs and vice versa for autophagosome biogenesis (Shpilka and Elazar, 2015).

1.2.7 LIR motif

The first discovery of the LC3-interacting region (LIR) motif of p62 and the Cvt cargo receptor Atg19 was by Terje Johansen in 2007 by a number of techniques including deletion mapping, point mutation analyses and X-ray crystallography (Pankiv *et al.*, 2007). The peptides of mammalian p62 and yeast Atg19 bound to LC3B and Atg8 respectively, revealed a common **W-x-x-L** motif, where x is represented as any amino acid (figure 1.7) (Ichimura *et al.*, 2008; Noda *et al.*, 2008; Birgisdottir, Lamark and Johansen, 2013). There are many other names for the motif, such as LC3-recognising sequence (LRS) and Atg8 interacting motif (AIM). Following the discovery of the

LIR motif in p62, a core consensus tetrapeptide LIR sequence, **[W/F/Y]XX[L/I/V]** was identified from 42 verified LIR motifs, with most LIR motifs possessing a W or an F at the aromatic position, and very few have Y (Birgisdottir, Lamark and Johansen, 2013). In this short LIR sequence, the 'x' represents any amino acid residue. The square brackets enclose certain residues which may occupy the single position. In the later years, Noda and colleagues further defined the LIR motif as **X_{-3} X_{-2} X_{-1}[W/F/Y]X_1X_2 [L/I/V]** (Noda, Ohsumi and Inagaki, 2010; Kalvari *et al.*, 2014). In 2014, Kalvari and colleagues (Nezis Lab) published a study in which they developed the iLIR database, a web based in silico tool allowing the identification of LIR motifs and hence novel LIR containing proteins (LIRCPs). During the development of the iLIR database, the group kept the six residue positions of the LIR motifs with position three occupied by the conserved [W/F/Y] aromatic residues and position occupied by [ILV] aliphatic residues, which was in line with the defined canonical LIR motif (Alemu *et al.*, 2012; Kalvari *et al.*, 2014). The resulting motif was termed xLIR motif (and also 'relaxed') which has the following expression; **[ADEFGLPRSK] [DEGMSTV] [WFY] [DEILQTV] [ADEFHIKLMPSTV] [ILV]** (Kalvari *et al.*, 2014).

The Atg8/LC3 sequence contains a C-terminal, core Ubl domain where the conserved 'ubiquitin fold' is located and an N-terminal arm that contains two α-helices closed onto the Ubl domain. The N-terminal and Ubl domain interface is where the LIR-containing peptide is situated, forming the site where the LIR motif binds and is labelled as the LIR docking site (LDS). The LDS possess a crevice shape that consists of two hydrophobic pockets HP1 and HP2 in the Ubl domain which interacts with the side chains of the [W/F/Y] and [L/I/V] residues of the LIR motif (figure 1.7) (Birgisdottir, Lamark and Johansen, 2013; Johansen and Lamark, 2020). Studies have

shown that LIR motifs bind to the LDS as an extended β-sheet (Noda, Ohsumi and Inagaki, 2010; Birgisdottir, Lamark and Johansen, 2013; Wild, McEwan and Dikic, 2014; Johansen and Lamark, 2020).

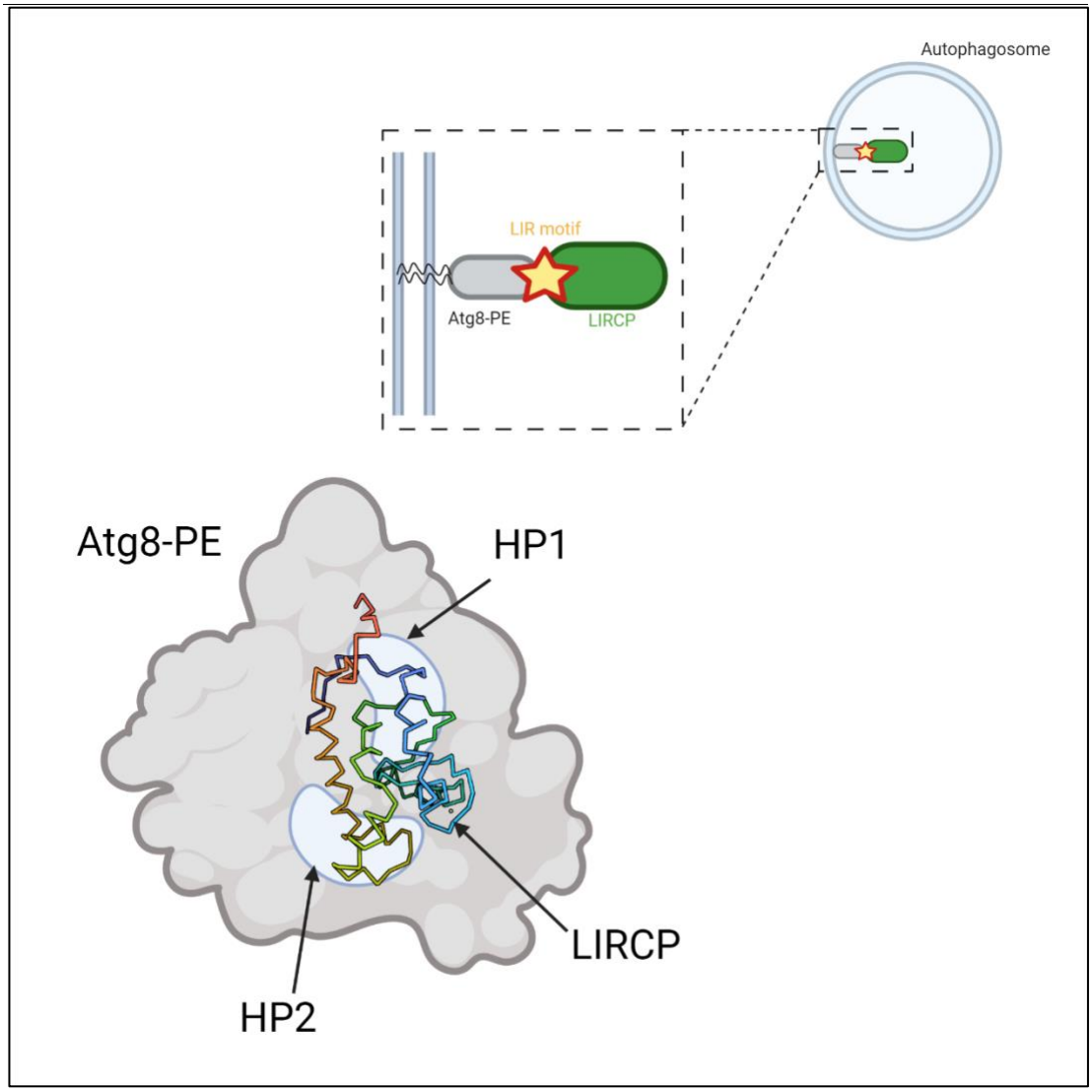

Figure 1.7. LIR-LDS interaction. Schematic overview of the interaction between Atg8 and LIR containing proteins (LIRCP) via the LIR motif. An example of LIR-LDS interaction showing Atg8-PE interacting with a LIR containing protein. The side chain of position 3 in LIR motif interacts with hydrophobic pocket 1 (HP1) and side chain of position 6 interacts with hydrophobic pocket 2 (HP2) (Created with BioRender.com).

Proteins can interact with Atg8 proteins in a LIR-independent manner too. In *C. elegans*, LIR motifs do not exist in autophagy receptors (Birgisdottir, Lamark and Johansen, 2013) and studies have shown that many proteins identified to interact with Atg8 are not affected by a mutated LIR docking site, the site at which the LIR motif of Atg8-interacting protein binds to the Atg8 (Behrends *et al.*, 2010; Birgisdottir, Lamark and Johansen, 2013). LIR-motif-mediated interactions have been shown to also be involved in autophagosome formation and maturation regulation, since

functional LIR motifs have also been identified in components of the core autophagic machinery, proposing that not all LIR-containing proteins act as SARs (Birgisdottir, Lamark and Johansen, 2013). For example, studies show evidence of a LIR-dependent interaction between Atg1 and Atg8, and that this interaction is also conserved and maintained in mammals as they found that ULK1 also interacted with autophagosomes in a LIR-dependent manner (Kraft *et al.*, 2012; Birgisdottir, Lamark and Johansen, 2013). Other autophagic machinery components that also possess functional LIR motifs include mammalian Atg13, FIP200, Atg4B (Atg13, Atg17 and Atg4B in *Drosophila* respectively) (Birgisdottir, Lamark and Johansen, 2013).

A number of techniques can be used to identify LIR-dependent Atg8-interacting proteins, bioinformatics searches, proteomics, phage display and yeast two-hybrid to name a few. Identification of LIR motifs have been possible using strategies such as deletion mapping, protein-protein interaction assays and testing deletion and point-mutated constructs (Birgisdottir, Lamark and Johansen, 2013).

1.2.8 Autophagy in ageing and age-related diseases

Basal level of autophagy is essential for quality control in the cell as it is vital for homeostasis. Evidence from previous genetic studies show that defects in basal autophagy are linked to disease conditions such as neurodegenerative diseases, cancer and inflammation. For example, knockout of Atg5 in mice neural cells revealed an accumulation of abnormal proteins and phenotypes of defects in motor function (Hara *et al.*, 2006; Yin, Pascual and Klionsky, 2016). Such findings further support the notion that autophagy functions as ‘house-keeper’ process in the cell. Not only is the accumulation of misfolded and damaged proteins and defective organelles a sign of

ageing, but it also is the cause of ageing. It is evident that the removal of such protein aggregates and dysfunctional organelles helps to ameliorate cellular function, avoid cell death, resulting in extended lifespan (Terman, Gustafsson and Brunk, 2007; Yin, Pascual and Klionsky, 2016). In a simple model, dysfunctional autophagy is associated with cellular degeneration and premature ageing, however on the other hand when autophagy levels are augmented at the whole-body level in different model organisms, it promotes longevity (Rubinsztein, Mariño and Kroemer, 2011; Yin, Pascual and Klionsky, 2016). Despite the fact that the specific mechanism by which autophagy contributes to anti-ageing is still yet unknown, the regulation of autophagy is said to be a promising target of enhancing healthy aging (Yin, Pascual and Klionsky, 2016).

1.2.8.1 Age-related factors and autophagy

Reactive oxygen species (ROS) including free radicals, hydrogen peroxide and hydroxyl radicals is primarily generated in the mitochondria by the electron transport chain (ETC). Excessive ROS causes oxidative stress, damaging cells, proteins, DNA and organelles, which can contribute to cellular ageing (Finkel and Holbrook, 2000; Balaban *et al*, 2005; Chen *et al*, 2009; Indo *et al*, 2015; Cheon *et al*, 2019). Under normal physiological conditions, there is interplay of autophagy and the redox response; autophagy can be induced by ROS and autophagy can regulate ROS levels in cells, reducing their toxic effects and decreasing oxidative damage (Li *et al*, 2013; Cheon *et al*, 2019). Under starvation conditions, autophagy can be induced by ROS-induced activation of AMPK (Li *et al*, 2013). When ROS production is blocked, the activation of AMPK is reduced and mTOR pathway activation is increased which in

turn leads to reduction of starvation-induced autophagy (Li *et al*, 2013). Cells are protected against excessive ROS by antioxidant enzymes such as glutathione (GSH), superoxide dismutase (SOD), peroxidase (GPX) and catalase (CAT), however antioxidant enzyme function is disrupted by cellular aging (Balaban *et al*, 2005, Finkel and Holbrook, 2000). The peroxisome proliferator-activated receptor gamma coactivator 1-alpha (PGC-1a) modulates antioxidant genes in response to oxidative stress downstream of AMPK. Hence, cells that undergo decreased AMPK activity resulting in mitochondrial ROS levels to increase, experience premature aging (Rabinovitch *et al*, 2017; Cheon *et al*, 2019). As cells age, the mitochondria undergo morphological and functional changes as there is a decline in mitochondrial inner membrane function, ETC function and mitochondrial integrity. This in turn leads to cellular energy deficiency and impairment of normal cellular activity (Shigenaga *et al*, 1994). The clearance of damaged mitochondria is mediated by autophagy (mitophagy). Hence any, disruptions in the autophagic process results in accumulation of damaged mitochondria and oxidative stress, contributing to cellular ageing (Graef and Nunnari, 2011; Lee *et al*, 2012; Hansen *et al*, 2018; Cheon *et al*, 2019).

DNA damage, caused by ultraviolet (UV) light and toxins or even ROS, is associated with cellular dysfunction (Cheon *et al*, 2019). Mitochondrial DNA (mtDNA) is more susceptible to damage by ROS than nuclear DNA (Maynard *et al*, 2009). Mutations within the mtDNA has been shown to accumulate with ageing and deletions in mtDNA have been shown to be more frequent in ageing brain (Kauppila *et al*, 2016; Cheon *et al*, 2019). A decline in DNA repair resulting in accumulation of DNA damage contributes to cellular senescence. Senescent cells accumulate during ageing. In addition, compromised DNA repair causing mutations in nuclear and mitochondrial genes has been associated with ageing. All in all, defects in the DNA

repair system have been implicated in ageing. Studies have shown *in vitro* increased double strand breaks in DNA and ineffective non-homologous end joining in senescent cells (Seluanov *et al*, 2004). Studies have reported a close association of DNA repair to autophagy. The selective autophagy receptor, p62, is involved in the regulation of DNA repair systems through the recruitment of DNA repair proteins (BRCA1, Rad51, RAP80) in a p62 dependent manner (Cheon *et al*, 2019). Hence studies have shown p62 accumulation, through loss of autophagy, disrupts DNA damage responses (Wang *et al*, 2016). Moreover, under autophagy deficiency conditions, the recruitment of DNA repair proteins by p62 to double strand breaks is compromised (Wang *et al*, 2016; Cheon *et al*, 2019).

Telomeres are repeated DNA sequences at the end of linear chromosomes consisting of six base pairs, TTAGGG (Cheon *et al*, 2019). Telomeres function during DNA replication to protect genetic information and protect ends of chromosomes against damage, hence promoting genetic stability (Henriques and Ferreira, 2012; Eitan *et al*, 2014). The lengths of telomeres are regulated by a telomerase, which consists of two components: telomerase RNA competent (TERC) and telomerase reverse transcriptase (TERT) (Cheon *et al*, 2019). As cells age, telomerase activity functionally declines in most somatic cells. On the contrary, telomerase activity is sustained in germ cells and cancer cells. Lack of telomerase activity causes telomeres to progressively shorten with cell division and DNA replication. The inability of the DNA repair machinery to restore telomeres leads to cell senescence and ageing (Henriques and Ferreira, 2012; Eitan *et al*, 2014; Boccardi *et al*, 2015). Studies have shown disrupted telomere function, increased genetic stability and a higher prevalence of cancer in aged mice with telomere deficiency (Rudolph *et al*, 1999). It has been reported through previous studies the association between telomere biology and

autophagy (Aoki *et al*, 2007; Ali *et al*, 2016; Nassour *et al*, 2019). Studies found increased levels of autophagy related proteins and cytoplasmic vacuoles in stressed cells associated with deprotected telomeres (Nassour *et al*, 2019). Most interestingly, TERT induces autophagy through binding to and subsequent suppression of mTORC1 kinase. Studies revealed knockdown of TERT leads to disrupted autophagy under basal and starvation conditions by increasing mTORC1 activity (Ali *et al*, 2016; Cheon *et al*, 2019).

The immune system normally eliminates senescent cells. The immune system, however, deteriorates with ageing resulting in weakened tissue homeostasis due to accumulated senescent cells (Sun *et al*, 2018). Senescent cells, through a process called senescence-associated secretory phenotype (SASP), releases pro-inflammatory factors, proteases, chemokines, macrophage inflammatory proteins and growth factors (Munoz-Espin and Serrano, 2014; Childs *et al*, 2015; Sun *et al*, 2018), allowing immune cells to be migrated and recruited to influence tissue repair. Persistent release of these SASP factors by senescent cells can cause chronic inflammation and tissue dysfunction (Freund *et al*, 2010). With ageing, SASP activity increases (Kiecolt-Glaser *et al*, 2003; Cheon *et al*, 2019). It has been shown for example, the inflammatory cytokine TNF-α and pro-inflammatory factor IL-8 are overexpressed with age (Kiecolt-Glaser *et al*, 2003; Tsukamoto *et al*, 2015; Ong *et al*, 2018). Most interestingly, studies have reported the interaction of the autophagic machinery with the immune system and controls inflammation, further showing the association of impaired autophagy with various inflammatory diseases (Levine *et al*, 2011; Deretic *et al*, 2013). Previous studies have observed reduced SASP secretion via mTORC1 by rapamycin, which is a mTOR inhibitor and autophagy inducer (Laberge *et al*, 2015). Other studies have stated a delay in SASP secreted products (IL-6 and IL-8) when

ATG5 and ATG7 are knockdown (Young *et al*, 2009). All in all, these findings indicate an essential role of autophagy in SASP which in turn is associated with ageing (Cheon *et al*, 2019).

1.2.8.2 Age-related diseases and autophagy

Accumulations of misfolded amyloid beta (Aβ) and neurofibrillary tangles (tau phosphorylation) can advance cell function damage and homeostasis impairment. It has been observed in studies using animal models to study Alzheimer's disease (AD), the protective effects of autophagy against accumulations of misfolded amyloid beta and neurofibrillary tangles (Frake *et al*, 2015). Dysfunctional autophagy in AD animal models can increase intracellular Aβ and neurofibrillary tangles (Frake *et al*, 2015). Studies have reported impairment of autophagosome clearance in AD due to noticeable accumulation of autophagosomes (Nixon, 2007). Other studies in post-mortem brains of AD have detected an increase in hyperactivated mTOR levels (An *et al*, 2003; Hung *et al*, 2009; Ihara *et al*, 2012). Additionally, in an AD model, dysfunctional autophagy can heighten cognitive impairment (Nilsson *et al*, 2013). On the contrary, when autophagy is reinforced, AD-related signs are reduced in AD animal models. For example, studies showed a decrease in Aβ deposition with rapamycin treatment, extending longevity in AD models (Rubinsztein *et al*, 2011; Frake *et al*, 2015; Singh *et al*, 2017).

Moreover, it has been suggested that age associated SASP and oxidative stress may contribute to AD pathology (Yao *et al*, 2004; Alcolea *et al*, 2015). Studies in AD models highlight reactive microglia closely located to Aβ plaques (Wang *et al*, 2015; Heckmann *et al*, 2019). Since proinflammatory cytokines are released by reactive

microglia, studies have displayed increased levels of specific cytokines in AD patients (TNF-α, IL-1β, IL-6, IL-12 and IL-18), indicating close association of the immune system to AD pathology and symptoms (Swardfager *et al*, 2010). There are close associations between oxidative stress and Aβ (Hensley *et al*, 1994). Oxidative stress can be caused by Aβ (Hensley *et al*, 1994) and it can also stimulate Aβ deposition (Misonou *et al*, 2000; Drake *et al*, 2003).

Genetic mutations in several genes can cause Parkinson's disease (PD) (LRRK2, SNCA, DJ-1, PRKN, PINK1) and these genes have close associations to autophagy, including mitophagy. Dysfunctional autophagy has been a key driver of pathology in PD (Alegre-Abarrategui *et al*, 2009; Lopes da Fonseca and Outeiro, 2014; Menzies *et al*, 2017). A key PD characteristic with impaired autophagy are Lewy bodies consisting of accumulated alpha-synuclein (Volpicelli *et al*, 2014). It has been reported that overexpression of α-synuclein leads to ATG9 mislocation resulting in dysfunctional macroautophagy (Winslow *et al*, 2010). The degradation of damaged mitochondria by autophagy is mediated by the recruitment of Parkin to the mitochondria by PINK1. Hence, mutations in PINK1 and Parkin disrupts this function (Vives-Bauza *et al*, 2010). It has been reported in PD patients impaired DNA repair system (Sepe *et al*, 2016; Cheon *et al*, 2019). Studies in mice have revealed that mutations of the key factor (ERCC1) in the nucleotide excision repair (NER) pathway can result in augmented dopaminergic neuron injury, loss of dopaminergic neurons in the striatum, DNA damage, accumulated α-synuclein and abnormal mitochondria (Sepe *et al*, 2016). Additional studies have shown a decline in autophagy and augmented cellular senescence in ERCC1-mutated mice. When these mice are treated with rapamycin, autophagy is enhanced and cellular senescence is reduced (Takayama *et al*, 2017; Cheon *et al*, 2019).

Amyotrophic lateral sclerosis (ALS) is a disease characterised by motor neuron loss within the CNS and degeneration of neuromuscular junctions. Familial forms of ALS is caused by mutations of genes such as SOD1, p62, C9ORF72 and TDP-43 to name a few (Renton *et al*, 2014; Menzies *et al*, 2017). Many of these ALS genes are involved in autophagy and lysosomal function (Menzies *et al*, 2017). For example, when p62 is mutated, it is no longer able to recognise LC3B and hence not recruited to the phagophore (Goode *et al*, 2016). The removal of TDP-43 is mediated by autophagy and the ubiquitin-proteasome system (UPS). Abnormal cytoplasmic accumulation of TDP-43 is observed in ALS tissues which could not be degraded by autophagy or UPS (Scotter *et al*, 2014). Motor function is improved, and accumulations of TDP-43 is reduced in TDP-43 Tg mice brain when treated with autophagy inducers such as rapamycin, spermidine, carbamazepine and tamoxifen (Wang *et al*, 2012). Interestingly, deletion of C9ORF72 gene results in impaired autophagy and endocytosis as C9ORF72 has a fundamental role in mediating endosomal trafficking for endosomal transport and autophagy (Farg *et al*, 2014; Cheon *et al*, 2019).

Overall, the above findings confirm the possible associations of dysfunctional autophagy and factors of cellular aging and that this interplay may advance age-related pathology and diseases. Impaired autophagy may contribute to the toxicity of accumulated disease proteins and hence contribute to AD, PD and ALS (Cheon *et al*, 2019). Targeted therapeutic approaches to enhance autophagy has been reported in various animal models to ameliorate diseases associated with toxicity of aggregate-prone proteins (Menzies *et al*, 2017; Siddiqi *et al*, 2019). Thus, pharmacological or genetic tools that function to modulate autophagy may be promising clinical interventions to combat age-related diseases (Cheon *et al*, 2019).

1.3 Interplay between autophagy and endosomal trafficking

Autophagy is closely related to endocytosis at the stage of endosomal trafficking from early endosomes to lysosomes. Endocytosis is the importing of nutrients and macromolecules from outside of the cell into the cell. The process acts as a companion route to autophagy. Both autophagy and endocytosis have converging steps and common participating molecules (figure 1.8) (Hyttinen *et al.*, 2013). In endocytosis, the early endosome is attached to Rab5 on its surface. The early endosome matures to the late endosome and Rab5 is replaced with Rab7. Rab7 is a common participating molecule in both autophagy and endocytosis as Rab7 is also located on the autophagosomal outer membrane. Just like the autophagosome, the late endosome also fuses with the lysosome leading to degradation of cellular material. During endocytosis and autophagy, the fusion of the late endosome (sometimes also early endosome) with late autophagosome can also occur, forming an amphisomes, which later fuses with lysosomes for complete degradation (Hyttinen *et al.*, 2013).

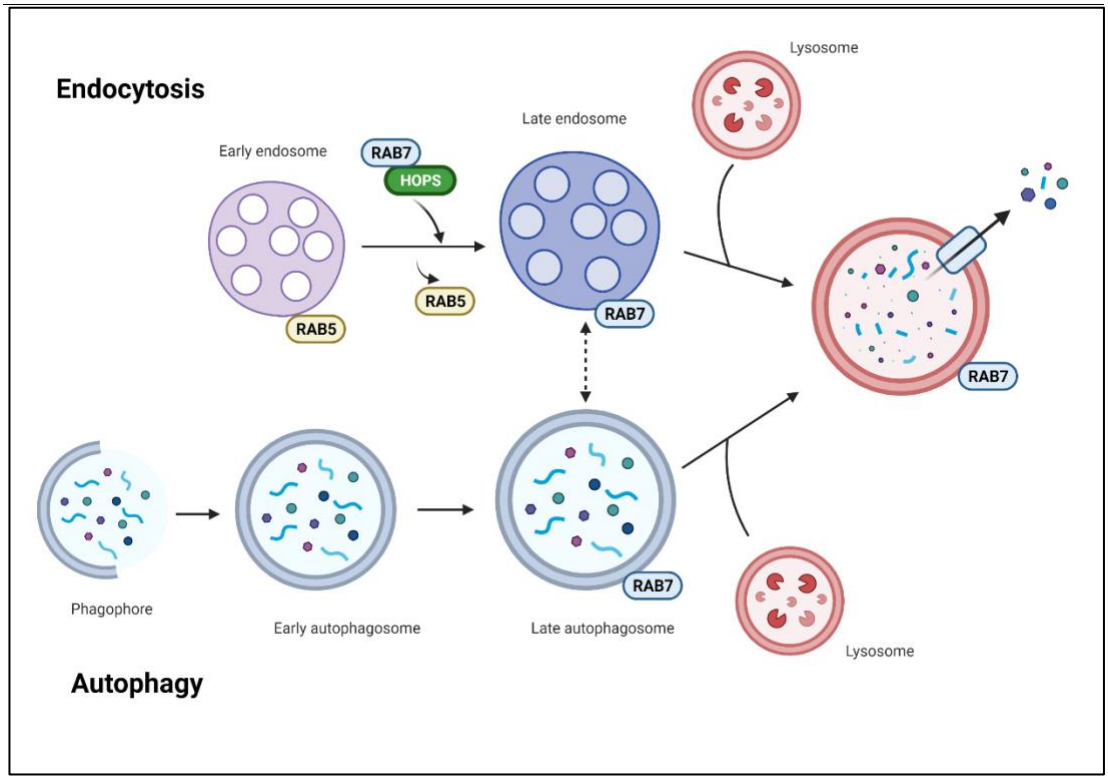

Figure 1.8. Endocytosis and autophagy. Upper panel showing endocytosis, starting from early endosome formation with Rab5 attached to its surface. Maturation of early endosome to late endosome with Rab5 changing to Rab7. The late endosome fuses with lysosome forming hybrid organelle. Bottom panel showing autophagy, from phagophore formation, early autophagosome formation to late autophagosome maturation (attached to Rab7 also). Late autophagosome fuses with lysosome to form autolysosomes. Late endosome can fuse with late autophagosome (Created with BioRender.com).

The endomembrane system permits various functions of the eukaryotic cell to be compartmentalized. For example, degradation occurs in lysosomes. This allows for higher degree of cell specialization. This system relies on the dynamic interactions between different compartments, facilitated by vesicle trafficking between them. Intracellular trafficking involves the formation and budding of membrane vesicles from a donor membrane, transport and subsequent fusion with the target membrane, leading to transport of cargo from donor to target organelle. Intracellular trafficking is regulated and orchestrated by several proteins and protein complexes such as adaptor and coat proteins, GTP-binding proteins (GTPases), SNARE proteins and tethering proteins (Søreng, Neufeld and Simonsen, 2017).

1.4 ADP-ribosylation factor (Arf) GTPase activating protein 3 (ArfGAP3)

A recent yeast two hybrid screening by Nezis laboratory (unpublished) in 3rd instar larvae and whole fly head samples revealed a library of *Drosophila* Atg8a interacting proteins, in which we identified a high confidence interaction (level B and C) between Atg8a and ADP-ribosylation factor (Arf) GTPase activating protein 3 (ArfGAP3) in both *Drosophila* whole fly head and 3rd instar larvae. The selected interaction domain (SID) identified in the yeast two hybrid screening is the domain predicted to be involved in the interaction. In 3rd instar larvae, the SID was from residue 293 to 409 and residues 206 to 414 in whole fly head.

ArfGAP3 is a GTPase activating protein (GAP) and belongs to the ArfGAP family of multidomain proteins. All ArfGAPs share a common domain within the N-terminus of their protein sequence, ArfGAP domain. This domain consists of a conserved zinc-binding motif. ArfGAPs regulate membrane trafficking and remodelling of the actin cytoskeleton through the regulation of the ADP-ribosylation factor (Arf) proteins. The multi domain of the ArfGAPs allows them to function dependently and independently of Arf proteins (Inoue and Randazzo, 2007). ArfGAPs facilitate the conversion of Arf-GTP into Arf-GDP by promoting the hydrolysis of GTP that is bound to Arf proteins (figure 1.9) (Inoue and Randazzo, 2007; Rodrigues *et al*, 2016).

Arf proteins are a family of GTP-binding proteins that belong to the sub-family of Ras superfamily. There are six Arf proteins that are categorized, based on the amino acid sequence (Moss *et al*, 1998), into three classes: class I, class II and class III. Arf1, Arf2 and Arf3 belong to class I, Arf4 and Arf5 are class II and class III includes Arf6 (Moss *et al*, 1998; Inoue and Randazzo, 2007). Arf1 is a well-studied

Arf protein (Randazzo *et al*, 2000; Donaldson *et al*, 2005). There are several pathways the Arf1 protein functions in; Golgi-endoplasmic reticulum retrograde transport, intra-Golgi transport, trafficking from mtrans Golgi network to endosomes and transport within endocytic pathway (Randazzo *et al*, 2000; Donaldson *et al*, 2005). Another extensively studied Arf protein is Arf6, which has implications in endocytosis, phagocytosis and receptor recycling (Donaldson, 2003; D'souza-Schorey and Chavrier, 2006).

Arf protein function is governed by binding and hydrolysis of GTP, hence the cycling between GTP bound Arf and GDP-bound Arf is key for its function (Inoue and Randazzo, 2007). This process is required for the dissociation of coat proteins from Golgi-derived membranes and vesicles. The dissociation of coat proteins is a pre-requisite for the fusion of these vesicles with target compartments (Søreng, Neufeld and Simonsen, 2017). The cycling is regulated by the action of guanine nucleotide exchange factors (GEFs) and GTPase activating proteins (GAPs) (figure 1.9). Human ArfGAP1 was the first ArfGAP discovered to regulate Arf1 protein at the Golgi apparatus (Cukierman *et al*, 1995).

Arfs function in membrane trafficking involves recruiting coat proteins for cargo sorting into vesicles and recruiting and activating enzymes involved in altering membrane lipid composition (Donaldson and Jackson, 2011). Moreover, both Arf1 and Arf6 has been implicated in regulation of the cytoskeleton. Arf1 has been shown to associate with focal adhesion dynamics (Norman *et al*, 1998) and Arf6 has been shown to have functional relevance in invadopodia formation and peripheral membrane ruffle formation (Donaldson *et al*, 2003; Hashimoto *et al*, 2004).

The human genome consists of at least 24 genes that translate to proteins with ArfGAP domains (Inoue and Randazzo, 2007). Furthermore, another set of proteins

categorised as ARF-like (ARL) proteins have broader roles than Arfs and are implicated in a number of similar functions such as recruitment of coat complexes for vesicle budding (Donaldson and Jackson, 2011), however the role of ArfGAPs in regulating ARL proteins have not yet been extensively studied.

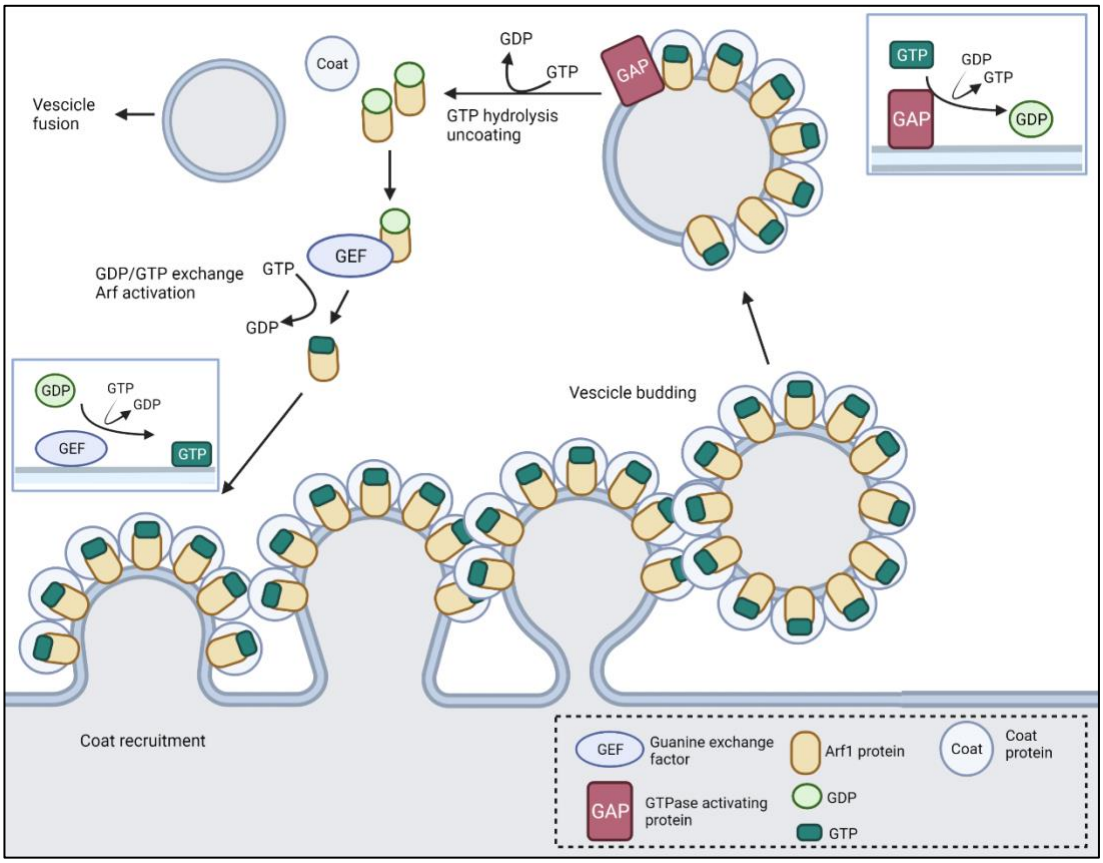

Figure 1.9. ARF GDP/GTP cycle. Arf1 protein is activated upon GDP to GTP exchange via GEF, which recruits coat proteins for vesicle formation followed by vesicle budding. GAP protein hydrolyses the GTP bound to Arf1 protein, resulting in dissociation of coat proteins (Created with BioRender.com).

1.4.1 ArfGAP3 in protein transport from Golgi to endosomes

ArfGAP3 also been reported to regulate Arf1 activity (Liu et al, 2001; Frigerio *et al*, 2007; Weimer et al, 2008; Shiba *et al*, 2013). There has been significant evidence suggesting that ArfGAP3 is involved in the process of protein transport from the Trans-Golgi network to endosomes (figure 1.10). A study by Shiba *et al* in 2013

showed that ArfGAP3 localises to the trans-Golgi network. HeLa cells were double stained for ArfGAP3 and trans-Golgi or cis-Golgi markers (TGN46 and GM130 respectively). Confocal imaging results illustrated ArfGAP3 co-localised with TGN46 more than the GM130 (Shiba *et al.*, 2013). When cargo is ready to be trafficked from donor to target organelle, areas of the TGN are coated with clathrin and adaptors namely Golgi-localized γ-ear-containing ADP-ribosylation factor binding proteins (GGAs) and this forms clathrin coated vesicles (Søreng, Neufeld and Simonsen, 2017). The same study double transfected cells with HA-tagged ArfGAP3 and FLAG-tagged various GGAs and carried out immunoprecipitation with anti-FLAG and western blotting with anti-HA. They discovered that HA-tagged ArfGAP3 coprecipitated with all GGAs, further suggesting that ArfGAP3 associates with GGAs. Furthermore, to examine if ArfGAP3 influenced the association of these coat proteins with TGN/endosomes, they measured the ratio of Golgi to cytosol for GGA in both control and ArfGAP3 KD cells. In ArfGAP3 KD cells, a small but significant decrease was observed in Golgi/endosomal association of GGA1 and GGA2, indicating ArfGAP3 regulates these two GGAs in particular (Shiba *et al.*, 2013).

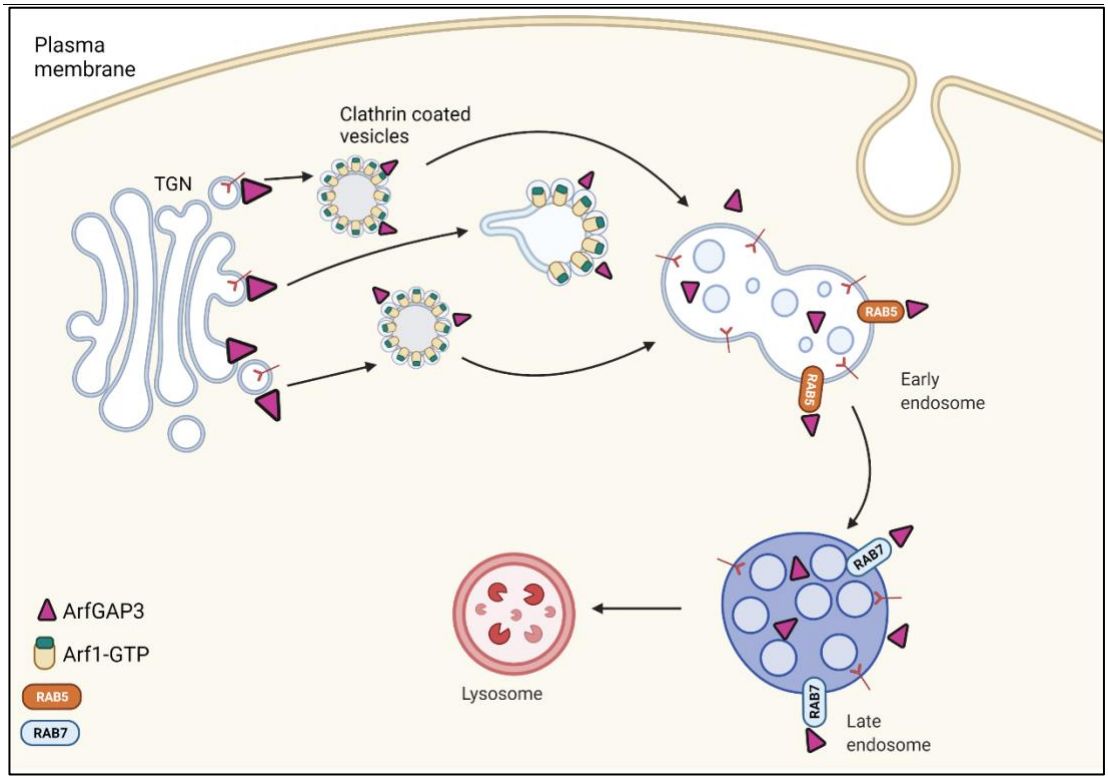

Figure 1.10. ArfGAP3 in protein transport from trans-Golgi network to endosomes. ArfGAP3 associates with TGN. Areas of the TGN membrane form vesicles via recruitment of coat proteins (GGAs) mediated by the activation of Arf1 protein. Vesicles traffic to early endosomes, where upon dissociation by Arf1-GTP hydrolysis via ArfGAP3, the vesicles then fuse with early endosomes. Early endosomes, which have a Rab5 attached to its membrane, then matures to late endosomes. The Rab5 is exchanged to a Rab7 on the membrane. ArfGAP3 associates with Rab5 and Rab7. Late endosomes fuse with lysosomes or with late autophagosomes which can later fuse with lysosomes (Created with BioRender.com).

Figure 1.10 demonstrates the fusion of these vesicles with the early endosomes. In order to the fusion to take place, the coat proteins must dissociate, and this is facilitated by GTP-bound Arf1 hydrolysis mediated by ArfGAP3. Shiba *et al* study also found that ArfGAP3 predominantly localises to early endosomes. They carried out confocal studies with markers HA-tagged Rab4 for early/recycling endosomes, GFP-tagged Rab5 for early endosomes and RFP-tagged Rab7 for early/late endosomes. ArfGAP3 co-localised with Rab5 more than Rab7 and Rab4, postulating that ArfGAP3 could have a key role in trafficking from early to late endosomes. This further suggests ArfGAP3 has a functional role in the endocytic pathway (Shiba *et al.*, 2013).

There are not any studies published yet showing any association of ArfGAP proteins to autophagy, however a recent study reported findings demonstrating the role of ARF-like protein ARL8 as a positive regulator of lysosomal fusion events in *Drosophila* (Boda et al, 2019). This study opened a new avenue to explore potential roles of Arf proteins and ArfGAPs in lysosomal degradative pathways.

1.5 Arfs and Rabs in the regulation of lipid droplet development and lipolysis

It is well known that Rab7 is a regulator of autophagosome and late endosome maturation (Feng, Press and Wandinger-Ness, 1995; Gutierrez *et al.*, 2004; Garcia, Vevea and Pon, 2018). Recent studies have revealed that Rab7 as well as Rab5 and Rab2 accumulate on lipid droplets under nutrient starvation conditions (Bartz *et al.*, 2007; Garcia, Vevea and Pon, 2018). Additionally, the studies have also indicated that Rab7 activation is prerequisite for the recruitment of autophagosome and lysosomal marker proteins to the lipid droplets (Garcia, Vevea and Pon, 2018). Studies also suggest Rab5 mediates docking of endosomes to the lipid droplets (Bartz *et al.*, 2007). Furthermore, other proteins that have also been identified on lipid droplets include Arf1 (*Drosophila* ArfGAP3 regulates Arf1 protein) and ArfGAP1 (Human homolog of *Drosophila* ArfGAP3) (Bartz *et al.*, 2007). Interestingly, a study published in 2010 by Hommel *et al* shows that an Arf-like GTPase ARFRP1 regulates lipid droplet growth and lipolysis as knockdown of ARFRP1 results in hinderance in normal enlargement of lipid droplets (Hommel *et al.*, 2010). In summary, the Arf proteins, Arf GTPases and Rab proteins all seem to play a role also in lipid droplet development and lipolysis.

Chapter 2

Thesis aims & hypothesis

2.1 Thesis aims

The principal objective of this PhD project is to characterize the function of the ArfGAP3 protein in the relationship between endosomal trafficking and selective autophagy during the course of ageing.

This project is divided into three stages; stage 1 entail experiments to confirm biochemically Atg8a and ArfGAP3 interaction followed by identification of specific structural motifs of ArfGAP3 that facilitates this interaction. Stage 2 of the project focuses on deciphering the role of ArfGAP3 in the interplay between autophagy and endosomal trafficking. Stage 3 of the project involves investigating the physiological relevance of ArfGAP3 during ageing.

2.2 Hypothesis

Late endosomes (also early endosomes) have the ability to fuse with late autophagosomes. Both autophagy and endocytosis have a common participating molecule, Rab7, which promotes the fusion of autophagosomes and late endosomes with lysosomes (Hyttinen *et al.*, 2013) (figure 2.1). Recent yeast-two hybrid screening by Nezis Lab has confirmed an interaction between *Drosophila* Atg8a and ArfGAP3

(unpublished), validating a role of ArfGAP3 in the autophagic pathway. Previous studies have also highlighted an association between ArfGAP3 and Rab7 (Shiba *et al.*, 2013). Hence, we hypothesize that ArfGAP3, possibly through Rab activity, is a positive regulator of lysosomal fusion events with autophagosomes and endosomes.

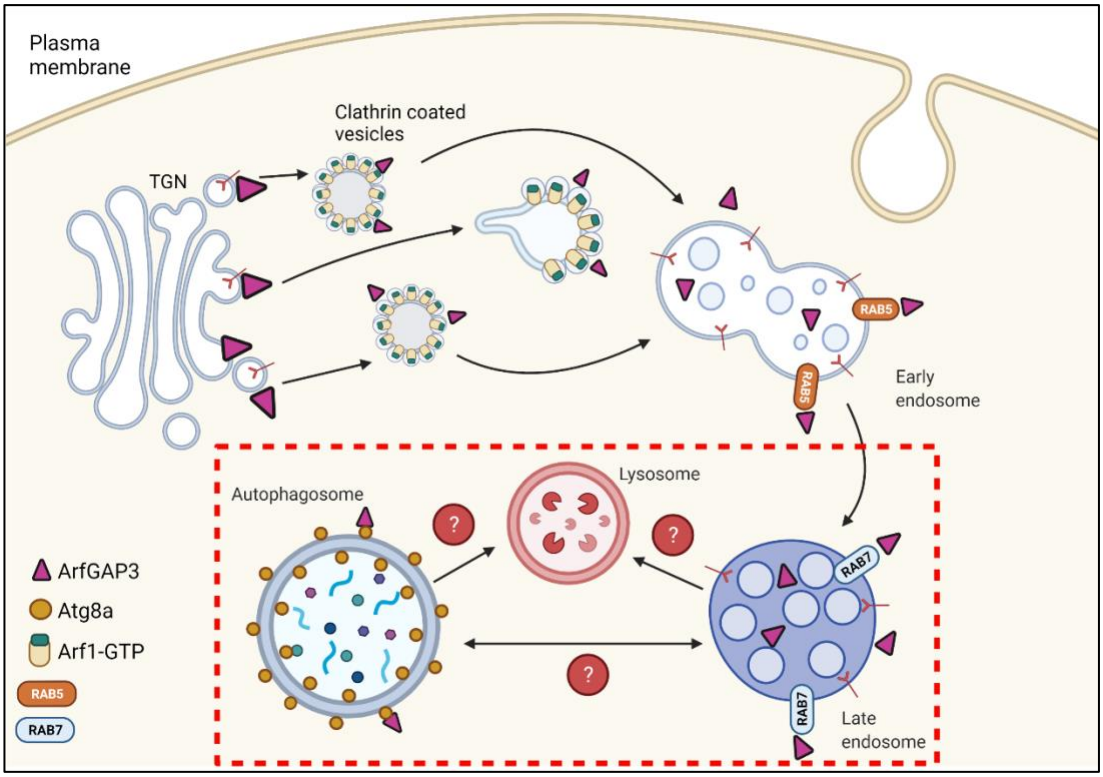

Figure 2.1. Schematic diagram illustrating hypothesis of this PhD project. ArfGAP3 has been shown to play a role in protein transport from the trans-Golgi network to endosomes as studies have highlighted its associations with TGN, vesicle coat proteins (GGAs) through the hydrolysis of GTP bound Arf1 protein, early and late endosomes, via associations with Rab5 and Rab7 respectively. Autophagy and endocytosis have converging steps and common participating molecule, Rab7, which promotes fusion of autophagosomes and endosomes to lysosomes. Since ArfGAP3 has been shown previously in Nezis Lab to interact with Atg8a in *Drosophila* and previously been shown to associate with Rab7-positive endosomes, we hypothesize that ArfGAP3, possibly through Rab7 activity, has a functional role in regulating the fusion of autophagosomes and endosomes with lysosomes (Created with BioRender.com)

Chapter 3

Materials and methods

3.1 Chemicals and reagents

Table 3.1. Chemicals and reagents. List of chemicals and reagents used in experiments and source of purchase.

Chemicals and reagents	Source
2-Mercaptoethanol	Sigma Aldrich (M3148)
16% formaldehyde	ThermoFisher Scientific (28908)
Absolute ethanol	SLS Stores
Acrylamide	AccuGel (SLS stores)
Agarose	SLS Stores
APS (Ammonium persulfate)	SLS sores
Bovine Serum Albumin	Sigma Aldrich (A7906)
Bromophenol blue sodium	Sigma Aldrich (B8026)
cOmplete ULTRA Tablets, Mini, EDTA-free, EASYpack Protease Inhibitor Cocktail Tablets	Roche (05892791001)
ECL reagent	Amersham (RPN2209)
EDTA	SLS Preparation room
EGTA	Sigma Aldrich (E4378)
Gel extraction kit	Qiagen
Gluthathione Sepharose 4B	Sigma Aldrich (GE17-0756-01)
Glycerol	Sigma Aldrich (G6279)
GoTaq qPCR Master Mix kit	Promega (A6002)
Igepal CA-630	MP (198596)
Imidazol	Sigma Aldrich (I2399)
Instant Blue (Coomassie staining)	Expedon (ISB1L)
IPTG	SLS stores
NaCl	SLS preparation room
Lysozyme	Fisher Scientific (10249843)
PCR/DNA purification kit	NEB/Qiagen
Plasmid miniprep kit	NEB/Qiagen
Ponceau S	Sigma Aldrich (P3504)
Precision Plus Protein™ Dual colour standards	BIO-RAD (1610374)
ProLong™ Gold Antifade Reagent	Invitrogen by ThermoFisher Scientific

Protein assay dye reagent concentrate	Bio-RAD
Protein G Sepharose 4 FastFlow	GE Healthcare (11524935)
REVERTAID kit 100RXN	Fisher Scientific (K1622)
Sodium deoxycholate	Alfa Aesar (B20759)
SDS	SLS preparation room
Sucrose	Sigma Aldrich (16104)
TEMED	Sigma Aldrich (T9281)
Tris HCl	SLS preparation room
Triton X-100	Sigma Aldrich (T8787)
Tween-20	Sigma Aldrich (P9416)

3.2 *Drosophila melanogaster* husbandry and genetic principles

3.2.1 Fly stocks

Table 3.2. *Drosophila* fly stocks. List of fly stocks used in experiments with full genotype and source of purchase.

Fly name	Genotype	Source
w1118	w[1118]	Bloomington *Drosophila* Stock Centre (ID 3605)
cg::Gal4 (fat body driver)	w[1118]; P{w[+mC]=Cg-GAL4.A}2	Bloomington *Drosophila* Stock Centre (ID 7011)
Pros Gal4 (garland nephrocyte driver)	w*; P{GAL4-pros.MG}3	Bloomington *Drosophila* Stock Centre (ID 80572)
Ubi::Gal4 (whole body driver)	w[*]; P{w[+m*]=Ubi-GAL4.U}2/CyO	Bloomington *Drosophila* Stock Centre (ID 32551)
da::Gal4; mkrs/TM6b (whole body driver)	w[*]; P{w[+mW.hs]=GAL4-da.G32}2; MKRS/TM6B, Tb[1]	Bloomington *Drosophila* Stock Centre (ID 55851)
elav::Gal4/CyO (II) (brain driver)	elav::Gal4/CyO	Bloomington *Drosophila* Stock Centre (ID 8765)
luc-RNAi	y[1] v[1]; P{y[+t7.7] v[+t1.8]=TRiP.JF01355}attP2	Bloomington *Drosophila* Stock Centre (ID 31603)
FLPout mCherry-Atg8a/SM66b	yw, hsflp; UAS-mCherry-Atg8a; Ac>CD2>Gal4/SM66b	Radu Tusco, University of Warwick
FLPout GFP-mCherry-Atg8a	yw, hsflp; UAS-GFP-mCherry-Atg8a; Ac>CD2>Gal4	Anne Claire Jacomin, University of Warwick
hs::Flp FRT82B	yw, hsflp; FRT82B ubi>GFP	Yun Fan, University of Warwick
MARCM FRT80	yw, hsflp; FRT80B ubi>GFP	Yun Fan, University of Warwick
CgGal4, mCh-Atg8a	Cg-GAL4 UAS-mCherry-Atg8a	Anne Claire Jacomin, University of Warwick

CgGal4, GFP-Atg8a	Cg-GAL4 UAS-GFP-GFP-Atg8a	Gabor Juhász, Eotvos Lorand University Hungary
3xmCherryAtg8a GFP	hsflp; UAS DCR2; 3xmcherry Atg8a – Act -CD2-Gal4, UAS – 2xEGFP	Gabor Juhász, Eotvos Lorand University Hungary
Atg7 (d14)/CyO-GFP	Atg7[d14]	Gábor Juhász, Eotvos Lorand University Hungary
Atg7 (d77)	Atg7[d77]	Gábor Juhász, Eotvos Lorand University Hungary
ArfGAP3 mutants e0250	w[1118]; PBac{w[+mC]=RB}ArfGAP3[e01250]	Bloomington *Drosophila* Stock Centre (86009)
ArfGAP3 mutants d00510	w[1118]; P{XP}ArfGAP3d00510	Bloomington *Drosophila* Stock Centre
UAS ArfGAP3 WT DsRed ^{4B}/cyo	UAS;ArfGAP3^{4B}/cyo	Ruth Johnson, Wesleyan University
UAS ArfGAP3 WT DsRed ^{3e}/cyo	UAS;ArfGAP3^{DsRED3e}/cyo	Ruth Johnson, Wesleyan University
UAS ArfGAP3 WT DsRED ^{PD}/cyo	UAS;ArfGAP3-PD^{DsRed3B}/TM6B	Ruth Johnson, Wesleyan University
UAS ArfGAP3 RNAi/cyo (RJ)	UAS;ArfGAP3 RNAi/cyo	Ruth Johnson, Wesleyan University
UAS ArfGAP3 RNAi VDRC A	P{VSH330410}attP40	Vienna *Drosophila* Resource Centre (VDRC ID 330410)
UAS ArfGAP3 RNAi VDRC B	w^{1118}; P{GD12053}v35123	Vienna *Drosophila* Resource Centre (VDRC ID 35123)
UAS ArfGAP3 RNAi Bloom 31156	y[1] v[1]; P{y[+t7.7] v[+t1.8]=TRiP.JF01649}attP2	Bloomington *Drosophila* Stock Centre (ID 31156)
UAS ArfGAP3 RNAi Bloom B 61993	y[1] v[1]; P{y[+t7.7] v[+t1.8]=TRiP.HMJ23619}attP40/CyO	Bloomington *Drosophila* Stock Centre (ID 61993)
UAS ArfGAP3 FLAG WT (M3)	W^{118};UAS-3xFLAG-dArfGAP3;+/+	BestGene Inc, US
UAS ArfGAP3 FLAG LM1 (M1)	W^{118};UAS-3xFLAG-dArfGAP3LIR;+/+	BestGene Inc, US

3.2.2 Ectopic gene expression

Gene expression is activated in *Drosophila melanogaster* using the bipartite UAS/GAL4 system. The yeast derived protein GAL4, is a transcriptional activator in this system. GAL4 is a desirable tool for gene activation as it lacks endogenous targets within *Drosophila* (Cho, Bang and Toh, 2014). The GAL4 protein has a specific enhancer known as the upstream activation sequence (UAS). Fly lines expressing a protein of interest in a specific tissue can be generated by the UAS/GAL4 system. One fly line must express the UAS together with the specific gene of interest. A separate fly line must express the GAL4 with a tissue-specific promoter. Upon flies from each line crossing, in the resulting progeny, the tissue-specific promoter drives the expression of GAL4 protein, which in turn binds to the UAS, resulting in gene of interest expression at the tissue for which the promoter is specific for (figure 3.1) (McGuire, Roman and Davis, 2004; Cho, Bang and Toh, 2014).

An advantage of using this system is that both UAS and GAL4 are carried in different parental lines so these flies are viable even if they are carrying an inactive form of a toxic gene. (McGuire, Roman and Davis, 2004; Cho, Bang and Toh, 2014). Due to the range of tissue-specific promoters available, the UAS/GAL4 system is a favourable tool to study the effects of various genes through their over-expression or misexpression at various tissue locations (Osterwalder *et al.*, 2001).

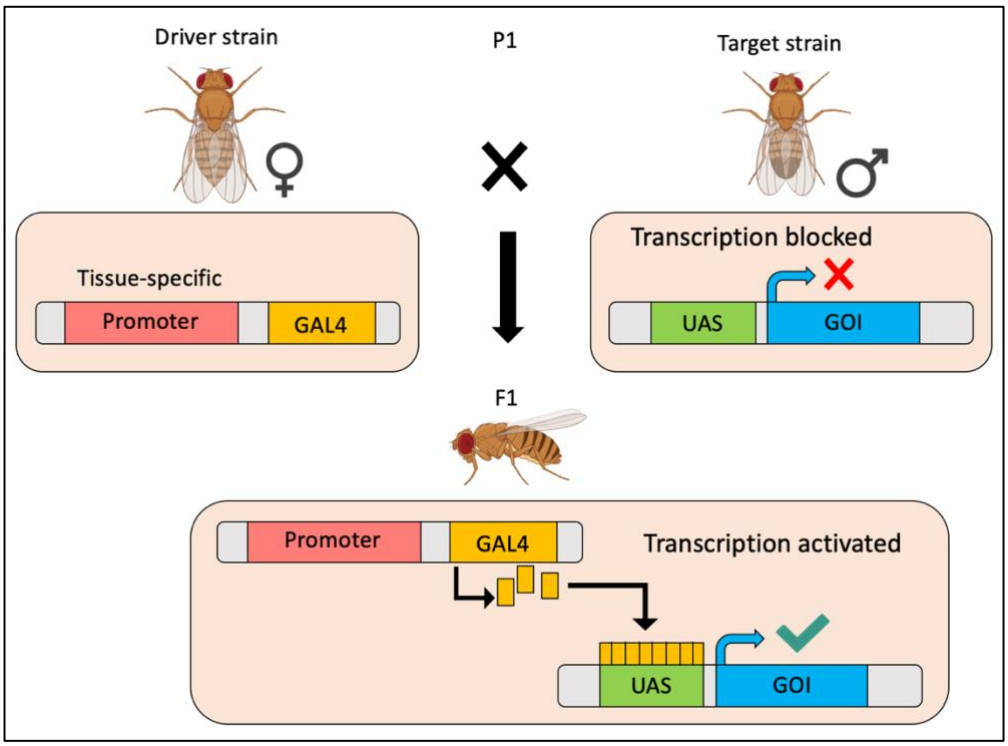

Figure 3.1. Ectopic gene expression using UAS/GAL4 system. The parental driver strain carries the GAL4 transcription activator which is under the control of a tissue-specific promoter. The parental target strain carries the UAS enhancer with the gene of interest, where transcription is blocked. Upon crossing, in the progeny flies, transcription of the gene of interest is activated as GAL4 binds to UAS.

The drivers used for the experiments in this thesis are summarised in table 3.2, the most common one being Cg::Gal4 which expresses the gene in the *Drosophila* fat body.

3.2.3 Fly maintaining conditions

All stock flies were kept at 18°C and transferred into new tubes of fly food roughly every four weeks. Flies used for experiments in this thesis, crosses and aging flies were kept at 25°C, and virgin collection fly tubes were kept at 18°C.

3.2.4 Fly food recipe

Fly food was made by the University of Warwick School of Life Science preparation room technicians. The recipe for 1 litre of fly food consisted of; 42g inactive yeast (Genesee Scientific), 60g cornmeal polenta (TRS Asia's Finest Food), 130g sucrose, 5.5g bacto agar (BD), 30ml 10% w/v nipagin solution (methyl 4-hydroxybenzoate – Sigma) dissolved in absolute ethanol and 1 litre super Q deionised water.

3.3 Fluorescence and Immunofluorescence microscopy

3.3.1 Buffers and reagents for IF

All buffers and reagents for immunofluorescence (IF) were prepared fresh as a working stock at the time of the experiment. Phosphate buffer saline (PBS) was used to make all buffers and dilute reagents. 4% formaldehyde diluted in PBS was used to fix all *Drosophila* tissues. Two separate buffers were used for IF washes and antibody incubations. PBX buffer for washes was prepared with 0.2% triton x-100 in a working stock volume of PBS (30ml). For antibody incubations, 0.2% BSA was prepared in a working stock volume of PBX (30ml).

3.3.2 Antibodies and dyes for IF

Table 3.3. Antibodies and dyes for immunofluorescence. List of antibodies and dyes used in IF experiments, with brief description, dilution used and source of purchase.

Antibodies & Dyes	Description	Dilution	Source
IF primary antibodies (diluted in PBX + 0.2% BSA buffer)			
Anti- Rab5	Rabbit polyclonal *Drosophila* early endosome marker	1:500	Abcam (ab31261)
Anti- Rab7	Mouse monoclonal	3-5ug/ml	Developmental Studies Hybridoma Bank (DSHB), University of Iowa
Anti- Cathepsin L	Rabbit polyclonal	1:1000	Abcam (ab58991)
Anti- FLAG M2	Mouse monoclonal	1:500	Sigma Aldrich (F1804)
IF Dyes (diluted in PBS)			
Lysotracker- RED	DND-99 Red Fluorescent dye	1:1000	ThermoFisher Scientific (L7528)
DAPI (Hoechst)		1:1000	
Bodipy	493/503 lipid probe	1:1000	ThermoFisher Scientific (D3922)
IF secondary antibodies (diluted in PBX + 0.2% BSA buffer)			
Anti-Rabbit IgG 488A	Goat, (H+L), highly cross-absorbed, CF™	1:1000	Sigma Aldrich SAB4600045
Anti- Rabbit IgG 568	Goat, (H+L), highly cross-absorbed, CF™	1:1000	Sigma Aldrich SAB4600086
Anti- Mouse IgG 488A	Goat, (H+L), highly cross-absorbed, CF™	1:1000	Sigma Aldrich SAB4600042

Anti- Mouse IgG 568	Goat, (H+L), highly cross-absorbed, CF™	1:1000	Sigma Aldrich SAB4600082

3.3.3 Dissections

For immunofluorescence experiments, *Drosophila* fly 3rd instar larvae tissues (fat bodies, brain, garland nephrocytes) were dissected in PBS using very fine dissecting tweezers (Dumostar #55). The dissected tissues were transferred into cell-strainer baskets (Corning Falcon #352235). These baskets were placed in 48-well plates which was used to carry out all incubations.

3.3.4 Summary of IF experiments

Table 3.4. Immunofluorescence experiments. Summary of crosses, experimental details and antibodies/dyes used for all IF experiments

Experimental cross	Experimental details	Antibodies/dyes used
CgGal4, GFP-Atg8a x UAS ArfGAP3 WT DsRED 4B CgGal4, GFP-Atg8a x UAS ArfGAP3 WT DsRED PD	Co-localisation analysis of ArfGAP3 and Atg8a to confirm interaction	DAPI
Flpout mCherry Atg8a x UAS FLAG WT ArfGAP3 (M3) Flpout mCherry Atg8a x UAS FLAG ArfGAP3 LM1 (M1)	Co-localisation analysis of ArfGAP3 and Atg8a to confirm interaction	DAPI

3xmCherry Atg8a GFP x UAS ArfGAP3 RNAI (RJ)	Clonal analysis of number of autophagosomes in control and ArfGAP3 RNAi cells for investigating autophagic flux	DAPI
FLPout GFP-mCherry-Atg8a x UAS luciferase RNAI FLPout GFP-mCherry-Atg8a x UAS ArfGAP3 RNAI (RJ)	Clonal analysis of autophagosomes and autolysosomes in control and ArfGAP3 RNAi cells for investigating autophagic flux	DAPI
CgGal4 x luciferase RNAI CgGal4 x UAS ArfGAP3 WT DsRed^{4B} CgGal4 x UAS ArfGAP3 RNAI (VDRC B) CgGal4 x UAS ArfGAP3 RNAI (RJ)	Lysotracker analysis to examine lysosome number and morphology in control and ArfGAP3 RNAi cells	Lysotracker, DAPI
CgGal4 x UAS ArfGAP3 DsRED 4B	Co-localisation of ArfGAP3 and Rab5/Rab7	Anti-Rab5, anti-Rab7, DAPI
CgGal4 x UAS ArfGAP3 RNAI (RJ)	TEM analysis of autophagic machinery	N/A
CgGal4 x luciferase RNAI CgGal4 x UAS ArfGAP3 RNAI (RJ) CgGal4 x UAS ArfGAP3 RNAI (VDRC B)	Standard IF investigation accumulation of Rab7 in fat body cells.	Anti-Rab7, DAPI
CgGal4 x luciferase RNAI	Co-localisation analysis of Rab7 an cathepsin L	Anti-Rab7, anti-Cathepsin-L, DAPI

CgGal4 x UAS ArfGAP3 RNAI (RJ) CgGal4 x UAS ArfGAP3 RNAI (VDRC B)	for investigating endosome – lysosome fusion.	
ProsGal4 x UAS luciferase RNAI ProsGal4 x UAS ArfGAP3 RNAI (RJ)	Standard IF investigation accumulation of Rab7 in garland nephrocytes.	Anti-Rab7, DAPI
WT (W118) CgGal4 x UAS ArfGAP3 RNAI (RJ)	Bodipy staining to investigate lipid droplet size in control and ArfGAP3 RNAi cells.	Bodipy, DAPI
ElavGal4 x UAS ArfGAP3 WT (M3)	Standard IF to examine the expression of ArfGAP3 in larval brain	Anti-FLAG, DAPI

3.3.5 Co-localisation studies

Standard IF protocol; fed and starved (4hours or 24 hours starvation in 20% sucrose solution) larvae fat bodies (3rd instar development stage) were dissected. Dissected fat bodies were fixed with 4% PFA for 30 minutes RT, washed 3 x 10 minutes with PBX buffer at RT and blocked in PBX + BSA buffer for 1 hour at RT. Fat bodies were incubated with primary antibody overnight at 4 °C (on shaker). Dissected tissues were then incubated with secondary antibody for 2 hours at RT followed by 3 x 10 minutes washes in PBX + BSA buffer, further followed by 3 x 10 minutes PBS washes at RT. DAPI staining was carried out for 30minutes in a dark box at RT. Fat bodies were mounted using ProLong^{TM} Gold Antifade Reagent on microscope slides, sealed with nail varnish and viewed under confocal microscope. Coloc2 plugin was used in ImageJ

to quantify co-localisation of DsRed-ArfGAP3 and GFP-Atg8a signals using Pearson's correlation coefficient.

3.3.6 Clonal analysis

Four hours starved 3rd instar larvae (20% sucrose solution) fat bodies were dissected from crosses for clonal analysis experiments summarized in table 3.4. Prior to dissection, embryos 0 – 18hours after egg laying were subjected to heat shock for 20 minutes at 37°C. Dissected fat bodies were fixed, washed, stained with DAPI and mounted the same as described in the standard IF protocol under co-localization studies.

3.3.7 Garland nephrocyte staining

Pros Gal4 driver fly line is a specific driver for expression in garland nephrocytes. Garland nephrocytes are located around the oesophagus forming a garland-like ring structure as seen in figure 3.2 (Helmstädter, Huber and Hermle, 2017). Since garland nephrocyte cells are too small to be visible by light microscope during dissection, the top end of the midgut, proventriculus region with the oesophagus was dissected. Fed third instar larvae garland nephrocytes were fixed in 4% PFA for 30 minutes and subjected to standard immunofluorescence as described above staining for endogenous Rab7. Garland nephrocytes were mounted on microscope slides and viewed under confocal microscope. Fiji software was used to quantify the number of Rab7-positive puncta in control and ArfGAP3.RNAi cells. Statistical analysis was carried out using GraphPad Prism 7.

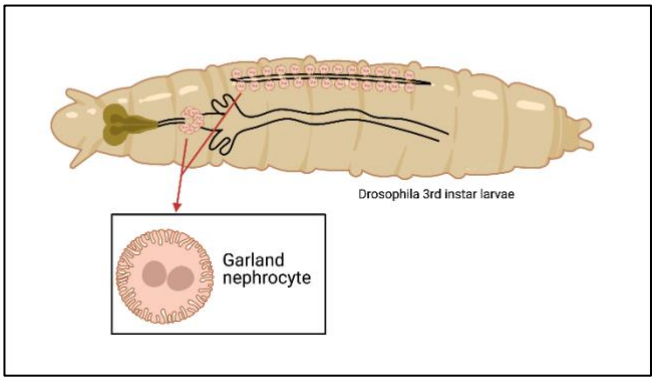

Figure 3.2. Location of garland nephrocytes. A schematic diagram showing the positioning of garland nephrocytes (green) in a ring-like structure around the oesophagus (created with BioRender.com).

3.3.8 Confocal microscopy acquisition

Confocal microscopy acquisition was carried out using the Carl Zeiss LSM80 in the School of Life Science imaging suite. Most images were taken using 63x objective lens, and occasionally 10x and 100x lenses were also used. Images were acquired using the zen image processing software and the .czi files were later analysed using Fiji.

3.3.9 Image analysis

Images after acquisition were analysed using FIJI program. For all co-localisation experiments in this thesis, the in-built plugin 'Coloc 2' was used to measure the signal overlap between two channels. Each image was separated into individual channels that were used during acquisition, i.e green channel reprenting GFP, red channel representing mCherry and blue channel representing DAPI. The channel associated with Atg8a positive puncta was subjected to threshold adjustment to only select puncta. Noise was decreased by using the despeckle tool and the watershed function was applied to create a binary image. The resulting highlighted particles were added to the ROI (region of interest manager). The ROI was applied to the second channel (for example, Rab7, ArfGAP3, cathepsin L) and the Coloc2 plugin was applied to

determine a Pearson's correlation coefficient value. For image analysis that involved counting number of particles (i.e. Autophagosomes, lysosomes, endosomes), the same steps as above were applied up until the watershed function. The built-in 'Analyse particle' tool was applied to analyse the number of particles in the selected area. Lysosome diameter and lipid droplet diameter was measured using the built in 'analyse particle' tool in FIJI. The same steps as mentioned above prior to 'analyse particle' application was applied to the image so the threshold selected the correct particles. The area of each particle was measured and converted to diameter size (µm) using equation [2*SQRT(area/pi())] in excel.

3.4 Western blotting

3.4.1 Buffers for lysate extraction

RIPA buffer was used for fly larvae and whole fly lysate extraction. The buffer was made with 10mM Tris-HCl (pH 8.0), 1mM EDTA, 0.5mM EGTA, 1% Triton X-100, 0.1% sodium deoxycholate, 0.1% SDS, 140mM NaCl. At time of experiment, one protease inhibitor tablet was added per 10ml of RIPA buffer.

3.4.2 Buffers for western blotting

A 10x stock of protein gel running buffer was obtained from the SLS media room where the buffer was made. Running buffer consisted of 250mM Tris base, 2M glycine and 1% SDS and was diluted down to 1x for experimental use. Western blotting transfer buffer was also obtained from the SLS media room. A 10x stock of Transfer

buffer consisted of 250mM Tris, 2M glycine. The final transfer buffer made at time of experiment consisted of the 10x buffer diluted in water with 20% ethanol to make a 1x dilution of transfer buffer. The transfer buffer was kept cold. For the washes in between antibody incubations, 1x TBS and 1x TBS-Tween buffer was used. 5% blocking buffer, used to block the membrane prior to primary antibody incubation, was prepared with 2.5g of BSA diluted in 50ml of 1x TBS-T buffer. 1% BSA TBS-T buffer, used to dilute antibodies, was prepared with 0.5g of BSA diluted in 50ml of 1x TBS-T buffer.

3.4.3 Antibodies for western blotting

Table 3.5. Antibodies for western blotting. List of antibodies used in western blotting experiments, dilution used and source of purchase.

Antibodies	Dilution	Experiment	Source
	WB primary antibodies (diluted in 1% BSA TBS-T)		
Monoclonal guinea pig anti- ArfGAP3 1545	1:500	Chapter 5.2, 5.3	Ruth Johnson, Wesleyan University
Monoclonal mouse anti- HIS	1:2000	Chapter 4.4	Abcam ab18184
Monoclonal rabbit anti- Ref2P	1:2000	Chapter 6.5	Abcam ab178440
Polyclonal rabbit anti- beta actin	1:2000	Chapter 5.3, 6.5	Abcam ab8227
Monoclonal mouse anti- tubulin	1:50,000	Chapter 5.2, 5.3	Sigma Aldrich T5168
	WB secondary antibodies (diluted in 1% BSA TBS-T)		
Goat anti-Rabbit IgG (H+L) HRP	1:1000	Chapter 5.3, 6.5	Invitrogen 31460

Rabbit anti- Mouse IgG (H+L) HRP	1:1000	Chapter 4.4, 5.2, 5.3	Invitrogen 31450
Goat anti- Guinea pig IgG (H+L) HRP	1:1000	Chapter 5.2, 5.3	Abcam ab102372

3.4.4 Lysate extraction

One week old flies were homogenised with a pestle in RIPA buffer (with protease inhibitor), incubated on ice for 30 minutes prior to 20 minutes centrifugation at 12000 rcf at 4°C. The supernatant was collected for the experiment or stored at -80°C.

3.4.5 Determining protein concentration

Protein estimation (BSA assay) was carried out for each lysate prior to western blotting. A BSA standard curve was set up to measure the protein concentration by measuring the absorbance of known concentrations of BSA at λ = 595nm. Linear BSA dilutions were set up in cuvettes as below followed by adding 200µl of BIO-RAD dye. After incubating for 5 minutes, the absorbances were taken on GENESYS^{TM} 10S Vis spectrophotometer.

[BSA] (µg/ml)	**dH_2O (µl)**	**BSA µl of (100µg/ml)**
0	800	0
1	790	10
2.5	775	25
5	750	50

10	700	100
15	650	150
20	600	200

Two cuvettes were set up for each sample with 800µl of dH_2O, one with 2µl of sample and the other with 4µl of sample. 200µl of BIO-RAD dye was added to each cuvette, mixed well and absorbance readings were taken.

3.4.6 Preparation of loading samples

Samples were diluted in RIPA buffer and 4x laemmli buffer to have a protein content of 100µg in 100µl. In order to denature the proteins, lysates were boiled for 5 minutes at 95°C. The samples were stored at -20°C or subjected to SDS-PAGE electrophoresis.

3.4.6.1 Laemmli Buffer

Laemmli buffer was used to denature the protein sample prior to SDS-PAGE electrophoresis. A 4x stock solution of laemmli buffer was prepared without β-mercaptoethanol for long-term storage at room temperature. BIO-RAD recipe for 4x laemmli buffer was used, with contained; 277.8mM Tris-HCl pH 6.8, 44.4% (v/v) glycerol, 4.4% SDS, 0.02% bromophemol blue and H_2O to a final volume of 100ml. At the time of experiment, the working volume of 4x laemmli buffer was supplemented with 5% β-mercaptoethanol.

3.4.7 Gel casting

For SDS-PAGE gel electrophoresis, Bis-Tris polyacrylamide gels were prepared and used. Gels were made fresh at the time of experiment using the below recipes.

Resolving gel	**8%**		**12%**	
Number of gels	1	2	1	2
H2O (ml)	2.78	5.56	2	4
Tris 1.5M pH 8.8 (ml)	1.5	3	1.5	3
30% acrylamide (ml)	1.6	3.2	2.4	4.8
SDS 10% (µl)	60	120	60	120
APS 10% (µl)	60	120	60	120
TEMED (µl)	5	10	5	10
Total (ml)	6	12	6.02	12.04

Stacking gel	**1**	**2**	**3**	**4**
Number of gels				
Pre-mix (ml)	2	3	5	6
APS 10% (µl)	40	60	100	120
TEMED (µl)	3	4	7	8

Pre-mix stacking gel

H2O (ml)	22.8
Acrylamide 30% (ml)	6.8
Tris 0.5M pH 6.8 (ml)	10
SDS 10% (ml)	0.4
Total (ml)	40

3.4.8 SDS-PAGE and transfer to membrane

The gels were assembled in the gel mounts and placed inside an electrophoresis tank filled with 1x protein running gel buffer. The first well for every gel was loaded with 3µl of BIO-RAD protein gel ladder. The remaining gel wells were loaded with 10µl - 20µl of sample, which ran through the stacking gel at 75 V and through the resolving gel at 150 V at room temperature. For western blots that were going to be probed with ArfGAP3 antibody, the samples were left to run through a 12% gel for approximately 4 to 6 hours for optimal separation of proteins.

After SDS-PAGE, the separated proteins on the gel were transferred onto one of two membranes; nitrocellulose or PVDF. The layering of transfer sponges, filter papers, membrane and gel were assembled in a tray of cold 1x transfer buffer and then placed into the BIO-RAD transfer equipment inside new tanks filled with cold 1x transfer buffer. Transfer to a nitrocellulose membrane was carried out at 100 V for 1 hour at room temperature.

3.4.9 Immunoblotting

Membranes were blocked at room temperature in 5% BSA TBS-T blocking solution. Primary antibody was incubated overnight at 4°C. Membranes were washed 3x in 1x TBS-T for 10mins each at room temperature, followed by secondary antibody incubation at room temperature for 1 hour. A further 3x TBS-T washes were carried out for 10minutes each at room temperature, followed by a single wash with 1x TBS. A 1:1 ratio of ECL mix was made and membranes were incubated for 2 minutes. The membranes were then exposed to CL-XposureTM Film (ThermoScientific 34089) for a specific amount of time,and passed through a developer.

3.5 Molecular genetics

3.5.1 Cloning of N-terminus HIS-tagged ArfGAP3

The cloning of N-terminus HIS-tagged ArfGAP3 was carried out by Dr Stavroula Petridi (Post-doc in Nezis Lab). The ArfGAP3 plasmid, UAS-ArfGAP3-PB-RFP was kindly gifted by Ruth Johnson. PCR amplification of the ArfGAP3 insert using the NdeI and NheI restriction enzymes was carried out (primers outlined in 3.6.4). A PCR clean up was carried out on the PCR product using PCR purification kit (Monarch T1030L) yielding 238.2ng/μl of ArfGAP3 PCR product. The amount of p28 vector acquired was 233.15ng/μl. Digestion of the PCR product and p28 vector was carried out using the NdeI and NheI restriction enzymes. For all digestion reactions, 1μg of DNA was used. The digestion reactions were set up as summarised below.

Digestion reactions	**ArfGAP3 product**	**PCR p28 vector**
CutSmart buffer	5 µl	5 µl
NdeI	1µl	1µl
NheI	1µl	1µl
DNA	4.19 µl	4.28 µl
H_2O	38.8 µl	38.72 µl
Total	50 µl	50 µl

Digestions were incubated for 30 minutes at 37°C, 20 minutes at 65°C and final 20 minutes at 80°C. The digestions ran on a 0.7% agarose gel at 100 V and bands of interest were excised. Gel extraction (Qiagen kit 2806) of excised bands was carried out, yielding 21.6 ng/µl of ArfGAP3 and 34ng/µl of p28, followed by ligation reaction. For the ligation reaction, a 100ng of cut vector was needed and two different ligation reactions were set up, 1:1 and 1:3 vector: insert ratios. The formulas for ligation reactions are summarised below.

$$\boldsymbol{Ligation\ 3{:}1}$$

$$\boldsymbol{Insert\ mass\ (ng) = 3\ x\ \left(\frac{Insert\ length}{Vector\ length}\right)\ x\ Vector\ mass}$$

$$\boldsymbol{Ligation\ 1{:}1}$$

$$\boldsymbol{Insert\ mass\ (ng) = 1\ x\ \left(\frac{Insert\ length}{Vector\ length}\right)\ x\ Vector\ mass}$$

Using the above formulas, the insert mass was calculated; for 1:1 ratio 31.46ng of cut ArfGAP3 was needed and for 3:1 ratio 94.37ng of cut ArfGAP3 was needed. The ligation reactions were set up as summarised below.

Ligation ratios	**1:1**	**1:3**
Cut p28 vector	2.94 µl	2.94 µl
Cut ArfGAP3 insert	1.46 µl	4.37 µl
T4 ligase buffer	2 µl	2 µl
T4 ligase	1 µl	1 µl
H_20	12.6 µl	9.69 µl
Total	20 µl	20 µl

The above ligation reactions were incubated at 16°C overnight followed by inactivation of the T4 ligase at 65°C for 10 minutes. Transformation of E. coli cells was carried out where 1µl of the ligation reaction was added into 50µl of competent cells. This was left to incubate for 30 minutes on ice followed by immediate heat shock at 42°C for 30 seconds. The cells were further incubated on ice for 2 minutes and then 200µl of SOC medium was added which was then incubated at 37°C for 1 hour with 300rpm shaking. Agar plates supplemented with kanamycin were plated with these ligation cell samples and incubated at 37°C overnight.

To select the successfully ligated colonies, colony cracking was performed. A stock of 5x cracking buffer was prepared using the recipe; 25g sucrose, 40ml dH_2O, 5ml 5M NaOH and 2.5ml 10% SDS. A stock of 6x bromophenol blue loading dye was prepared using recipe; 3ml glycerol, 25mg bromophenol blue and dH_2O up to 10ml. To 1ml aliquot of 5x cracking buffer, 200µl of bromophenol blue was added. The colony cracking reaction was set up as summarised below.

Colony cracking reaction

Cracking buffer + loading dye	5µl
P1 resuspension buffer	5µl
Overnight culture or single colony	15µl

Colonies to be tested were also patched onto fresh agar plates to grow overnight. The above colony cracking reaction was then loaded directly onto a 0.7% agarose gel to verify successfully ligated colonies at expected band length. For the colonies that indicated the ArfGAP3 insert was successfully ligated, mini-prep DNA purification kit (Qiagen kit 27106) was used to carry out mini preps on overnight cultures of the colonies. The DNA from the mini prep was then digested with NdeI and NheI (used for the PCR cloning in 3.6.1, to confirm the presence of the ArfGAP3 insert. DNA of the colonies were also sent off for sequencing (GATC sequencing).

3.5.2 Site directed mutagenesis

ArfGAP3 LIR motif mutation constructs (LIR1 and LIR2) were generated via site directed mutagenesis. PAGE purified forward and reverse primers (primers outlined in 3.6.4) were designed to incorporate a 2 point mutation into the ArfGAP3 sequence at the third and sixth amino acid position within the LIR motifs. Both amino acids at these positions were altered to alanine amino acid, outlined below. Alanine was chosen as a substitution because it is a neutral amino acid and it has the least effect on the structure of that area of the protein.

ArfGAP3 LIR1 mutant primer design:

392 to 397	**LGYETI**
2-point mutation (alanine)	**LGAETA**

Protein sequence to nucleotide sequence of LIR motif:

L G Y E T I

5' - CTG GGC TAC GAG ACA ATT - 3'

Protein sequence to nucleotide sequence of LIR mutation

L G A E T A

5' - CTG GGC GCC GAG ACA GCT - 3'

ArfGAP3 LIR2 mutant primer design:

37 to 42	**PTWSSV**
2-point mutation (alanine)	**PTASSA**

Protein sequence to nucleotide sequence of LIR motif 2:

P T W S S V

5' - CCC ACC TGG TCC TCC GTT - 3'

Protein sequence to nucleotide sequence of LIR mutation

P T A S S A

5' - CCC ACC GCG TCC TCC GCT - 3'

Reactions for site directed mutagenesis were set up as summarised below.

Site directed mutagenesis reaction

10x pfu ultra buffer	5µl
dsDNA template (ArfGAP3 wildtype plasmid 100ng)	1.45µl
10µM forward primer	2.5µl
10µM reverse primer	2.5µl
dNTP mix	2µl
DMSO	1.5µl
dH2O	34.05µl
Pfu ultra HF DNA polymerase (to be added last)	1µl

Site directed mutagenesis PCR of ArfGAP3 wildtype cDNA (above reaction) was subjected to 95°C for 30 seconds, 55°C for 1 minute and 68°C for 7 minutes for 18 cycles. DPN1 digestion was carried out followed by transformation into NEB® 10-beta competent cells (New England Biolabs C3019H). Successful colonies were picked for overnight liquid cultures and mini-preps were carried out to extract DNA, concentrations were measured using a Nanodrop. DNA samples were sent off GATC sequencing.

3.5.3 Cloning of FLAG-tagged wildtype ArfGAP3 and LIR mutant

In order to generate wildtype ArfGAP3 and LIR mutant transgenic flies, the WT and LIR mutant ArfGAP3 sequences had to be cloned into a FLAG UAS plasmid to send off to BestGene Inc (US). Figure 3.3 shows a schematic overview of the method used for this cloning. Two restriction sites, XhoI and XbaI, were introduced into the HIS-tagged ArfGAP3 p28 plasmid via PCR (primers outlined in 3.6.4). The PCR was set to 95°C for 30 seconds, 64.1°C for 30 seconds and 72°C for 1 minute for 25 cycles. The PCR product (ArfGAP3 plasmid with XhoI and XbaI insertions) was subjected to PCR clean-up to determine DNA concentrations. This was followed by digestion of the PCR product with XhoI and XbaI restriction enzymes to excise the ArfGAP3 gene with XhoI and XbaI overhangs. Digestion of the recipient UAS FLAG-tagged plasmid with XhoI and XbaI was carried out simultaneously. The digestion protocol was the same as outlined above in subchapter 3.6.1, only this time using XhoI and XbaI restriction enzymes. The two digested products were ligated using the same protocol outlined also in subchapter 3.61, the amount of vector and insert varied depending on the calculated concentrations. The resulting ligated colonies were then verified by colony cracking and GATC sequencing (protocol also outlined in subchapter 3.6.1). The successfully generated UAS FLAG-tagged WT and LIR mutant ArfGAP3 plasmids were shipped to BestGene Inc. in US to generate the new transgenic WT and LM1 ArfGAP3 fly lines.

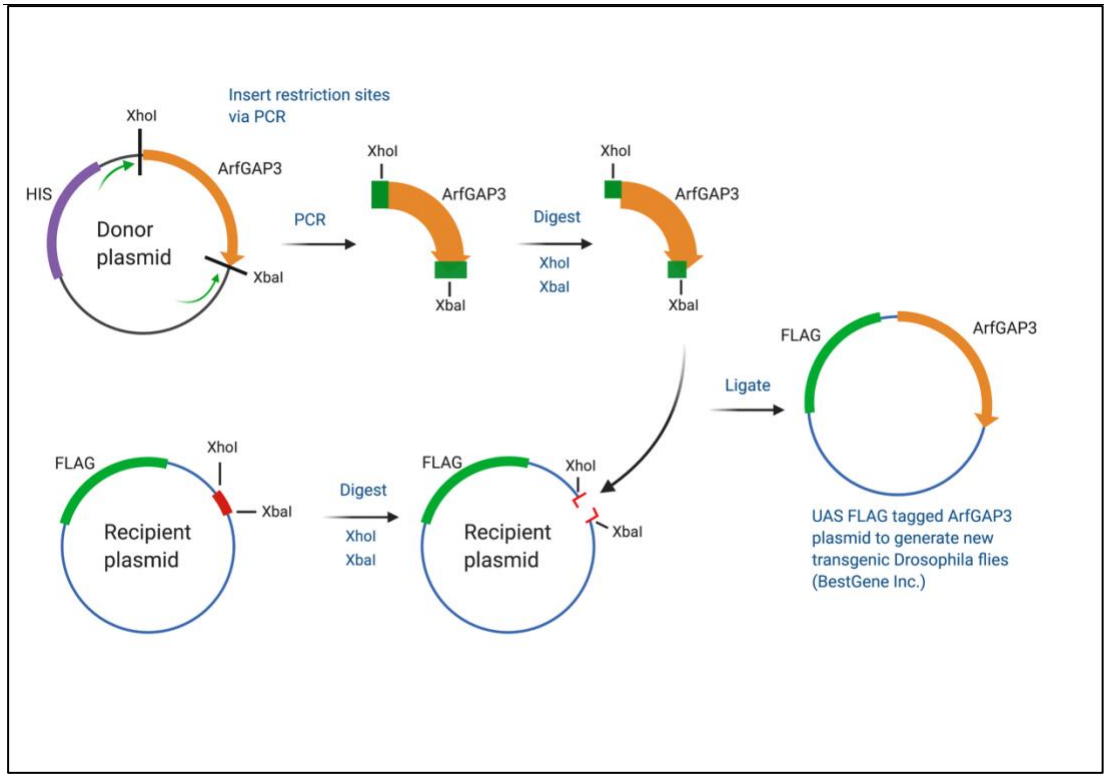

Figure 3.3. Cloning of FLAG-tagged wildtype ArfGAP3 and LIR mutant. Restriction sites XhoI and XbaI were introduced into the HIS tagged ArfGAP3 p28 plasmid via PCR, followed by digestion with XhoI and XbaI to remove the ArfGAP3 gene of interest with XhoI and XbaI overhangs. The UAS FLAG-tagged recipient plasmid was also digested with XhoI and XbaI. The excised ArfGAP3 gene was ligated with the recipient plasmid to create UAS FLAG tagged ArfGAP3 construct (Created with BioRender.com)

3.5.4 Primers

All primers that were used in cloning of N-terminus HIS-Tagged ArfGAP3, site directed mutagenesis for LIR constructs and cloning of UAS FLAG-tagged WT and LIR mutant ArfGAP3 plasmids are outlined below, written in the 5’ to 3’ direction. Primers were ordered from Integrated DNA Technologies (IDT).

Table 3.6. Primers for cloning. Primer sequence of primers used for all cloning experiments written in 5’ to 3’ direction.

Primer name	Primer sequence
Cloning of N-terminus HIS-tagged ArfGAP3	
NdeI forward for ArfGAP3	5’ CCGCATATGATGGACATGGCCAGTCCAGCAGCAGGA 3’
NheI reverse for ArfGAP3	5’ TGGCAAGACAAGTACGGTCGCTAAGCTAGCCCG 3’
Site directed mutagenesis for LIR constructs (PAGE purified)	
ArfGAP3 LIR mutant 1 forward	5’ GATGCGCTGGGCGCCGAGACAGCTGAGCCTATTGGG 3’
ArfGAP3 LIR mutant 1 reverse	5’ CCCAATAGGCTCAGCTGTCTCGGCGCCCAGCGCATC 3’
ArfGAP3 LIR mutant 2 forward	5’ AAGGCTCCCACCGCGTCCTCCGCTACCTATGGCATC 3’
ArfGAP3 LIR mutant 2 reverse	5’ GATGCCATAGGTAGCGGAGGACGCGGTGGGAGCCTT 3’
Cloning of UAS FLAG-tagged WT and LIR mutant ArfGAP3	
XhoI forward for ArfGAP3	5’ CCGCTCGAGATGGACATGGCCAGTCCAGCAGCAGGA 3’
XbaI reverse for ArfGAP3	5’ TGGCAAGACAAGTACGGTCGCTAAGTCTAGACCG 3’

3.6 GST pulldown

3.6.1 Buffers for GST pulldown

The GST pulldown protocol consisted the use of four different buffers; lysis buffer, high salt wash buffer, low salt wash buffer and imidazole wash buffer. The lysis buffer was prepared with 25mM tris pH7.4, 100mM NaCl and 2mM EDTA in dH_2O. On the day of the experiment the buffer was supplemented with 0.01% β-mercaptoethanol, protease inhibitor (1x tablet per 10ml) and 1μg/ml lysozyme. High salt wash buffer was prepared with 25mM tris pH 7.4, 500mM NaCl and 2mM EDTA. Low salt wash buffer was prepared with 25mM tris pH7.4, 50mM NaCl and 2mM EDTA. Imidazole wash buffer was prepared with 25mM tris pH 7.4, 100mM NaCl, 2mM EDTA and 10mM imidazole (this buffer needs to be protected from light).

3.6.2 Protein expression in E. coli

Pre-cultures of GST, GST-Atg8a, GST-Atg8a LDS mutant, N-HIS ArfGAP3 WT and N-HIS ArfGAP3 LIR mutants 1 and 2 were set up by picking a single colony from respective culture plates and inoculating in LB medium supplemented with the appropriate antibiotics. These pre-cultures were incubated at 37°C overnight in a thermal shaker. The following day, 100ml main culture was inoculated at 1:100 with the pre-culture and incubated at 37°C in a thermal shaker until the OD_{600} reached 0.6. Once the optimal OD was reached, 1ml of this culture (before induction) was collected. Protein expression was induced by addition of 0.5mM IPTG in the main culture followed by 16 hours incubation at 16°C. Another 1ml of this culture (after

induction) was collected. The before and after induction cultures were centrifuged in a top-bench centrifuge for 30 seconds at maximum speed. Supernatant was discarded and the pellets were resuspended in 200µl of 1x laemmli buffer, denatured at 95°C for 5 minutes. Samples were loaded (5µl) and ran on an 8% gel followed by Coomassie blue gel staining or western blotting to check for protein expression.

3.6.3 Lysate preparation

The IPTG induced main cultures were centrifuged. Oak Ridge Centrifuge tubes (ThermoScientific 3119-0050) were used in a pre-cooled (4°C) high speed centrifuge with the JA-20 rotor. Cultures were centrifuged at 7,000 rpm for 15 minutes at 4°C. The supernatant was discarded and the pellet was resuspended in 1.5ml lysis buffer (with β-mercaptoethanol, protease inhibitor and lysozyme). The resuspended pellets were transferred into 15ml falcon tubes and subjected to sonication on ice. Sonication parameters were 35% amplitude, 10 sec pulse and 5 sec OFF for 1x 3 minute pulse time. Sonicated lysates were then transferred into the high speed centrifugation tubes and equilibrated with lysis buffer for equal weight. Lysates were centrifuged at 20,000 rpm for 20 minutes at 4°C. The supernatant was collected in 2ml sterile Eppendorf tubes, a 100µl of this supernatant was collected separately for inputs (100µl of 2x laemmli buffer was added to inputs).

3.6.4 Protein purification

3.6.4.1 Preparation of Glutathione Sepharose beads

Glutathione Sepharose 4 Fast Flow beads were used for the pulldowns. The appropriate volume of beads was removed from the bottle and transferred into an Eppendorf tube for use. The beads were sedimented by centrifugation at 500g for 5 minutes. The supernatant was removed and the beads were washed with dH_2O by centrifugation at maximum speed for 30 seconds. The supernatant was removed and this was cycle with dH_2O was repeated four times, followed by a wash with lysis buffer (without β-me, protease inhibitor, lysozyme). After the final wash, beads were resuspended with equal volume of lysis buffer (with β-me, protease inhibitor, lysozyme).

3.6.4.2 Purification of bait and prey proteins

The cell lysates of bait (GST, GST-Atg8a and GST-Atg8a LDS mutant lysates) and prey proteins (ArfGAP3 lysates) were added to the prepared Glutathione beads (100µl) and incubated for 40 minutes at 4°C. The bait protein beads were then sedimented by centrifugation at 500g for 5 minutes, 100µl of the supernatant was collected as flow-through (100µl of 2x laemmli buffer was added to flow-through). The remaining supernatant was removed. The prey protein beads were sedimented by centrifugation at 500g for 5 minutes, the pellet was discarded and the supernatant was collected and kept on ice. A 100µl of the prey supernatant was collected as flow-through. The bait protein beads were washed with high salt wash buffer by

centrifugation at 500g for 5 minutes. Supernatant was removed and beads were washed with lysis buffer (with β-me, protease inhibitor, lysozyme), centrifuged at 500g for 5 minutes. The supernatant was removed.

3.6.5 Protein-Protein interaction assay (In vitro pulldown)

The lysates of the prey proteins (ArfGAP3) was added to the bait protein beads and incubated on a roller at 4°C for 2 hours, followed by centrifugation at 500g for 5 minutes. A 100µl of supernatant was collected as flow-through again (100µl of 2x laemmli buffer was added to flow-through), the remaining supernatant was discarded. The sedimented beads were then washed with lysis buffer (with β-me, protease inhibitor, lysozyme) by centrifugation at 500g for 5 minutes and the supernatant was removed. The beads were washed with imidazole buffer by centrifugation at 500g for 5 minutes and the supernatant was removed. To these pulldown beads, 150µl of 2x laemmli buffer was added and samples were heated at 95°C for 5 minutes.

3.6.6 SDS-PAGE and immunoblotting for pulldown

The pulldown beads, inputs and flow-through samples were all subjected to SDS-PAGE (8% gel), transferred onto a nitrocellulose membrane and immunoblotted for anti-HIS primary antibody 1:2000 (method outlined in 3.4.10). For loading control, the membrane was washed in 0.2% ponceau staining for 1 hour at room temperature.

3.7 Immunoprecipitation

3.7.1 Buffers for IP

RIPA buffer was also used for immunoprecipitation lysate preparation. The RIPA buffer was made fresh using the same recipe outlined in 3.4.1, adding 1x protease inhibitor tablet per 10ml of working stock volume.

3.7.2 Preparation of Protein G Sepharose beads

Protein G Sepharose 4 FastFlow beads were used for immunoprecipitation. The beads were pre-cleared by washing with 4x with dH2O, followed by 4x with RIPA buffer (without protease inhibitor). Between each wash, beads were sedimented by centrifugation at maximum speed for 1 minute at 4°C. An equal volume of RIPA buffer (with protease inhibitor) was added to the beads.

3.7.3 Lysate preparation

Third instar larvae were homogenised with a pestle in RIPA buffer (with protease inhibitor), incubated on ice for 30 minutes prior to 20 minutes centrifugation at 12000 rcf at 4°C. The supernatant was collected for the experiment or stored at -80°C. A small volume of lysate, 50µl, was kept aside as input and protein estimation was performed as outlined in 3.4.6.

3.7.4 Removal of non-specific binding proteins

The larvae lysate was incubated with 60µl of pre-clear beads for 40 minutes at 4°C on a roller (rotating) to remove any non-specific binding proteins. The beads were sedimented by pre-cooled (4°C) top-bench centrifugation at maximum speed for 1 minute. The supernatant was collected and sedimented beads were discarded.

3.7.5 Immunoprecipitation

To the lysate supernatant, 40µl of pre-cleared beads and 2µl of anti-FLAG antibody was added and incubated overnight at 4°C on a rotating roller. This was followed by 3x washed with RIPA buffer (with protease inhibitor), beads were sedimented between each wash by centrifugation at maximum speed for 1 minute at 4°C. Supernatant was discarded and the beads were collected. To the 40µl of beads, 60µl of 2x laemmli buffer was added. Samples were heated at 95°C for 5 minutes.

3.7.6 SDS-PAGE and immunoblotting for IP

IP samples and inputs were loaded (5µl) on 2x 8% gels and subjected to SDS-PAGE. One of the gels was transferred to a nitrocellulose membrane and immunoblotted for monoclonal mouse anti-FLAG 1:1000 (method outlined in 3.4.10). The second gel was stained with Coomassie blue for band detection and excision.

3.8 Mass spectrometry

3.8.1 Proteomics and data analysis of mass spectrometry

Proteomics protocol was carried out in the School of Life Science Proteomics Laboratory. The excised bands of interest was diced into small cubes of 2-4mm and placed in an eppendorf (1.5ml). The gel segments were distained using 50% ethanol 50mM ammonium bicarbonate (ABC) for 20 minutes at room temperature on a shaker (650rpm). The liquid was removed and the gel segments were dehydrated in 100% ethanol for 5 minutes at room temperature shaking at 650rpm, causing the gel to turn white. The next step involved reduction/alkylation, where the gel segments were treated with 10mM TCEP 40mM CAA for 5 minutes at 70°C, with regular intervals of gentle vortex. The gel segments were washed 3x with 50% ethanol 50mM ABC for 20 minutes at room temperature, shaking at 650rpm. The liquid was discarded and the gel segments were dehydrated in 100% ethanol for 5 minutes at room temperature, shaking at 650rpm. The liquid was removed. Gel segments were then hydrated with 2.5ng/µl trypsin for 10 minutes at room temperature. The gel segments were covered with 50mM ABC and incubated overnight at 37°C.

The following day, the liquid around the gel pieces was collected in a new tube and kept aside. In order to extract the peptides, gel segments were treated with 25% acetonitrile 5% formic acid and subjected to sonication for 5 minutes at room temperature. The liquid extractions were collected and combined with the overnight liquid that was set aside. This sonication step was repeated another two times. With the lid open, the Eppendorf with collected liquid was placed into a Speed-Vac for 2 hours. The peptides were concentrated, by bringing the volume down to 20µl. The

resulting peptides were resuspended in 30µl 2% CAN 0.1% TFA to bring the final volume to 50µl. This was transferred into a spin column and centrifuged at maximum speed for 5 minutes. The sample was transferred to a Mass Spec vial ready for Cleidi Zampronio in the Proteomics Lab to run the samples in the mass spectrometer. Mass spectrometry results were analysed using the Scaffold4 program.

3.9 PCR and Real time-qPCR

3.9.1 RNA extraction

RNA extraction was carried out under the fume hood and only sterile equipment was used. Ambion RNA extraction kit was used. Lysis buffer was prepared for each sample from the extraction kit and supplemented with β-me to make a final concentration of 10µl/ml. Third instar larvae were homogenized in the lysis buffer with a mortar and pestle and centrifuged at 12000 rcf for 2 minutes at room temperature. The supernatant was transferred to a new tube and an equal volume of 70% ethanol was added, mixed by vortex and 700µl was transferred into a spin column. The column was centrifuged at 12000 rcf for 15 seconds at room temperature. The flow-through was discarded, 700µl of wash buffer (I) was added to the column and centrifuged at 12000 rcf for 15 seconds at room temperature. The wash with wash buffer (I) was repeated twice. The column was then washed with 500µl wash buffer (II) and centrifuged at 12000 rcf for 15 seconds at room temperature. An additional centrifugation step took place for column drying at 12000 rcf for 1 minute. The collection tube was discarded and replaced with a recovery tube. A volume of 50µl of RNAse free water was added to

the column, incubated for 1 minute and centrifuged at 12000 rcf for 2 minutes. The eluted RNA was then either subjected to reverse transcription or stored at -80°C.

3.9.2 Reverse transcription

The concentration of the eluted RNA was determined using the NanoDrop Spectrophotometer. DNA removal and cDNA synthesis kits were sourced from ThermoScientific.

3.9.2.1 DNA removal

Once the concentration of the eluted RNA was determined, the next step involved DNA removal by setting up the following reaction.

DNA removal

RNA	1µg
10x reaction buffer	1µl
DNAse I	1µl
dH_2O	Up to 10µl

The above reaction was incubated at 37°C for 30 minutes, followed by addition of 1µl of 50mM EDTA and further incubated at 65°C for 10 minutes.

3.9.2.2 cDNA synthesis

The cDNA was synthesised by setting up the following reaction.

cDNA synthesis

RNA	1µg
5x reaction buffer	4µl
10mM dNTP	2µl
Random primers	1µl
Ribolock	1µl
RevertAid	1µl
Total	20µl

The above reaction was incubated at 25°C for 5 minutes, 42°C for 60 minutes and at 70°C for a final 5 minutes.

3.9.3 PCR

For end-point PCR, ThermoScientific DreamTaq™ Green PCR master mix kit (K1081) was used. The PCR reaction was prepared in PCR tubes as outlined below. PCR run settings were adjusted according to primer Tm and amplicon size.

End-point PCR reaction mix	**x1**	**x2**	**x3**	**x4**	**x5**	**x6**
Master mix (2x)	25µl	50µl	75µl	100µl	125µl	150µl
H2O	13µl	26µl	39µl	52µl	65µl	78µl
Forward primer	5µl	10µl	15µl	20µl	25µl	30µl
Reverse primer	5µl	10µl	15µl	20µl	25µl	30µl
cDNA	2µl	4µl	6µl	8µl	10µl	12µl

3.9.4 Gel electrophoresis

The PCR product ran on a 0.7% agarose gel in 1x TAE buffer. Electrophoresis was carried out at 100 V for approximately 1 hour. Bands were either visualised using a UV trans-illuminator.

3.9.5 RT-qPCR

For qPCR, 1:100 dilution of the cDNA was prepared and the following reaction was set up. All reagents used for qPCR was sourced from Promega.

RT-qPCR reaction mix	**x1**	**x3 +1**	**x6 +1**	**x9 +1**	**x12 +1**	**x15 +1**
Master mix (2x)	12.5µl	50µl	87.5µl	125µl	162.5µl	200µl
H2O	6.5µl	26µl	45.5µl	65µl	84.5µl	104µl
Forward primer (10µM)	0.5µl	2µl	3.5µl	5µl	6.5µl	8µl
Reverse primer (10µM)	0.5µl	2µl	3.5µl	5µl	6.5µl	8µl
Total	20µl	80µl	140µl	200µl	260µl	320µl

The reaction mix was set up in Mx3000P® 96-well plates from Agilent Technologies. To each tube in the plate, 5µl of the diluted cDNA was added and pipetted up and down to mix thoroughly. Agilent Technologies Stratagene Mx3005P machine, located in the School of Life Science Genomics Facility Lab, was used to run the qPCR plate. The qPCR data was analysed using the MxPro QPCR Software.

3.10 Transmission Electron Microscopy

CgGal4 driver was crossed with UAS ArfGAP3 RNAI (old) line to create progeny expressing ArfGAP3 RNAI in the *Drosophila* fat bodies. Fed and 4hrs starved (20% sucrose) ArfGAP3 RNAI third instar larvae from the mentioned cross and ArfGAP3 mutant third instar larvae fat bodies were dissected and fixed in 2% glutaraldehyde in PBS for 1.5 hours at room temperature. The fat body tissues were washed 3x in PBS at room temperature for 5 minutes each, followed by 3x washes with dH_2O. From this point onwards Dr Saskia Bakker (SLS imaging suite) continued the protocol for TEM in the imaging suite as outlined in 'Preparation of Drosophila follicles for transmission electron microscopy' by Palara et al, 2016. TEM images were acquired in the imaging suite by Dr Saskia Bakker using the Jeol 2100Plus TEM. Acquired TEM images were further analysed using FIJI.

3.11 Lifespan assay

Survival (longevity) assay was performed on UAS ArfGAP3 RNAi (VDRC B) and UAS luciferase RNAi (control) flies to measure lifespans and check how the flies age. A cohort of 100 control flies and 100 ArfGAP3 RNAi flies, both males and females

separate, were collected. Flies were collected 24 hours of hatching and placed in multiple tubes (max 20-25 flies in each) supplemented with *Drosophila* food and kept in 25°C incubator to age. The flies were transferred to fresh vials every 2 to 3 days and number of dead flies were recorded at each transfer.

3.12 Climbing assay

A climbing assay was performed on the same cohort of flies collected for the lifespan assay to test the climbing ability of 1 week, 4 weeks and 8 weeks old flies. A maximum of 20 flies were transferred into separate climbing vials. These climbing vials were split into 3 segments, <1.5 cm (low), 1.5-6cm (middle) and 6-11.5cm (high). Once flies were transferred to the climbing vials, they were left to rest for 20 minutes. The flies were tapped down and number of flies climbing segment by segment was recorded twice within a 20 second period, at 10 and 20 seconds after vial was tapped down. This provided an indication of the initial reflex response at 10 seconds and a prolonged response at 20 seconds. For each segment the proportion of flies were calculated. In order to carry out statistical analysis, there were 3 vials for each genotype at each age criteria and each experiment was carried out 3 times with rest periods between each test.

3.13 Statistical analysis

Graphpad Prism version 8 was used for all statistical analyses in this thesis. When testing for statistical significance between two conditions, an unpaired student's t-test was performed. A one-way ANOVA was performed for statistical analysis for multiple comparisons. A statistical significance was considered when the p value was

below 0.05. For confocal experiments, the N number has been stated in each figure legend. For western blotting analysis, statistical analysis was carried out on 3 biological replicates (lysates from different sets of flies).

Part II

Results

Chapter 4

ArfGAP3 is a novel Atg8a-interacting protein

4.1 Chapter introduction: Yeast-two hybrid reveals ArfGAP3 as Atg8a-interacting protein

A popular expression that fits the investigation of proteins is "A man is known by the company he keeps". In order to characterise the function of a target protein, the most common technique is to identify its interacting partners. From this approach, it is possible to deduce the protein's function based on the interacting proteins function (Felgueiras, Silva and Fardilha, 2018). The presence of complex networks formed by interactions between different components, primarily proteins, is a fundamental property in all complex biological systems. These interactions are key for all levels of cellular function, to name a few, cell homeostasis, signalling, synthesis of biomolecules, metabolism, architecture etc (Brückner *et al.*, 2009). There are a number of techniques used to investigate protein-protein interactions. Yeast-two hybrid is a high-throughput screening by which protein-protein interactions are identified and is an in vivo approach (Felgueiras, Silva and Fardilha, 2018).

Since Atg8a is an important marker of *Drosophila* autophagy, a recent yeast-two hybrid screen was performed by colleagues in Nezis Laboratory in both *Drosophila melanogaster* 3rd instar larvae and whole fly head for Atg8a-interacting proteins. The results from this screen identified the GTPase activating protein, ArfGAP3, as an Atg8a-interacting protein. The screen also identified the selected interacting domain (SID) as the Atg8a-interacting domain within the ArfGAP3

sequence in the third instar larvae and whole fly head, at 293 to 409 and 206 to 414 residues respectively (figure 4.1). The yeast-two hybrid screen also revealed that the interaction between the two proteins was of 'high-confidence' (denoted as level B interaction) in the *Drosophila* larvae and of 'good confidence' (denoted as level C interaction) in the *Drosophila* whole fly head. Hence, ArfGAP3 was selected as a promising candidate to investigate further its role in autophagy. This chapter summarises the findings that confirms ArfGAP3 is a novel Atg8a-interacting protein.

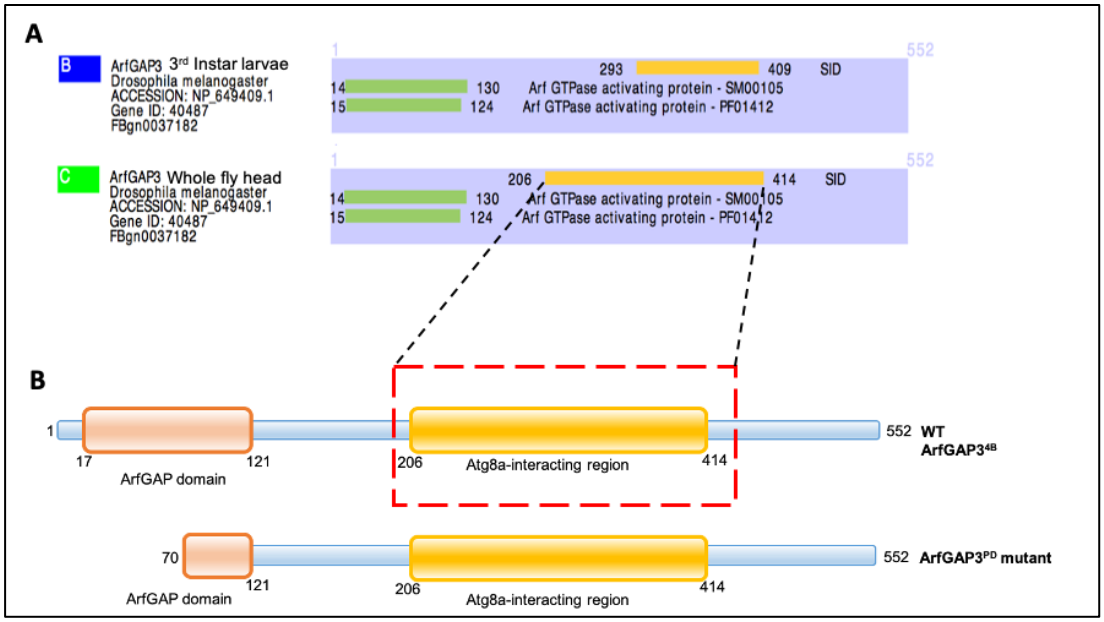

Figure 4.1. ArfGAP3 is an Atg8a-interacting protein. A) Yeast-two hybrid screening by Nezis lab revealed ArfGAP3 as an Atg8a-interacting protein. In *Drosophila* 3rd instar larvae, there is a 'high confidence' interaction between the two proteins (level B) and in *Drosophila* whole fly head, there is a 'good confidence' interaction (level C). The yeast-two hybrid screen also reveals the 'selected interacting domain' (SID – in yellow) which is known to be the Atg8a-interacting domain. The SID within the ArfGAP3 sequence in third instar larvae is between residues 293 and 409, and between 206 and 414 in the whole fly head. B) schematic illustration of wildtype ArfGAP3 and ArfGAP3 mutant sequence highlighted with the Atg8a-interacting region (in yellow) and the ArfGAP domain.

4.2 ArfGAP3 co-localises with Atg8a in *Drosophila melanogaster*

In order to confirm the interaction of ArfGAP3 with Atg8a by co-localisation studies, Cg-Atg8aGFP-Gal4 flies were crossed with UAS-ArfGAP3 WT line tagged with DsRed. The resulting progeny of flies expressed GFP tagged Atg8a positive autophagosomes and DsRed tagged WT ArfGAP3 in fat bodies. A mutant line for ArfGAP3 (denoted PD on flybase), which has the first 70 amino acids deleted (figure 4.1B) and tagged with DsRed, was also crossed with Cg-Atg8a-GFP-Gal4 and used for comparison. Immunofluorescence with DAPI staining was carried out on fed and 24 hour starved fat bodies. For this initial co-localisation experiment, we did not use ArfGAP3 antibody. In preliminary fluorescence microscopic analysis of fat bodies with the ArfGAP3 antibody, the antibody did not produce a clear strong signal that was reliable to use for the co-localisation experiment. Hence, we used the overexpression system approach. The tissues were mounted onto microscopic slides and immediately observed with confocal microscopy.

As expected, wildtype ArfGAP3 fed fat bodies showed diffused cytoplasmic staining of both Atg8a and ArfGAP3 as both proteins are localised to the cytosol (figure 4.2A). Under starved conditions, when autophagy is initiated, both ArfGAP3 and Atg8a localised to autophagosomes in both ArfGAP3 WT and mutant lines. However, merged analysis only showed wildtype DsRed-ArfGAP3 co-localised with GFP-Atg8a-positive autophagosomes post starvation induced autophagy compared to its truncated form DsRed-ArfGAP3-PD which showed no co-localisation (figure 4.2B/C). This confirmed ArfGAP3 and Atg8a are co-localised for subsequent interaction and indicates that the first 70 amino acid region is essential for the

interaction with Atg8a in addition to the selected Atg8a-interacting domain predicted by the yeast two hybrid screening.

To quantify ArfGAP3-Atg8a co-localisation observed, the Pearson's correlation coefficient was calculated from all images for both WT and mutant ArfGAP3. Pearson's correlation coefficient was the chosen algorithm to quantify the overlap of the GFP and DsRed signals in comparison to the commonly used Mander's coefficient since the latter is more suitable for cell culture in which the cells are organised in a single layer as Mander's coefficient is very susceptible to background noise. On the other hand, *Drosophila* fat body tissues vary in tissue thickness and orientation and so acquisition settings constantly need to be changed. For this reason, Pearson's correlation coefficient is an ideal choice for quantifying the overlap of signals as it is less affected by acquisition setting changes (Adler and Parmryd, 2010). The stronger the co-localisation, the closer the Pearson's coefficient to 1. If there is no co-localisation, the Pearson's coefficient will be closer to -1. Quantification analysis confirms that the ArfGAP3- Atg8a colocalization was lost with the ArfGAP3 PD mutant line, as the average Pearson's Coefficient was significantly reduced by 1.276 in the ArfGAP3 PD mutant (-0.5915) compared to WT ArfGAP3 (0.6843). An unpaired two-tailed t-test was performed as statistical analysis, confirming the difference in co-localisation between WT ArfGAP3 and mutant ArfGAP3 was highly significant, $p < 0.0001$ (figure 4.2D).

Using the overexpression of protein system comes with imitations. Overexpression of any protein can be damaging to a cell as it exhausts resources to produce and traffic proteins (Stoebel *et al*, 2008; Bolognesi and Lehner, 2018). In addition, overexpression of a protein can burden cellular machinery responsible for protein production, maturation of proteins, localization of proteins, all of which

demands high levels of energy (Shah *et al*, 2013; Rice and McLysaght, 2017). However, a study by Eguchi et al in yeast, reports that overexpression of a protein only becomes destructive and causes protein burden to the cell when it forms 15% of the cell's total protein content (Bolognesi and Lehner, 2018; Eguchi *et al*, 2018).

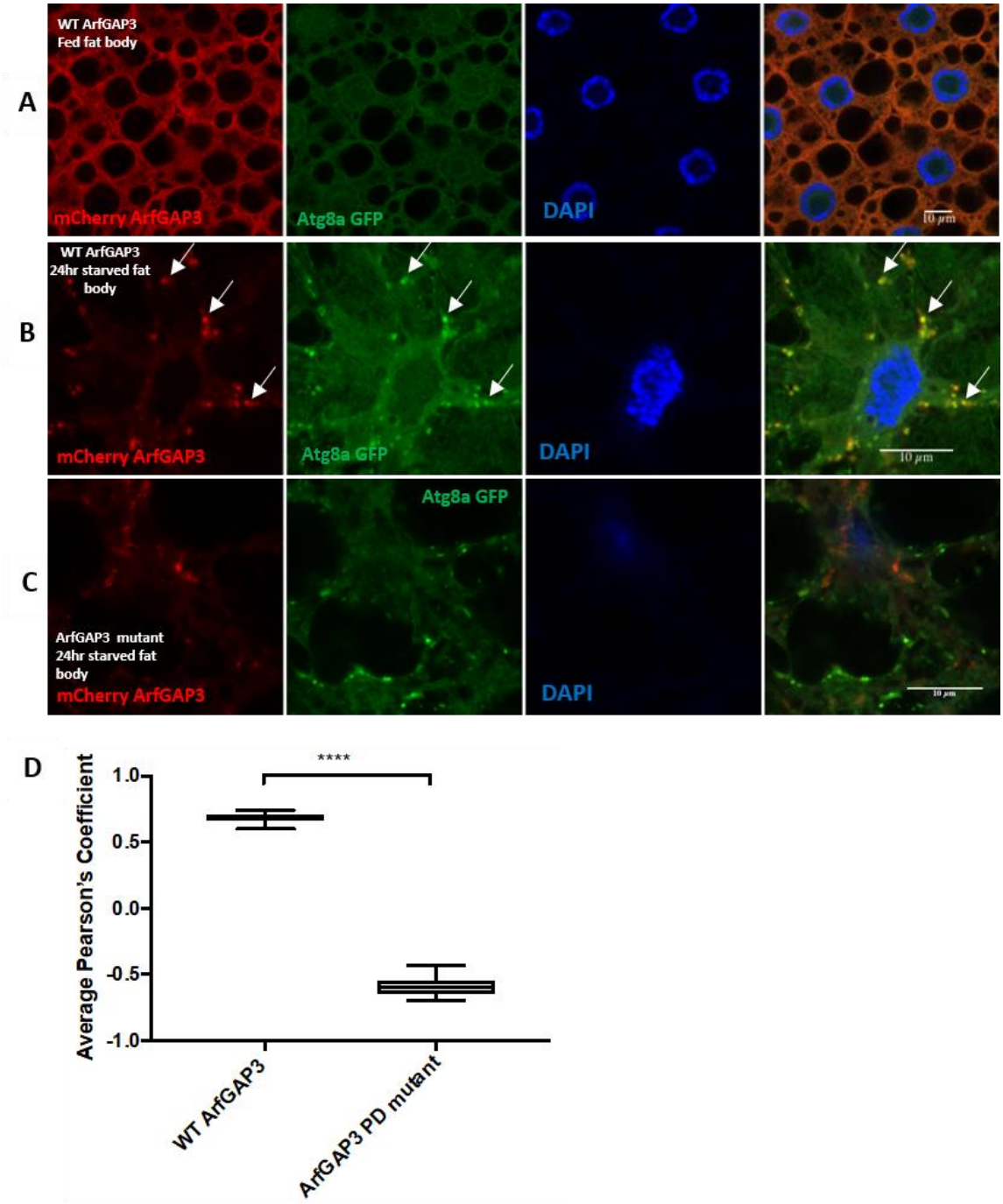

Figure 4.2. ArfGAP3 co-localises to Atg8a in *Drosophila*. Confocal sections of fat bodies captured at 63x magnification from A) fed third instar larvae from cross cg::Atg8aGFP-GAL4 x UAS ArfGAP3^{DsRED4B}, B) 24 hr starved larvae from cross cg::Atg8aGFP-GAL4 x UAS ArfGAP3^{DsRED4B} and c) 24 hr starved larvae from cross cg::Atg8aGFP-GAL4 x UAS ArfGAP3-PD^{DsRED3B} clonally expressing DsRED ArfGAP3 and GFP-Atg8a. ArfGAP3-PD is the truncated form of the protein, with a deletion in the first 70 amino acids. Scale bars are 10μm, n = 50 D) Coloc2 plugin in FIJI was used to quantify co-localisation of DsRED and GFP signals using Pearson's Correlation Coefficient. Average Pearson's Coefficient was significantly reduced by 1.276 in the ArfGAP3 PD mutant (-0.5915) compared to WT ArfGAP3 (0.6843). An unpaired two-tailed t-test was performed as statistical analysis, confirming the difference in co-localisation between WT ArfGAP3 and mutant ArfGAP3 was highly significant, p <0.0001.

4.3 Exploring the LIR motifs in ArfGAP3 protein sequence.

Nezis laboratory, in collaboration with Kalvari *et al*, developed a database called the iLIR at the University of Warwick (https://ilir.warwick.ac.uk) (Kalvari *et al*, 2014). This server is able to screen *Drosophila* protein sequences in FASTA format for putative LIR motifs, the significant motif responsible for the interaction with Atg8a protein. Both relaxed (xLIR) and conventional (WxxL) LIR motifs, described in subchapter 1.2.7, can be identified using this tool. The blast search will also reveal the primary sequence and the amino acid position of each LIR motif, the position specific scoring matrix (PSSM) score as well as an 'Anchor' result. The PSSM score is a measure of confidence for a motif in biological sequences. Several functionally related sequences are aligned to generate the matrix. The matrix displays log-based values that gives a score representing the presence of a particular residue in that aligned position. The higher the score, the more frequent the residue at that position of the alignment (Kalvari *et al*, 2014; Jacomin *et al*, 2017). The anchor results provide an indication if the motif is present within an intrinsically disordered region (Anchor region) (Meszaros *et al*, 2009) and is a key indicator high confidence protein-protein interaction (Mei *et al*, 2014). The lack of stable secondary and tertiary protein structures is a key feature for intrinsically disordered proteins. For this reason, upon binding to other macromolecules, these proteins can take up a fixed three-dimensional structure (Mei *et al*, 2014). Thus, the iLIR database recognises LIR motifs within Anchor regions as reliable functional LIR motifs.

The ArfGAP3 protein sequence was screened using the iLIR software which produced several hits of LIR motifs (figure 4.3). The results from the iLIR blast showed 7 potential LIR motifs, of which the one was highlighted in red as the xLIR

(relaxed) LIR motif and the following 6 are classed as conventional LIR motifs. This xLIR is the most likely LIR motif that is involved in the interaction with Atg8a due to its high PSSM score and location within an anchor region. The xLIR is located between residues 392 and 397 within the ArfGAP3 sequence. Most interestingly, this LIR motif is also located within the Atg8a-interacting region (residues 206 to 414) which was identified through the Y2H screening, further suggesting this particular LIR motif could be a key LIR motif for the interaction with Atg8a.

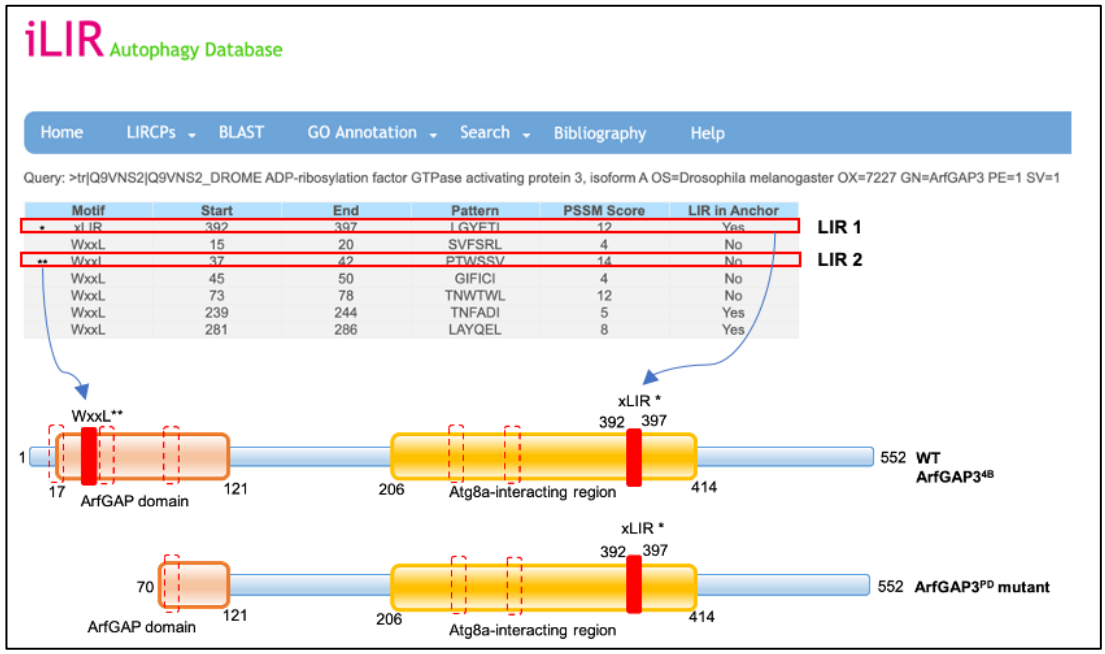

Figure 4.3. Exploring the LIR motifs in *Drosophila* ArfGAP3 sequence. Screenshot of the iLIR blast results for ArfGAP3 protein sequence highlighted seven LIR motifs, of which the top hit in the table, xLIR, was identified as the relaxed LIR motif (the most probable LIR motif involved in the interaction). WxxL motifs are conventional LIR motifs. Highlighted in red are the two LIR motifs that were selected for further investigations due to its high PSSM score and location within the sequence.

4.4 ArfGAP3 interacts with Atg8a in a LIR dependent manner.

To prove ArfGAP3 and Atg8a interact biochemically, a GST-pull down experiment was carried out. Three separate bacterial cultures expressing GST, GST-Atg8a and GST-Atg8a LDS$^{K48A, Y49A}$ (LIR docking site) mutant were set up. Cultures of wildtype N-HIS ArfGAP3 were also set up. A sample of the cultures before and after the IPTG

induction were subjected to SDS-PAGE, Coomassie blue staining and western blotting probed for anti-HIS tag to check for expression of each protein. All four proteins were expressed successfully in the cultures, a more intense band is observed for all cultures after IPTG induction (figure 4.4A).

Upon successful expression of N-terminus HIS-tagged ArfGAP3, three separate pull downs were carried out with wildtype ArfGAP3: 1) GST, 2) GST-Atg8a and 3) GST-Atg8a LDS $^{K48A, Y49A}$ mutant. The GST only with wildtype ArfGAP3 was carried out as a control pulldown to confirm that any interaction seen was solely with Atg8a and not with GST. The GST only pull down with wildtype ArfGAP3 showed no interaction as expected. There was a strong interaction observed between GST-Atg8a and wildtype (WT) ArfGAP3, even at low exposure when developing the western blot. The GST-Atg8a LDS pulldown showed a clear reduction in band intensity, showing the interaction is significantly reduced by 10-fold in the Atg8a LDS mutant compared to wildtype Atg8a (figure 4.4). All bands shown in the western blot were included in the quantification and statistical analysis revealed that the reduction in interaction was highly significant ($p=0.0002$). These results further support that there is an interaction between ArfGAP3 and Atg8a and suggests that the interaction is LIR dependent.

Since the interaction between ArfGAP3 and Atg8a shows to be LIR dependent, the next step was to further confirm this observation by checking the interaction when the LIR motif was mutated. Two mutant constructs of ArfGAP3 were created, which had different LIR motifs mutated by site directed mutagenesis. The first mutant construct had the xLIR motif, LGYETI, mutated and was denoted as LIR1. The second mutant construct had the conventional LIR motif, PTWSSV, mutated and was denoted as LIR2 (Figure 4.3). For both LIR motifs, the third and sixth amino acid residues

were altered to an alanine residue. The resulting sequence was LGAETA for LIR1 and PTASSA for LIR2. Alanine was the chosen amino acid residue for the mutation as it is a neutral amino acid, and it has the least effect on the structure of the motif. GATC sequencing was carried out to check if the two-point mutations were successful. Both ArfGAP3 LIR mutated constructs (LM1 and LM2) showed the LIR motifs were successfully mutated. The sequencing results show nucleotide bases 'TA' and 'AT' in the third and sixth amino acid codons were changed to bases 'GC' and 'GC' respectively in LIR motif 1 and bases 'TG' and 'GT' in the same amino acid positions were changed to bases 'GC' in LIR motif 2 (figures 4.5A and 4.6A).

4.4.1 ArfGAP3 interacts with Atg8a via LGYETI LIR motif

The three separate GST pull downs (GST, GST-Atg8a and GST-Atg8a LDS) were carried out with ArfGAP3 LIR1 mutant (LM1) alongside simultaneous pulldowns with WT ArfGAP3. A strong interaction was observed again between GST-Atg8a and WT ArfGAP3. As seen the first time, the interaction between Atg8a and WT ArfGAP3 was significantly reduced in the GST-Atg8a LDS by 10-fold ($p<0.0001$) (figure 4.5C/D). In the simultaneous pulldown with ArfGAP3 LM1, an interaction was observed between GST-Atg8a and ArfGAP3 LM1 (figure 4.5E/F), however, this interaction was reduced by 3-fold compared to the interaction observed with WT ArfGAP3 (figure 4.5G). This strongly suggested that the LIR1 motif (LGYETI) is a functional LIR motif that mediates the interaction between Atg8a and ArfGAP3.

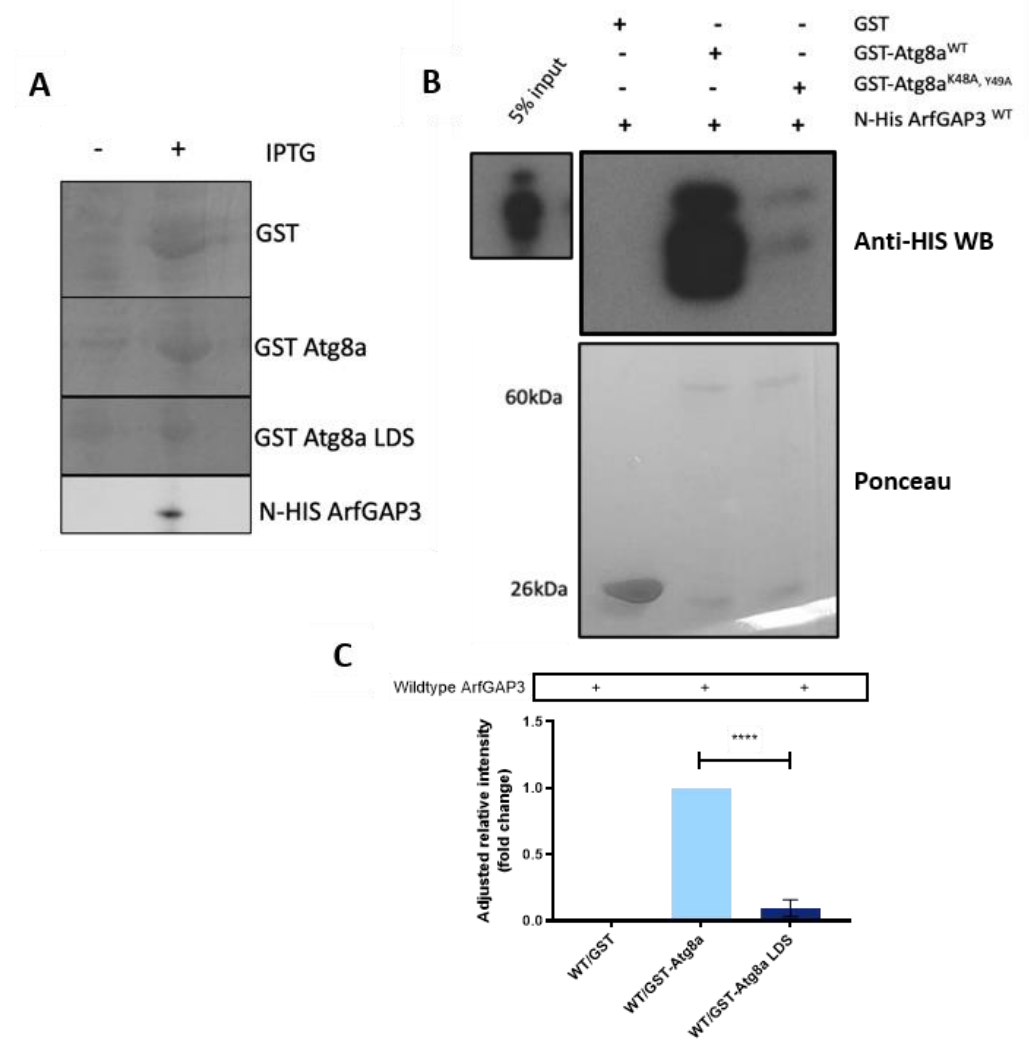

Figure 4.4. ArfGAP3 interacts with Atg8a in a LIR dependent manner. A) Protein expression in Rosetta bacteria. Bacterial cultures were treated with 0.5mM IPTG for GST, GST-Atg8a, GST-Atg8a LDS and N-HIS ArfGAP3. All proteins were expressed post IPTG induction. B) Three separate pull downs were carried out simultaneously with WT ArfGAP3. Ponceau staining was used for normalisation. For all three pulldowns, n = 3. A significant reduction in ArfGAP3 – Atg8a interaction is observed in the GST-Atg8a LDS mutant pulldown compared to GST-Atg8a. C) Band intensity quantification was carried out using FIJI and statistical analysis (one way ANOVA) carried out using GraphPad Prism 7, p value =0.0002, error bars denote SEM.

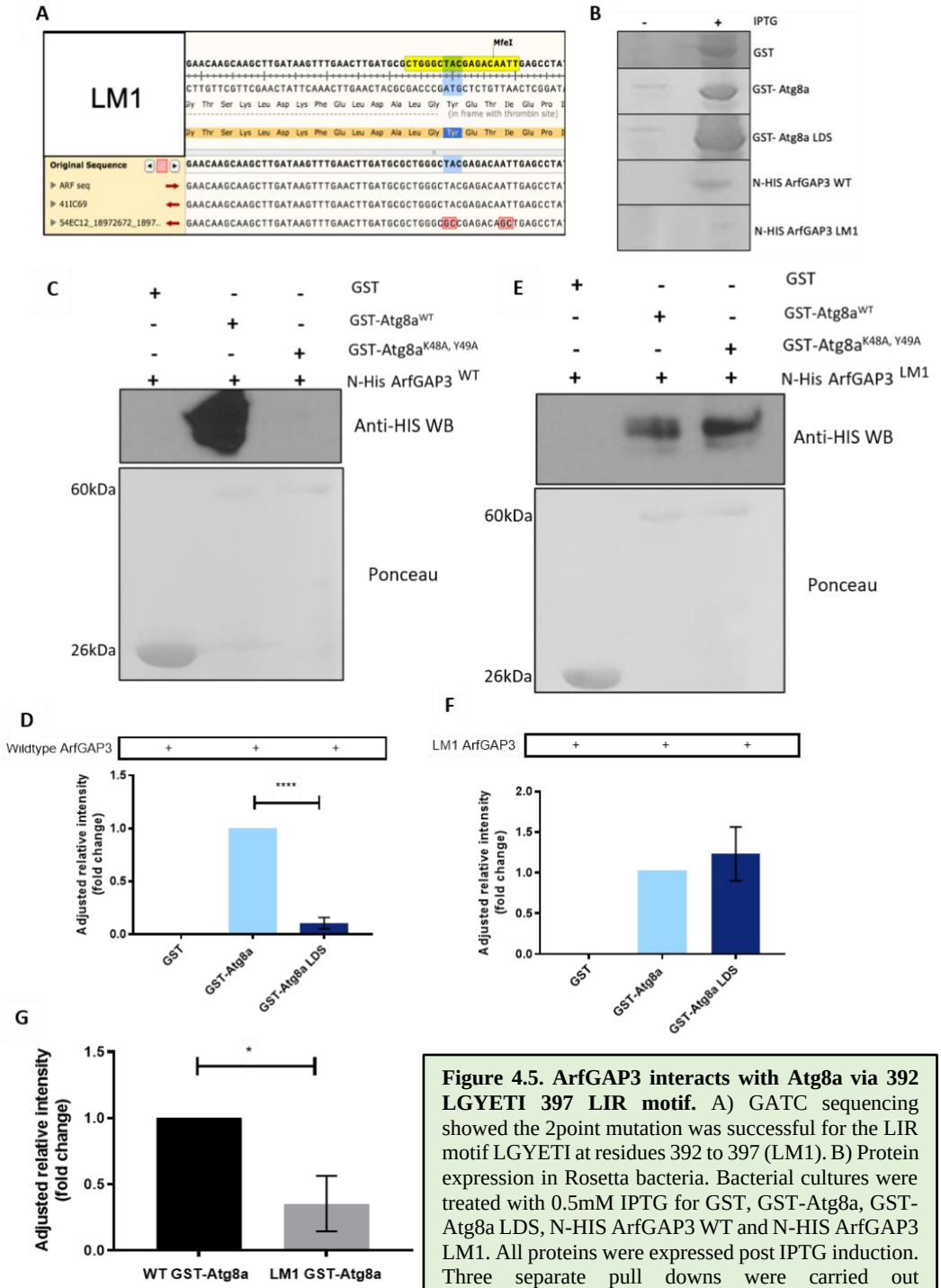

Figure 4.5. ArfGAP3 interacts with Atg8a via 392 LGYETI 397 LIR motif. A) GATC sequencing showed the 2point mutation was successful for the LIR motif LGYETI at residues 392 to 397 (LM1). B) Protein expression in Rosetta bacteria. Bacterial cultures were treated with 0.5mM IPTG for GST, GST-Atg8a, GST-Atg8a LDS, N-HIS ArfGAP3 WT and N-HIS ArfGAP3 LM1. All proteins were expressed post IPTG induction. Three separate pull downs were carried out simultaneously with both WT ArfGAP3 (C) and LM1 ArfGAP3 (E). Ponceau staining was used for normalisation. For all pulldowns, n = 3. G) A significant reduction in ArfGAP3 – Atg8a interaction is observed in the GST pulldown with LM1 compared to WT. D/F/G) Band intensity quantification was carried out using FIJI and statistical analysis (T-test and one way ANOVA) carried out using GraphPad Prism 7. Error bars denote SEM. P values; pull down with ArfGAP3 WT <0.0001, comparing GST-Atg8a WT pulldown and GST-Atg8a LM1 pulldown 0.0368.

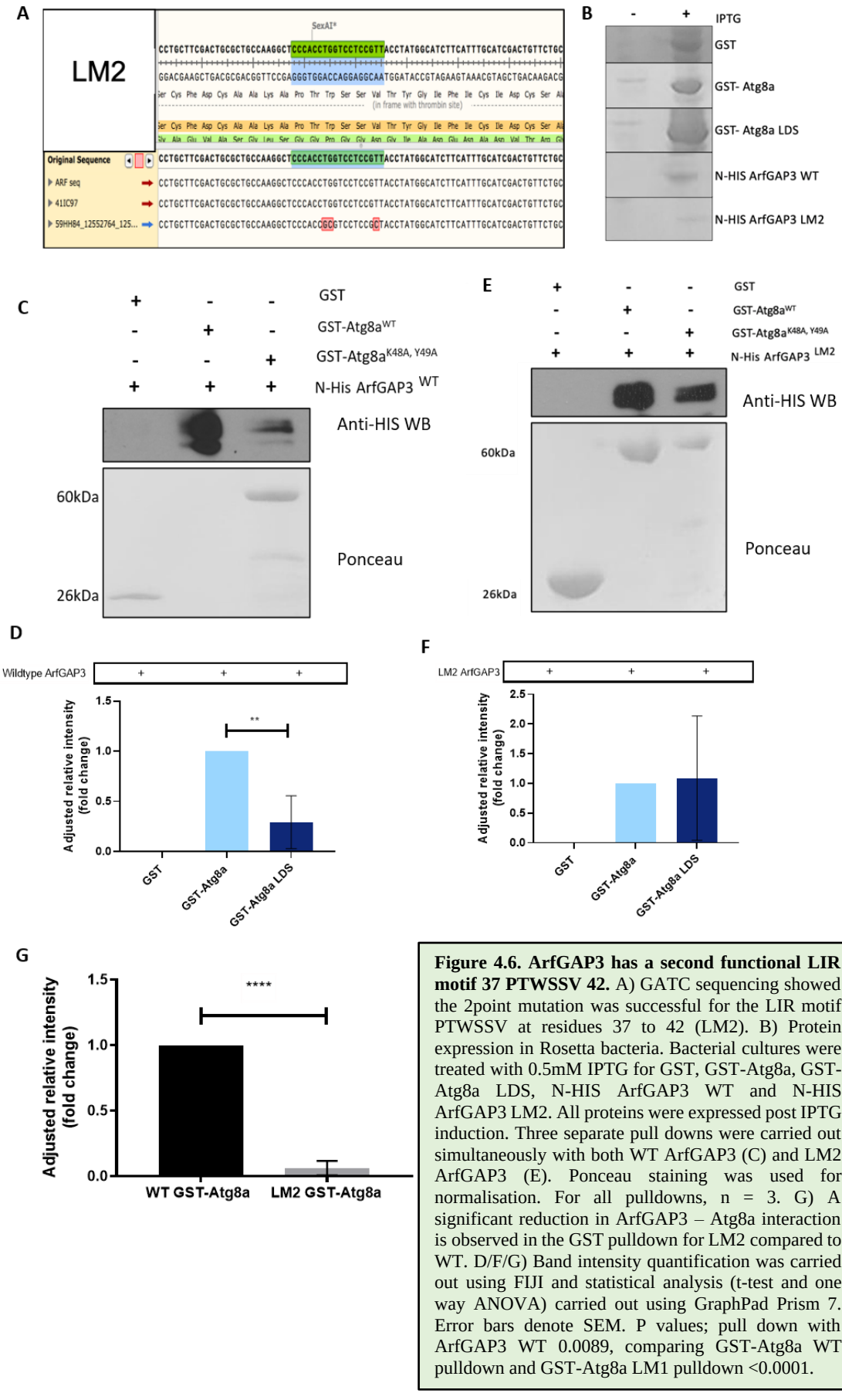

Figure 4.6. ArfGAP3 has a second functional LIR motif 37 PTWSSV 42. A) GATC sequencing showed the 2point mutation was successful for the LIR motif PTWSSV at residues 37 to 42 (LM2). B) Protein expression in Rosetta bacteria. Bacterial cultures were treated with 0.5mM IPTG for GST, GST-Atg8a, GST-Atg8a LDS, N-HIS ArfGAP3 WT and N-HIS ArfGAP3 LM2. All proteins were expressed post IPTG induction. Three separate pull downs were carried out simultaneously with both WT ArfGAP3 (C) and LM2 ArfGAP3 (E). Ponceau staining was used for normalisation. For all pulldowns, n = 3. G) A significant reduction in ArfGAP3 – Atg8a interaction is observed in the GST pulldown for LM2 compared to WT. D/F/G) Band intensity quantification was carried out using FIJI and statistical analysis (t-test and one way ANOVA) carried out using GraphPad Prism 7. Error bars denote SEM. P values; pull down with ArfGAP3 WT 0.0089, comparing GST-Atg8a WT pulldown and GST-Atg8a LM1 pulldown <0.0001.

4.4.2 ArfGAP3 has a second functional LIR motif.

The three separate GST pull downs (GST, GST-Atg8a and GST-Atg8a LDS) were also carried out with ArfGAP3 LIR2 mutant (LM2) alongside simultaneous pulldowns with WT ArfGAP3. The pulldowns were carried out three times for statistical analysis. The strong interaction between Atg8a and WT ArfGAP3 was seen for the third time in the GST-Atg8a pull down and this interaction was reduced in the GST-Atg8a LDS pulldown by 3-fold (figure 4.6C/D). The pulldown carried out with ArfGAP3 LM2 showed an interaction between Atg8a and ArfGAP3 LM2 (figure 4.6E). Although the interaction between ArfGAP3 LM2 and GST-Atg8a (figure 4.6E/F) compared to the interaction between WT ArfGAP3 and GST-Atg8a (figure 4.6C/D) does not appear significantly different in the western blotting analysis, quantification analysis carried out with all replicates in GraphPad prism showed the interaction between Atg8a and ArfGAP3 was reduced by 16-fold in the pulldown with ArfGAP3 LM2 compared to the pulldown with WT ArfGAP3. Statistical analysis confirmed this reduction in interaction was highly significant ($p<0.0001$) (figure 4.6G). Due to time constraints, more pulldown repeats could not be carried out. Although these pulldown results suggested that ArfGAP3 has a second functional LIR motif (PTWSSV), the LIR mutant pulldowns (LIR1 and LIR2) will need to be repeated for better represented western blots since there were some variations in results. Hence, by increasing the number of repeats, this will help further support and reliably conclude the pulldown observations.

The GST pulldown data indicates that Atg8a and ArfGAP3 interact via LIR1 and LIR2 motifs since both LIR mutants of ArfGAP3 exhibit reduced interaction with Atg8a. The results here showed that the site-directed mutagenesis via alanine scanning

was a successful approach to determine specific residues responsible for the interaction. This is in line with a recent study that investigated the change in binding affinity of proteins upon point mutations, in which they revealed 85 out of 110 mutated proteins showed decreased binding affinities (Wang *et al*, 2020). In addition, the GST pull down data suggests the inactivation of one or the other LIR motifs is solely not sufficient to completely block the interaction, instead it only reduces the interaction. However, in both cases, there is still some level interaction present. Previous studies have reported it is possible to have more than one functional LIR motif. For example, mATG4 consists of two functional LIR motifs. One of the LIR motifs is the N-terminal LIR, APEAR which is involved in binding and deletion of ATG8-PE. The other LIR motif is the C-terminal LIR involved in constitutive binding to ATG8 (Abreu *et al*, 2017; Park *et al*, 2019). Since there is more than one functional LIR motif, only one can bind to the LDS pocket of Atg8a at any given time during interaction, it could be LIR1 or alternatively LIR2. If both LIR motifs are required functionally for the interaction, this gives insights that there could be a second binding site that could possibly bind the LIR motif. A new interface between plant Atg8 and its interacting proteins was discovered in *Arabidopsis* (Marshall *et al*, 2015; Marshall *et al*, 2019), which is also conserved in both yeast and human (Lei and Klionsky, 2019) and has been identified as the interaction interface for LIR-LDS independent interaction with Atg8. This alternative interface was identified as the ubiquitin-interacting motif (UIM)-UIM docking site (UDS). Experimental data revealed that the UDS domain is located opposite to the LDS domain on Atg8 and hence this brought to light the possibility that LIR-containing proteins and UIM-containing proteins can bind simultaneously to Atg8 (Lei and Klionsky, 2019). Interestingly, proteins that do not possess the UIM motif are still able to bind to Atg8 via the UDS interface (Lei and

Klionsky, 2019). Taking this into account, it could be possible that the LIR motifs could also bind to the UDS domain and thus this gives rise to the possibility of ArfGAP3 interacting with Atg8a via the LIR1 and LIR2 motifs binding to LDS and UDS domains of Atg8a. This notion could possibly also explain why the interaction of ArfGAP3 is not fully eliminated, rather significantly reduced, with GST-Atg8a LDS. If this is the case, ArfGAP3 LIR motifs might be able to bind to the UDS domain but with lower specificity and affinity compared to the LDS domain. This will be further discussed in the later discussion chapter.

When comparing the GST pulldown results observed for both LIR1 and LIR2 motif, it is clearly noticeable that the overall reduction in interaction with the LIR2 mutant is higher than the reduction in interaction with LIR1 mutant (figure 4.5G and 4.6G). A possible explanation for this is that the LIR2 motif has a higher binding affinity to the LDS pocket on Atg8a than the LIR1 motif. It has been reported that the tryptophan residue (W), in the highly conserved third position within the consensus LIR motif, binds to the HP1 pocket of the LIR docking site more strongly than phenylalanine (F) and tyrosine (Y) residues (Johansen and Lamark, 2020). A previous study showed that altering the tyrosine residue (Y) to a tryptophan residue (W) within the NBR1 LIR motif had enhanced its binding affinity by 7.5-fold (Rozenknop *et al*, 2011; Johansen and Lamark, 2020).

A band was also seen in the GST-Atg8a LDS pull down with ArfGAP3 LM1 (figure 4.5E) and ArfGAP3 LM2 (figure 4.6E). At first, this seemed to not be a significant result and it was assumed this was most likely was due to false-positive protein interactions. In theory, since the third and sixth amino acid residues in both LIR1 and LIR2 motifs are mutated and the third and sixth amino acids of the LIR docking site on Atg8a are also mutated, this causes a change in binding affinity and

ligand specificity, resulting in no interaction. Hence, the two proteins would not be able to take up the "lock and key" conformation for effective binding. A study in 2019 demonstrated an amino acid point mutation by substitution can dramatically change the binding affinity and ligand specificity of proteins (Ricatti *et al*, 2019). A common overlooked issue in GST-pulldown assays is nucleic acid contamination in protein preparations, causing possible false-positive interactions as observed between the ArfGAP3 LIR mutant constructs and GST-Atg8a LDS. Nucleic acid, being a negative charged polymer, has the ability to adhere to basic surfaces on proteins, facilitating the interaction of the immobilized bait protein with the target protein. Thus, contaminating nucleic acid may contribute to false positive protein interactions or general background (Nguyen and Goodrich, 2006). A solution to overcome false-positive interactions due to contaminated nucleic acids would be to subject the protein preparations to micrococcal nuclease treatment, following the protocol outlined in Nguyen and Goodrich, 2006.

In order to further conclude on how the two LIR motifs are responsible for the interaction between Atg8a and ArfGAP3, a GST pull down should be carried out with an ArfGAP3 construct that would have a double mutation, for both LIR1 and LIR2 motifs and examine simultaneously the role of the UDS domain for this interaction if any. Additionally, data can further be supported with other protein-protein interaction assay such as co-immunoprecipitation.

4.5 Generating wildtype ArfGAP3 and LIR mutant ArfGAP3 transgenic flies.

The GST-pulldown experiments provided good biochemical evidence that Atg8a and ArfGAP3 interact and that these two LIR motifs are essential for the interaction. The next step was to clone these sequences into a UAS FLAG plasmid to send off to BestGene Inc (US), a company that can generate new transgenic fly lines that will express these proteins. These flies can then be used for further experiments. The cloning method for this involved using restriction enzymes to excise the ArfGAP3 gene from the current p28 plasmid and insert it into the new UAS FLAG plasmid. The UAS FLAG plasmid that was used had a TAK1 gene inserted which had to be excised using XhoI and XbaI restriction enzymes (figure 4.7A).

The TAK1 gene was successfully excised out of the UAS FLAG plasmid using restriction enzymes XhoI and XbaI. Since these two restriction enzymes were not located on either end of the ArfGAP3 gene in the p28 plasmid, XhoI and XbaI restriction enzyme sites were introduced via PCR cloning at these locations for WT ArfGAP3, ArfGAP3 LM1 and ArfGAP3 LM2. The ArfGAP3 gene was successfully excised using XhoI and XbaI and re-ligated into the UAS FLAG plasmid (figure 4.7). Successful colonies were selected and checked via GATC sequencing, which showed that the WT ArfGAP3 (figure 4.7B) and ArfGAP3 LM1 (figure 4.7C) colonies had successfully incorporated the ArfGAP3 gene into the UAS FLAG plasmid, however ArfGAP3 LM2 colonies did not. The WT and LM1 ArfGAP3 plasmid samples were sent off to BestGene Inc to generate the new UAS FLAG ArfGAP3 WT and LM1 transgenic fly lines.

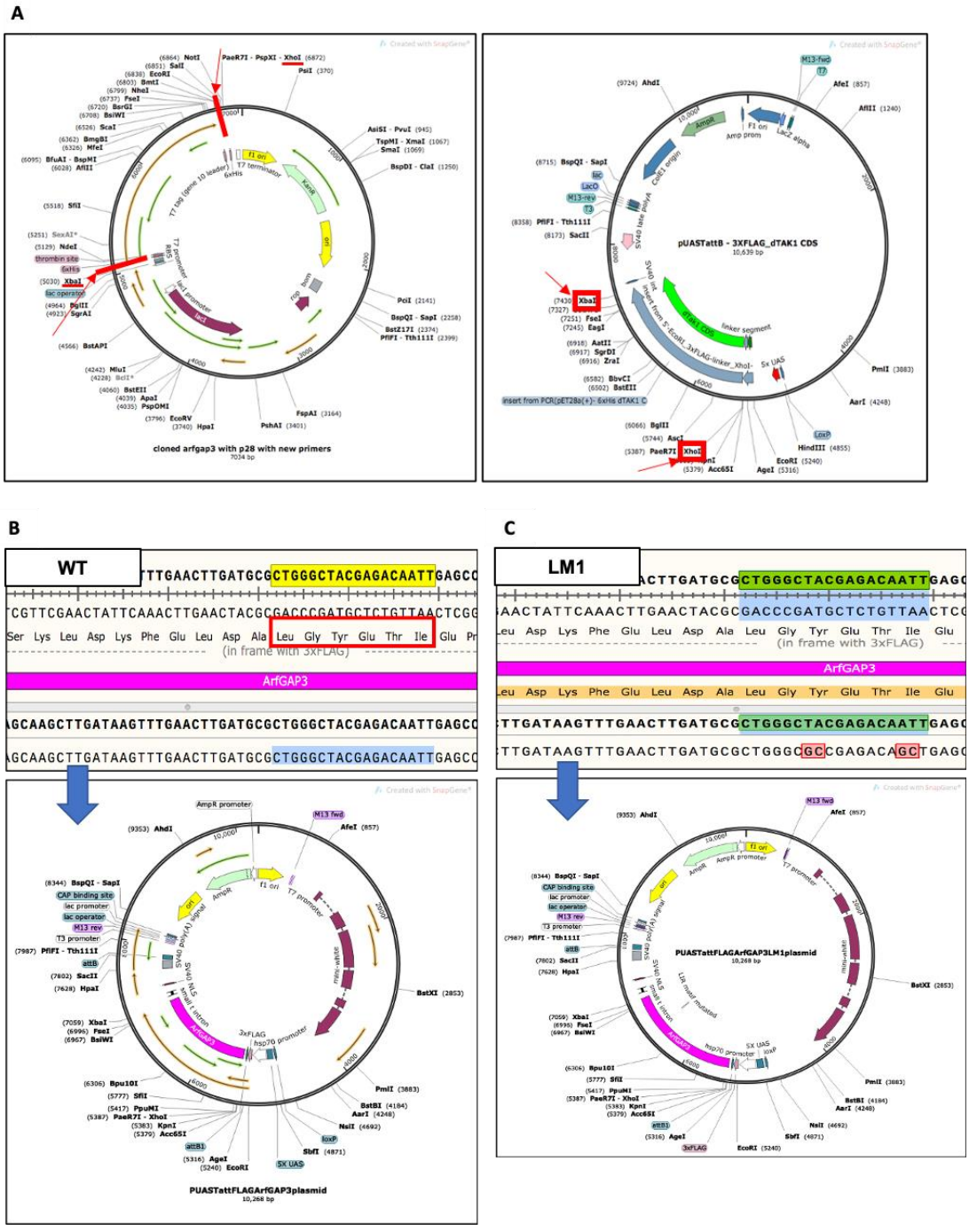

Figure 4.7. Cloning of WT and LM1 ArfGAP3 gene into UAS FLAG plasmid. A) Plasmid map of WT ArfGAP3 in pet28 vector (left), red marks highlighting sites of restriction enzymes XhoI and XbaI for digestion. Plasmid map of UAS FLAG Tak1 vector (right), red markings highlighting XbaI and XhoI sites for digestion. B) Successful cloning of WT ArfGAP3 sequence into UAS FLAG vector. GATC sequencing results (top left box) showing WT ArfGAP3 LIR1 motif unaltered. Yellow highlighted WT LIR1 motif in reference ArfGAP3 sequence. Blue highlighted WT LIR1 motif in WT ArfGAP3 colonies post cloning. Plasmid map (bottom left box) showing successful incorporation of WT ArfGAP3 sequence into UAS FLAG tagged plasmid. C) Successful cloning of LM1 ArfGAP3 sequence into UAS FLAG vector. GATC sequencing results (top right box) showing ArfGAP3 LIR1 motif mutated at 3rd and 6th residue positions (highlighted in red) of LIR motif in ArfGAP3 LIR1 mutant colonies. Green highlighted LIR1 motif in reference ArfGAP3 sequence. Plasmid map (bottom right box) showing successful incorporation of ArfGAP3 LIR1 mutant sequence into UAS FLAG tagged plasmid.

4.5.1 ArfGAP3 colocalises with Atg8a in new transgenic flies

Once the new transgenic fly lines were generated, the co-localisation of Atg8a and ArfGAP3 and the interaction via the LIR 1 motif was verified in these new lines. For this particular co-localisation experiment, the UAS FLAG ArfGAP3 WT and LM1 transgenic lines was crossed with Flpout mCherry Atg8a driver line. The progeny generated mCherry clones expressing Atg8a positive autophagosomes and an anti-FLAG GFP antibody was used to probe for ArfGAP3 WT and LM1.

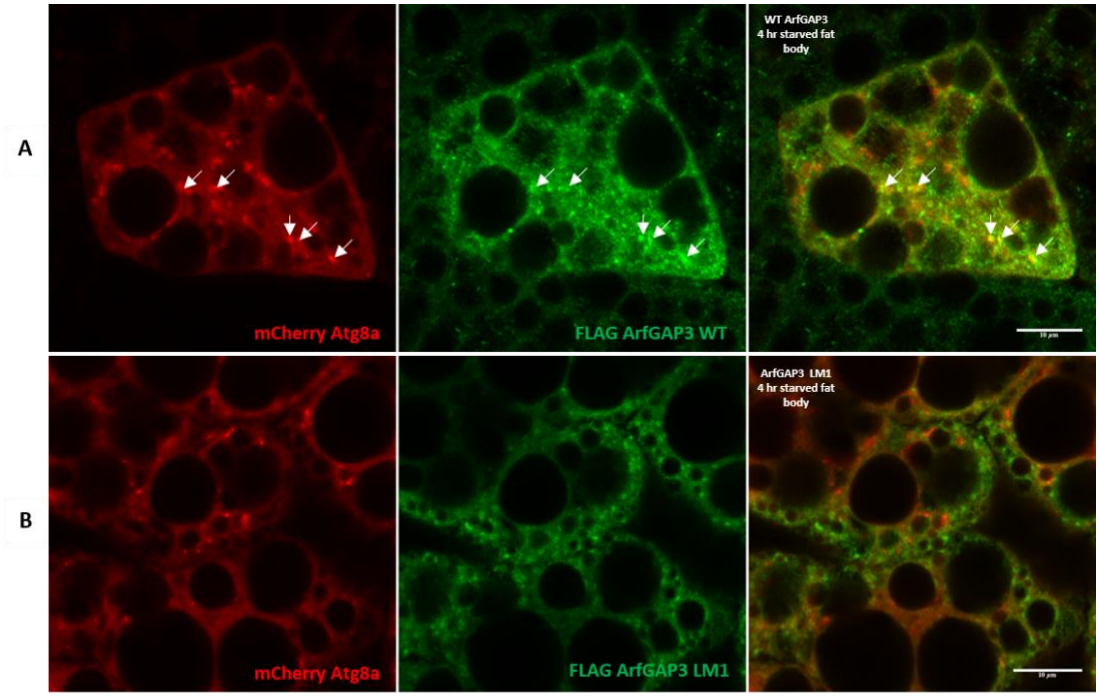

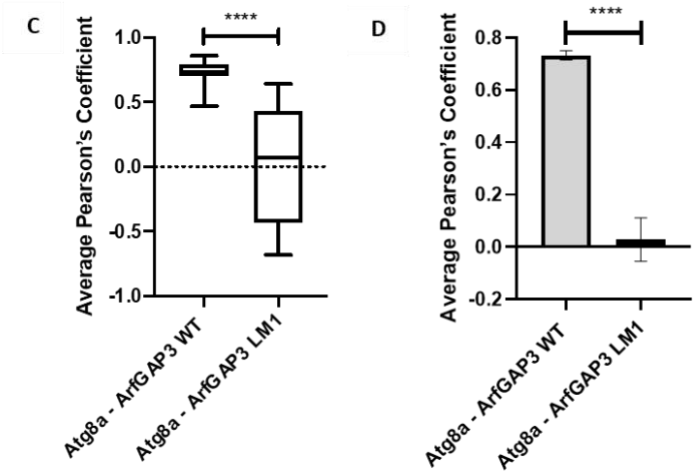

Figure 4.8. ArfGAP3 co-localises with Atg8a in new UAS FLAG ArfGAP3 transgenic flies. Confocal sections of fat bodies captured at 63x magnification from A) 4 hours starved third instar larvae from cross FlpoutmCherryAtg8a x UAS FLAG WT ArfGAP3 and B) 4 hr starved larvae from cross FlpoutmCherryAtg8a x UAS FLAG ArfGAP3 LM1 expressing mCherry Atg8a and GFP FLAG ArfGAP3. Scale bars are 10μm, n=30. C and D) Coloc2 plugin in FIJI was used to quantify co-localisation of mCherry and GFP signals using Pearson's Correlation Coefficient. Average Pearson's Coefficient was significantly reduced by 25-fold in the FLAG ArfGAP3 LIR mutant (0.02821) compared to FLAG WT ArfGAP3 (0.7329). C) Data represented as a box plot with whiskers denoting min to max values (GraphPad prism). D) Data represented as column bar graph with error bars denoting SEM. An unpaired two-tailed t-test was performed as statistical analysis, confirming the difference in co-localisation between WT ArfGAP3 and ArfGAP3 LIR mutant was highly significant, $p<0.0001$. Error bars represents SEM.

As observed previously, FLAG WT ArfGAP3 was seen to co-localise with mCherry positive Atg8a puncta. On the contrary, the FLAG ArfGAP3 LM1 did not co-localise with mCherry positive Atg8a puncta, strengthening the statement that ArfGAP3 interacts with Atg8a via the LIR 1 motif (392 LGYETI 397). Quantification analysis confirmed that the ArfGAP3- Atg8a colocalization was lost in the UAS FLAG ArfGAP3 LM1 line, as the average Pearson's Coefficient was significantly reduced by 25-fold in the FLAG ArfGAP3 LIR mutant (0.02821) compared to FLAG WT ArfGAP3 (0.7329), $p <0.0001$ (figure 4.8). The quantified data was represented as a box plot with whiskers representing minimum and maximum values. Since the whiskers can be mistaken as error bars, the quantified data was also represented as a column bar graph with error bars denoting SEM to further illustrate the data is significant as the error bars do not overlap. The data here shows that the interaction between ArfGAP3 and Atg8a is almost eliminated. Whilst this agrees with the observations that LIR1 motif is a functional LIR motif responsible for the interaction between ArfGAP3 and Atg8a, it does not support the notion that LIR2 motif is a second functional LIR motif that is also responsible for the interaction. For clearer conclusions, this experiment will need to be conducted in flies expressing FLAG ArfGAP3 LM2 and FLAG tagged ArfGAP3 flies expressing the double LIR mutant

(LIR1 and LIR2) for comparative analysis. In addition, having a higher ‘n’ number for image quantification will ensure a more conclusive observation.

Chapter 5

Deciphering the role of ArfGAP3 in the interplay between selective autophagy and endosomal trafficking

5.1 Chapter introduction: ArfGAP3 in membrane trafficking

ArfGAP family of proteins consist of an ArfGAP catalytic domain that facilitates the hydrolysis of GTP bound to Arf proteins, which regulates membrane trafficking (Shiba and Randazzo, 2012). ArfGAP3 mediates the hydrolysis of GTP bound to Arf1. One of the many cellular functions that Arf1 proteins and other Arf proteins are associated with is trafficking from the trans Golgi network (TGN) (Inoue and Randazzo, 2007). Previous studies have also demonstrated a functional role of ArfGAP3 in protein transport from the trans-Golgi network to endosomes, in which they show in HeLa cells a clear co-localisation of ArfGAP3 with early and late endosomal markers, Rab5 and Rab7 respectively. The study proposed that ArfGAP3 could possibly be involved in endosomal trafficking through the regulation of transport from early endosomes to late endosomes (Shiba *et al.*, 2013).

Chapter 4 validated a clear interaction present between ArfGAP3 and the autophagosomal protein Atg8a, strongly advocating a likely functional role of ArfGAP3 in the autophagic pathway. This chapter reports further results that suggest

a functional role of ArfGAP3 in the interplay between selective autophagy and endosomal trafficking.

5.2 ArfGAP3 is selectively degraded by autophagy

Atg8a is a protein embedded in the inner autophagosomal membrane and so in theory most Atg8a interacting proteins are usually degraded by autophagy. Since the co-localisation studies and GST pull down studies demonstrated a clear interaction between ArfGAP3 and Atg8a, biochemical analysis of ArfGAP3 was carried out in 7-day old wildtype (w118), ArfGAP3 mutant$^{e0/250}$ and two strains of autophagy mutant flies, Atg8a mutant and Atg7 mutant whole fly lysates to examine the levels of endogenous ArfGAP3 in the whole fly. Fly lysate samples were subjected to SDS-PAGE and western blotting and probed for anti-ArfGAP3.

In Atg8a mutants, autophagy is disrupted, and hence we would expect to see an accumulation of cytosolic material tagged for degradation (proteins, organelles etc) since they cannot be degraded. As seen in figure 5.1, there is an accumulation of endogenous ArfGAP3 protein (60kDa) in Atg8a mutant compared to wildtype. Even though the loading control is less in Atg8a mutant, with normalisation the quantification analysis still shows an increase in ArfGAP3 protein levels.

To further confirm the band observed was ArfGAP3, whole fly lysates of 7-day old ArfGAP3 mutants were also added to the experiment as well as Atg7 mutants as another autophagy mutant sample. The results were as expected, an accumulation in endogenous ArfGAP3 protein (60kDa) was seen in both autophagy mutant flies and a reduction in ArfGAP3 mutants flies compared to wildtype flies. The tubulin loading

control (50kDa) was also equal for all samples. Statistical analysis, t-test, was carried out which confirmed the accumulation of endogenous ArfGAP3 in Atg8a mutants as significant ($p = 0.0129$) and a significant reduction in ArfGAP3 in ArfGAP3 mutants ($p = 0.0023$) (figure 5.1). Overall, these results indicate ArfGAP3 is selectively degraded by autophagy.

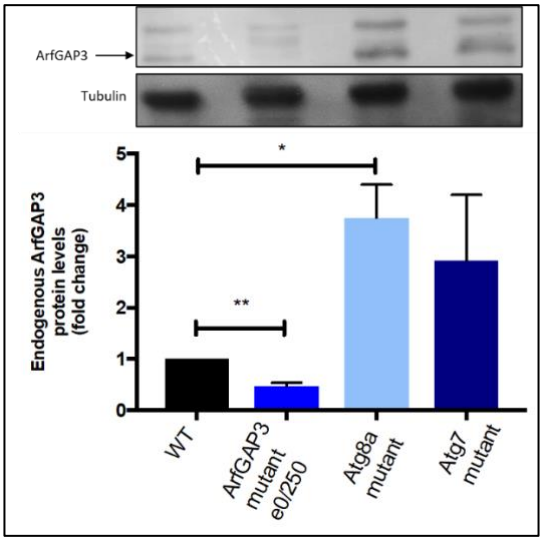

Figure 5.1 ArfGAP3 is selectively degraded by autophagy. Full fly lysates from W118 wild type (WT), ArfGAP3 mutants (e0/250) and Autophagy mutant flies (Atg8a mutant and Atg7 mutant) were subjected to SDS-PAGE (8% gel) and western blotting for ArfGAP3 endogenous protein. Tubulin was used as a loading control. The expected band for ArfGAP3 was ~60kDa and for tubulin ~50kDa. T-test analysis was carried out for significance p value ($p < 0.05$). Error bars represents SD.

5.3 Testing the efficiency of ArfGAP3 knockdown transgenic flies

The efficiency of the UAS ArfGAP3 RNAi line, given to us by Ruth Johnson, was tested by QPCR and western blotting on larvae samples (figure 5.2A&B). As expected, the qPCR results showed a clear reduction in mRNA levels of ArfGAP3 in cg ArfGAP3 RNAi larvae samples compared to wildtype. Two different ArfGAP3 RNAi larvae samples were tested for protein levels via western blotting, one focussing on ArfGAP3 expression in larvae fat bodies (Cg ArfGAP3 RNAi) and the other focussing on ArfGAP3 expression in the whole larval body (Da ArfgAP3 RNAi). As expected, there was a reduction in ArfGAP3 protein levels in ArfGAP3 RNAi larvae fat bodies samples compared to wildtype ArfGAP3 and Atg8a mutant, however, no

protein expression of ArfGAP3 was seen in wildtype only sample which is contrary to what was expected. On the other hand, some ArfGAP3 protein expression was seen in all whole larval body samples, however the loading control was not equal for all of the samples and so this result could not be reliable. Overall, the western blotting results for this ArfGAP3 RNAi efficiency cannot be concluded for definite as the loading control shows uneven loading. Even though the expression of ArfGAP3 was reduced in the cg ArfGAP3 RNAi samples compared to the positive control (cg ArfGAP3 DsRED) in both QPCR and western blotting (figure 5.2), the data from this western blot could not be used convincingly due to uneven loading control for all samples. The blot quality was not clear to interpret but was only displayed here to show that we were not able to obtain clear results here despite the multiple efforts to optimise the western blotting experiment using this ArfGAP3 RNAi flies. Since we were unable to achieve conclusive data here after multiple repeats, we moved onto sourcing a new ArfGAP3 RNAi fly line to work with (discussed below). The only experiment that was successful using this ArfGAP3 RNAi fly line was the qPCR analysis showing a clear reduction in ArfGAP3 mRNA levels in the RNAi line compared to control.

Since the results varied in protein levels between fat bodies and whole body with the UAS ArfGAP3 RNAi fly line from Ruth Johnson, a new set of ArfGAP3 RNAi lines were purchased from Vienna *Drosophila* Resource Centre (VDRC) and Bloomington *Drosophila* Stock Centre (BDSC) and denoted UAS ArfGAP3 RNAI-VDRC A, VDRC B and Bloom 31156. The protein levels via western blotting were examined using the new UAS ArfGAP3 RNAi fly lines (figure 5.2C). For the new RNAi lines, the whole fly driver DaGal4 was used to silence ArfGAP3 in the whole *drosophila* body. Whole fly lysates of 1 week old flies were used for the western

blotting experiment. Western blots were quantified using FIJI to measure band intensities for both ArfGAP3 protein and the loading control tubulin. The ArfGAP3: tubulin ratio was calculated and normalised to WT control. The results were much more promising, as a clear reduction in ArfGAP3 protein compared to controls was observed in two of the three new RNAi lines, VDRC B and Bloomington 31156. With the ArfGAP3 antibody we noticed multiple bands in the western blotting analysis due to its polyclonal nature. After subjecting the samples to SDS-PAGE for 4hours, we were able to obtain the band separation as seen in figure 5.2C. The bands highlighted by the red arrow in figure 5.2C are specific for ArfGAP3 as these bands were observed at 60kDa, the molecular weight of ArfGAP3. At 60kDa, we can see ArfGPA3 expression in WT, luciferase RNAi, ArfGAP3 WT DsRED, ArfGAP3 mutant and atg8a mutants. We noticed the clear accumulation in ArfGAP3 in the Atg8a mutant compared to WT which agrees with the western blot data in figure 5.1, and so this was another indication that these bands were specific for ArfGAP3. The RNAi fly line that was chosen henceforth to use for the RNAi experiments was UAS ArfGAP3 VDRC B alongside the original UAS ArfGAP3 RNAi fly line from Ruth Johnson. From this point forward, the latter RNAi line will be denoted as UAS ArfGAP3 RNAi (RJ) and the former will be UAS ArfGAP3 RNAi (VDRC B). A limitation in this analysis was using the luciferase RNAi line for comparison with the VDRC ArfGAP3 RNAi line as the luciferase RNAi line is a TriP line. TriP lines are entirely different in genotype than the VDRC GD RNAi lines. Here, the appropriate control for comparison is the WT fly line, as displayed in figure 5.2C.

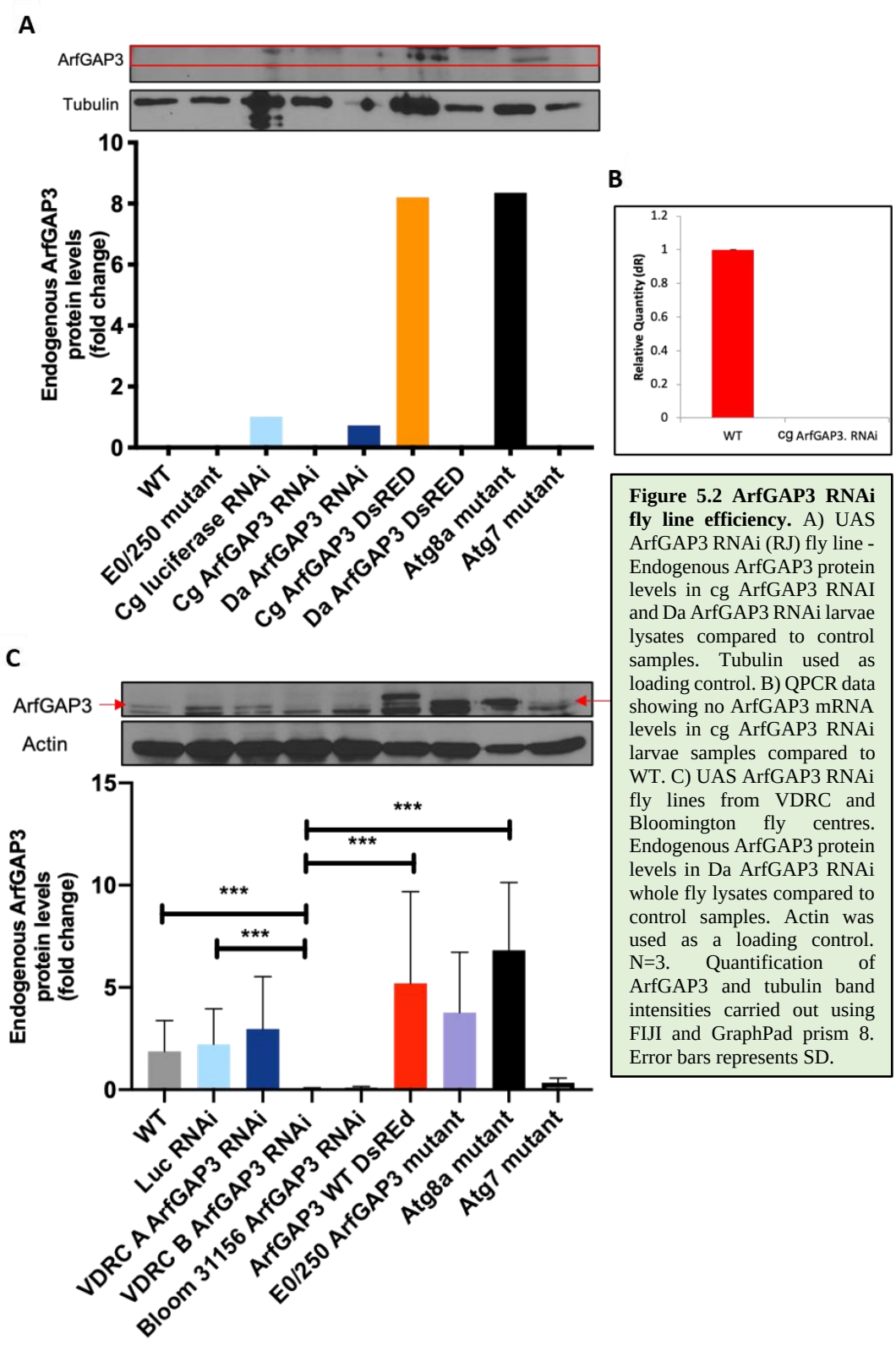

Figure 5.2 ArfGAP3 RNAi fly line efficiency. A) UAS ArfGAP3 RNAi (RJ) fly line - Endogenous ArfGAP3 protein levels in cg ArfGAP3 RNAI and Da ArfGAP3 RNAi larvae lysates compared to control samples. Tubulin used as loading control. B) QPCR data showing no ArfGAP3 mRNA levels in cg ArfGAP3 RNAi larvae samples compared to WT. C) UAS ArfGAP3 RNAi fly lines from VDRC and Bloomington fly centres. Endogenous ArfGAP3 protein levels in Da ArfGAP3 RNAi whole fly lysates compared to control samples. Actin was used as a loading control. N=3. Quantification of ArfGAP3 and tubulin band intensities carried out using FIJI and GraphPad prism 8. Error bars represents SD.

5.4 The effect of ArfGAP3 on the autophagic flux

5.4.1 Knockdown of ArfGAP3 affects autophagosomes number

To see what effect, knock down of ArfGAP3 levels in cells was having on autophagy, a transgenic *Drosophila* line expressing *Drosophila* Atg8a tagged with mCherry with a heat shock induced FLPout Gal4/UAS GFP system was crossed with *Drosophila* UAS ArfGAP3 RNAi (RJ) line. This produced progeny expressing mCherry Atg8a and generating some GFP expressing cells which expressed ArfGAP3 RNAi (ArfGAP3 knock down) and surrounding cells that did not express GFP and hence did not express ArfGAP3 RNAi (figure 5.3). This produced a ‘mosaic’ pattern. The number of mCherry Atg8a puncta were quantified in each ArfGAP3 RNAi GFP clonal cell and compared with the number of mCherry Atg8a puncta in the surrounding control non-GFP cells.

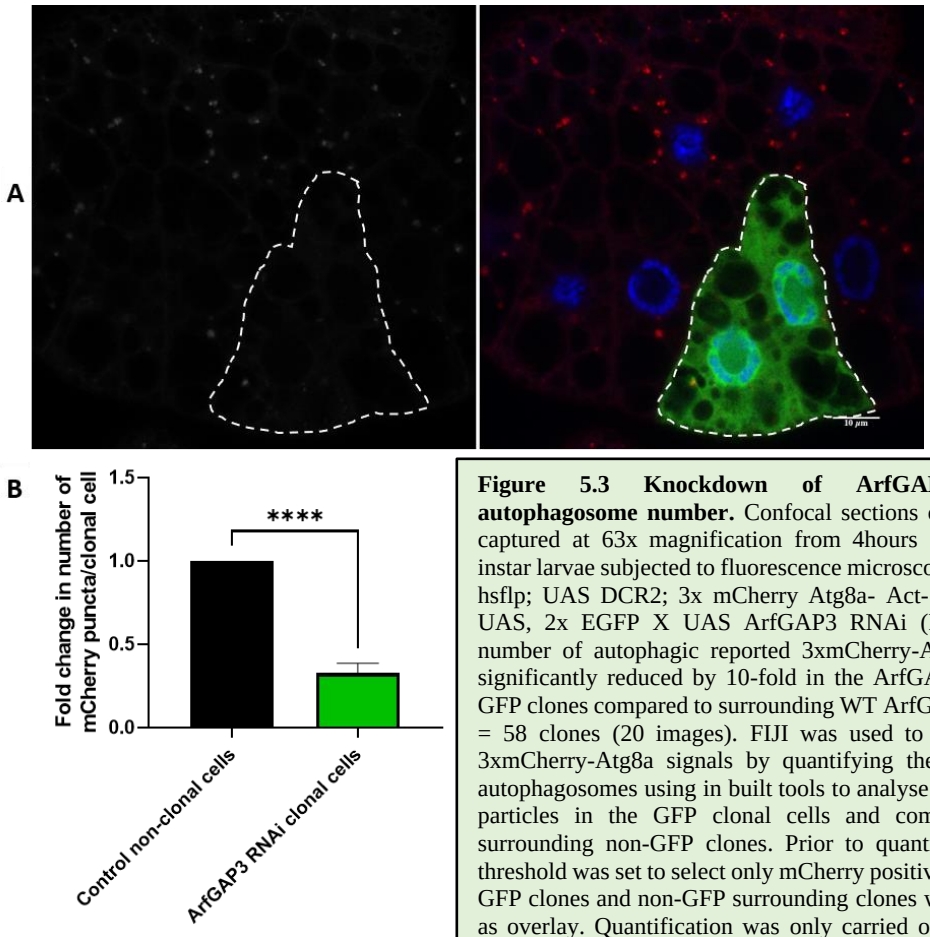

Figure 5.3 Knockdown of ArfGAP3 affects autophagosome number. Confocal sections of fat bodies captured at 63x magnification from 4hours starved third instar larvae subjected to fluorescence microscopy. A) Cross hsflp; UAS DCR2; 3x mCherry Atg8a- Act- CD2- Gal4, UAS, 2x EGFP X UAS ArfGAP3 RNAi (RJ). B) The number of autophagic reported 3xmCherry-Atg8a dots is significantly reduced by 10-fold in the ArfGAP3 silenced GFP clones compared to surrounding WT ArfGAP3 cells. N = 58 clones (20 images). FIJI was used to quantify the 3xmCherry-Atg8a signals by quantifying the number of autophagosomes using in built tools to analyse and quantify particles in the GFP clonal cells and compare to the surrounding non-GFP clones. Prior to quantification, the threshold was set to select only mCherry positive puncta, the GFP clones and non-GFP surrounding clones were selected as overlay. Quantification was only carried out limited to threshold within overlay area. Error bar represents SEM.

Most GFP clone cells that expressed ArfGAP3 RNAi showed less mCherry Atg8a-positive autophagosomes compared to surrounding non-clones (figure 5.3). In a few cases, some non-GFP clones showed a reduction in autophagosome number which most likely indicates clearance of autophagosomes through fusion with lysosomes suggesting the autophagosomes in those GFP clones were accumulating. FIJI was used to quantify the mCherry-Atg8a signals by quantifying the number of autophagosomes using the built-in tools to analyse and quantify particles in the GFP clonal cells and compare to the surrounding non-GFP clones. Prior to quantification, the threshold was set to select only mCherry positive puncta, the GFP clones and non-GFP surrounding clones were selected as overlay. Quantification was only carried out limited to

threshold within overlay area. Quantification was performed in 58 GFP positive ArfGAP3 RNAi expressing clones and compared to surrounding non-GFP clones. The number of autophagosomes in GFP positive ArfGAP3 RNAi clones were normalised to number of autophagosomes in surrounding non-GFP control cells. Statistics revealed a significant 3-fold decrease in the number of autophagosomes in ArfGAP3 RNAi GFP clonal cells compared to surrounding control cells.

In theory if the autophagic flux downstream of autophagosome formation is disrupted, there would be an accumulation of autophagosomes, which we did see in some clones but not all. The data here does not confidently suggest that the autophagic flux is disrupted. The results could be interpreted in two ways; 1) less Atg8a positive autophagosomes are formed in RNAi cells compared to control cells so the knockdown of ArfGAP3 seems to disrupt events upstream of autophagosome formation or 2) knockdown of ArfGAP3 does not hinder the clearance of autophagosomes via fusion with lysosomes and hence autophagic flux is normal. Neither of these two explanations fit with the data presented in figure 5.5 in the following subchapter. For more conclusive results on this data, this experiment would need to be repeated and supported by biochemical evidence, such as an autophagy flux assay (western blotting) showing Atg8 levels in ArfGAP3 RNAi cells compared to control cells.

5.4.2 Knockdown of ArfGAP3 affects lysosomal size (diameter).

Following the discovery, that low levels of ArfGAP3 affects autophagosome number, the effect of ArfGAP3 silencing on lysosome function was investigated. Lysotracker RED staining was carried out immediately on 4 hours sucrose starved dissected and PFA fixed fat bodies expressing ArfGAP3 RNAi (VDRC B), ArfGAP3 RNAi (RJ) and WT ArfGAP3 to visualise autophagy induced lysosomes. The tissues were mounted and viewed by confocal microscopy immediately.

Typically, the number of lysosomes in mammalian cells can be between 50 to 1000, normally around 500, and can decrease to less than 50 upon starvation (Xu and Ren, 2015). Studies have reported in *Drosophila* control fat bodies, upon starvation, number of lysosomes can range between 75 to 100/area (Takats *et al*, 2013; Hegedus *et al*, 2016). Quantification of lysotracker red staining in the *Drosophila* fat bodies and statistical analysis revealed there was a significant difference in the number of lysosomes between WT ArfGAP3 and ArfGAP3 RNAi VDRC B. The average number of lysosomes in WT ArfGAP3 fat bodies was around 126 lysosomes, which significantly increased 3-fold in ArfGAP3 RNAi VDRC B fat bodies (average number of lysosomes, 331). There was no significant difference in the number of lysosomes in ArfGAP3 RNAi (RJ) fat bodies compared to WT ArfGAP3 (figure 5.4A/C). The data here could further be supported by examining endogenous lysosomal proteins via western blotting in WT ArfGAP3 and ArfGAP3 RNAi fat body lysates.

On the contrary, a considerable difference in the size of the lysosomes was noticed. The diameter of the lysosome is heterogenous and has been established to range from 0.05μm to 0.5μm which can increase up to 1.5μm in diameter upon

starvation in mammalian cells (Xu and Ren, 2015). In *Drosophila*, lysosome diameter ranges from 0.5μm to 1μm, increasing up to 1.5μm upon starvation (Lorincz *et al*, 2017). Under starvation conditions, upon autophagy induction, lysotracker red positive autolysosomes were observed in all fat body tissues (figure 5.4B). Autolysosomes in WT ArfGAP3 fat bodies ranged from 0.5μm to 2μm, with an average lysosome size of 1μm. Most interestingly, lysosomes in fat bodies expressing ArfGAP3 RNAi were considerably larger ranging from 1.5μm to 5μm, with an average lysosome sizes of around 2μm and 2.5μm in ArfGAP3 RNAi VDRC B and ArfGAP3 RNAi RJ fat bodies respectively (figure 5.4B). Statistical analysis revealed that the increase in lysosome size in ArfGAP3 RNAi fat bodies compared to control WT ArfGAP3 was highly significant ($p<0.0001$) (figure 5.4D). A question arose whether the fat body cells were larger in ArfGAP3 RNAi lines compared to control and if this accounted for the increase in autolysosome size. Upon analysing the area of fat body cells in FIJI, the area of the fat body cells in ArfGAP3 RNAi tissues did not differ from control WT tissues and hence did not account for the increase in autolysosome size. The data here suggests that ArfGAP3 is crucial for normal lysosome functioning since enlarged lysosomes could be an indication of accumulated cellular cargo due to disrupted degradation. Further experiments to support this data should involve acquiring z-stack images by confocal microscopy to quantify 3D representations of autolysosome size since images in this experiment were taken as a single slice.

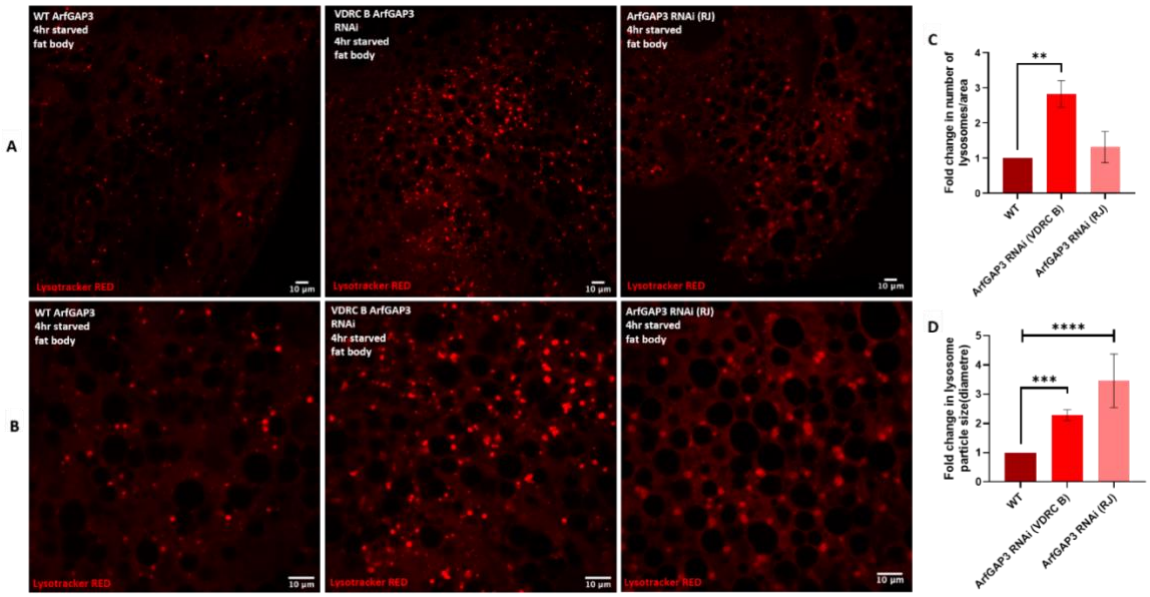

Figure 5.4 Knockdown of ArfGAP3 affects lysosomal size (diameter). A/B) Confocal sections of fat bodies subjected to fluorescence microscopy captured at 63x magnification from 4hours starved third instar larvae stained with lysotracker RED in control WT ArfGAP3 (left panel), ArfGAP3 RNAi (VDRC B) (middle panel) and ArfGAP3 RNAI (RJ) (right panel). All fly lines were crossed with fat body specific CgGal4 driver. Scale bars are 10µm. WT n=17 images, ArfGAP3 RNAi n=16 images. Panel A displaying number of lysotracker-red positive autolysosomes. Panel B displaying magnified images to show changes in lysosome diameter. C) The number of lysosomes at the same magnification in each genotype were quantified using FIJI and statistical analysis (one-way ANOVA) was carried out using GraphPad Prism 8. Statistical analysis showed a significant increase in number of lysosomes in ArfGAP3 RNAi (VDRC B) compared to control, p=0.0084. D) Lysosome diameter was measured using the built in 'analyse particle' tool in FIJI. The area of each particle was measured and converted to diameter size using equation [2*SQRT(area/pi())] in excel. Statistical analysis (one-way ANOVA) revealed the difference in lysosomal size in diameter between WT ArfGAP3 and both ArfGAP3 RNAi's were highly significant, p<0.0001. Error bars represent SEM.

5.4.3 Knockdown of ArfGAP3 affects autophagosome-lysosome fusion

The crucial step for complete degradation in the process of autophagy involves the fusion of autophagosomes to lysosomes to form autolysosomes which carry the necessary enzymes for degrading cellular material. Since knockdown of ArfGAP3 was seen to effect autophagosome number and lysosomal size, the next element of the autophagic flux to evidently explore was the effect of ArfGAP3 on autophagosome-lysosome fusion. A number of confocal studies can help examine any disruptions to the autophagic flux.

Another transgenic *Drosophila* line expressing tandem tagged mCherry-GFP-Atg8a with a FLPout system was crossed with UAS ArfGAP3 RNAi (RJ). This produced a progeny expressing GFP clones with GFP Atg8a positive puncta. It also produced red clones in the same area with mCherry puncta representing autolysosomes. These clones expressed ArfGAP3 RNAi, hence represented ArfGAP3 knockdown. In brief, the mCherry puncta represent autolysosomes because the acidic hydrolases in autolysosomes causes the quenching of GFP fluorescence signal upon fusion of autophagosomes with lysosomes, resulting in mCherry fluorescing autolysosomes (DeVorkin and Gorski, 2014; Lorincz *et al*, 2017). Hence this experiment is a good method to see if the autophagic flux is being disrupted as when both channels (GFP and mCherry) are merged we would expect to see more red puncta representing autolysosomes if the autophagic flux is normal and functioning. On the other hand, small GFP and mCherry-positive puncta would represent autophagosomes and yellow puncta can be an indication of autolysosomes unable to degrade cargo, suggesting that the autophagic flux is disrupted (Lorincz *et al*, 2017).

The dissected fat bodies were subjected to fluorescence microscopy with DAPI staining. Mounted tissues viewed under confocal microscopy. Confocal images from this experiment suggested that there was a disruption in the autophagic flux when ArfGAP3 was knocked out, as merged image analysis showed a mix of mCherry and GFP autophagosomes and some yellow puncta (figure 5.5B). In the control cells, only mCherry positive autolysosomes were observed (figure 5.5A). Quantification analysis showed a higher Pearson's correlation coefficient for ArfGAP3 RNAi cells compared to control cells, confirming the mCherry and GFP signals overlapped more in ArfGAP3 RNAi cells than in control cells (figure 5.5). Thus, this suggests that the

autophagic flux is disrupted in the absence of ArfGAP3 because there are autophagosomes present which have not been able to fuse with lysosomes. Alternatively, the data could also suggest increased number of autophagosome due to increased formation or accumulation of autophagosomes in ArfGAP3 RNAi cells. Although this explanation would not fit the results observed in figure 5.3 where we show decreased number of autophagosomes in ArfGAP3 RNAi fat body cells, the interpretation seems more accurate for data in figure 5.5, as we see impaired autophagosome-lysosome fusion in ArfGAP3 RNAi cells compared to control. If fusion is hindered, there would be an accumulation of autophagosomes observed.

An alternative approach to examine the effect of ArfGAP3 on the autophagic flux would be to cross cgGal4 mCherry Atg8a driver flies with UAS ArfGAP3 RNAi, the resulting progeny flies would express mCherry positive Atg8a puncta in ArfGAP3 RNAi fat bodies, which can be immunostained with cathepsin-L antibody for labelling lysosomes. The co-localisation of mCherry autophagosomes with cathepsin-L positive lysosomes can then be measured and quantified.

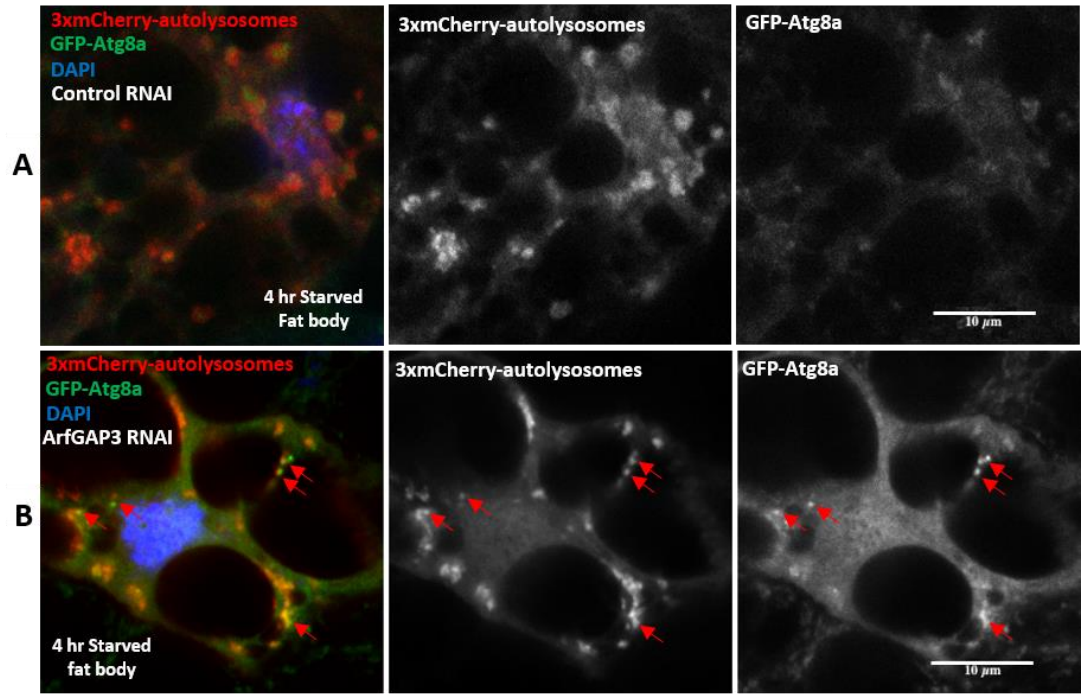

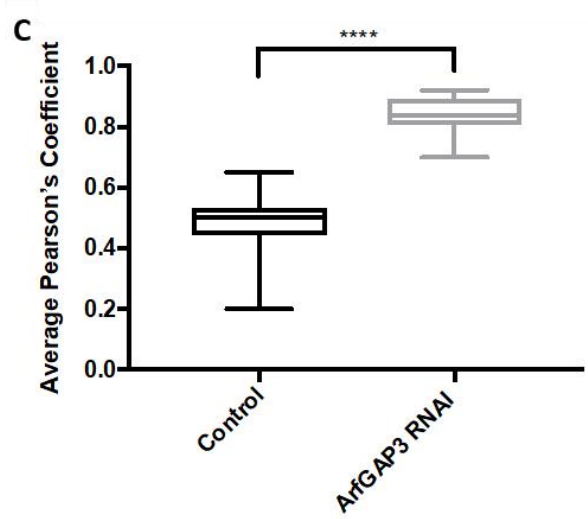

Figure 5.5 Knockdown of ArfGAP3 affects autophagosome-lysosome fusion. Confocal sections of fat bodies subjected to fluorescence microscopy captured at 63x magnification from 4hours starved third instar larvae. A) Cross FLPout tandem GFP-mCherry Atg8a X control RNAi showing clear mCherry signals of autolysosomes compared to B) cross FLPout tandem GFP-mCherry Atg8a X UAS ArfGAP3 RNAi (RJ) where merged signals of mCherry and GFP can be seen indicating disruption to autophagic flux. C) Coloc2 plugin in FIJI was used to quantify co-localisation of mCherry and GFP signals using Pearson's Correlation Coefficient. Scale bar 10μm, n=30 images. Statistical analysis using GraphPad Prism indicates significant difference in Pearson's correlation coefficient between ArfGAP3 RNAi cells and control cells, $p<0.0001$. Error bars represent SD.

5.5 The effect of ArfGAP3 on the endocytic flux

5.5.1 ArfGAP3 co-localises with Rab5 and Rab7 in Drosophila melanogaster

Previous studies have shown that ArfGAP3 could possibly be associated with early and late endosomes. ArfGAP3 co-localised to Rab5 (early endosome marker) and Rab7 (late endosome marker) in HeLa cells suggesting ArfGAP3 could play a role in endosomal trafficking in mammalian cells (Shiba *et al.*, 2013). To test if this observation was also true in *Drosophila melanogaster*, DsRed tagged UAS ArfGAP3 WT flies were crossed with the CgGAL4 driver to express ArfGAP3-DsRed in larval fat bodies. These fat bodies were subjected to immunofluorescence with the early and late endosomal markers, Rab5 and Rab7 respectively.

In starved larval fat bodies, DsRed tagged ArfGAP3 co-localised with Rab5 and Rab7 (figure 5.6), as the average Pearson's Coefficients were closer to +1, 0.7 and 0.6 respectively (figure 5.6). A control fly line was not used here. This experiment was not done for any comparison purposes, merely to show that ArfGAP3 co-localised to Rab7 and Rab5 in *Drosophila*. The data here supports the findings in the study by Shiba *et al*, 2013. Their study also showed that ArfGAP3 co-localised with Rab5 more than Rab7. Herein, ArfGAP3 also co-localised more with Rab5 than Rab7 (figure 5.6), however, the focus from here onwards was on Rab7 as it is a common participating molecule in both autophagy and endocytosis.

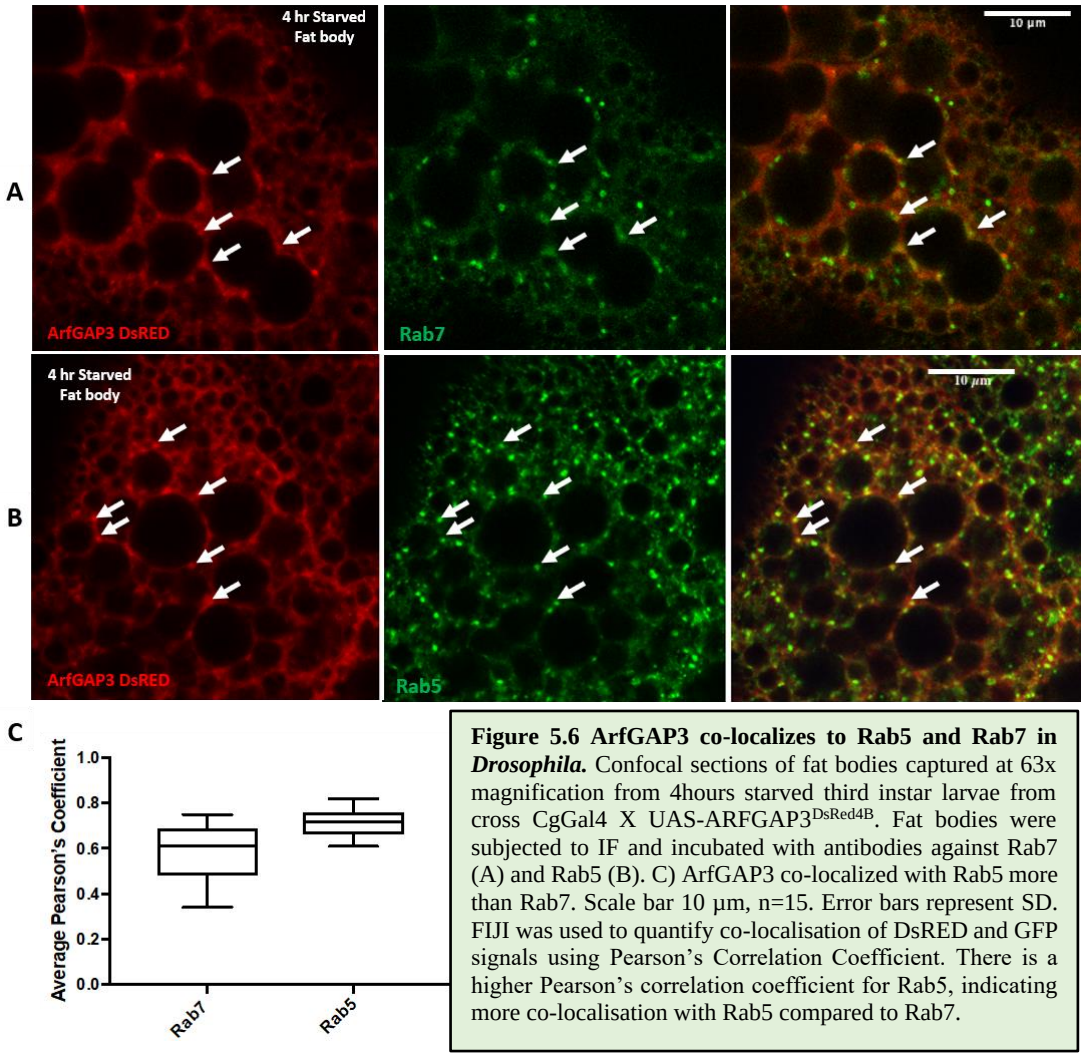

Figure 5.6 ArfGAP3 co-localizes to Rab5 and Rab7 in *Drosophila.* Confocal sections of fat bodies captured at 63x magnification from 4hours starved third instar larvae from cross CgGal4 X UAS-ARFGAP3^{DsRed4B}. Fat bodies were subjected to IF and incubated with antibodies against Rab7 (A) and Rab5 (B). C) ArfGAP3 co-localized with Rab5 more than Rab7. Scale bar 10 µm, n=15. Error bars represent SD. FIJI was used to quantify co-localisation of DsRED and GFP signals using Pearson's Correlation Coefficient. There is a higher Pearson's correlation coefficient for Rab5, indicating more co-localisation with Rab5 compared to Rab7.

5.5.2 Knockdown of ArfGAP3 effects endosome trafficking.

A recent study published in 2019 by Gabor Juhasz group showed that a small GTPase protein Arl8 is a general positive regulator of lysosomal fusion events. In the study by Gabor, TEM was carried out on Arl8 RNAi and control starved garland nephrocytes. In control and Arl8 RNAi cells, endosomes and lysosomes were observed, however in Arl8 RNAi cells the endosomes were much larger (Boda et al., 2019).

Since ArfGAP3 is a GTPase activating protein, there could be similar functional links of ArfGAP3 to lysosomal fusion events. Hence, similar TEM analysis was also carried out in UAS ArfGAP3 RNAi (RJ) and ArfGAP3 mutant fed and starved fat bodies and was compared to TEM analysis of WT fed and starved fat bodies which was done previously in the laboratory by Dr Ioannis Nezis. The WT fed fat bodies show clear representations of mitochondria and cytoplasm with endoplasmic reticulum (white arrows) (figure 5.7A'). Under starved conditions, when autophagy is initiated, autophagosomes and autolysosomes can be seen as expected (figure 5.7A''). The autophagosomes can be distinguished by the appearance of double membrane vesicles with smaller cargo in the autophagosome lumen (white arrows left panel). The autolysosome structures appear more dense and larger in size compared to autophagosomes (white arrows right panel). On the contrary, both fed and starved ArfGAP3 RNAi fat body cells showed an accumulation of vesicles (red arrows) (figure 5.7B). However, in the starved cells, when autophagy was initiated, lysosomes were also observed. Multiple vesicles were observed surrounding the lysosome as if fusion is occurring or about to take place (figure 5.7B right panel). ArfGAP3 mutant fed and starved fat bodies also showed accumulation of these vesicles (red arrows), although the staining of the mutant cells was not as clear as ArfGAP3 RNAi cells (figure 5.7C). These vesicular structures are of different shapes and sizes in the starved fat bodies, however more consistent in shape in the fed fat bodies. The morphology of these vesicles is irregular in the ArfGAP3 RNAi starved fat bodies. In comparison to the TEM images of Arl8 RNAi fat bodies published in Gabor's study, these vesicular structures observed in the ArfGAP3 RNAi fat bodies could also possibly be endosomes as seen in Gabor's study.

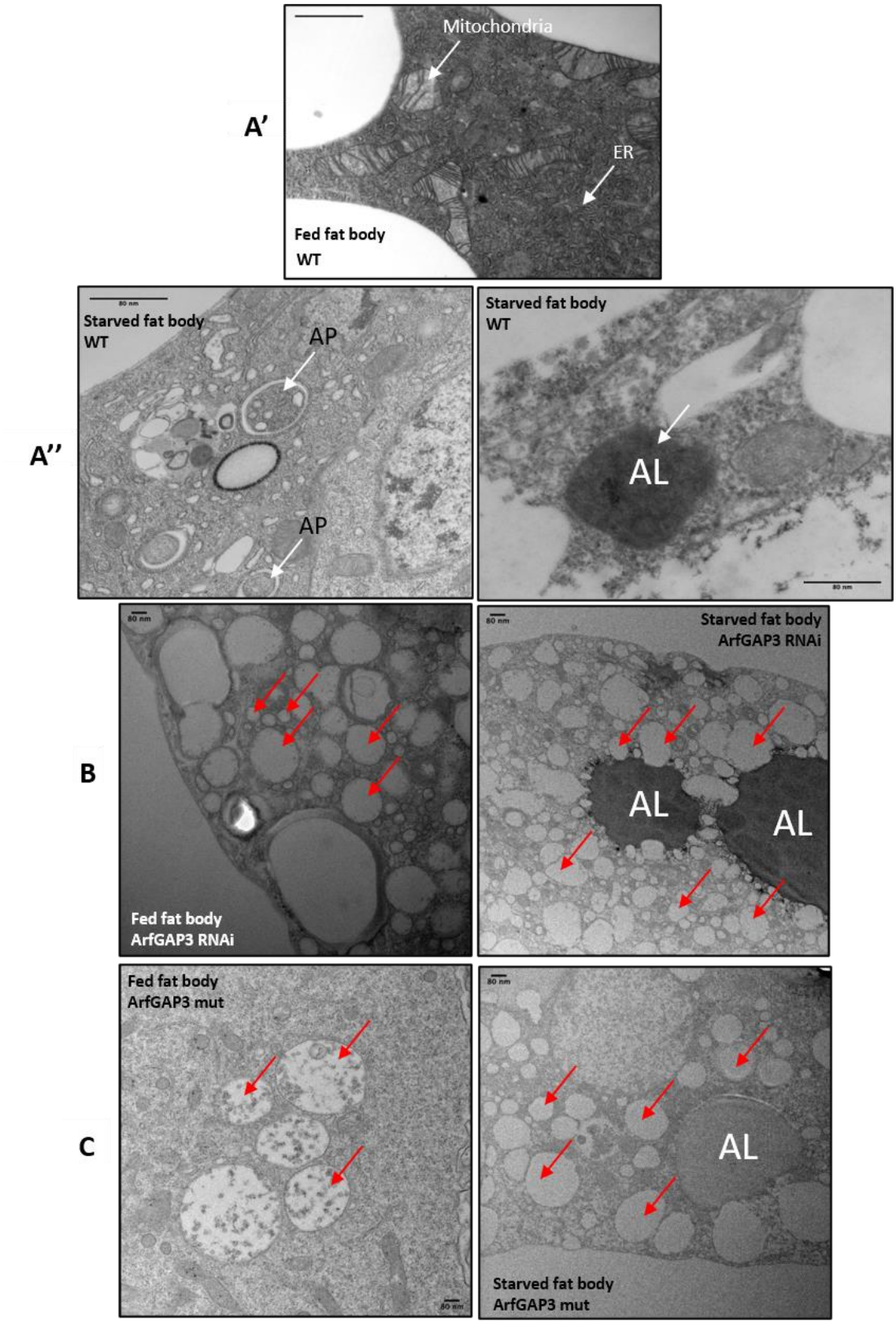
A'
Mitochondria
ER
Fed fat body
WT
A''
Starved fat body
WT
AP
AP
Starved fat body
WT
AL
B
Fed fat body
ArfGAP3 RNAi
Starved fat body
ArfGAP3 RNAi
AL
AL
C
Fed fat body
ArfGAP3 mut
AL
Starved fat body
ArfGAP3 mut

Figure 5.7 Knockdown of ArfGAP3 affects endosomal trafficking. Ultrastructure of fat body cells from fed WT third instar larvae shows clear structures of ER, mitochondria etc (A') and WT 4hrs starved larvae fat bodies show presence of autophagosomes and lysosomes (A''), n=4. B) Fed and 4hrs starved CgGal4 UAS ArfGAP3 RNAi (RJ) larvae fat bodies show accumulation of endosome-like vesicles. In starved cells (right panel) these accumulated vesicles have altered morphology to the vesicles seen in fed conditions. N = 21. C) Fed and 4hrs starved ArfGAP3 mutant larvae fat bodies also show accumulation of endosome-like vesicles. N=39. Images taken with Dr Saskia Bakker and Dr Ioannis Nezis (School of Life Science imaging suite).

Since it was thought that the accumulated vesicles observed in the TEM images could possibly also be endosomes, starved 3rd instar larval fat bodies expressing ArfGAP3 RNAi were subjected to immunofluorescence for Rab7. The driver line, cgGal4, was crossed with UAS ArfGAP3 RNAi (RJ) fly line. Wildtype and luciferase RNAi fat bodies were used as controls. Rab7-positive endosomes were observed in both WT and luciferase RNAi fat body cells (figure 5.8A). There was a 2-fold increase in endosome number in luciferase RNAi compared to WT, however statistical analysis showed the change was not significant. A possible explanation for this could be due to the small n number for quantification and the large deviation in number of endosomes for luciferase RNAi fat bodies. A larger n number for quantification should give a more accurate statistical significance. Rab-7 positive endosomes had accumulated in starved ArfGAP3 RNAi fat bodies, with a significant 4-fold increase in endosome number compared with WT (figure 5.8B), further suggesting that the accumulated vesicles seen in TEM analysis of ArfGAP3 RNAi fat bodies, could potentially be endosomes. In addition, some endosomes in the ArfGAP3 RNAi fat body cells were observed to be slightly bigger and abnormal in shape compared to endosomes in WT and luciferase RNAi cells, correlating to the change in vesicle morphology seen in the TEM analysis under starvation conditions in ArfGAP3 RNAi cells. Endosome size varies between early endosomes and late endosomes. Studies in *Drosophila* have shown late endosome vesicle size around 70-80nm (0.7-0.8µm)

(Ganley *et al*, 2004). The limitation of the analysis here however is that we did not have an internal control for endosome size changes and quantification analysis of endosome size was not carried out. A few internal controls that could be used to compare endosome size to would be Rab5-positive early endosomes and Atg8a-positive autophagosomes. To assess the specific morphological features, TEM images immunolabelled for endocytic and autophagic structures would also be good alternative experiments to complement this data.

The accumulation of Rab7 positive endosomes was later verified using the new UAS ArfGAP3 RNAi (VDRC B) fly line to confirm the observations seen in the UAS ArfGAP3 RNAi (RJ) line was reliable. As observed in figure 5.8C'-D, the number of Rab7 positive endosomes is significantly increased in the UAS ArfGAP3 RNAi (VDRC B) fat bodies compared to the control luciferase RNAi fat bodies. Quantification analysis clarified a fourfold increase in endosome number in the ArfGAP3 RNAi line compared to control (figure 5.8D). In addition, image acquisition at a higher magnification, showed endosome morphology in the ArfGAP3 RNAi VDRC B fly line was seen more prominent (clear ring-like structures) (figure 5.8C''). A limitation in this analysis is as mentioned in chapter 4, that the luciferase RNAi is a TriP line which is a different genetic background to the VDRC B ArfGAP3 RNAi line. In theory, having a control against a completely unrelated protein can be a comparable control, but only if the genetic background is the same.

In Gabor's study, immunostaining for endogenous Rab7 was carried out in larval garland nephrocytes in control and Arl8 RNAi cells. Garland nephrocytes were the chosen tissue because nephrocytes are known as an "excretory" organ by endocytosis. In flies, the endocytic cargo can be sorted by nephrocytes for either

degradation by lysosome or recycling back into haemolymph. Hence, nephrocytes are used as a model to study endocytosis due to its high endocytic activity (Boda *et al.*, 2019). In their study, enlarged Rab7-positive late endosomes were seen when Arl8 was silenced. Immunostaining for endogenous Rab7 was carried out in the control (luciferase RNAi) and ArfGAP3 RNAi garland nephrocytes (figure 5.9A). When ArfGAP3 was silenced, there was an increase in Rab-7 positive endosomes by almost 2-fold compared to control, however this was not significant (figure 5.9B). The immunofluorescence staining was not as clear as in Gabor's study, where the Rab-7 positive endosome ring structure was seen very clearly and hence easier to quantify. Nevertheless, some rab-7 positive ring structures could be seen in the ArfGAP3 RNAi cells. Again, the limitation in the analysis of this data was using luciferase RNAi as the control line, WT (w118) would have been a better control. To support the Rab7 data in this sub-chapter, western blot data showing accumulation of endogenous Rab7 in control and ArfGAP3 RNAi fly lysates will have to be carried out as future experiments.

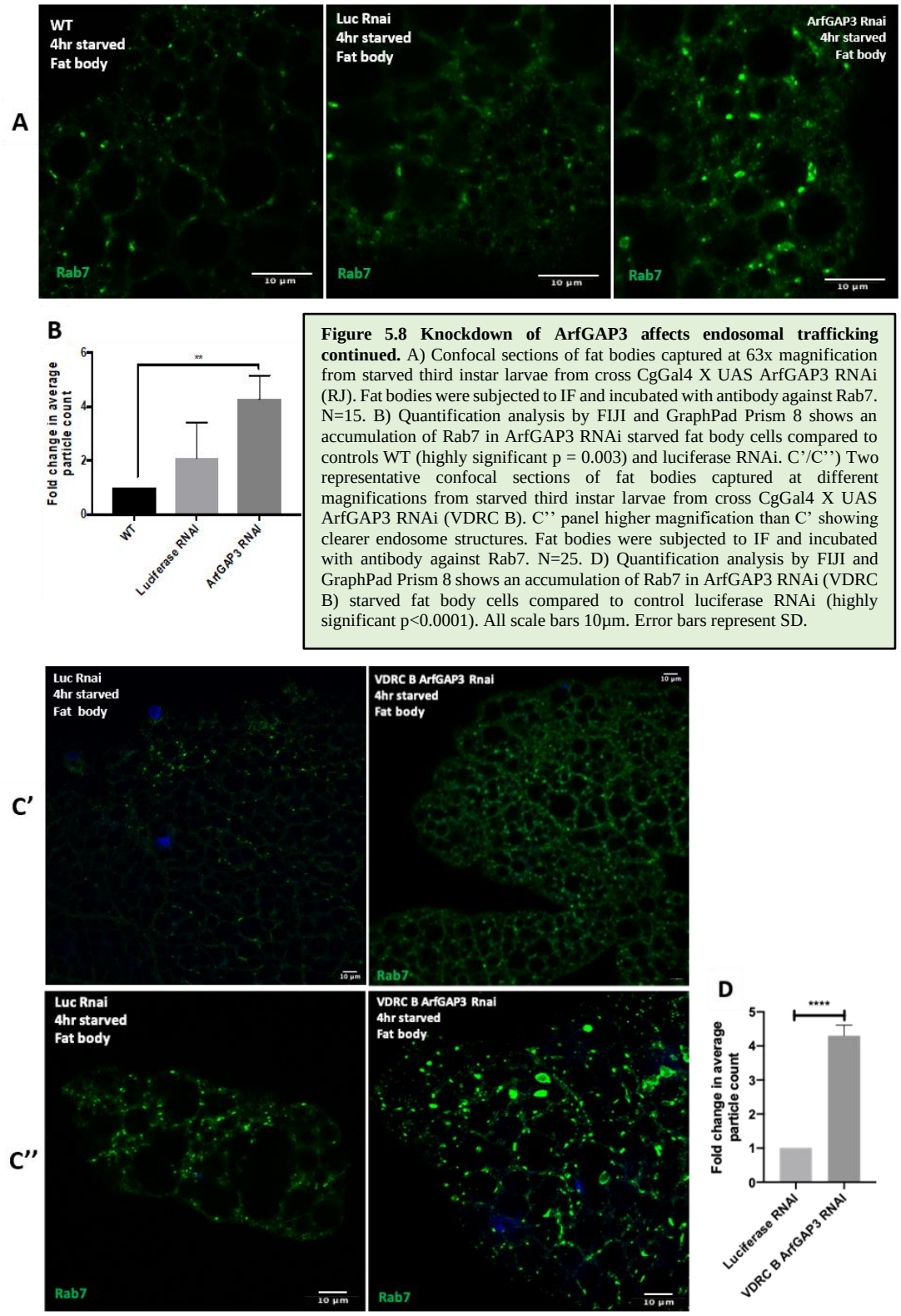

Figure 5.8 Knockdown of ArfGAP3 affects endosomal trafficking continued. A) Confocal sections of fat bodies captured at 63x magnification from starved third instar larvae from cross CgGal4 X UAS ArfGAP3 RNAi (RJ). Fat bodies were subjected to IF and incubated with antibody against Rab7. N=15. B) Quantification analysis by FIJI and GraphPad Prism 8 shows an accumulation of Rab7 in ArfGAP3 RNAi starved fat body cells compared to controls WT (highly significant p = 0.003) and luciferase RNAi. C'/C'') Two representative confocal sections of fat bodies captured at different magnifications from starved third instar larvae from cross CgGal4 X UAS ArfGAP3 RNAi (VDRC B). C'' panel higher magnification than C' showing clearer endosome structures. Fat bodies were subjected to IF and incubated with antibody against Rab7. N=25. D) Quantification analysis by FIJI and GraphPad Prism 8 shows an accumulation of Rab7 in ArfGAP3 RNAi (VDRC B) starved fat body cells compared to control luciferase RNAi (highly significant p<0.0001). All scale bars 10µm. Error bars represent SD.

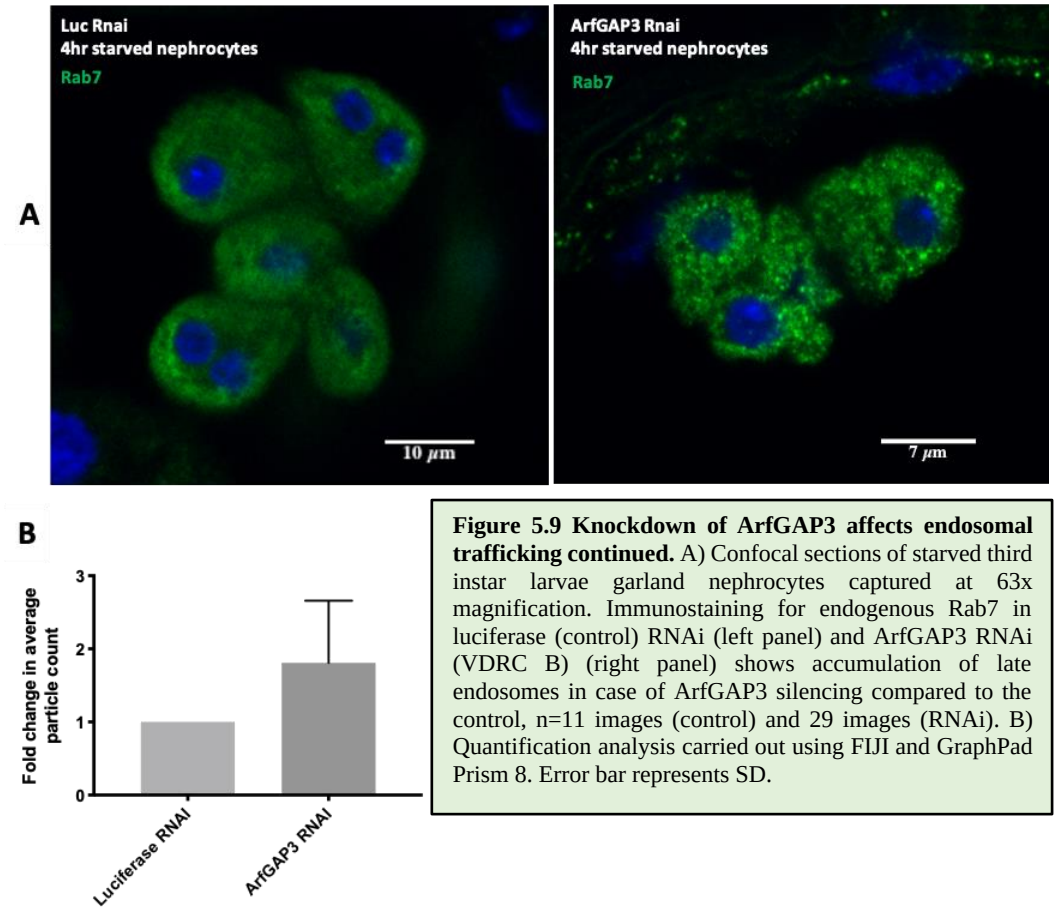

Figure 5.9 Knockdown of ArfGAP3 affects endosomal trafficking continued. A) Confocal sections of starved third instar larvae garland nephrocytes captured at 63x magnification. Immunostaining for endogenous Rab7 in luciferase (control) RNAi (left panel) and ArfGAP3 RNAi (VDRC B) (right panel) shows accumulation of late endosomes in case of ArfGAP3 silencing compared to the control, n=11 images (control) and 29 images (RNAi). B) Quantification analysis carried out using FIJI and GraphPad Prism 8. Error bar represents SD.

5.5.3 Knockdown of ArfGAP3 disrupts endosome-lysosome fusion

After examining the effect of low levels of ArfGAP3 on the autophagic flux and hence autophagosome-lysosome fusion, next we approach to investigate endosome-lysosome fusion. Since ArfGAP3 has been previously shown to co-localise to Rab5 and Rab7, it was considered that ArfGAP3 could also possibly be involved in endosome-lysosome fusion events.

To address whether ArfGAP3 is involved in regulating endosome-lysosome fusion, immunofluorescence was carried out on WT (W118) (control), luciferase RNAi (control) and ArfGAP3 RNAi (VDRC B) 4-hour sucrose starved larval fat

bodies for Rab7 (late endosome marker) and cathepsin-L (lysosomal protein), to check for co-localisation (figure 5.10). It is expected that if the endosome-lysosome fusion events are not disrupted, clear overlapping of both Rab7 and cathepsin-L signals should be seen. On the other hand, if endosome-lysosome fusion is disrupted, both signals should not overlap. Quantification of the Rab7 and Cathepsin-L signals were analysed using generating a Pearson's correlation coefficient followed by statistical analysis.

As expected, in both controls, WT (W118) and luciferase RNAi, there was clear co-localisation of Rab7 positive endosomes and cathepsin-L positive lysosomes, verifying normal endosome-lysosome fusion events (figure 5.10 A&B). The average Pearson's correlation coefficient was 0.67 for WT (W118) and 0.6 for luciferase RNAi (figure 5.10D). On the contrary, in starved ArfGAP3 RNAi (VDRC B) fat bodies, the co-localisation of Rab7 positive endosomes with cathepsin-L positive lysosomes reduced by 1.5-fold, giving an average Pearson's correlation coefficient of 0.4. Statistical analysis (one-way ANOVA) revealed that the difference in average Pearson's correlation coefficient between the controls and ArfGAP3 RNAi was highly significant ($p<0.0001$). As mentioned previously, the luciferase RNAi was an incorrect control used for the VDRC B ArfGAP3 RNAi line. In addition, the significant difference in Rab7 and cathepsin-L co-localisation between luciferase RNAi and VDRC B ArfGAP3 RNAi revealed by statistical analysis is questionable since the error bars overlap largely. On the other hand, the significant difference in Rabb7 and cathepsin-L co-localisation between the appropriate WT (w118) control and VDRC B ArfGAP3 RNAi is a more reliable result as the error bars do not overlap. The data here signifies that endosome-lysosome fusion was disrupted in ArfGAP3

RNAi starved fat bodies and hence low levels/absence of ArfGAP3 affects endocytic activity.

5.6 Knockdown of ArfGAP3 does not affect endosome-autophagosome fusion

Endocytosis and autophagy can functionally interact. In other words, the endocytic and autophagic pathways can interconnect on the occasion when autophagosomes fuse with late endosomes (multivesicular bodies, MVBs) to form amphisomes, which can then mature or fuse with lysosomes to form autolysosomes (Tooze, Abada and Elazar, 2014). In this study, data leans towards the possibility that low levels of ArfGAP3 disrupts autophagosome-lysosome fusion and subsequently disrupts the autophagic flux, however this is not fully conclusive until further experiments are carried out to support this notion. In addition, there was compelling evidence that low levels of ArfGAP3 disrupts endosome-lysosome fusion and hence endocytic flux was also disrupted. Therefore, investigating the effect of ArfGAP3 on trafficking of endosomes to autophagosomes and hence autophagosome-endosome fusion was the next approach.

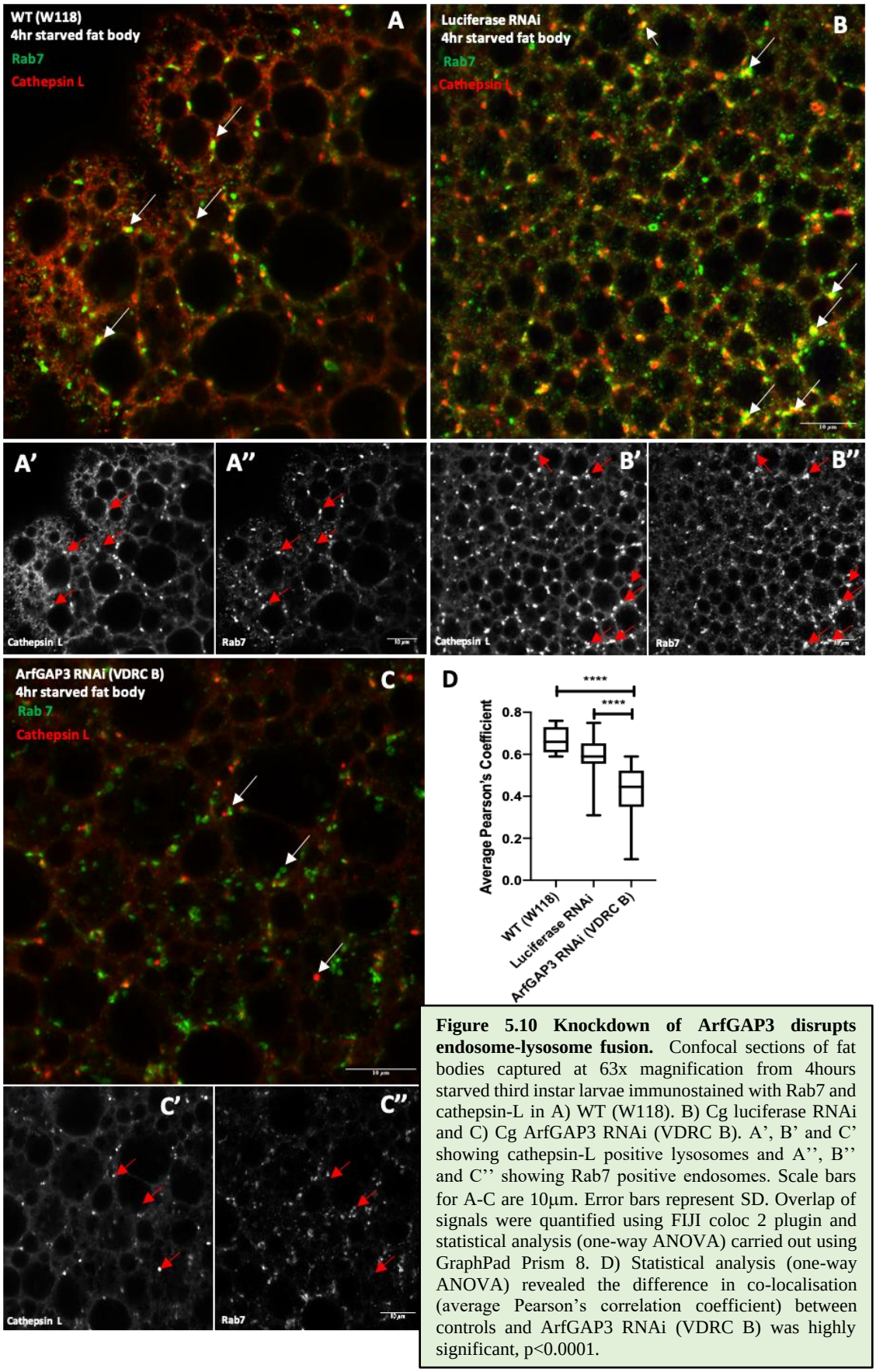

Figure 5.10 Knockdown of ArfGAP3 disrupts endosome-lysosome fusion. Confocal sections of fat bodies captured at 63x magnification from 4hours starved third instar larvae immunostained with Rab7 and cathepsin-L in A) WT (W118). B) Cg luciferase RNAi and C) Cg ArfGAP3 RNAi (VDRC B). A', B' and C' showing cathepsin-L positive lysosomes and A'', B'' and C'' showing Rab7 positive endosomes. Scale bars for A-C are 10μm. Error bars represent SD. Overlap of signals were quantified using FIJI coloc 2 plugin and statistical analysis (one-way ANOVA) carried out using GraphPad Prism 8. D) Statistical analysis (one-way ANOVA) revealed the difference in co-localisation (average Pearson's correlation coefficient) between controls and ArfGAP3 RNAi (VDRC B) was highly significant, $p<0.0001$.

5.6.1 Knockdown of ArfGAP3 does not disrupt autophagosome- endosome fusion.

In order to examine whether ArfGAP3 mediates the trafficking of endosomes to autophagosomes, flies expressing mCherry tagged Atg8a in fat bodies were crossed with UAS ArfGAP3 RNAi (VDRC B) flies. ArfGAP3 was silenced in the fat bodies of the resulting progeny. Luciferase RNAi flies was used as control. Dissected fat bodies were immunostained with Rab7.

Since ArfGAP3 was shown to mediate fusion of autophagosomes and endosomes with lysosomes, it was assumed that ArfGAP3 possibly also mediated the fusion of autophagosomes and endosomes. Nevertheless, this was not the case observed through confocal microscopy. In control cells, in some cases Rab7 positive late endosomes were seen to co-localise with mCherry-Atg8a positive autophagosomes (figure 5.11A). However, in other cases, there was no clear overlap of the Rab7 and mCherry-Atg8a signals, but the endosomes were seen to locate around mCherry-Atg8a positive autophagosomes that were also slightly bigger in size, as if perhaps fusion was about to take place (figure 5.11B).

In fat bodies expressing ArfGAP3 RNAi, some overlap of Rab7 and mCherry-Atg8a signals was also observed (figure 5.11C). Like in the control cells, where there was no clear overlap of Rab7-GFP and mCherry Atg8a signals, endosomes surrounding slightly larger mCherry-Atg8a positive autophagosomes was also noticed in some cases. The endosomes surrounding the autophagosomes seen in these confocal images were like what was observed in the TEM experiment images in figure 5.7, where the “endosome-like” vesicles surrounded the lysosomes. Quantification analysis revealed that there was no significant difference in co-localisation between

Rab7 positive endosomes and mCherry-Atg8a positive autophagosomes when ArfGAP3 was knockdown compared to control RNAi cells (p=0.06) (figure 5.11E). The data here suggests that ArfGAP3 knock down does not affect autophagosome-endosome fusion. However, since luciferase RNAi is an inappropriate control to use for VDRC B ArfGAP3 RNAi, repeating this experiment using WT (w118) should be the next approach to clarify this data and conclusion.

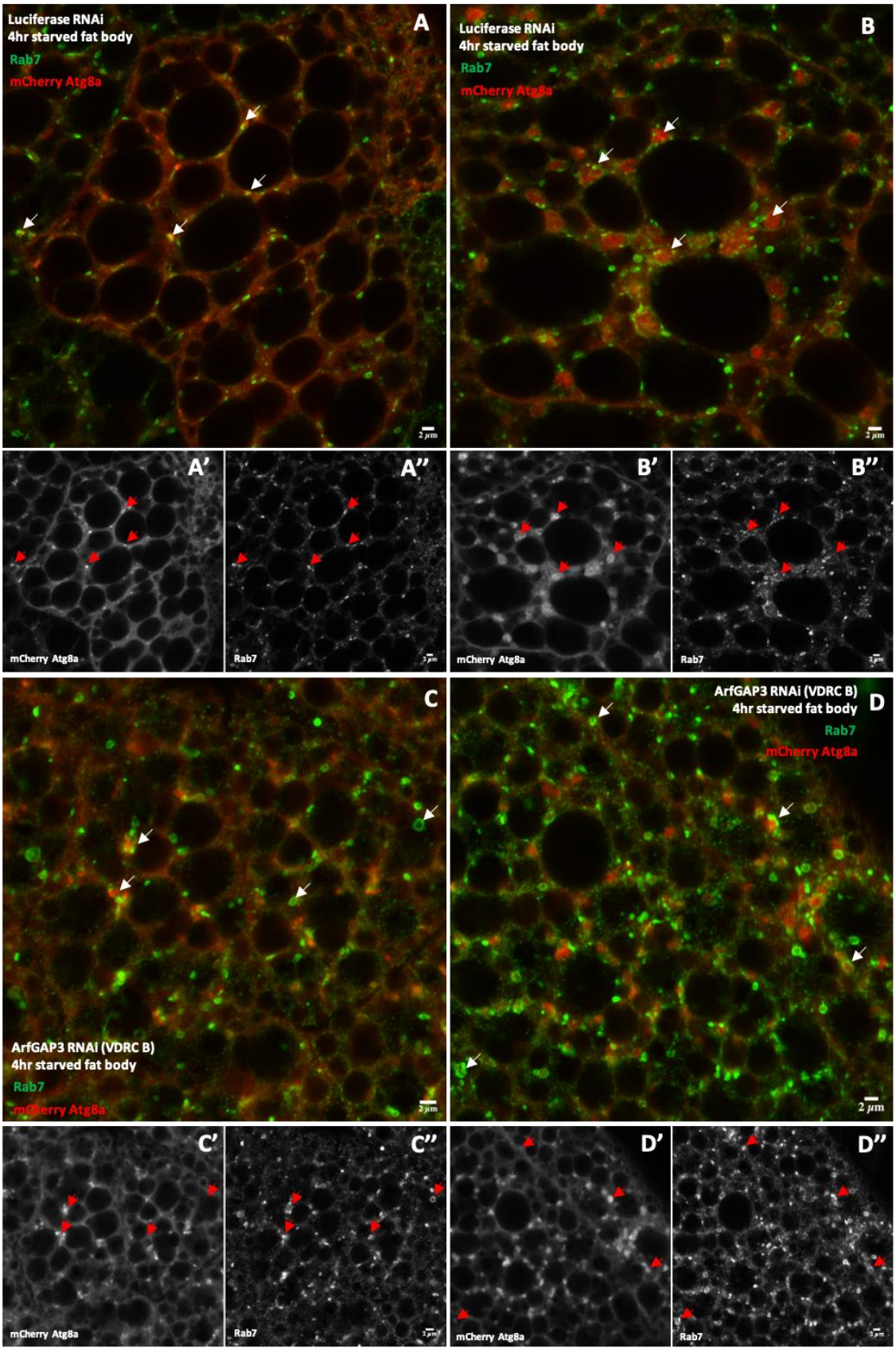
Luciferase RNAi
4hr starved fat body
Rab7
mCherry Atg8a
A
B
A'
A''
B'
B''
mCherry Atg8a
Rab7
C
D
ArfGAP3 RNAi (VDRC B)
4hr starved fat body
Rab7
mCherry Atg8a
C'
C''
D'
D''
2 μm

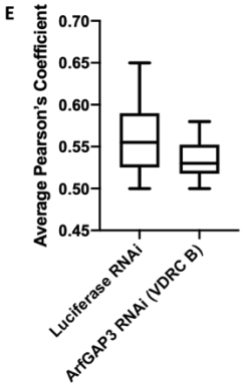

Figure 5.11 Knockdown of ArfGAP3 does not disrupt autophagosome-endosome fusion. Confocal sections of fat bodies captured at 63x magnification from 4hours starved third instar larvae expressing mCherry Atg8a and immunostained with Rab7 in A-B) luciferase RNAi (control) and C-D) ArfGAP3 RNAi (VDRC B). A and B are two representative images of luciferase RNAi. C and D are two representative images if ArfGAP3 RNAi VDRC B. A', B' and C' showing mCherry Atg8a autophagosome in respective genotypes. A'', B'' and C'' are showing Rab7 endosomes in respective genotypes. Scale bars for A-D are 2µm. Error bars represent SD. Overlap of signals were quantified using FIJI coloc 2 plugin and statistical analysis (T-tests) carried out using GraphPad Prism 8. E) Statistical analysis revealed there was no significant difference in co-localisation (average Pearson's correlation coefficient) between luciferase RNAi and ArfGAP3 RNAi (VDRC B), $p<0.06$.

5.7 ArfGAP3 in the interplay between autophagy and lipophagy

Recent studies have shown that lipid droplets regulate autophagosome biogenesis and there has been growing evidence showing that also autophagy regulates lipophagy (Singh *et al.*, 2009; Shpilka and Elazar, 2015; Garcia, Vevea and Pon, 2018). Certain proteins that have also been identified on lipid droplets (LD) include Arf1 (ArfGAP3 regulates Arf1 protein) and ArfGAP1 (Human homolog of *Drosophila* ArfGAP3) (Bartz *et al.*, 2007). As mentioned in Chapter 1.5, the study by Hommel *et al* showed that knockdown of Arf-like GTPase, ARFRP1, results in hinderance in normal development of lipid droplets and therefore regulates lipid droplet growth and lipolysis (Hommel *et al.*, 2010). In essence, Arf proteins, Arf GTPases and Rab proteins all seem to have functional relevance in lipid droplet development and lipolysis.

Since studies show possible links of mammalian ArfGAP1 and ARFRP1 to lipid droplet regulation, the effect of *Drosophila* ArfGAP3 on lipid droplet development was the final approach to investigate in this chapter.

5.7.1 The effect of ArfGAP3 in lipid droplet development

Lipid droplets are located in *Drosophila* fat body cells. To examine the effect of ArfGAP3 on lipid droplet development, UAS ArfGAP3 RNAi (RJ) flies were crossed with the CgGal4 driver, resulting in progeny flies expressed ArfGAP3 RNAi in fat bodies. Dissected fat bodies were then stained with a lipid droplet dye, BODIPY. The size of the lipid droplets was compared between WT (W118) control and ArfGAP3 RNAi (RJ).

Lipid droplets in the control cells varied in size, with the largest LD size of around 15μm. The average size of LD in WT control cells was around 9μm. On the contrary, the lipid droplets in fat bodies expressing ArfGAP3 RNAi were much bigger in size. The average size of LD increased to around 14μm and the largest LD was around 20μm. Statistical analysis, t-test, revealed that the increase in average LD size in ArfGAP3 RNAi fat bodies compared to WT LDs was highly significant (figure 1.12). The lipid droplet sizes in control cells were in the expected range of 'normal' lipid droplet development as previous studies in *Drosophila* have published average LD size in controls also around 9μm and largest around 14μm (Fan *et al.*, 2017). Therefore, this data strongly confirms that the enlargement of LDs is abnormal in ArfGAP3 RNAi fat bodies and suggests that ArfGAP3 is key for normal LD development.

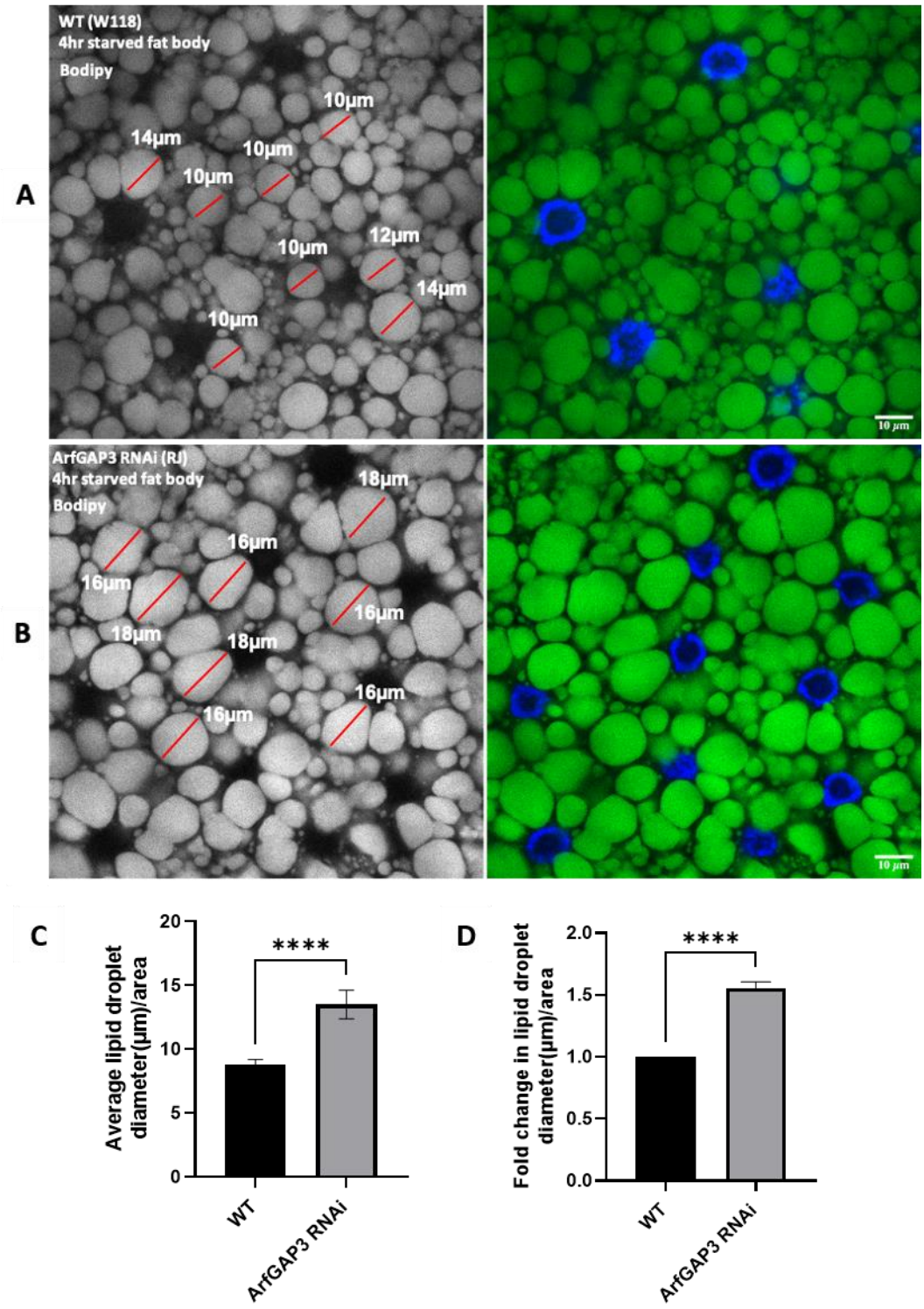

Figure 5.12 Knockdown of ArfGAP3 causes enlargement of lipid droplets. Confocal sections of fat bodies captured at 63x magnification from 4hours starved third instar larvae stained with BODIPY in A) WT (W118) (control) and B) ArfGAP3 RNAi (RJ). Scale bars are 10µm, n=12 images. C) Quantification showing average LD diameter (µm)/area. D) Quantification showing fold change in LD diameter (µm)/area. LD diameter was measured using the built in 'analyse particle' tool in FIJI. The area of each particle was measured and converted to diameter size (µm) using equation [2*SQRT(area/pi())] in excel. Statistical analysis (T-tests) carried out using GraphPad Prism 8. Analysis revealed a significant increase in lipid droplet size in ArfGAP3 RNAi (RJ) compared to control cells ($p<0.0001$).

The data in this chapter suggests a possible role of ArfGAP3 in the endolysosomal pathway as knockdown of ArfGAP3 resulted in an accumulation of endosomes and disrupted downstream endosome-lysosome fusion. Even though the data indicates knockdown of ArfGAP3 influences lysosome size, some of the data in this chapter is open to question and interpretation, in particularly figure 5.3 and figure 5.5, examining the effect of ArfGAP3 on the autophagic flux. On one hand we see less autophagosomes in ArfGAP3 RNAi cells compared to control in figure 5.3, which in theory signifies normal autophagic flux, suggesting that the knockdown of ArfGAP3 aids normal autophagic flux. However, examining the effect of ArfGAP3 on autophagosome-lysosome fusion suggested otherwise, that knockdown of ArfGAP3 disrupts fusion of these compartments and hence disrupts autophagic flux. Interestingly, in figure 5.5, we do see autophagic structures in the ArfGAP3 RNAi cells and mostly only autolysosomes in the control cells indicating clearance of autophagosomes through normal autophagic flux compared to RNAi cells. Figures 5.11C' and 5.11D' also show mCherry positive autophagic structures in ArfGAP3 RNAi cells. The data in figure 5.5 suggests there could be an accumulation of autophagosomes in ArfGAP3 RNAi cells compared to control (not quantified), which, if true, would fit the interpretation that knockdown of ArfGAP3 disrupts autophagic flux, since fusion is impaired, there should in theory be an accumulation of autophagosomes. Further experiments and repeats will need to be carried out to clarify this data, by performing autophagic flux assays by western blotting to see if endogenous levels of Atg8a accumulates in ArfGAP3 RNAi fly lysates.

Chapter 6

Investigating the physiological relevance of ArfGAP3 during ageing

6.1 Chapter introduction: Autophagy and endolysosomal system in ageing.

Autophagic activity has been shown to decline with age, being the likely causative factor of accumulation of damaged cytosolic macromolecules and organelles during ageing (Lipinski *et al*, 2010; Maruzs *et al*, 2019). A study in 2010 showed the essential role of ROS as a mediator upstream to the activation of type III PI3 kinase, which is key for autophagy induction. Moreover, they also reported the transcriptional down-regulation of autophagy during normal aging in human brain (Lipinski *et al*, 2010). Dysfunctional autophagy and endolysosomal system are key pathological features that worsen age-associated diseases, e.g., neurodegeneration. Defects in autophagy has been implicated in age-related diseases such as Alzheimer's disease (AD), Parkinson's disease (PD), Huntington's disease (HD), Frontal Temporal Dementia (FTD) etc since these diseases exhibit pathological characteristics of accumulated proteins leading to chronic aggregation (Reggiori and Klumperman, 2016). Observations in certain studies have shown the decline in effects of these toxic protein aggregates by upregulating autophagy by using chemical inducers of autophagy like rapamycin (Metcalf *et al*, 2012). The treatment of rapamycin has been reported to augment

clearance of mutant huntingtin protein aggregation, resulting in subsequent protection against toxicity in mammalian cells and animal models of HD (Berger *et al*, 2006; Ravikumar *et al*, 2006; Sarkar *et al*, 2009; Metcalf *et al*, 2012). In addition, defects in the endolysosomal system has also been implicated in AD where levels of Rab5 and Rab7 have been shown to be upregulated in the brain (Reggiori and Klumperman, 2016; Xu *et al*, 2018). A study on post-mortem human brain tissue from patients with mild cognitive impairment and AD showed Rab5 and Rab7 was selectively up regulated in the hippocampus, basal forebrain and frontal cortex compared to brain tissues from patients with no cognitive impairment (Ginsberg *et al*, 2010).

There have not been any published studies showing any relevance of ArfGAP3 in age-related physiology, however, it became an avenue to explore after discovering ArfGAP3's significant relations to autophagy and endolysosomal system. In Chapter 5, the function of ArfGAP3 in the interplay between autophagy and endosomal trafficking was established. This chapter will explore further findings that suggest any physiological importance of ArfGAP3 in autophagy during ageing.

6.2 Lifespan of ArfGAP3 knockdown transgenic flies is reduced

The effect of absence of ArfGAP3 was examined on lifespan of adult *Drosophila* flies. For this survival assay, DaGal4 driver flies (driver for whole body expression) was crossed with UAS ArfGAP3 RNAi (VDRC B) flies. The progeny flies had ArfGAP3 knockout throughout the whole body. Luciferase RNAi flies were used as control.

It has been documented that on average wildtype male adult *Drosophila* flies can live up to ~50 days at 25°C, generally having a shorter lifespan than females

(Linford *et al.*, 2013). In the case of luciferase RNAi control, the average lifespan for male flies was 71 days and 74 days for female flies. On the contrary the average lifespan for ArfGAP RNAi male and female flies was 60 and 62 days respectively. Comparison of the survival curves using Log-rank (Mantel-Cox) test revealed that the difference in average lifespans between luciferase RNAi and ArfGAP3 RNAi males was highly significant (chi square = 8.072, p = 0.0045), however there was no significant difference in the average lifespan between luciferase RNAi and ArfGAP3 RNAi female flies (chi square = 0.7186, p=0.3966) (figure 6.1). In summary, the lifespan data revealed that for both genotypes the females lived longer than males, however knockdown of ArfGAP3 affected the lifespan of male flies than female flies compared to respective male and female control flies. This data suggests that ArfGAP3 expression, in a sex biased manner, positively contributes to longevity. Many species exhibit sex-biased differences in traits. In *Drosophila* it has been reported that females have the tendency to live longer than males, as also the case for humans and any other species where the XY sex chromosome is male (Tower and Arbeitman, 2009). In *Caenorhabditis elegans*, the hermaphrodites possess the XX chromosome and tend to live longer than males, which only possess one X chromosome. On the contrary, the heterogametic sex in most bird species is female, and for these species, the males tend to live longer than females (Tower and Arbeitman, 2009). Certain genetic and environmental factors have been observed to have a greater effect in one sex over the other (Partridge *et al*, 2005; Tower, 2006). These factors is discussed in detail in the discussion chapter 7.3.

Since these aging experiments were conducted towards the end of the PhD timeline, the previous ArfGAP3 RNAi experiments discussed in chapter 5 had been

carried out prior to obtaining these lifespan results. Thus, sex of flies was not considered at the time of the earlier ArfGAP3 RNAi experiments. Going forward, sex selection will need to be implemented in experimental design as appropriate controls. The limitation in the lifespan analysis here is that the genetic background of the luciferase RNAi and ArfGAP3 VDRC B RNAi lines were not the same, so using WT (w118) as another control would have been appropriate. Going forward, the genetic background of control flies should be verified to avoid any background effects occurring.

6.3 Knockdown of ArfGAP3 does not affect climbing ability of *Drosophila* flies

To characterise the phenotype by assessing the physiological differences between ArfGAP3 RNAi flies and luciferase RNAi control flies, a series of climbing assays were conducted to examine the locomotor behaviour of the two genotypes. The climbing assay was carried out on 7 days and 4 weeks old flies, where the flies were transferred into climbing vials, tapped down to the bottom, followed by recording the number of flies that climbed up to each segment in the climbing vial (low, middle and high) at 10 and 20 seconds.

As the flies aged to 4 weeks, their ability to climb had significantly reduced compared to 7 days for both luciferase RNAi and ArfGAP3 RNAi male and female flies, as 80-90% of the flies remained at the lowest segment of the climbing vial, unable to climb further up (figure 6.2) (tables 6.1 and 6.2). On the other hand, there was no significant difference in climbing ability between the two genotypes at 7 days and 4 weeks (figure 6.2) (tables 6.3 and 6.4) at each time point. For both of the control

luciferase RNAi and ArfGAP3 RNAi flies, the female flies showed better locomotor behaviour at both time points, as a larger proportion of female flies were recorded in the higher segments (6-11.5cm) of the climbing vial compared to male flies. On the whole, these results suggest that lack of expression of ArfGAP3 does not hinder the negative geotaxis and climbing ability of *Drosophila*.

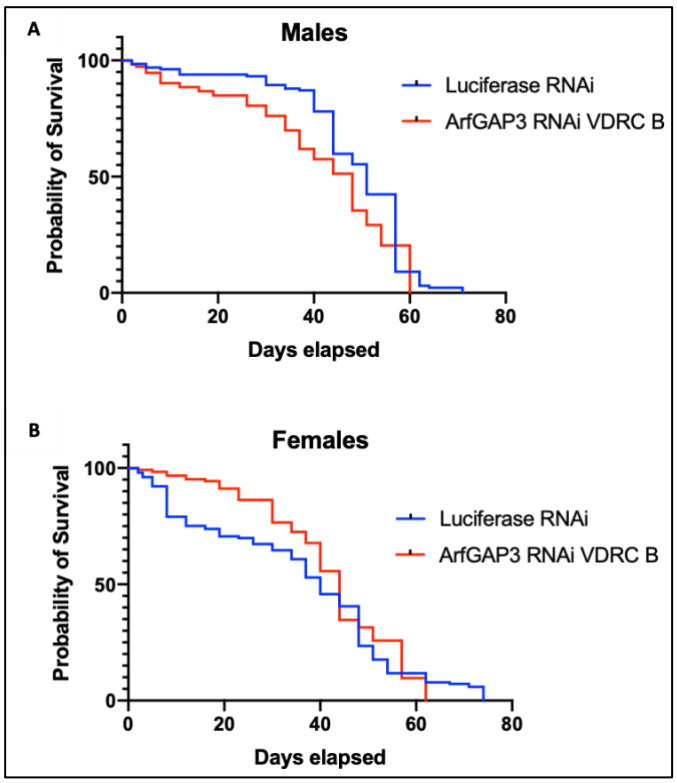

Figure 6.1 Longevity of ArfGAP3 knockdown transgenic flies is reduced. Survival curves showing probability of survival over time for A) ArfGAP3 RNAi VDRC B and luciferase RNAi male flies and B) ArfGAP3 RNAi VDRC B and luciferase RNAi female flies. ArfGAP3 RNAi male flies demonstrated a significantly reduced average lifespan compared to luciferase RNAi control flies (chi square 8.072, p=0.0045) whereas the females flies did not (chi square 0.7186, p=0.3966). N=3 lifespan assays with different biological replicates and 3 technical replicates. Statistical analysis carried out using log-rank (Mantel Cox) test using GraphPad prism 8.

6.4 Expression of ArfGAP3 in the brain

Drosophila ArfGAP3 has been shown to play a crucial role in the patterning of the *Drosophila* pupal eye (Johnson *et al.*, 2011). Moreover, the lifespan and climbing assay suggest some physiological relevance of ArfGAP3 during aging. Naturally, the next approach was to examine where ArfGAP3 is expressed in the brain.

6.4.1 ArfGAP3 is expressed in larval brain

In order to examine expression of ArfGAP3 in the *Drosophila* larval brain, ElavGal4 flies (driver for expression in brain) were crossed with UAS ArfGAP3 WT flies tagged with FLAG and the progeny larval brains were immunostained with anti-FLAG. ArfGAP3 was predominantly expressed in the optic lobes of the larvae brain (figure 6.3). ArfGAP3 expression in the optic lobes agrees with the study highlighting the role of ArfGAP3 in *Drosophila* pupal eye patterning. Additionally, it was also interesting to observe that some expression was also seen in the central brain area and ventral nerve cord. This could possibly indicate that ArfGAP3 may have a larger role within the brain.

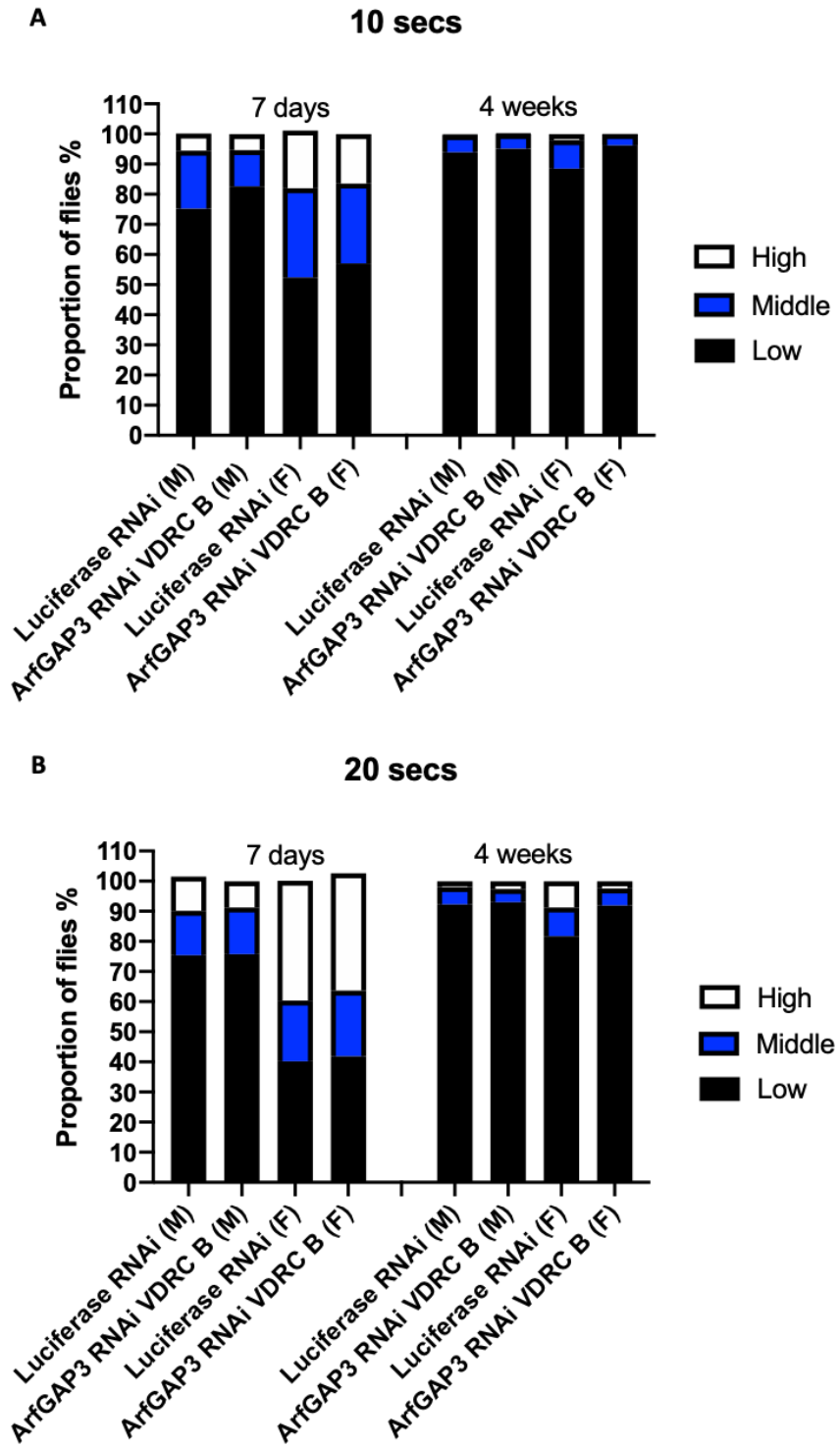

Figure 6.2 Knockdown of ArfGAP3 does not affect climbing ability of *Drosophila* flies. Climbing assay results illustrated as bar charts showing proportion of flies that climbed to each segment; low (<1.5cm), middle (1.5-6cm) and high (6-11.5cm). Number of flies were recorded at A) 10secs and B) 20 seconds. N = 3 climbing assay replicates with different biological replicates and 3 technical replicates.

Table 6.1. Climbing ability significantly reduced in aged control and ArfGAP3 RNAi flies. Table summarises the climbing abilities between 7 days and 4 weeks old flies within the same genotype. Proportion of flies were recorded at low, middle and high segments of the climbing vial at 10 seconds after tapping the flies down. Statistical analysis, t-test, for each segment was carried out using GraphPad Prism 8.

	Males			
Height climbed in 10 secs	Control proportion % (7days)	Control proportion % (4 weeks)	p value	Significant difference?
Low	75.19	93.89	0.00218851	**
Middle	19.26	5.74	0.01677334	*
High	5.74	0.37	0.01336915	*
	Males			
Height climbed in 10 secs	ArfGAP3 RNAi proportion % (7days)	ArfGAP3 RNAi proportion % (4 weeks)	p value	Significant difference?
Low	82.59	95.15	0.01507041	*
Middle	12.04	4.85	0.07305235	NS
High	5.37	0.37	0.01030884	*
	Females			
Height climbed in 10 secs	Control proportion % (7days)	Control proportion % (4 weeks)	p value	Significant difference?
Low	52.41	88.48	0.00273006	**
Middle	29.63	9.48	0.00138551	**
High	19.07	2.04	0.02158861	**
	Females			
Height climbed in 10 secs	ArfGAP3 RNAi proportion % (7days)	ArfGAP3 RNAi proportion % (4 weeks)	p value	Significant difference?
Low	57.04	96.19	0.0065981	**
Middle	26.48	3.81	0.0016198	**
High	16.48	0.00	0.09759703	NS

Table 6.2. Climbing ability significantly reduced in aged control and ArfGAP3 RNAi flies continued. Table summarises the climbing abilities between 7 days and 4 weeks old flies within the same genotype. Proportion of flies were recorded at low, middle and high segments of the climbing vial at 20 seconds after tapping the flies down. Statistical analysis, t-test, for each segment was carried out using GraphPad Prism 8.

	Males			
Height climbed in 20 secs	Control proportion % (7days)	Control proportion % (4 weeks)	p value	Significant difference?
Low	75.37	92.28	0.00093384	***
Middle	14.81	5.78	0.01755428	*
High	11.30	1.94	0.00315142	**
	Males			
Height climbed in 20 secs	ArfGAP3 RNAi proportion % (7days)	ArfGAP3 RNAi proportion % (4 weeks)	p value	Significant difference?
Low	75.74	92.98	0.00311735	**
Middle	15.56	4.43	0.00402372	**
High	8.70	2.59	0.0360677	*
	Females			
Height climbed in 20 secs	Control proportion % (7days)	Control proportion % (4 weeks)	p value	Significant difference?
Low	40.19	81.70	0.00074694	***
Middle	20.19	9.54	0.00019574	***
High	39.81	8.76	0.00053848	***
	Females			
Height climbed in 20 secs	ArfGAP3 RNAi proportion % (7days)	ArfGAP3 RNAi proportion % (4 weeks)	p value	Significant difference?
Low	41.85	91.85	0.00400631	**
Middle	21.85	5.74	0.00732658	**
High	38.89	2.41	0.00797953	**

Table 6.3. Knockdown of ArfGAP3 does not affect climbing ability of *Drosophila* flies. Table summarises the climbing abilities at 7 days and 4 weeks between the two genotypes, control (luciferase RNAi) and ArfGAP3 RNAi. Proportion of flies were recorded at low, middle and high segments of the climbing vial at 10 seconds after tapping the flies down. Statistical analysis, t-test, for each segment was carried out using GraphPad Prism 8.

	Males			
Height climbed in 10 secs	Control proportion % (7days)	ArfGAP3 RNAi proportion % (7days)	p value	Significant difference?
Low	75.19	85.93	0.00803305	**
Middle	19.26	8.70	0.00556539	**
High	5.74	5.37	0.82756472	NS
	Males			
Height climbed in 10 secs	Control proportion % (4 weeks)	ArfGAP3 RNAi proportion % (4 weeks)	p value	Significant difference?
Low	93.89	95.15	0.60344496	NS
Middle	5.74	4.85	0.72510834	NS
High	0.37	0.37	1	NS
	Females			
Height climbed in 10 secs	Control proportion % (7days)	ArfGAP3 RNAi proportion % (7days)	p value	Significant difference?
Low	49.07	63.70	0.00503712	**
Middle	31.63	26.48	0.11352326	NS
High	20.41	9.81	0.05013428	*
	Females			
Height climbed in 10 secs	Control proportion % (4 weeks)	ArfGAP3 RNAi proportion % (4 weeks)	p value	Significant difference?
Low	88.48	96.19	0.03481163	*
Middle	9.48	3.81	0.07985007	NS
High	2.04	0.00	0.00038817	***

Table 6.4. Lack of ArfGAP3 expression does not change locomotor behaviour in flies continued. Table summarises the climbing abilities at 7 days and 4 weeks between the two genotypes, control (luciferase RNAi) and ArfGAP3 RNAi. Proportion of flies were recorded at low, middle and high segments of the climbing vial at 20 seconds after tapping the flies down. Statistical analysis, t-test, for each segment was carried out using GraphPad Prism 8.

	Males			
Height climbed in 20 secs	Control proportion % (7days)	ArfGAP3 RNAi proportion % (7days)	p value	Significant difference?
Low	75.37	85.74	0.01156985	*
Middle	14.81	8.22	0.0506365	*
High	11.30	6.04	0.03399655	*
	Males			
Height climbed in 20 secs	Control proportion % (4 weeks)	ArfGAP3 RNAi proportion % (4 weeks)	p value	Significant difference?
Low	92.28	92.98	0.77962084	NS
Middle	5.78	4.43	0.36426308	NS
High	1.94	2.59	0.68934405	NS
	Females			
Height climbed in 20 secs	Control proportion % (7days)	ArfGAP3 RNAi proportion % (7days)	p value	Significant difference?
Low	40.19	55.19	0.02852101	*
Middle	20.19	18.52	0.61614718	NS
High	39.81	28.89	0.04521815	*
	Females			
Height climbed in 20 secs	Control proportion % (4 weeks)	ArfGAP3 RNAi proportion % (4 weeks)	p value	Significant difference?
Low	81.70	91.85	0.04580351	*
Middle	9.54	5.74	0.12881116	NS
High	8.76	2.41	0.05677405	*

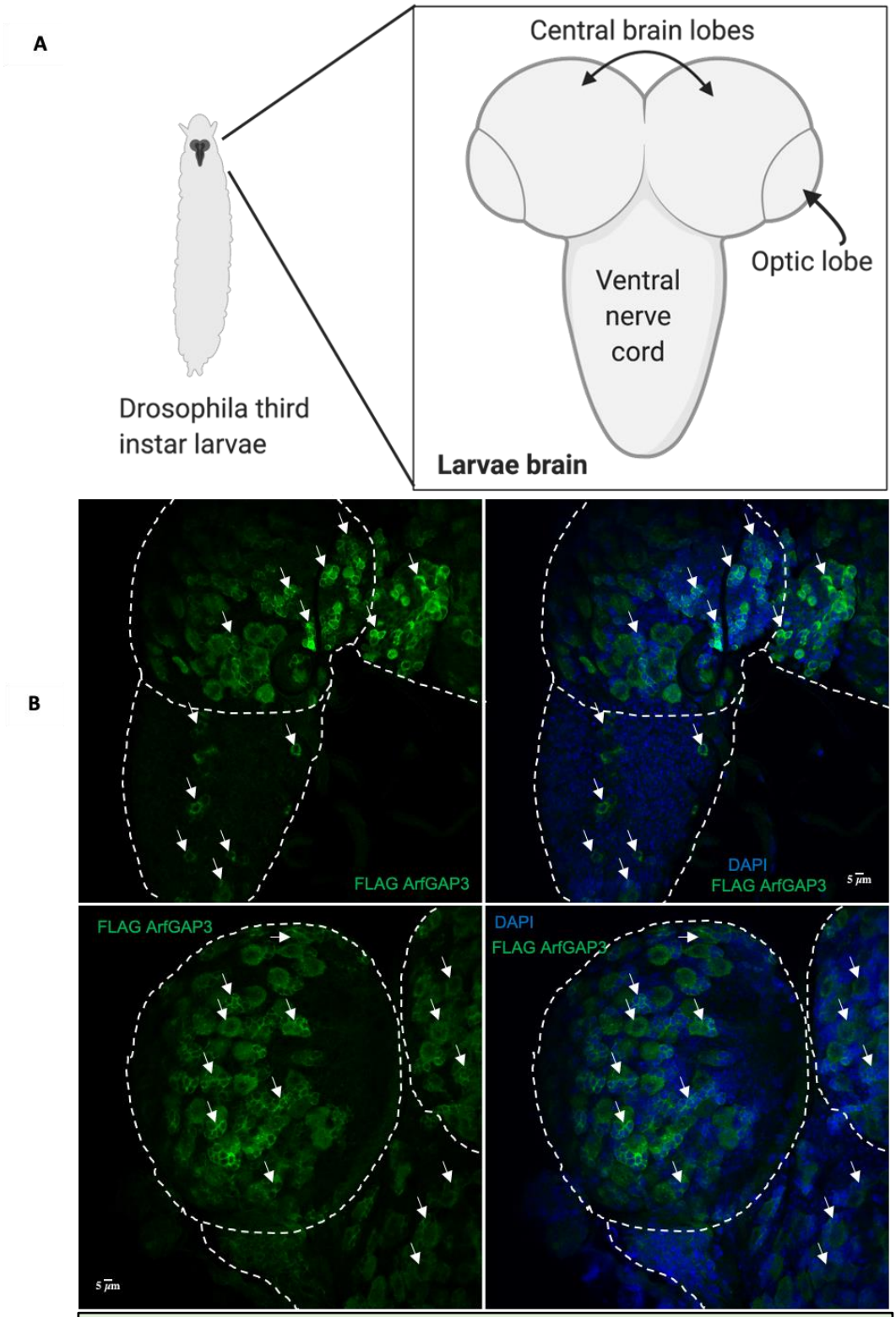

Figure 6.3 ArfGAP3 is expressed predominantly in larval brain optic lobes. A) Schematic diagram illustrating the anatomy of a *Drosophila* larval brain. B) Confocal sections of *Drosophila* larval brain captured at 60x magnification from fed third instar larvae. Scale bars are 5µm. Images were analysed using FIJI. White arrows showing majority of ArfGAP3 expression in optic lobes, and some expression in central brain and ventral nerve cord.

6.5 Knockdown of ArfGAP3 results in accumulation of Ref(2)P in aged flies

Ref(2)P, the *Drosophila* p62 homologue, is a polyubiquitin binding protein which has a significant role in autophagy. It primarily functions to anchor ubiquitinated proteins tagged for degradation to the autophagosome membrane and hence accumulation of Ref(2)P is a clear sign of autophagy disruption (Nezis *et al.*, 2008; Nezis and Stenmark, 2012). Hence, investigating levels of Ref(2)P in aged ArfGAP3 knockdown flies is a good approach to examine the effect of ArfGAP3 on autophagy in aged flies.

Levels of Ref(2)P were investigated in UAS ArfGAP3 RNAi (VDRC B) 7 days and 4 weeks old flies. Wildtype (W118) and luciferase RNAi 7 days and 4 weeks old flies were used as controls. Ref(2)P protein levels had significantly increased in all three genotypes at 4 weeks compared to 7 days. There was a fivefold increase in Ref(2)P levels in 4 week old ArfGAP3 RNAi flies compared to 7 days old and statistical analysis confirmed this increase was highly significant. At 4 weeks old, ArfGAP3 RNAi flies had the highest levels of Ref(2)P accumulation compared to 4 week old WT and luciferase RNAi, further suggesting lack of ArfGAP3 expression contributes to Ref(2)P accumulation, not just the age-related decrease in autophagy function observed in the case with both WT and luciferase RNAi control flies (figure 6.4).

Although a significant difference in Ref((2)P levels was observed between ArfGAP3 RNAi and WT (w118), there are limitations in analysis in the context of aging, since the lifespan assay was not carried out using WT (w118) as a control line. This data would have more significant relevance to autophagy disruption in aged flies with reliable lifespan assay carried out in the same genotypes.

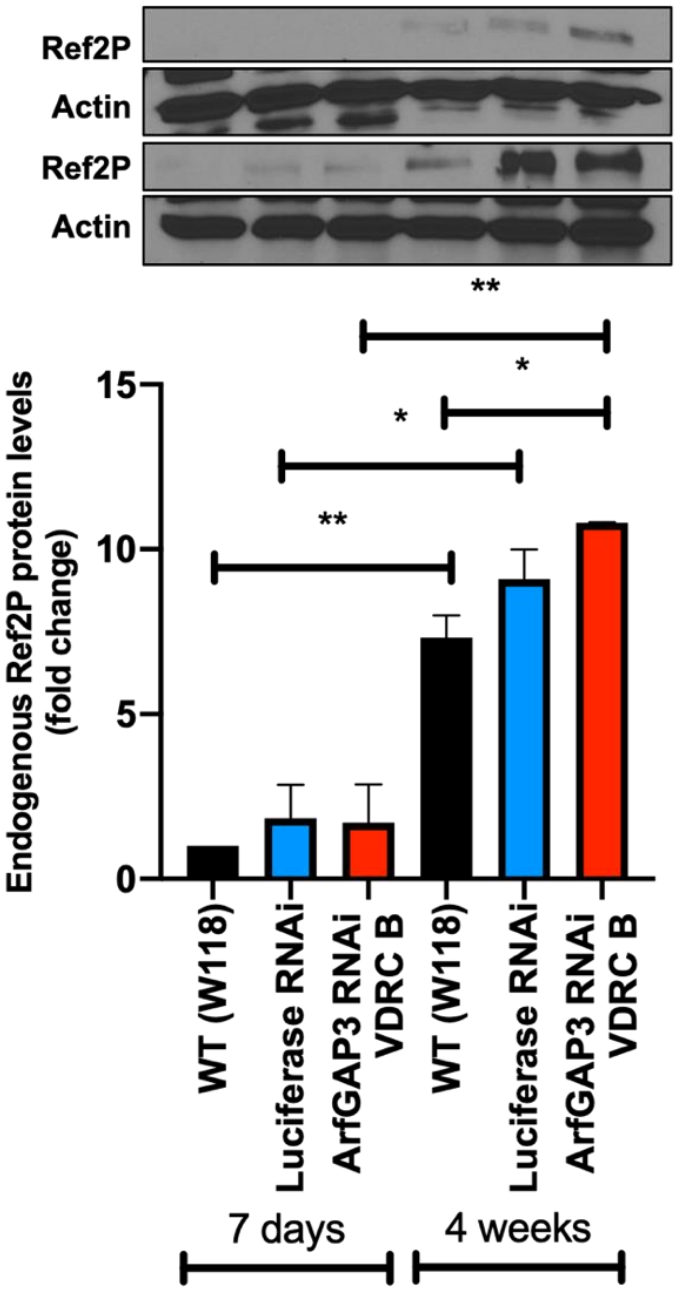

Figure 6.4 Ref(2)P accumulates in 4 weeks old aged flies lacking ArfGAP3 expression. Full fly lysates from 7day old and 4 week old wild type (W118), luciferase RNAi and ArfGAP3 RNAi (VDRC B) flies were subjected to SDS-PAGE (10% gel) and western blotting for Ref(2)P protein. Actin was used as a loading control. The expected band for Ref(2)P was ~100kDa and for actin ~42kDa. N=3 replicates. T-test analysis was carried out for significance p value ($p < 0.05$) confirming a significant increase in Ref(2)P levels in 4 weeks old ArfGAP3 RNAi flies compared to WT and luciferase RNAi flies.

Overall, the data in this chapter is open to questions since the lifespan assay results were not conclusive as the luciferase RNAi line was used as the control, which has a different genetic background to ArfGAP3 VDRC B and so genetic background effects could influence the data. Going forward, the lifespan experiments will need to be repeated using WT (w118) flies as control and if the results support the observations as seen in figure 6.1, then the Ref(2)P accumulation observed in ArfGAP3 RNAi flies compared to WT (w118) will be conclusive.

Part III

Discussion & Conclusions

Chapter 7

Discussion and conclusions

ArfGAP3 has previously determined known functions in membrane trafficking as a GTPase activating protein that hydrolyses GTP-bound Arf1 protein (Inoue and Randazzo, 2007). The recent yeast-two hybrid screening carried out by previous members of our lab revealed ArfGAP3 as an Atg8a-interacting protein. Amongst the many potential candidates, ArfGAP3 was selected for further investigation because it had a high confidence interaction with Atg8a as well as its known key roles in membrane trafficking through regulating Arf1 activity, hence giving rise to the notion that ArfGAP3 could have functional associations with autophagy and endosomal trafficking.

7.1 ArfGAP3 is an Atg8a-interacting protein and a positive regulator of the endocytic flux

To validate the yeast-two hybrid findings and identify if the interaction between ArfGAP3 and Atg8a was LIR dependent or not, the interaction was investigated by *in-vitro* GST pull down analysis. In Chapter 4, *Drosophila* ArfGAP3 was confirmed to interact with Atg8a in a LIR dependent manner. Using the iLIR database generated by Nezis lab, it was also revealed that ArfGAP3 had several hits as potential LIR motifs. Analysing the iLIR database, it was predicted that the xLIR (relaxed) motif, LGYETI, was the most probable LIR motif involved in the interaction with Atg8a.

GST- pull down analysis confirmed the xLIR motif, LGYETI, was a LIR motif responsible for the interaction of ArfGAP3 with Atg8a. However, a second functional LIR motif, PTWSSV, was also identified for ArfGAP3. This was first observed by co-localisation studies, when signals of ArfGAP3-DsRed and Atg8a-positive GFP puncta did not overlap in mutant flies lacking the PTWSSV LIR motif. Overall, these results strongly suggest that ArfGAP3 and Atg8a interact in a LIR dependent manner, with a primary LIR motif responsible for the interaction and a secondary LIR motif that also aids the interaction.

Previous studies have reported it is possible to have more than one functional LIR motif. For example, mATG4 consists of two functional LIR motifs. One of the LIR motifs is the N-terminal LIR, APEAR which is involved in binding and deletion of ATG8-PE. The other LIR motif is the C-terminal LIR involved in constitutive binding to ATG8 (Abreu *et al*, 2017; Park *et al*, 2019). If both ArfGAP3 LIR motifs are required functionally for the interaction, this gives insights that there could be a second binding site that could possibly bind the LIR motif. As mentioned in chapter 4, a new interface between plant Atg8 and its interacting proteins was discovered in *Arabidopsis* (Marshall *et al*, 2015; Marshall *et al*, 2019), which is also conserved in both yeast and human (Lei and Klionsky, 2019). This new interface, identified as the ubiquitin-interacting motif (UIM)-UIM docking site (UDS), is responsible for LIR-LDS independent interaction with Atg8. Experimental data revealed that the UDS domain is located opposite to the LDS domain on Atg8 and hence this brought to light the possibility that LIR-containing proteins and UIM-containing proteins can bind simultaneously to Atg8 (Lei and Klionsky, 2019). Interestingly, proteins that do not possess the UIM motif are still able to bind to Atg8 via the UDS interface (Lei and Klionsky, 2019). Taking this into account, it could be possible that the LIR motifs

could also bind to the UDS domain and thus this gives rise to the possibility of ArfGAP3 interacting with Atg8a via the LIR1 and LIR2 motifs binding to LDS and UDS domains of Atg8a.

Once it was established that ArfGAP3 and Atg8a physically interact, knowing its exact role in the autophagic process was the next to investigate. There are many roles of Atg8 proteins including; driving the formation of autophagosomes (elongation and closure), recruiting autophagy receptors and adaptors for selective removal of damaged proteins and organelles and facilitating autophagosome – lysosome fusion. Examples of selective receptors are mammalian p62 (*Drosophila* Ref(2)P), NDP52 and NBR1. Both autophagy receptors and adaptors contain LIR motifs. The selective receptors can also be engulfed into the autophagosome and degraded by lysosomes with the selective cargo tagged for degradation, however autophagy adaptors are autophagy interactors that are not selectively degraded by autophagy (Wirth *et al.*, 2019). To assess whether ArfGAP3 could possibly be a selective autophagy receptor or adaptor, checking the levels of the protein in autophagy mutants, where the autophagic machinery is compromised, is an ideal approach. This approach was previously shown by previous members of the lab, where they showed the *Drosophila* protein Kenny had accumulated in autophagy mutant flies and hence was selectively degraded by autophagy (Tusco *et al.*, 2017). In this case, it would be expected to see an accumulation of ArfGAP3 in autophagy mutants if it is a selective autophagy receptor. In Chapter 5, ArfGAP3 is shown to accumulate in autophagy mutants compared to controls. This is because the autophagic machinery is compromised and hence unable to degrade ArfGAP3. The data here highly supports the notion that ArfGAP3 could potentially be a selective autophagic receptor since the data provides

evidence that ArfGAP3 accumulates in autophagy mutants and hence is selectively degraded by autophagy.

Functional autophagic flux is defined by the completion of autophagosome formation and lysosomal clearance (Ntsapi *et al.*, 2016). Autophagosomes are intermediate structures in the autophagic pathway. Thus, at any given time, the number of autophagosomes detected is consequently the balance between rate of autophagosome formation and rate of autophagosome conversion into autolysosomes. For this reason, an increase in autophagosome number compared to basal levels can either represent induction of autophagy or suppression of downstream steps in the autophagic pathway. A decrease in autophagosome number compared to basal levels would indicate a blockage or disruption in any step upstream of autophagosome formation (Mizushima, Yoshimorim and Levine, 2010). In Chapter 5, we see the number of autophagosomes significantly reduced in ArfGAP3 RNAi cells compared to control cells after autophagy induction. Initial interpretation of data suggested that knockdown of ArfGAP3 is responsible for the disruption in events upstream to autophagosome formation, resulting in fewer autophagosomes being formed. It is important to note that autophagosome formation is not completely halted in the absence of ArfGAP3, however it is significantly reduced. This result could highlight the significance of ArfGAP3 in autophagosome formation. Events upstream of autophagosome maturation include nucleation and elongation. Since it was well established in Chapter 4 that ArfGAP3 physically interacts with Atg8a, and Atg8 proteins are embedded in the inner membrane of the phagophore/autophagosome (Johansen and Lamark, 2020). One possibility is that ArfGAP3 aids in the elongation of the phagophore to form the autophagosome, which is mediated by the interaction with Atg8a on the inner membrane of the phagophore.

On the other hand, the results are open to question and alternative interpretations. This is because we later observe in figure 5.5, autophagic structures in the ArfGAP3 RNAi cells. Figures 5.11C' and 5.11D' also show mCherry positive autophagic structures in ArfGAP3 RNAi cells. The data in figure 5.5 suggests there could be an accumulation of autophagosomes in ArfGAP3 RNAi cells compared to control (not quantified), which, if true, would fit the interpretation that knockdown of ArfGAP3 disrupts autophagic flux, since fusion is impaired, there should in theory be an accumulation of autophagosomes.

Once it was established that ArfGAP3 is selectively degraded by autophagy and to help better understand the role of ArfGAP3 in autophagy, we investigated its effects downstream of autophagosome formation. In Chapter 5, we show that lysosome fusion with endosomes is compromised when ArfGAP3 is knockdown, indicating strong links of ArfGAP3 to endolysosomal fusion events. Since there was no definitive result in chapter 5 showing accumulation of autophagosomes in ArfGAP3 RNAi cells, the question whether ArfGAP3 also regulates autophagosome-lysosome fusion remains open until further experiments such as assessing the autophagic flux by western blotting confirms the notion that it does regulate fusion events with autophagosomes.

The common participating molecule in both autophagy and endosomal trafficking is the presence of Rab7 on both the autophagosomal membrane and the endosomal membrane. Rab7 is a key molecule that promotes the autophagosomes and endosomes to fuse with lysosomes (Hyttinen *et al.*, 2013). In Chapter 5, ArfGAP3 was shown to co-localise to both Rab7-positive late endosomes and Rab5-positive early endosomes in *Drosophila* fat body cells. This correlated with a previous study where

they showed ArfGAP3 co-localised to early and late endosomes in HeLa cells (Shiba *et al.*, 2013).

A number of tethering proteins and complexes are involved in the fusion between autophagosomes and lysosomes and endosome-lysosome fusion; SNAREs, HOPs, PLEKHM1 and EPG5 (Yim and Mizushima, 2020). The HOPs, PLEKHM1 and EPG5 simultaneously interact with both autophagosomal and lysosomal proteins to mediate fusion. For example, PLEKHM1 and EPG5 interact with Atg8/LC3 on the autophagosomal membrane and lysosomal small GTPase Rab7 on the lysosomal membrane, forming a bridge between both organelles to aid fusion. Comparably, PLEKHM1 and HOPs complex also bind to another lysosomal small GTPase Arl8b^{GTP} on the lysosomal membrane. Whilst PLEKHM1 binds to Atg8/LC3 on the autophagosomal membrane, the HOPs complex interacts with the SNARE complex Qa-SNARE STX17 on the autophagosomal membrane (Yim and Mizushima, 2020). Similarly, HOPS, PLEKHM1, SNAREs, Rab7 and Arl8b also mediate fusion of endosomes with lysosomes (de Araujo *et al.*, 2020) (figure 7.1). Likewise, the same tethering proteins are involved in endosome-lysosome fusion, where HOPS and PLEKHM1 act as bridge in the interaction between GTPase Arl8bGTP on the lysosomal membrane and Rab7 on the endosomal and lysosomal membrane (Yim and Mizushima, 2020) (figure 7.1).

Arl8 is a conserved Arf-like protein from the same subfamily as ArfGAP3 (Boda *et al.*, 2019). In previous studies Arl8 has been described as a lysosomal motility regulator essential for various cellular functions associated with the endolysosomal system (Nakae *et al.*, 2010; Boda *et al.*, 2019). Furthermore, Arl8 has also been shown to be fundamental for normal endosomal pathway functioning in *Drosophila* (Rosa-Ferreira, Sweeney and Munro, 2018; Boda *et al.*, 2019). Since ArfGAP3 is from the

same subfamily of proteins as Arl8, in principle it is possible for the two proteins to have similar functions. Now that it is established the ArfGAP3 and Atg8 interact, a possible explanation could be that ArfGAP3 may be functioning as a docking protein binding to Atg8 and/or Rab7 on the autophagosomal membrane and endosomal membrane and interacting with Rab7 on the lysosomal membrane. Alternatively, ArfGAP3 could also be situated on the lysosomal membrane like Arl8, interacting directly with Atg8 on the autophagosomal membrane to mediate fusion events. Verifying these possible interactions of ArfGAP3 with these tethering proteins and complexes by immunofluorescence and biochemical approaches will help to elucidate exactly how ArfGAP3 facilitates fusion between endosomes and lysosomes and possibly between autophagosomes and lysosomes once future experiments are conducted to elucidate this notion more clearly.

The *Drosophila* Arl8 study by Boda *et al* revealed that Arl8 is required for autophagosome-lysosome fusion. To test this, their study used a tool to detect autophagosome-lysosome fusion using mCherry-Atg8a expression in larval fat bodies with a lysosomal reporter. Normal fusion was detected when these two reporters co-localised, whilst separate signals indicated fusion defects. Their study showed clear overlapping structures in the control cells, confirming normal fusion events. The co-localisation was lost between autophagosomes and lysosomes in Arl8 silenced cells indicating clear fusion defects. Although we used a different but just as an effective tool to detect autophagosome – lysosome fusion (described in Chapter 5.4.3), our results for ArfGAP3 correlate with that observed for Arl8 their study. In ArfGAP3 knockdown fat body cells, autophagosome – lysosome fusion was disrupted compared to normal fusion events in control cells.

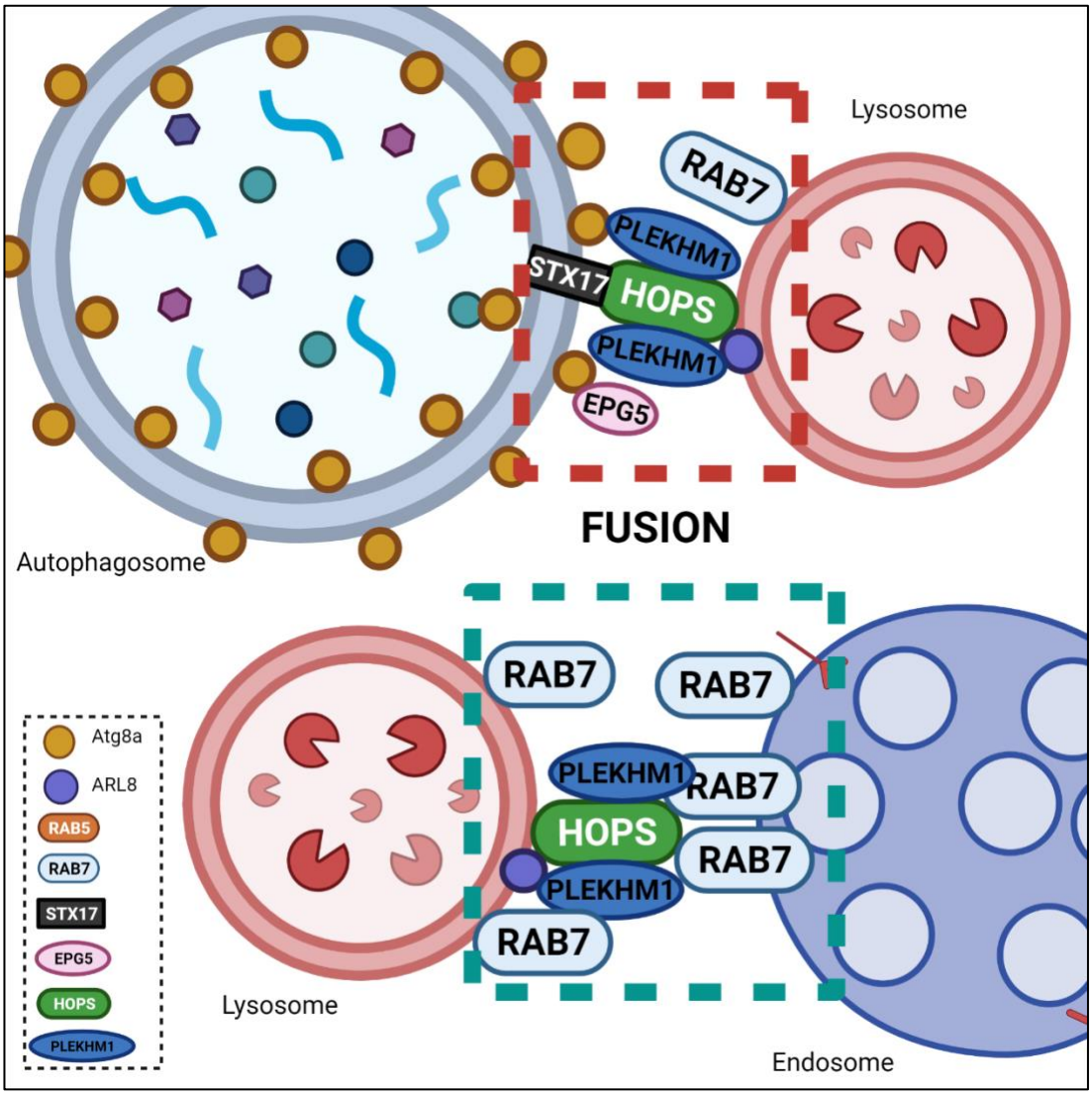

Figure 7.1 Key proteins and components of autolysosome and endolysosome system. Schematic diagram of key proteins and components essential for autophagosome-lysosome fusion and endosome-lysosome fusion, showing how proteins are assembled and interacting partners (Created with BioRender.com, de Araujo *et al*, 2020).

Interestingly, the *Drosophila* Arl8 study by Boda *et al* discovered that Arl8 is also required for endosome-lysosome fusion. The same approach in our study was used to detect endosome-lysosome fusion in larval fat bodies, immunostaining for Rab7 and cathepsin-L. Results from their study showed clear overlap of Rab7 and cathepsin-L in control cells, which was decreased in Arl8 mutant cells. Results from our study was also in agreement, as co-localisation of Rab7 and cathepsin L was decreased in

ArfGAP3 silenced cells compared to control cells. This strongly suggested endosome-lysosome fusion was also disrupted in ArfGAP3 RNAi cells compared to normal fusion events in control cells. Furthermore, the observed accumulation of endosomes in ArfGAP3 silenced cells also correlated with defects in endosome-lysosome fusion. This is because when fusion is compromised, endosomes are not able to fuse with lysosomes and hence will accumulate as more endosomes are formed and trafficked. Overall, the data here suggests with confidence that ArfGAP3 has functional relevance to lysosomal fusion events as it acts as a positive regulator.

Lysosomes are fundamental components of the autophagic pathway. Lysosomes are membrane-bound organelles containing acidic hydrolases that aid intracellular and extracellular cargo degradation (Bandyopadhyay *et al.*, 2014). In normal physiology, the canonical lysosome diameter is heterogenous ranging from 0.05μm to 0.5μm. Upon nutrient starvation, lysosome size can increase to 1.5μm in diameter due to membrane fusion. In essence, the larger structures are autolysosomes which are transient organelles that return back to the regular lysosome size of 0.5μm post lysosomal degradation (lysosome reformation) (Xu and Ren, 2015). In Chapter 5, nutrient starved (autophagy induced) control cells exhibited lysosomes that ranged from 0.5μm to 1.5μm in diameter, with an average size of 0.78μm. This was in agreement with the above published data for normal physiology. On the other hand, nutrient starved fat body cells lacking the expression of ArfGAP3 (ArfGAP3 RNAi cells) exhibited significantly larger lysosomes, ranging from 2μm to 5μm in diameter, with an average lysosome diameter of 3μm, fourfold larger than control lysosomes. The changes in lysosome size we see in our data has been previously shown in a study that investigated the lysosomal fusion and acidification relationship in *Drosophila*

(Mauvezin *et al*, 2015). The study showed control lysosomes between 0.5μm and 1μm in diameter, whereas in the V-ATPase RNAi cells, the lysosome size increased to 2μm-3μm in diameter upon starvation (Mauvezin *et al*, 2015). Enlarged lysosomes can be a sign of dysfunctional lysosomal degradation of cellular cargo, resulting in accumulation of the undigested cargo (Xu and Ren, 2015). The data here indicates that the knockdown of ArfGAP3 seems to be responsible for disrupting lysosomal degradation leading to accumulation of undigested materials in the lysosomal lumen resulting in enlarged, dysfunctional lysosomes.

The question that arose next was that if fusion of lysosomes with autophagosomes and endosomes is compromised, why and how is there a build-up of undigested cellular material in these lysosomes? In answer to this, it is important to note that macroautophagy is not the only autophagic pathway. The cellular content destined for lysosomal degradation can also arrive to the lysosome by chaperone-mediated autophagy and microautophagy, since these two types of autophagy can take place on the lysosome itself. The accumulation of undigested material in the lysosomes in this study suggests defects in the lysosomal degradation step, possibly indicating the absence of crucial enzymes and proteins that regulate and mediate this step. It has been reported that there are 50 lysosomal enzymes responsible for substrate degradation and more than 150 lysosomal membrane proteins (LMPs) key for lysosome stability and regulation. These lysosomal proteins are synthesised in the endoplasmic reticulum (ER), modified at the Golgi complex with mannose-6-phosphate (M6P) residues and traversed to the trans-Golgi network (TGN), the point at which these proteins are sorted to the endolysosomal system via clathrin-coated vesicles (Reggiori and Klumperman, 2016). As highlighted in the introduction of Chapter 5, ArfGAP3 has been shown to play a role in protein transport from TGN to endosomes, and has been

shown to associate with (co-localise to) the TGN, clathrin coat proteins and endosomes via Rab5 and Rab7 (Shiba *et al.*, 2013). Interestingly, lysosomal proteins modified with M6P binds to M6P receptor (MPR) in the TGN and are trafficked by clathrin-coated vesicles to the endosomes (Ghosh *et al*, 2003; Ghosh *et al*, 2004). This gives rise to the notion that ArfGAP3 may regulate the traffic of lysosomal proteins from TGN to endosomes. Thus, a possible explanation as to why the lysosome cannot degrade the accumulated cargo in the absence of ArfGAP3 may be because the compromised fusion of lysosomes with endosomes does not result in the successful delivery of these key lysosomal proteins to the lysosomal lumen to execute lysosomal degradation of cellular cargo. This in turn resulted in strikingly enlarged lysosomes.

Previous studies have reported findings suggesting that increase in levels of Rab7 hindered lysosome reformation, resulting in enlarged lysosomes (Yu *et al*, 2010). In the study, the authors had constitutively overexpressed Rab7 and found that it abolished lysosome reformation, which resulted in enlarged autolysosomes (Yu *et al*, 2010). Our data correlates with this study by Yu *et al*, as we show knockdown of ArfGAP3 results in an accumulation of Rab7 positive endosomes which in turn prevents lysosomal reformation resulting in enlarged lysosomes.

In addition, some of the enlarged lysosomes observed also seemed somewhat distorted in shape compared to spherical control lysosomes. A recent study demonstrated the use of ferroquine (FQ) as a promising drug candidate for cancer. In the study they showed FQ disrupted lysosomal function resulting in enlarged and distorted lysosomes (Kondratskyi *et al*, 2017). The distorted shape of lysosomes was like irregular circular structures which correlate to some distorted lysosome structures seen in our data. Damaged lysosomes can be selectively degraded by lysophagy. In lysophagy, the lysosomal membrane is ubiquitinated to initiate the uptake of the

damaged lysosome into the growing phagophore/autophagosome, which in turn fuses with a functional lysosome for degradation (Papadopoulos, Kravic and Meyer, 2020). We see lysosome enlargement and distortion with ArfGAP3 is knockdown. It could be possible to assume that there is some clearance of damaged lysosomes by lysophagy, however the rate of clearance (i.e., rate of lysophagy) is most likely reduced since majority of lysosomes seem enlarged.

The aberrant accumulation of lysosomal content within the lysosomal lumen due to defects in lysosomal degradation, export and trafficking causes conditions called Lysosomal Storage Diseases (LSDs). In LSD physiology, defects in autophagosome-lysosome fusion and lysosomal reformation causes the enlarged lysosome's lifespan to increase (Xu and Ren, 2015). This in turn leads to imbalance in the equilibrium between the input and output of lysosomal content. Thus, further resulting in a hinderance in autophagic and endocytic activity (Fukuda *et al*, 2006). A study in 2006 examined the compartments of autophagic and endocytic lysosomal degradative pathway in myoblasts deficient for lysosomal acid α-glucosidase (GAA) to comprehend lysosomal storage disease (Pompe disease). They discovered enlarged lysosome compartments and acidification defect of lysosomes in GAA knockout myoblasts (Fukuda *et al*, 2006). When lysosomal reformation is compromised, the lysosomes cannot return to the normal size needed to efficiently fuse with autophagosomes and endosomes. This could be another explanation why we see a decrease in lysosomal fusion with autophagosomes and endosomes in ArfGAP3 knockdown cells compared to control cells. In addition, the compromised lysosomal function within the cell results in a shortage of building-blocks, precursor proteins for biosynthetic pathways, ultimately leading to cellular starvation (Xu and Ren, 2015).

Taken together, our study provides evidence that ArfGAP3 is required for normal lysosome activity by regulating the trafficking of endosomes, that carry lysosomal proteins necessary for degradation, and positively regulates subsequent fusion of endosomes to lysosomes. The role of ArfGAP3 as a positive regulator of autophagosome fusion to lysosomes is still open to question as cannot be conclusive from our data, however it is a promising avenue to further examine with better experimental approaches and tools since we show in our data ArfGAP3 in an Atg8a-interacting protein via the LIR motif.

7.2 ArfGAP3 in the interplay between autophagy and lipophagy

In macrolipophagy, lipid droplets are engulfed by autophagosomes, which in turn fuse with lysosomes for lipid droplet degradation (Schulze *et al.*, 2017). Macrolipophagy was first studied in mouse starvation models. The studies have shown evidence of autophagosome and lysosome marker proteins to co-localise with lipid droplets under starvation conditions (Singh *et al.*, 2009; Garcia, Vevea and Pon, 2018). Previous studies show evidence of Rab7 as a regulator of autophagosome and late endosome maturation (Feng, Press and Wandinger-Ness, 1995; Gutierrez *et al.*, 2004; Garcia, Vevea and Pon, 2018). Recent studies have revealed under nutrient starvation conditions, the accumulation of Rab7, Rab5 and Rab2 on lipid droplets (Bartz *et al.*, 2007; Garcia, Vevea and Pon, 2018). There is evidence that activation of Rab7 is a prerequisite for the recruitment of autophagosome and lysosomal marker proteins to the lipid droplets (Garcia, Vevea and Pon, 2018). Lastly, many other proteins have been identified on lipid droplets including Arf1 and ArfGAP1 (Bartz *et al.*, 2007).

This is of interest because ArfGAP3 regulates Arf1 proteins and ArfGAP1 is the human homolog of *Drosophila* ArfGAP3.

In Chapter 5, we showed that lipid droplets were abnormally enlarged in ArfGAP3 RNAi fat body cells compared to control cells, suggesting ArfGAP3 regulates normal lipid droplet development. Intriguingly, an Arf-like GTPase, ARFRP1, has been shown to regulate lipid droplet growth and lipolysis. The study showed evidence that knockdown of ARFRP1 results in hinderance in normal development of lipid droplets (Hommel *et al.*, 2010). It is not known how ArfGAP3 could be regulating normal lipid droplet development, however possible theories include regulation of lipid droplet development by regulating Arf1 protein. Alternatively, regulation of lipid droplet development could be through the activity of Rab7 or Rab5 since Chapter 5 highlights ArfGAP3 co-localises to both Rab7 and Rab5 in *Drosophila,* which also agrees with previously published co-localisation in HeLa cells (Shiba *et al.*, 2013). Moreover, Chapter 5 shows that ArfGAP3 is also selectively degraded by autophagy. It could be possible that if ArfGAP3 is also situated on the lipid droplet, it can be internally degraded by lipophagy. To confirm if this is the case, further mass spectroscopy looking into protein interactors on *Drosophila* lipid droplets would be insightful. An additional approach to test the activation of lipophagy would be to verify the colocalization of a LD marker (BODIPY) with lysosomal marker (LAMP1) under autophagy induced conditions (Ward *et al.*, 2016).

Furthermore, Lipid droplets regulate autophagosome biogenesis as studies verify that both lipid droplet biogenesis and lipolysis are vital processes for autophagosome biogenesis. It has been highlighted that membrane flow from endoplasmic reticulum (ER) to LDs and vice versa is essential for autophagosome biogenesis (Shpilka and Elazar, 2015). Given that lipid droplet biogenesis is essential

for autophagosome biogenesis, this could be a possible explanation to why we see impairment in lipid droplet development and autophagosome formation in ArfGAP3 silenced cells compared to control cells. The picture that emerges is that in the presence of ArfGAP3, through possibly the regulation of Arf1 protein or activity of Rab7, normal lipid droplet development occurs, which is essential for autophagosome biogenesis. When ArfGAP3 is absent, this process is hindered. In summary, ArfGAP3 in accompany with the Arf proteins and Rab proteins all seem to play a role also in lipid droplet development. To get a complete picture of ArfGAP3's exact role in lipid droplet biogenesis, the next steps would be to further understand how ArfGAP3 regulates lipid droplet development. One approach could be to double stain Drosophila fat bodies with BODIPY (marker for LD's) and anti-ArfGAP3 to check for localisation of ArfGAP3 on LD surface. Alternatively, in control and ArfGAP3 knockdown fat body cells, check for co-localisation of ArfGAP3 with Rab7 and Rab5 on LD surfaces.

7.3 Possible implications of ArfGAP3 in age-related diseases

Once the role of ArfGAP3 in the interplay between autophagy and endosomal trafficking was investigated, we examined its physiological relevance during aging. Lifespan survival assay summarised in Chapter 6 showed reduced longevity in ArfGAP3 RNAi flies compared to control. It is important to note here that the reduced longevity was only significant in male flies but not in female flies. Overall, control flies lived on average 12 days longer than ArfGAP3 RNAi flies, suggesting that ArfGAP3 positively contributes to longevity, and does so significantly in a sex biased manner. This data correlates with the published literature reporting that females have

the tendency to live longer than males in *Drosophila*, as also the case for humans and any other species where the XY sex chromosome is male (Tower and Arbeitman, 2009). Additionally, in *Caenorhabditis elegans*, the hermaphrodites possess the XX chromosome and tend to live longer than males, which only possess one X chromosome. On the contrary, the heterogametic sex in most bird species is female, and for these species, the males tend to live longer than females (Tower and Arbeitman, 2009).

Additionally, physiological differences between the control flies and ArfGAP3 RNAi flies, assessed by climbing assays in Chapter 6, showed that there was no significant difference in climbing abilities of the flies between the two genotypes at 7 days. Although, there was a significant decrease in climbing abilities at 4 weeks for both control and ArfGAP3 RNAi flies, there was no significant difference again between the two genotypes at 4 weeks. The data here postulates that ArfGAP3 does not positively contribute to locomotor behaviour in flies.

Lifespan in *Drosophila* can be influenced by many genetic and environmental factors; fertility, temperature, mating status to name a few, and the effect of these factors between male and females is not equal. In some cases, certain factors, either enhancing or reducing longevity, can affect a particular sex more than the other. An example in *Drosophila* is quantitative trait locus (QTL) analysis, for which a number of loci influencing longevity is linked to the X-chromosome (Vermeulen, Bijlsma and Loeschcke, 2008). Other examples include genetic mutations that results in sex-dependent boost in longevity, i.e. chico1 in *Drosophila* (Clancy *et al.*, 2001). Mild stress is an example of an environmental factor that has been seen to increase lifespan in males more than females (Sorensen *et al*, 2007). The genetic architecture of lifespan differs between males and females in *Drosophila*, humans, and mice (Tower and

Arbeitman, 2009). Since males inherit a single X chromosome only, any recessive mutant phenotype linked to the X chromosome will be expressed. On the contrary in females, the additional X chromosome provides a wild-type copy of the gene and so the recessive phenotype is not suppressed. These recessive mutations could likely contribute to decreased lifespan in males more than females (Tower and Arbeitman, 2009). Inbreeding in species tend to cause these recessive mutations homozygous and has been shown in Drosophila to decrease lifespan (Vermeulen *et al*, 2008; Tower and Arbeitman, 2009). A quantitative trait loci (QTL) study in *Drosophila*, where they examined inbreeding effects on lifespan, showed male lifespan was affected more than females (Vermeulen *et al*, 2008).

Drosophila ArfGAP3 has been shown to play a crucial role in the patterning of the *Drosophila* pupal eye (Johnson *et al.*, 2011). Immunofluorescence analysis in Chapter 6 revealed ArfGAP3 in expressed in the third instar larval brain. Most of the expression was observed in the optic lobes which was expected and correlated with the above study highlighting the role of ArfGAP3 in the pupal eye. This study by Ruth Johnson together with the findings from our study showing knockdown of ArfGAP3 disrupts the endocytic flux strongly confirms the role of ArfGAP3 in the endolysosomal system. This is because the multiple signalling pathways required for proper eye development in the *Drosophila* compound eye are modulated by endocytosis. Hence regulators of autophagy are usually studied in Drosophila fat bodies and their role in the endocytic pathway can be studied in the compound eye (Lorincz *et al.*, 2016). The *Drosophila* compound eye is an organ well used for investigating function of autophagy in neurodegenerative disorders as the retinule cells in the compound eye are primary sensory neurones (Lorincz *et al.*, 2016; Lőrincz, Mauvezin and Juhász, 2017). Due to shorter lifecycles in Drosophila and less genetic

redundancy, researchers have more leverage when examining models of neurodegenerative diseases (Lorincz *et al.*, 2016). Some additional expression was also observed in the central brain and ventral nerve cord. The ventral nerve cord is responsible for higher order decisions such as climbing, reaching, jumping etc (Chen *et al.*, 2018). This coincides with the climbing assay, as we don't see any significant changes in locomotor behaviour, expression in the ventral nerve cord regions is lower than the optic lobes. Numerous studies have shown the *Drosophila* central brain involvement in a number of functions including navigation, sleep, visual memory, short and long term spatial memory (Franconville, Beron and Jayaraman, 2018; Xu *et al.*, 2020). It will be interesting to further investigate the effects of ArfGAP3 silencing in aged brain cells on the visual and spatial memory aspect, since this could have significant links to neurodegeneration.

In Chapter 6, we showed that ArfGAP3 knockdown disrupted autophagy in 4 week old flies as levels of Ref(2)P was seen to significantly accumulate in ArfGAP3 RNAi flies compared to control flies. This was a clear indication that cellular cargo destined for lysosomal degradation was accumulating either in autophagosomes or lysosomes, since Ref(2)P anchors ubiquitinated proteins tagged for degradation to the autophagosomal membrane (Nezis *et al.*, 2008; Nezis and Stenmark, 2012). Low autophagic flux has been associated with many neurodegenerative diseases due to the accumulation of diseased proteins and neurotoxicity (Menzies, Moreau and Rubinsztein, 2011; Ntsapi *et al.*, 2016). Most interestingly, most lysosome related disorders (LSDs) pathology involves neurodegeneration due to accumulation of cytoplasmic aggregates as a result of autophagy impairment (Pastores and Maegawa, 2013; Reggiori and Klumperman, 2016).

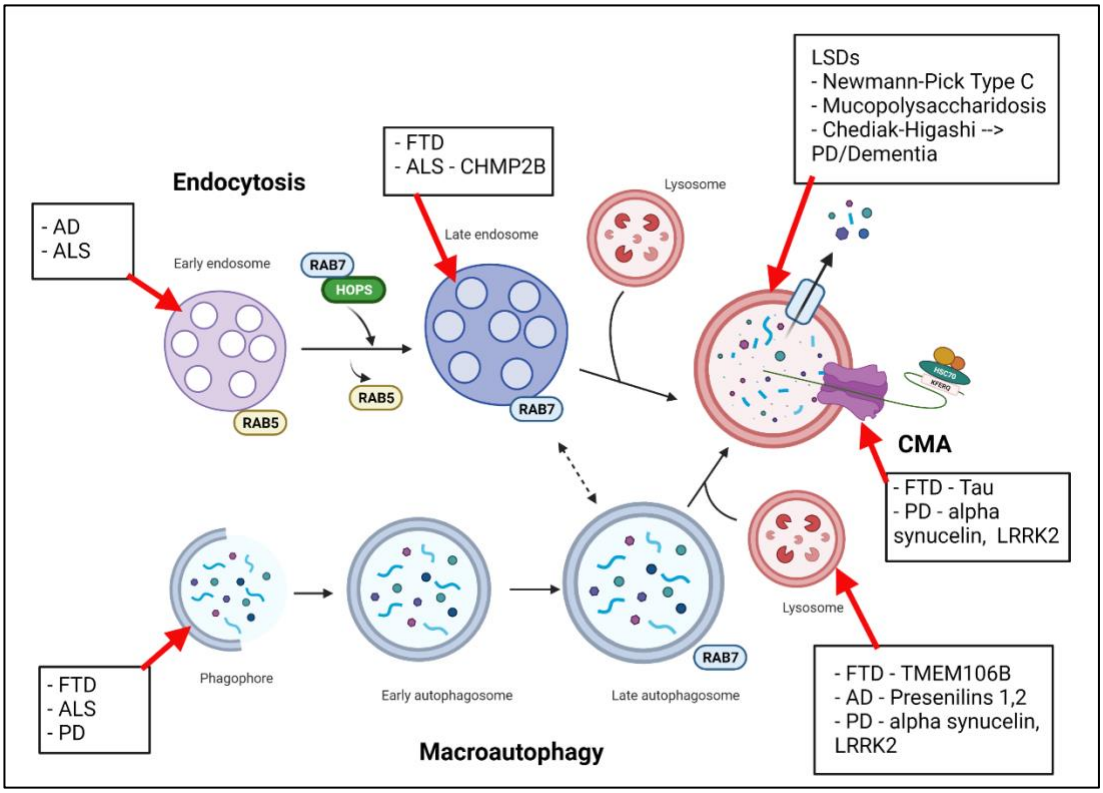

Figure 7.2. Interplay between autophagy and endolysosomal pathway and the neurological disorders related to different compartments of the lysosomal degradative pathways. Endolysosomal pathway (top panel), macroautophagy (bottom panel) and merging of both pathways (dotted arrow). In the endosomal pathway the early endosome, formed by the internal budding of the cell membrane, is either matured to recycling endosome (which then matures to late endosome) or directly matures to a late endosome. The late endosome fuses with the lysosome forming an endolysosome allowing degradation to occur. The autophagic pathway involves the formation of the phagophore, which matures into a double membrane autophagosome. The autophagosome fuses with the lysosome forming an autolysosome resulting in cellular degradation. Both pathways merge at the point where endosomes and autophagosomes fuse to form an amphisome, which in turn fuses with a lysosome for degradation. There is extensive crosstalk between different compartments of the autophagic and endocytic pathways, any defects in components in pathway to lysosomes will result in disruption to lysosomal function. AD – Alzheimer's disease, ALS – Amyotrophic lateral schlerosis, PD – Parkinson's disease, FTD – Frontal temporal dementia, LSD – lysosome storage disorder. (Created with BioRender.com, Reggiori and Klumperman, 2016).

The pathophysiological connection between autophagy and endolysosomal system is also associated to several neurodegenerative diseases such as Alzheimer's Disease (AD), Parkinson's Disease (PD), Huntington's Disease (HD), and Amyotrophic Lateral Sclerosis (ALS), since the pathology of all these conditions involves aggregation of aberrant proteins (figure 7.2). Fundamentally, upregulation of autophagy can ameliorate the toxic effects of accumulated aggregates (Tan *et al.*,

2014; Ntsapi *et al.*, 2016). Strikingly, previous studies have shown that the dysfunctional lysosomal proteolysis is an early pathological event in AD and the subsequent progression of the disease consists of pathological changes including accumulation of late endosomes (Nixon, 2005; Ntsapi *et al.*, 2016).

Taken together, there is growing evidence that the autophagic pathway and endocytic pathways are naturally interconnected at many levels of organisation and regulation in health and disease. The picture that emerges is that any defects in any one of the two pathways could also affect the progression of the other pathway. In addition, a hinderance in the endolysosomal system may trigger corrections to cellular defects by autophagy and vice versa (Ntsapi *et al.*, 2016) (figure 7.2).

7.4 Concluding remarks.

Limited research has been published on *Drosophila* ArfGAP3 and hence there is inadequate knowledge of its exact physiological relevance in key cellular mechanisms. Although previous studies have revealed its significant role in membrane trafficking to endosomes and its possible affiliation to endosomal trafficking, the mechanistic details of this and its functional importance downstream of endosomal trafficking interconnecting to autophagy has been unclear.

This study confirms ArfGAP3 as a novel Atg8-interacting protein in *Drosophila*. We show knockdown of ArfGAP3 expression potentially has an effect on autophagosome-lysosome fusion, but this was open to interpretation. Knockdown of ArfGAP3 resulted in accumulated endosomes leading to disrupted endosome-lysosome fusion and dysfunctional lysosomal degradation. All in all, knockdown of ArfGAP3 expression results in low endocytic flux and possibly autophagic flux, which

can be linked to the pathological features described above for neurodegenerative diseases such as AD and PD.

In principle, ArfGAP3 possibly aids autophagosome-lysosome fusion via the established LC3-mediated interaction with Atg8. In addition, possibly Rab7 activity, ArfGAP3 ensures normal trafficking of late endosomes to the lysosome for endosome-lysosome fusion, aiding the transport of essential lysosomal proteins and thus mediating normal functioning of lysosomes in addition to facilitating normal lipid droplet development. There is convincing evidence from this study to conclude that ArfGAP3 is a **positive regulator** of the endocytic flux. Figure 7.3 summarises the proposed functional relevance of *Drosophila* ArfGAP3 in the autophagic and endolysosomal pathway.

Our study for the first time proposes a potential significant role of *Drosophila* ArfGAP3 in the interplay between autophagy and endosomal trafficking, further strengthening the notion that autophagy and the endolysosomal system are very well interconnected at the level of organisation and regulation in health and disease.

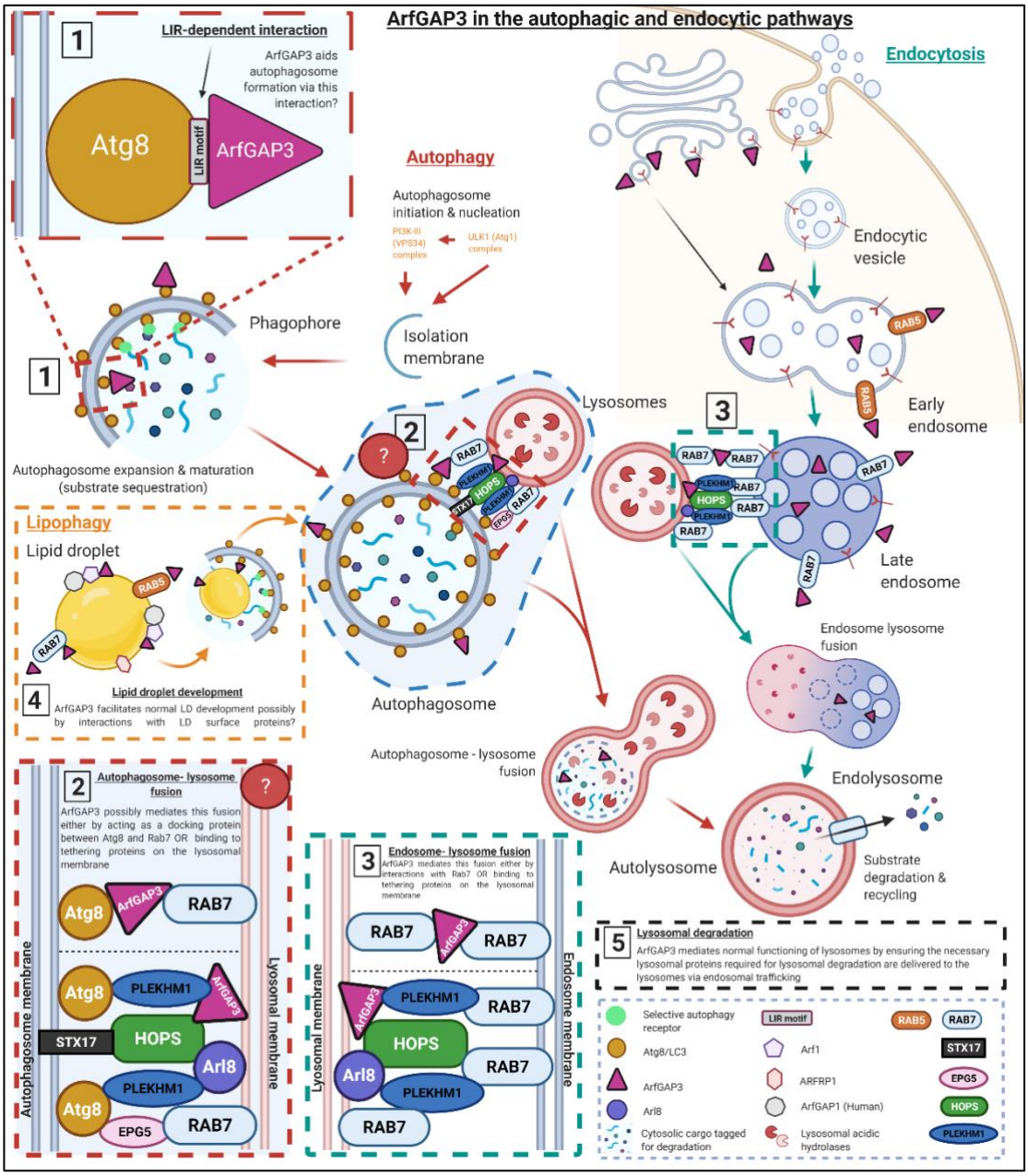

Figure 7.3. *Drosophila* ArfGAP3 is a positive regulator of the endocytic flux. 1) ArfGAP3 interacts with Atg8 in a LIR-dependent manner, confirmed by yeast-two hybrid screening, confocal co-localisation and GST-pull down assay. We show ArfGAP3 is essential for autophagosome formation as knockdown of ArfGAP3 results in fewer autophagosomes formed. ArfGAP3 possibly aids autophagosome formation via this LIR mediated interaction with Atg8. 2) Data suggest ArfGAP3 possibly mediates autophagosome-lysosome fusion shown herein by confocal tandem fusion in ArfGAP3 knockdown cells fusion events were less observed. ArfGAP3 mediates this fusion either by acting as a docking protein between Atg8 and Rab7 or binding to tethering proteins (HOPS and PLEKHM1) on the lysosomal membrane. However, this is open to question until further clarified. 3) ArfGAP3 mediates endosome-lysosome fusion shown herein by confocal co-localisation in ArfGAP3 knockdown cells fusion events were less observed. ArfGAP3 mediates this fusion either by interactions with Rab7 or binding to tethering proteins (HOPS and PLEKHM1) on the lysosomal membrane. 4) ArfGAP3 facilitates normal lipid droplet development as knockdown of ArfGAP3 resulted in abnormally enlarged lipid droplets. It could be interacting with certain LD surface proteins to promote normal LD development. 5) ArfGAP3 mediates normal functioning of lysosomes as ArfGAP3 knockdown cells showed enlarged autolysosomes, indicating accumulation of undigested cellular cargo. ArfGAP3 mediates normal lysosome function by ensuring the necessary lysosomal proteins required for lysosomal degradation are delivered to the lysosomes by regulating endosomal trafficking. (Created with BioRender.com).

Bibliography

Abreu S, Kriegenburg F and Gomez-Sanchez R (2017) Conserved Atg8 recognition sites mediate Atg4 association with autophagosomal membranes and Atg8 deconjugation. EMBO Rep 18, 765-780

Adams, M. D. *et al.* (2000) 'The genome sequence of Drosophila melanogaster', *Science*, 287(5461), pp. 2185–2195.

Adler, J. and Parmryd, I. (2010) 'Quantifying colocalization by correlation: The pearson correlation coefficient is superior to the Mander's overlap coefficient', *Cytometry Part A*, 77(8), pp. 733–742.

Agarwal, Shivani *et al.* (2015) 'Autophagy and endosomal trafficking inhibition by Vibrio cholerae MARTX toxin phosphatidylinositol-3-phosphate-specific phospholipase A1 activity', *Nature Communications*. Nature Publishing Group, 6, pp. 1–11.

Agola, J. O. *et al.* (2011) 'Rab GTPases as regulators of endocytosis, targets of disease and therapeutic opportunities', *Clinical Genetics*, 80(4), pp. 305–318.

Alcolea D, Martínez-Lage P, Sánchez-Juan P, Olazarán J, Antúnez C, Izagirre A, Ecay-Torres M, Estanga A, Clerigué M, Guisasola MC, Sánchez Ruiz D, Marín Muñoz J, Calero M, Blesa R, Clarimón J, Carmona-Iragui M, Morenas-Rodríguez E, Rodríguez-Rodríguez E, Vázquez Higuera JL, Fortea J, Lleó A (2015) Amyloid precursor protein metabolism and inflammation markers in preclinical Alzheimer disease. Neurology 85:626-633.

Alemu, E. A. *et al.* (2012) 'ATG8 family proteins act as scaffolds for assembly of the ULK complex: Sequence requirements for LC3-interacting region (LIR) motifs', *Journal of Biological Chemistry*, 287(47), pp. 39275–39290.

Ali M, Devkota S, Roh JI, Lee J, Lee HW (2016) Telomerase reverse transcriptase induces basal and amino acid starvation-induced autophagy through mTORC1. Biochem Biophys Res Commun 478:1198-1204.

An WL, Cowburn RF, Li L, Braak H, Alafuzoff I, Iqbal K, Iqbal IG, Winblad B, Pei JJ (2003) Up-regulation of phosphorylated/activated p70 S6 kinase and its relationship to neurofibrillary pathology in Alzheimer's disease. Am J Pathol 163:591-607.

Aoki H, Iwado E, Eller MS, Kondo Y, Fujiwara K, Li GZ, Hess KR, Siwak DR, Sawaya R, Mills GB, Gilchrest BA, Kondo S (2007) Telomere 3' overhang-specific DNA oligonucleotides induce autophagy in malignant glioma cells. FASEB J 21:2918-2930.

de Araujo, M. E. G. *et al.* (2020) 'Lysosomal size matters', *Traffic*, 21(1), pp. 60–75.

Arrese, E. L. and Soulages, J. L. (2010) 'Insect Fat Body: Energy, Metabolism, and Regulation', *Annual Review of Entomology*, 55(1), pp. 207–225.

Ashford, T. P. and Porter, K. R. (1962) 'Cytoplasmic components in hepatic cell lysosomes', *Journal of Cell Biology*, 12, pp. 198–202.

Balaban RS, Nemoto S, Finkel T (2005) Mitochondria, oxidants and aging. Cell 120:483-495.

Bandyopadhyay, D. *et al.* (2014) 'Lysosome transport as a function of lysosome diameter', *PLoS ONE*, 9(1), pp. 18–23.

Bandyopadhyay, U. *et al.* (2008) 'The Chaperone-Mediated Autophagy Receptor Organizes in Dynamic Protein Complexes at the Lysosomal Membrane', *Molecular and Cellular Biology*, 28(18), pp. 5747–5763.

Barbosa, M. C., Grosso, R. A. and Fader, C. M. (2019) 'Hallmarks of aging: An autophagic perspective', *Frontiers in Endocrinology*, 10(JAN), pp. 1–13.

Barja, G. (2017) ‘The Cell Aging Regulation System (CARS)’, *Reactive Oxygen Species*, 3(9), pp. 148–183.

Barlowe, C. K. and Miller, E. A. (2013) ‘Secretory protein biogenesis and traffic in the early secretory pathway’, *Genetics*, 193(2), pp. 383–410.

Bartel, B. (2015) ‘Proteaphagy-Selective Autophagy of Inactive Proteasomes’, *Molecular Cell*. Elsevier Inc., 58(6), pp. 970–971.

Bartz, R. *et al.* (2007) ‘Dynamic activity of lipid droplets: Protein phosphorylation and GTP-mediated protein translocation’, *Journal of Proteome Research*, pp. 3256–3265.

Bassett A, Karran E, Miller BL, Fleming A, Rubinsztein DC (2019) Felodipine induces autophagy in mouse brains with pharmacokinetics amenable to repurposing. Nat Commun 10:1817.

Bayer, K. and Jungbauer, A. (2007) *Advances in biochemical engineering science, Journal of Biotechnology*, 132(2), pp. 97-98
Behrends, C. *et al.* (2010) ‘Network organization of the human autophagy system’, *Nature*. Nature Publishing Group, 466(7302), pp. 68–76.

Bento, C. F. *et al.* (2013) ‘The role of membrane-trafficking small GTPases in the regulation of autophagy’, *Journal of Cell Science*, 126(5), pp. 1059–1069.

Berger Z, Ravinkumar B, Menzies FM, Oroz LG, Underwood BR, Pangalos MN, Schmitt I, Wullner U, Evert BO, O’Kane CJ and Rubinsztein DC (2006) Rapamycin alleviates toxicity of different aggregate-prone proteins. Human Molecular Genetics. 15:433-442

Bernales, S., Schuck, S. and Walter, P. (2007) ‘ER-phagy: Selective autophagy of the endoplasmic reticulum’, *Autophagy*, 3(3), pp. 285–287.

Bhujabal, Z. *et al.* (2017) ‘FKBP8 recruits LC3A to mediate Parkin-independent

mitophagy', *EMBO reports*, 18(6), pp. 947–961.

Bier, E. (2005) 'Drosophila, the golden bug, emerges as a tool for human genetics', *Nature Reviews Genetics*, 6(1), pp. 9–23.

Birgisdottir, Å. B., Lamark, T. and Johansen, T. (2013) 'The LIR motif - crucial for selective autophagy', *Journal of Cell Science*, 126(15), pp. 3237–3247.

Boccardi V, Pelini L, Ercolani S, Ruggiero C, Mecocci P (2015) From cellular senescence to Alzheimer's disease: the role of telomere shortening. Ageing Res Rev 22:1-8.

Boda, A. *et al.* (2019) 'Drosophila Arl8 is a general positive regulator of lysosomal fusion events', *Biochimica et Biophysica Acta - Molecular Cell Research*, 1866(4), pp. 533–544.

Bodemann, B. O. *et al.* (2011) 'RalB and the exocyst mediate the cellular starvation response by direct activation of autophagosome assembly', *Cell*. Elsevier Inc., 144(2), pp. 253–267.

Bolognesi B and Lehner B (2018) Protein overexpression: Reaching the limit. ELife 7:e39804

Brehme, M. and Voisine, C. (2016) 'Model systems of protein-misfolding diseases reveal chaperone modifiers of proteotoxicity', *DMM Disease Models and Mechanisms*, 9(8), pp. 823–838.

Brückner, A. *et al.* (2009) 'Yeast two-hybrid, a powerful tool for systems biology', *International Journal of Molecular Sciences*, 10, pp. 2763–2788.

Buchan, J. R. *et al.* (2013) 'Eukaryotic stress granules are cleared by autophagy and Cdc48/VCP function', *Cell*, 153(7), p. 1461.

Carlsson, S. R. and Simonsen, A. (2015) 'Membrane dynamics in autophagosome

biogenesis', *Journal of Cell Science*, 128(2), pp. 193–205.

Carroll, B. *et al.* (2013) 'The TBC/RabGAP Armus Coordinates Rac1 and Rab7 Functions during Autophagy', *Developmental Cell*. Elsevier Inc., 25(1), pp. 15–28.

Chang, Y.-Y. and Neufeld, T. P. (2009) 'An Atg1/Atg13 Complex with Multiple Roles in TOR-mediated Autophagy Regulation', *Molecular Biology of the Cell*, 20, pp. 2004–2014.

Chang, Y.-Y. and Neufeld, T. P. (2010) 'Autophagy takes flight in Drosophila', *Febs Letters*, 584(7), pp. 1342–1349.

Chauhan, S. *et al.* (2016) 'TRIMs and Galectins Globally Cooperate and TRIM16 and Galectin-3 Co-direct Autophagy in Endomembrane Damage Homeostasis', *Developmental Cell*. Elsevier Inc., 39(1), pp. 13–27.

Chen, C. L. *et al.* (2018) 'Imaging neural activity in the ventral nerve cord of behaving adult Drosophila', *Nature Communications*, 9(1).

Chen, Q. *et al.* (2019) 'ATL3 Is a Tubular ER-Phagy Receptor for GABARAP-Mediated Selective Autophagy', *Current Biology*. Elsevier Ltd., 29(5), pp. 846–855.

Chen Y, Azad MB, Gibson SB (2009) Superoxide is the major reactive oxygen species regulating autophagy. Cell Death Differ 16:1040-1052

Cheon SY, Kim H, Rubinsztein DC and Lee JE (2019) Autophagy, Cellular Aging and Age-related Human Diseases. Experimental Neurobiology 28(6):643-657

Childs BG, Durik M, Baker DJ, van Deursen JM (2015) Cellular senescence in aging and age-related disease: from mechanisms to therapy. Nat Med 21:1424-1435**.**

Chino, H. *et al.* (2019) 'Intrinsically Disordered Protein TEX264 Mediates ER-phagy', *Molecular Cell*. Elsevier Inc., 74(5), pp. 909–921.

Cho, D. H. *et al.* (2018) 'Pexophagy: Molecular mechanisms and implications for health and diseases', *Molecules and Cells*, 41(1), pp. 55–64.

Cho, K. S., Bang, S. M. and Toh, A. (2014) 'Lipids and Lipid Signaling in Drosophila Models of Neurodegenerative Diseases', in *Omega-3 Fatty Acids in Brain and Neurological Health*. Academic Press, pp. 327–336. Available at: https://www.sciencedirect.com/science/article/pii/B9780124105270000260.

Chu, C. T. *et al.* (2013) 'Cardiolipin externalization to the outer mitochondrial membrane acts as an elimination signal for mitophagy in neuronal cells', *Nature Cell Biology*, 15(10), pp. 1197–1205.

Clancy, D. J. *et al.* (2001) 'Extension of life-span by loss of CHICO, a Drosophila insulin receptor substrate protein', *Science*, 292(5514), pp. 104–106.

Cohen-Kaplan, V. *et al.* (2016) 'The ubiquitin-proteasome system and autophagy: Coordinated and independent activities', *International Journal of Biochemistry and Cell Biology*. Elsevier Ltd, 79, pp. 403–418.

Csizmadia, T. *et al.* (2018) 'Molecular mechanisms of developmentally programmed crinophagy in Drosophila', *Journal of Cell Biology*, 217(1), pp. 361–374.

Cukierman E, Huber I, Rotman M, Cassel D (1995) The ARF1 GTPase-activating protein: zinc finger motif and Golgi complex localization. Science 270:1999–2002

Das, G., Shravage, B. V. and Baehrecke, E. H. (2012) 'Regulation and function of autophagy during cell survival and cell death', *Cold Spring Harbor Perspectives in Biology*, 4(6), pp. 1–14.

Dembla, M. *et al.* (2014) 'ArfGAP3 Is a Component of the Photoreceptor Synaptic Ribbon Complex and Forms an NAD(H)-Regulated, Redox-Sensitive Complex with RIBEYE That Is Important for Endocytosis', *Journal of Neuroscience*, 34(15), pp. 5245–5260.

Denton, D. and Kumar, S. (2018) 'Ribophagy: New receptor discovered', *Cell Research*. Springer US, 28(7), pp. 699–700.

Deosaran, E. *et al.* (2013) 'NBR1 acts as an autophagy receptor for peroxisomes', *Journal of Cell Science*, 126(4), pp. 939–952.

Deretic V, Saitoh T, Akira S (2013) Autophagy in infection, inflammation and immunity. Nat Rev Immunol 13:722-737.

DeVorkin, L and Gorski, S.M. (2014) 'Monitoring autophagy in Drosophila using fluorescent reporters in the UAS-GAL4 system'. *Cold Spring Harb Protoc*, 9 pp. 967-72

Dikic, I. *et al.* (2011) 'Phosphorylation of the Autophagy Receptor Optineurin Restricts Salmonella Growth', *Science*, 333(6039), pp. 228–233.

Donaldson JG (2003) Multiple roles for Arf6: sorting, structuring, and signal-ing at the plasma membrane. J Biol Chem 278:41573–41576.

Donaldson JG, Honda A, Weigert R (2005) Multiple activities for Arf1 at the Golgi complex. Biochim Biophys Acta-Mol Cell Res 1744:364–373

Donaldson, J. G. and Jackson, C. L. (2011) 'ARF family G proteins and their regulators: roles in membrane transport, development and disease', *Nature Reviews Molecular Cell Biology*. Nature Publishing Group, 12(6), pp. 362–375.

Dong, X. and Levine, B. (2013) 'Autophagy and viruses: Adversaries or allies?', *Journal of Innate Immunity*, 5(5), pp. 480–493.

Dou, Z. *et al.* (2015) 'Autophagy mediates degradation of nuclear lamina', *Nature*, 527(7576), pp. 105–109.

Drake J, Link CD, Butterfield DA (2003) Oxidative stress precedes fibrillar deposition of Alzheimer's disease amyloid beta-peptide (1-42) in a transgenic Caenorhabditis elegans model. Neurobiol Aging 24:415-420.

D'Souza-Schorey C, Chavrier P (2006) ARF proteins: roles in membrane trafficand beyond. Nat Rev Mol Cell Biol 7:347–358

Duffy, J. B. (2002) 'GAL4 system in Drosophila: A fly geneticist's Swiss army knife', *Genesis*, 34(1–2), pp. 1–15.

Dunn, K. W., Kamocka, M. M. and McDonald, J. H. (2011) 'A practical guide to evaluating colocalization in biological microscopy', *American Journal of Physiology - Cell Physiology*, 300(4), pp. 723–742.
de Duve, C. and Wattiaux, R. (1966) 'Functions of Lysosomes', *Annual Review of Physiology*, 28, pp. 435–492.

Ebrahimi-Fakhari, D. *et al.* (2014) 'Emerging role of autophagy in pediatric neurodegenerative and neurometabolic diseases', *Pediatric Research*, 75(1–2), pp. 217–226.

Eisenberg, T. *et al.* (2009) 'Induction of autophagy by spermidine promotes longevity', *Nature Cell Biology*. Nature Publishing Group, 11(11), pp. 1305–1314.

Eitan E, Hutchison ER, Mattson MP (2014) Telomere shortening in neurological disorders: an abundance of unanswered questions. Trends Neurosci 7:256-263.

Eguchi Y, Makanae K, Hasunuma T, Ishibashi Y, Kito K, Moriya H (2018) Estimating the protein burden limit of yeast cells by measuring expression limits of glycolytic proteins. Elife computational and systems biology 7:e34595

Fan, W. *et al.* (2017) 'Drosophila TRF2 and TAF9 regulate lipid droplet size and phospholipid fatty acid composition', *PLoS Genetics*, 13(3), pp. 1–21.

Farg MA, Sundaramoorthy V, Sultana JM, Yang S, Atkinson RA, Levina V, Halloran MA, Gleeson PA, Blair IP, Soo KY, King AE, Atkin JD (2014) C9ORF72, implicated in amytrophic lateral sclerosis and frontotemporal dementia, regulates endosomal trafficking. Hum Mol Genet 23:3579-3595.

Farre, J.-C. *et al.* (2008) 'PpAtg30 Tags Peroxisomes for Turnover by Selective Autophagy', *Developmental Cell*, 14(3), pp. 365–376.

Felgueiras, J., Silva, J. V. and Fardilha, M. (2018) 'Adding biological meaning to human protein-protein interactions identified by yeast two-hybrid screenings: A guide through bioinformatics tools', *Journal of Proteomics*. Elsevier B.V., 171, pp. 127–140.

Feng, Y., Press, B. and Wandinger-Ness, A. (1995) 'Rab 7: An important regulator of late endocytic membrane traffic', *Journal of Cell Biology*, 131(6 I), pp. 1435–1452.

Finkel T, Holbrook NJ (2000) Oxidants, oxidative stress and the biology of ageing. Nature 408:239-247.

Florey, O. (2018) 'The double life of autophagy proteins', *Nature Microbiology*. Springer US, 3(12), pp. 1334–1335.

Frake, R. A. *et al.* (2006) 'Autophagy and Neurodegeneration', *ACS Chemical Biology*, 1(May), pp. 211–213.

Frake RA, Ricketts T, Menzies FM, Rubinsztein DC (2015) Autophagy and neurodegeneration. J Clin Invest 125:65-74.

Franconville, R., Beron, C. and Jayaraman, V. (2018) 'Building a functional connectome of the drosophila central complex', *eLife*, 7, pp. 1–24.

Freund A, Orjalo AV, Desprez PY, Campisi J (2010) Inflammatory networks during cellular senescence: causes and consequences. Trends Mol Med 16:238-246.

Frigerio, G. *et al.* (2007) 'Two human ARFGAPs associated with COP-I-coated vesicles', *Traffic*, 8(11), pp. 1644–1655.

Fukuda T, Ewan L, Bauer M, Mattaliano RJ, Zaal K, Ralston E, Plotz PH and Raben N (2006) Dysfunction of endocytic and autophagic pathways in a lysosomal storage disease. Annals of neurology. 59(4):700-708

Fumagalli, F. *et al.* (2016) 'Translocon component Sec62 acts in endoplasmic reticulum turnover during stress recovery', *Nature Cell Biology*, 18(11), pp. 1173–1184.

Ganley IG, Carroll K, Bittova L and Pfeffer S (2004) Rab9 GTPase regulates late endosome size and requires effector interaction for its stability. Molecular Biology of the Cell. 15: 5420-5430

Gao, J. *et al.* (2018) 'Molecular mechanism to target the endosomal Mon1-Ccz1 GEF complex to the pre-autophagosomal structure', *eLife*, 7, pp. 1–18.

Garcia, E. J., Vevea, J. D. and Pon, L. A. (2018) 'Lipid droplet autophagy during energy mobilization, lipid homeostasis and protein quality control', *Frontiers in Bioscience - Landmark*, pp. 1552–1563.

Ge, L. *et al.* (2013) 'The ER–Golgi intermediate compartment is a key membrane source for the LC3 lipidation step of autophagosome biogenesis', *eLife*, 2, pp. 1–23.

Ghosh P, Dahms NM, Kornfeld S. (2003) Mannose 6-phosphate receptors: new twists in the tale. Nat Rev Mol Cell Biol 4:202–212.

Ghosh P, Kornfeld S. (2004) The GGA proteins: key players in protein sorting at the trans-Golgi network. Eur J Cell Biol 83:257–262

Ghosh, R. and Pattison, J. S. (2018) 'Macroautophagy and Chaperone-Mediated Autophagy in Heart Failure: The Known and the Unknown', *Oxidative Medicine and Cellular Longevity*, 2018(i).

Gillingham, A. K. and Munro, S. (2007) 'The Small G Proteins of the Arf Family and Their Regulators', *Annual Review of Cell and Developmental Biology*, 23(1), pp. 579–611.

Ginsberg SD, Mufson EJ, Counts SE, Wuu J, Alldred MJ, Nixon RA and Shaoli C (2010) Regional selectivity of rab5 and rab7 protein up regulation in mild cognitive impairment and Alzheimer's disease. Journal of Alzheimer's Disease. 22(2):631-639

Goldman, D. P., Cutler, D., Rowe, J. W., Michaud, P. C., Sullivan, J., Peneva, D., et al. (2013). Substantial health and economic returns from delayed aging may warrant a new focus for medical research. Health Aff. 32, 1698–1705

Goode A, Butler K, Long J, Cavey J, Scott D, Shaw B, Sollen-berger J, Gell C, Johansen T, Oldham NJ, Searle MS, Layfield R (2016) Defective recognition of LC3B by mutant SQSTM1/p62 implicates impairment of autophagy as a pathogenic mechanism in ALS-FTLD. Autophagy 12:1094-1104

Graef M, Nunnari J (2011) Mitochondria regulate autophagy by conserved signalling pathways. EMBO J 30:2101-2114.

Graef, M. *et al.* (2013) 'ER exit sites are physical and functional core autophagosome biogenesis components', *Molecular Biology of the Cell*, 24(18), pp. 2918–2931.

Grasso, D. *et al.* (2011) 'Zymophagy, a novel selective autophagy pathway mediated by VMP1-USP9x-p62, prevents pancreatic cell death', *Journal of Biological Chemistry*, 286(10), pp. 8308–8324.

Grumati, P. *et al.* (2017) 'Full length RTN3 regulates turnover of tubular endoplasmic reticulum via selective autophagy', *eLife*, 6, pp. 1–32.

Grumati, P. and Dikic, I. (2018) 'Ubiquitin signaling and autophagy', *Journal of Biological Chemistry*, 293(15), pp. 5404–5413.

Gutierrez, M. G. *et al.* (2004) 'Rab7 is required for the normal progression of the autophagic pathway in mammalian cells', *Journal of Cell Science*, 117(13), pp. 2687–2697.

Hailey, D. W. *et al.* (2010) 'Mitochondria Supply Membranes for Autophagosome Biogenesis during Starvation', *Cell*. Elsevier Ltd, 141(4), pp. 656–667.

Hanna, R. A. *et al.* (2012) 'Microtubule-associated protein 1 light chain 3 (LC3) interacts with Bnip3 protein to selectively remove endoplasmic reticulum and mitochondria via autophagy', *Journal of Biological Chemistry*, 287(23), pp. 19094–19104.

Hansen, T. E. and Johansen, T. (2011) 'Following autophagy step by step', *BMC Biology*, 9, pp. 2–5.

Hansen M, Rubinsztein DC, Walker DW (2018) Autophagy as a promoter of longevity: insights from model organisms. Nat Rev Mol Cell Biol 19:579-593

Hara, T. *et al.* (2006) 'Suppression of basal autophagy in neural cells causes neurodegenerative disease in mice', *Nature*, 441(7095), pp. 885–889.

Hashimoto S, Onodera Y, Hashimoto A, Tanaka H, Hamaguchi M,Yamada A, Sabe H (2004) Requirement for Arf6 in breast cancer invasive activities. Proc Natl Acad Sci U S A 101:6647–6652

He, C. and Klionsky, D. J. (2009) 'Regulation Mechanisms and Signalling Pathways of Autophagy', *Annual review of genetics*, 43(68), p. 67.

Heckmann BL, Teubner BJW, Tummers B, Boada-Romero E, Harris L, Yang M, Guy CS, Zakharenko SS, Green DR (2019) LC3-associated endocytosis facilitates β-amyloid clearance and mitigates neurodegeneration in Murine Alzheimer's disease. Cell 178:536-551.e14.

Heged s, K. *et al.* (2016) ‘The Ccz1-Mon1-Rab7 module and Rab5 control distinct steps of autophagy’, *Molecular Biology of the Cell*, 27(20), pp. 3132–3142.

Hegedus, K. *et al.* (2014) ‘The putative HORMA domain protein Atg101 dimerizes and is required for starvation-induced and selective autophagy in drosophila’, *BioMed Research International*, 2014.

Helmstädter, M., Huber, T. B. and Hermle, T. (2017) ‘Using the drosophila nephrocyte to model podocyte function and disease’, *Frontiers in Pediatrics*, 5(December), pp. 1–9.

Henriques CM, Ferreira MG (2012) Consequences of telomere shortening during lifespan. Curr Opin Cell Biol 24:804-808.

Hensley K, Carney JM, Mattson MP, Aksenova M, Harris M, Wu JF, Floyd RA, Butterfield DA (1994) A model for beta-amyloid aggregation and neurotoxicity based on free radical generation by the peptide: relevance to Alzheimer disease. Proc Natl Acad Sci U S A 91:3270-3274.

Heo, J. M. *et al.* (2015) ‘The PINK1-PARKIN Mitochondrial Ubiquitylation Pathway Drives a Program of OPTN/NDP52 Recruitment and TBK1 Activation to Promote Mitophagy’, *Molecular Cell*. Elsevier Inc., 60(1), pp. 7–20.

Hinners, I. (2003) ‘Changing directions: clathrin-mediated transport between the Golgi and endosomes’, *Journal of Cell Science*, 116(5), pp. 763–771.

Hommel, A. *et al.* (2010) ‘The ARF-Like GTPase ARFRP1 Is Essential for Lipid Droplet Growth and Is Involved in the Regulation of Lipolysis’, *Molecular and Cellular Biology*, 30(5), pp. 1231–1242.

Hosokawa, N. *et al.* (2009) ‘Nutrient-dependent mTORC1 Association with the ULK1–Atg13–FIP200 Complex Required for Autophagy’, *Molecular Biology of the Cell*, 20, pp. 1981–1991.

Hung SY, Huang WP, Liou HC, Fu WM (2009) Autophagy protects neuron from Abeta-induced cytotoxicity. Autophagy 5:502-510.

Hutchins, M. U., Veenhuis, M. and Klionsky, D. J. (1999) 'Peroxisome degradation in Saccharomyces cerevisiae is dependent on machinery of macroautophagy and the Cvt pathway', *Journal of Cell Science*, 112(22), pp. 4079–4087.

Hyttinen, J. M. T. *et al.* (2013) 'Maturation of autophagosomes and endosomes: A key role for Rab7', *Biochimica et Biophysica Acta - Molecular Cell Research*. Elsevier B.V., 1833(3), pp. 503–510.

Ichimura, Y. *et al.* (2000) 'A ubiquitin-like system mediates protein lipidation', *Nature*, 408(6811), pp. 488–492.

Ichimura, Y. *et al.* (2008) 'Structural basis for sorting mechanism of p62 in selective autophagy', *Journal of Biological Chemistry*, 283(33), pp. 22847–22857.

Ihara Y, Morishima-Kawashima M, Nixon R (2012) The ubiquitin-proteasome system and the autophagic-lysosomal system in Alzheimer disease. Cold Spring Harb Perspect Med2:a006361.

Indo HP, Yen HC, Nakanishi I, Matsumoto K, Tamura M, Nagano Y, Matsui H, Gusev O, Cornette R, Okuda T, Minamiyama Y, Ichikawa H, Suenaga S, Oki M, Sato T, Ozawa T, Clair DK, Majima HJ (2015) A mitochondrial superoxide theory for oxidative stress diseases and aging. J Clin Biochem Nutr 56:1-7.

Inoue, H. and Randazzo, P. A. (2007) 'Arf GAPs and their interacting proteins', *Traffic*, 8(11), pp. 1465–1475.

Itoh, T. *et al.* (2011) 'OATL1, a novel autophagosome-resident Rab33B-GAP, regulates autophagosomal maturation', *Journal of Cell Biology*, 192(5), pp. 838–853.

Jacomin AC, Samavedam S, Charles H and Nezis IP (2017) iLIR database: A web resource for LIR motif-containing proteins in eukaryotes, Autophagy 13:1782-1789

Jacomin, A.-C. *et al.* (2018) 'What we learned from big data for autophagy research', *Frontiers in Cell and Developmental Biology*, 6, pp. 1–14.

Jacomin, A.-C. *et al.* (2019) 'Impact of Autophagy and Aging on Iron Load and Ferritin in Drosophila Brain', *Frontiers in Cell and Developmental Biology*, 7(July), pp. 1–12.

Jennings, B. H. (2011) 'Drosophila-a versatile model in biology & medicine', *Materials Today*. Elsevier Ltd, 14(5), pp. 190–195.

Ji, C. H. and Kwon, Y. T. (2017) 'Crosstalk and interplay between the ubiquitin-proteasome system and autophagy', *Molecules and Cells*, 40(7), pp. 441–449.

Jiang, P. *et al.* (2014) 'The HOPS complex mediates autophagosome-lysosome fusion through interaction with syntaxin 17', *Molecular Biology of the Cell*, 25(8), pp. 1327–1337.

Jiang, S., Wells, C. D. and Roach, P. J. (2011) 'Starch-binding domain-containing protein 1 (Stbd1) and glycogen metabolism: Identification of the Atg8 family interacting motif (AIM) in Stbd1 required for interaction with GABARAPL1', *Biochemical and Biophysical Research Communications*. Elsevier Inc., 413(3), pp. 420–425.

Johansen, T. and Lamark, T. (2011) 'Selective autophagy mediated by autophagic adapter proteins', *Autophagy*, 7(3), pp. 279–296.

Johansen, T. and Lamark, T. (2020) 'Selective Autophagy: ATG8 Family Proteins, LIR Motifs and Cargo Receptors', *Journal of Molecular Biology*. The Authors, 432(1), pp. 80–103.

Johnson, R. I. *et al.* (2011) 'Role for a Cindr-Arf6 axis in patterning emerging

epithelia', *Molecular Biology of the Cell*, 22(23), pp. 4513–4526.

Juhász, G. *et al.* (2008) 'The class III PI(3)K Vps34 promotes autophagy and endocytosis but not TOR signaling in Drosophila', *Journal of Cell Biology*, 181(4), pp. 655–666.

Jung, W. *et al.* (2017) ' Lipophagy prevents activity-dependent neurodegeneration due to dihydroceramide accumulation in vivo ', *EMBO reports*, 18(7), pp. 1150–1165.

Kalvari, I. *et al.* (2014) 'iLIR: A web resource for prediction of Atg8-family interacting proteins', *Autophagy*, 10(5), pp. 913–925.

Kamada, Y. *et al.* (2000) 'Tor-mediated Induction of Autophagy Via an Apg1 Protein Kinase Complex', *The Journal of Cell Biology*, 150, pp. 1507–1513.

Kamada, Y. *et al.* (2010) 'Tor Directly Controls the Atg1 Kinase Complex To Regulate Autophagy', *Molecular and Cellular Biology*, 30(4), pp. 1049–1058.

Kauppila TES, Kauppila JHK, Larsson NG (2017) Mammalian mitochondria and aging: an update. Cell Metab 25:57-71

Kawasaki, F. *et al.* (2016) 'Small heat shock proteins mediate cell-autonomous and -nonautonomous protection in a Drosophila model for environmental-stress-induced degeneration', *DMM Disease Models and Mechanisms*, 9(9), pp. 953–964.

Khaminets, A. *et al.* (2015) 'Regulation of endoplasmic reticulum turnover by selective autophagy', *Nature*, 522(7556), pp. 354–358.

Khaminets, A., Behl, C. and Dikic, I. (2016) 'Ubiquitin-Dependent And Independent Signals In Selective Autophagy', *Trends in Cell Biology*. Elsevier Ltd, 26(1), pp. 6–16.

Khatter, D. *et al.* (2015) 'The small GTPase Arl8b regulates assembly of the mammalian HOPS complex on lysosomes', *Journal of Cell Science*, 128(9), pp. 1746–1761.

Kiecolt-Glaser JK, Preacher KJ, MacCallum RC, Atkinson Malarkey WB, Glaser R (2003) Chronic stress and age-related increases in the proinflammatory cytokine IL-6. Proc Natl Acad Sci U S A 100:9090-9095.

Kim, I., Rodriguez-Enriquez, S. and Lemasters, J. J. (2007) 'Selective degradation of mitochondria by mitophagy', *Archives of Biochemistry and Biophysics*, 462(2), pp. 245–253.

Kimmel, A. R. *et al.* (2010) 'Adoption of PERILIPIN as a unifying nomenclature for the mammalian PAT-family of intracellular lipid storage droplet proteins', *Journal of Lipid Research*, 51(3), pp. 468–471.

Kirkin, V. *et al.* (2009) 'A Role for NBR1 in Autophagosomal Degradation of Ubiquitinated Substrates', *Molecular Cell*, 33(4), pp. 505–516.

Kirkin, V. (2020) 'History of the Selective Autophagy Research: How Did It Begin and Where Does It Stand Today?', *Journal of Molecular Biology*. The Author, 432(1), pp. 3–27.

Klionsky, D. J. (2008) 'Autophagy revisited: A conversation with Christian de Duve', *Autophagy*, 4(6), pp. 740–743.

Knævelsrud, H. *et al.* (2013) 'Membrane remodeling by the PX-BAR protein SNX18 promotes autophagosome formation', *Journal of Cell Biology*, 202(2), pp. 331–349.

Knowles, T. P. J., Vendruscolo, M. and Dobson, C. M. (2014) 'The amyloid state and its association with protein misfolding diseases', *Nature Reviews Molecular Cell Biology*. Nature Publishing Group, 15(6), pp. 384–396.

Komatsu, M. *et al.* (2007) 'Homeostatic Levels of p62 Control Cytoplasmic Inclusion Body Formation in Autophagy-Deficient Mice', *Cell*, 131(6), pp. 1149–1163.

Kondratskyi A, Kondratska K, Abeele FV, Gordienko D, Dubois C, Toillon RA, Slomianny C, Lemiere S, Delcourt P, Dewailly E, Skryma R, Biot C and Prevarskaya N (2017) Ferroquine, the next generation antimalarial drug, has antitumor activity. Scientific reports. 7(15896): 1-15

Korac, J. *et al.* (2013) 'Ubiquitin-independent function of optineurin in autophagic clearance of protein aggregates', *Journal of Cell Science*, 126(2), pp. 580–592.

Kraft, C. *et al.* (2012) 'Binding of the Atg1/ULK1 kinase to the ubiquitin-like protein Atg8 regulates autophagy', *EMBO Journal*. Nature Publishing Group, 31(18), pp. 3691–3703.

Kriegenburg, F., Ungermann, C. and Reggiori, F. (2018) 'Coordination of Autophagosome–Lysosome Fusion by Atg8 Family Members', *Current Biology*. Elsevier Ltd, 28(8), pp. R512–R518.

Kroemer, G. (2015) 'Autophagy: druggable process that is deregulated in aging and human disease', *Journal of Clinical Investigation*, 125(1), pp. 1–4.

Kuchitsu, Y. and Fukuda, M. (2018) 'Revisiting Rab7 Functions in Mammalian Autophagy: Rab7 Knockout Studies', *Cells*, 7(11), p. 215.

Kuma, A. *et al.* (2002) 'Formation of the ~350-kDa Apg12-Apg5·Apg16 multimeric complex, mediated by Apg16 oligomerization, is essential for autophagy in yeast', *Journal of Biological Chemistry*, 277(21), pp. 18619–18625.

Kwon, Y. T. and Ciechanover, A. (2017) 'The Ubiquitin Code in the Ubiquitin-Proteasome System and Autophagy', *Trends in Biochemical Sciences*. Elsevier Ltd, 42(11), pp. 873–886.

Laberge RM, Sun Y, Orjalo AV, Patil CK, Freund A, Zhou L, Curran SC, Davalos AR, Wilson-Edell KA, Liu S, Limbad C, Demaria M, Li P, Hubbard GB, Ikeno Y, Javors M, Desprez PY, Benz CC, Kapahi P, Nelson PS, Campisi J (2015) MTOR

regulates the pro-tumorigenic senescence-associated secretory phenotype by promoting IL1A translation. Nat Cell Biol 17:1049-1061.

Lamark, T. and Johansen, T. (2012) 'Aggrephagy: Selective disposal of protein aggregates by macroautophagy', *International Journal of Cell Biology*, 2012.

Lamb, C. A., Yoshimori, T. and Tooze, S. A. (2013) 'The autophagosome: Origins unknown, biogenesis complex', *Nature Reviews Molecular Cell Biology*. Nature Publishing Group, 14(12), pp. 759–774.

Lazarou, M. *et al.* (2015) 'The ubiquitin kinase PINK1 recruits autophagy receptors to induce mitophagy', *Nature*, 524(7565), pp. 309–314.

Lecker, S. H., Goldberg, A. L. and Mitch, W. E. (2006) 'Protein degradation by the ubiquitin-proteasome pathway in normal and disease states', *Journal of the American Society of Nephrology*, 17(7), pp. 1807–1819.

Lee J, Giordano S, Zhang J (2012) Autophagy, mitochondria and oxidative stress: cross-talk and redox signalling. Biochem J 441:523-540.

Lee, Y. K. and Lee, J. A. (2016) 'Role of the mammalian ATG8/LC3 family in autophagy: Differential and compensatory roles in the spatiotemporal regulation of autophagy', *BMB Reports*, 49(8), pp. 424–430.

Lei Y and Klionsky DJ (2019) UIM-UDS: a new interface between ATG8 and its interactors. Cell Research. 29:507-508

Lemus, L. *et al.* (2016) 'An ER-Localized SNARE Protein Is Exported in Specific COPII Vesicles for Autophagosome Biogenesis', *Cell Reports*. The Authors, 14(7), pp. 1710–1722.

Lescat, L. *et al.* (2018) 'CMA restricted to mammals and birds: myth or reality?', *Autophagy*. Taylor & Francis, 14(7), pp. 1267–1270.

Levine B, Mizushima N, Virgin HW (2011) Autophagy in immunity and inflammation. Nature 469:323-335.

Li L, Chen Y, Gibson SB (2013) Starvation-induced autophagy is regulated by mitochondrial reactive oxygen species leading to AMPK activation. Cell Signal 25:50-65.

Li, C. and Yu, S. S. B. (2016) 'Rab proteins as regulators of lipid droplet formation and lipolysis', *Cell Biology International*, 40(10), pp. 1026–1032.

Li, W. W., Li, J. and Bao, J. K. (2012) 'Microautophagy: Lesser-known self-eating', *Cellular and Molecular Life Sciences*, 69(7), pp. 1125–1136.

Lim, J. and Yue, Z. (2015) 'Neuronal Aggregates: Formation, Clearance, and Spreading', *Developmental Cell*. Elsevier Inc., 32(4), pp. 491–501.

Lindner, A. B. and Demarez, A. (2009) 'Biochimica et Biophysica Acta Protein aggregation as a paradigm of aging', *BBA - General Subjects*. Elsevier B.V., 1790(10), pp. 980–996.

Linford, N. J. *et al.* (2013) 'Measurement of lifespan in Drosophila melanogaster', *Journal of Visualized Experiments*, (71), pp. 1–9.

Lipinski MM, Zheng B, Yan Z, Py BF, Ng A, Xavier R, Li C, Yankner BA, Scherzer CR and Yuan J (2010) Genome-wide analysis reveals mechanisms modulating autophagy in normal brain aging and in Alzheimer's disease. PNAS. 107(32):14164-14169

Liu, L. *et al.* (2012) 'Mitochondrial outer-membrane protein FUNDC1 mediates hypoxia-induced mitophagy in mammalian cells', *Nature Cell Biology*, 14(2), pp. 177–185.

Liu, X. *et al.* (2001) 'Functional characterization of novel human ARFGAP3', *FEBS Letters*, 490(1–2), pp. 79–83.

Longatti, A. *et al.* (2012) 'TBC1D14 regulates autophagosome formation via Rab11- and ULK1-positive recycling endosomes', *Journal of Cell Biology*, 197(5), pp. 659–675.

López-Otín, C. *et al.* (2013) 'The hallmarks of aging', *Cell*, 153(6), p. 1194-1217

Lopes da Fonseca T, Outeiro TF (2014) ATP13A2 and alpha-synuclein: a metal taste in autophagy. Exp Neurobiol 23:314-323.

Lorincz, P. *et al.* (2016) 'iFly: The eye of the fruit fly as a model to study autophagy and related trafficking pathways', *Experimental Eye Research*, 144, pp. 90–98.

Lörincz, P. *et al.* (2017) 'Rab2 promotes autophagic and endocytic lysosomal degradation', *Journal of Cell Biology*, 216(7), pp. 1937–1947.

Lőrincz, P. *et al.* (2016) 'MiniCORVET is a Vps8-containing early endosomal tether in drosophila', *eLife*, 5(JUNE2016), pp. 1–27.

Lőrincz, P., Mauvezin, C. and Juhász, G. (2017) 'Exploring Autophagy in Drosophila', *Cells*, 6(3), p. 22.

Lu, K., Psakhye, I. and Jentsch, S. (2014) 'Autophagic clearance of PolyQ proteins mediated by ubiquitin-Atg8 adaptors of the conserved CUET protein family', *Cell*. Elsevier Inc., 158(3), pp. 549–563.

Luzio, J. P., Gray, S. R. and Bright, N. A. (2010) 'Endosome-lysosome fusion', *Biochemical Society Transactions*, 38(6), pp. 1413–1416.

Maejima, I. *et al.* (2013) 'Autophagy sequesters damaged lysosomes to control lysosomal biogenesis and kidney injury', *EMBO Journal*. Nature Publishing Group, 32(17), pp. 2336–2347.

Mancias, J. D. *et al.* (2014) 'Quantitative proteomics identifies NCOA4 as the cargo receptor mediating ferritinophagy', *Nature*. Nature Publishing Group, 508(7498), pp.

105–109.

Mandell, M. A. *et al.* (2014) ‘TRIM proteins regulate autophagy: TRIM5 is a selective autophagy receptor mediating HIV-1 restriction’, *Autophagy*, 10(12), pp. 2387–2388.

Mandell, M. A. *et al.* (2017) ‘Correction: TRIM17 contributes to autophagy of midbodies while actively sparing other targets from degradation [J. Cell Sci. 129, (3562-3573)] 10.1242/jcs.190017’, *Journal of Cell Science*, 130(6), p. 3562-3573

Mardones G.A., Polishchuk R.S., Bonifacino J.S. (2008) Protein transport from the *trans*-Golgi network to endosomes. In: Mironov A.A., Pavelka M. (eds) The Golgi Apparatus. Springer, Vienna

Mariño, G. *et al.* (2014) ‘Self-consumption: The interplay of autophagy and apoptosis’, *Nature Reviews Molecular Cell Biology*. Nature Publishing Group, 15(2), pp. 81–94.

Marshall, R. S. *et al.* (2015) ‘Autophagic Degradation of the 26S Proteasome Is Mediated by the Dual ATG8/Ubiquitin Receptor RPN10 in Arabidopsis’, *Molecular Cell*. Elsevier Inc., 58(6), pp. 1053–1066.

Marshall RS, Hua Z, Mali S, McLoughlin F and Vierstra RD (2019) ATG8-binding UIM proteins define a new class of autophagy adaptors and receptors. Cell. 177(3): 766-781

Martinez-Lopez, N., Athonvarangkul, D. and Singh, R. (2015) ‘Autophagy and Aging’, *Advances in Experimental Medicine and Biology*, 847, pp. 73–87.

Maruzs, T. *et al.* (2019) ‘On the Fly: Recent Progress on Autophagy and Aging in Drosophila’, *Frontiers in Cell and Developmental Biology*, 7(July), pp. 1–15.

Masaldan, S. *et al.* (2018) ‘Iron accumulation in senescent cells is coupled with impaired ferritinophagy and inhibition of ferroptosis’, *Redox Biology*. Elsevier B.V., 14(September 2017), pp. 100–115.

Massey, A. C. *et al.* (2006) 'Consequences of the selective blockage of chaperone-mediated autophagy', *Proceedings of the National Academy of Sciences of the United States of America*, 103(15), pp. 5805–5810.

Massie, C. and Mills, I. G. (2006) 'The developing role of receptors and adaptors', *Nature Reviews Cancer*, 6(5), pp. 403–409.

Matsuura, A. *et al.* (1997) 'Apg1p, a novel protein kinase required for the autophagic process in Saccharomyces cerevisiae', *Gene*, 192(2), pp. 245–250.

Mauvezin C, Nagy P, Juhasz G and Neufeld TP (2015) Autophagosome-lysosome fusion is independent of V-ATPase-mediated acidification. Nature communications. 6(7007):1-14

Moss J and Vaughan M (1998) Molecules in the ARF Orbit. Journal of Biological Chemistry. 273(34):21431-21434

Maynard S, Schurman SH, Harboe C, de Souza-Pinto NC, Bohr VA (2009) Base excision repair of oxidative DNA damage and association with cancer and aging. Carcinogenesis 30:2-10

McEwan, D. G. *et al.* (2015) 'PLEKHM1 regulates autophagosome-lysosome fusion through HOPS complex and LC3/GABARAP proteins', *Molecular Cell*. Elsevier Inc., 57(1), pp. 39–54.

McGuire, S. E., Roman, G. and Davis, R. L. (2004) 'Gene expression systems in Drosophila: A synthesis of time and space', *Trends in Genetics*, 20(8), pp. 384–391.

McPhee, C. K. and Baehrecke, E. H. (2009) 'Autophagy in Drosophila melanogaster', *Biochimica et Biophysica Acta - Molecular Cell Research*. Elsevier B.V., 1793(9), pp. 1452–1460.

Mei Y, Minfei S, Soni G, Salem S, Colbert CL and Sinha SC (2014) Intrinsically Disordered Regions in Autophagy Proteins. Proteins 82(4): 565-578

Mejlvang, J. *et al.* (2018) 'Starvation induces rapid degradation of selective autophagy receptors by endosomal microautophagy', *The Journal of cell biology*, 217(10), pp. 3640–3655.

Melani, M. *et al.* (2017) 'Zonda is a novel early component of the autophagy pathway in *Drosophila*', *Molecular Biology of the Cell*, 28(22), pp. 3070–3081. doi: 10.1091/mbc.E16-11-0767.

Menzies, F. M. *et al.* (2017) 'Autophagy and Neurodegeneration: Pathogenic Mechanisms and Therapeutic Opportunities', *Neuron*, 93(5), pp. 1015–1034.

Menzies, F. M., Fleming, A. and Rubinsztein, D. C. (2015) 'Compromised autophagy and neurodegenerative diseases', *Nature Reviews Neuroscience*. Nature Publishing Group, 16(6), pp. 345–357.

Menzies, F. M., Moreau, K. and Rubinsztein, D. C. (2011) 'Protein misfolding disorders and macroautophagy', *Current Opinion in Cell Biology*. Elsevier Ltd, 23(2), pp. 190–197.

Meszaros B, Simon I and Dosztanyi (2009) Prediction of protein binding regions in disordered proteins. PLoS computational biology 5(5):e1000376

Metcalf DJ, Garcia-Arencibia M, Hochfeld WE and Rubinsztein DC (2012) Autophagy and misfolded proteins in neurodegeneration. Experimental Neurology. 238(1):22-28

Mijaljica, D., Prescott, M. and Devenish, R. J. (2011) 'Microautophagy in mammalian cells: Revisiting a 40-year-old conundrum', *Autophagy*, 7(7), pp. 673–682.

Mijaljica, D., Prescott, M. and Devenish, R. J. (2012) 'The intriguing life of Autophagosomes', *International Journal of Molecular Sciences*, 13(3), pp. 3618–3635.

Misonou H, Morishima-Kawashima M, Ihara Y (2000) Oxidative stress induces intracellular accumulation of amyloid beta-protein (Abeta) in human neuroblastoma cells. Biochemistry 39:6951-6959.

Mizuno-Yamasaki, E., Rivera-Molina, F. and Novick, P. (2012) 'GTPase Networks in Membrane Traffic', *Annual Review of Biochemistry*, 81(1), pp. 637–659.

Mizushima, N. (2010) 'The role of the Atg1/ULK1 complex in autophagy regulation', *Current Opinion in Cell Biology*. Elsevier Ltd, 22(2), pp. 132–139.

Mizushima, N. (2018) 'A brief history of autophagy from cell biology to physiology and disease', *Nature Cell Biology*. Springer US, 20(5), pp. 521–527.

Mizushima, N. and Komatsu, M. (2011) 'Autophagy: Renovation of cells and tissues', *Cell*. Elsevier Inc., 147(4), pp. 728–741.

Mizushima, N., Yoshimorim, T. and Levine, B. (2010) 'Methods in Mammalian Autophagy Research', *Cell*, 140(3), pp. 313–326.

Mochida, K. *et al.* (2015) 'Receptor-mediated selective autophagy degrades the endoplasmic reticulum and the nucleus', *Nature*, 522(7556), pp. 359–362.

Morel, E. and Codogno, P. (2018) 'A novel regulator of autophagosome biogenesis and lipid droplet dynamics', *EMBO reports*, 19(9), pp. 1–2.

Mortimore, G. E. and Schworer, C. M. (1977) 'Induction of autophagy by amino-acid deprivation in perfused rat liver', *Nature*, 270(5633), pp. 174–176.

Motley, A. M., Nuttall, J. M. and Hettema, E. H. (2012) 'Pex3-anchored Atg36 tags peroxisomes for degradation in Saccharomyces cerevisiae', *EMBO Journal*. Nature Publishing Group, 31(13), pp. 2852–2868. d

Mukherjee, A. *et al.* (2016) 'Selective endosomal microautophagy is starvation-inducible in Drosophila', *Autophagy*. Taylor & Francis, 12(11), pp. 1984–1999.

Mulakkal, N. C. *et al.* (2014) 'Autophagy in drosophila: From historical studies to current knowledge', *BioMed Research International*, 2014(C).

Muñoz-Espín D, Serrano M (2014) Cellular senescence: from physiology to pathology. Nat Rev Mol Cell Biol 15:482-496

Murakawa, T. *et al.* (2015) 'Bcl-2-like protein 13 is a mammalian Atg32 homologue that mediates mitophagy and mitochondrial fragmentation', *Nature Communications*. Nature Publishing Group, 6(May), pp. 1–14.

Nagy, P. *et al.* (2014) 'Atg17/FIP200 localizes to perilysosomal Ref(2)P aggregates and promotes autophagy by activation of Atg1 in Drosophila', *Autophagy*, 10(3), pp. 453–467.

Nakae, I. *et al.* (2010) 'The Arf-like GTPase Arl8 Mediates Delivery of Endocytosed Macromolecules to Lysosomes in Caenorhabditis elegans', *Molecular Biology of the Cell*, 21, pp. 2434–2442.

Nakatogawa, H., Ichimura, Y. and Ohsumi, Y. (2007) 'Atg8, a Ubiquitin-like Protein Required for Autophagosome Formation, Mediates Membrane Tethering and Hemifusion', *Cell*, 130(1), pp. 165–178.

Nassif, M., Woehlbier, U. and Manque, P. A. (2017) 'The enigmatic role of C9ORF72 in autophagy', *Frontiers in Neuroscience*, 1, pp. 1–10.

Nassour J, Radford R, Correia A, Fusté JM, Schoell B, Jauch A, Shaw RJ, Karlseder J (2019) Autophagic cell death restricts chromosomal instability during replicative crisis. Nature 565:659-663.

Nezis, I. P. *et al.* (2008) 'Ref(2)P, the Drosophila melanogaster homologue of mammalian p62, is required for the formation of protein aggregates in adult brain', *Journal of Cell Biology*, 180(6), pp. 1065–1071.

Nezis, I. P. (2012) ‘Selective autophagy in drosophila’, *International Journal of Cell Biology*, 2012.

Nezis, I. P. and Stenmark, H. (2012) ‘P62 at the interface of autophagy, oxidative stress signaling, and cancer’, *Antioxidants and Redox Signaling*, 17(5), pp. 786–793.

Nguyen TN and Goodrich JA (2006) Protein-protein interaction assays: eliminating false-positive interactions. Nat methods. 3(2):135
-139

Niccoli T and Partridge L (2012) Ageing as a risk factor for disease. Current Biology. 22(17):741-752.

Nilsson P, Loganathan K, Sekiguchi M, Matsuba Y, Hui K, Tsubuki S, Tanaka M, Iwata N, Saito T, Saido TC (2013) Aβ secretion and plaque formation depend on autophagy. Cell Rep 5:61-69

Nixon, R. A. (2005) ‘Endosome function and dysfunction in Alzheimer’s disease and other neurodegenerative diseases’, *Neurobiology of Aging*, 26(3), pp. 373–382.

Nixon RA (2007) Autophagy, amyloidogenesis and Alzheimer disease. J Cell Sci 120:4081-4091.

Noda, N. N. *et al.* (2008) ‘Structural basis of target recognition by Atg8/LC3 during selective autophagy’, *Genes to Cells*, 13(12), pp. 1211–1218.

Noda, N. N., Ohsumi, Y. and Inagaki, F. (2010) ‘Atg8-family interacting motif crucial for selective autophagy’, *FEBS Letters*, 584(7), pp. 1379–1385.

Norman JC, Jones D, Barry ST, Holt MR, Cockcroft S, Critchley DR (1998) ARF1 mediates paxillin recruitment to focal adhesions and potentiates Rho-stimulated stress fiber formation in intact and permeabilized Swiss3T3 fibroblasts. J Cell Biol 143:1981–1995

Novak, I. *et al.* (2010) 'Nix is a selective autophagy receptor for mitochondrial clearance', *EMBO Reports*, 11(1), pp. 45–51.

Ntsapi, C. *et al.* (2016) 'Autophagic Flux Failure in Neurodegeneration: Identifying the Defect and Compensating Flux Offset', in *Autophagy in Current Trends in Cellular Physiology and Pathology*, pp. 157–176.

Obara, K. *et al.* (2008) 'The Atg18-Atg2 complex is recruited to autophagic membranes via phosphatidylinositol 3-phosphate and exerts an essential function', *Journal of Biological Chemistry*, 283(35), pp. 23972–23980.

Ohsumi, Y. (2001) 'Molecular dissection of autophagy: Two ubiquitin-like systems', *Nature Reviews Molecular Cell Biology*, 2(3), pp. 211–216.

Olsvik, H. L. *et al.* (2019) 'Endosomal microautophagy is an integrated part of the autophagic response to amino acid starvation', *Autophagy*. Taylor & Francis, 15(1), pp. 182–183.

Ong SM, Hadadi E, Dang TM, Yeap WH, Tan CT, Ng TP, Larbi A, Wong SC (2018) The pro-inflammatory phenotype of the human non-classical monocyte subset is attributed senescence. Cell Death Dis 9:266.

Orvedahl, A. *et al.* (2010) 'Autophagy Protects against Sindbis Virus Infection of the Central Nervous System', *Cell Host and Microbe*, 7(2), pp. 115–127.

Osterwalder, T. *et al.* (2001) 'A conditional tissue-specific transgene expression system using inducible GAL4', *Proceedings of the National Academy of Sciences of the United States of America*, 98(22), pp. 12596–12601.

Pankiv, S. *et al.* (2007) 'p62/SQSTM1 binds directly to Atg8/LC3 to facilitate degradation of ubiquitinated protein aggregates by autophagy*[S]', *Journal of Biological Chemistry*, 282(33), pp. 24131–24145.

Papadopoulos, C., Kravic, B. and Meyer, H. (2020) 'Repair or Lysophagy: Dealing

with Damaged Lysosomes', *Journal of Molecular Biology*. Elsevier Ltd, 432(1), pp. 231–239.

Papandreou, M. E. and Tavernarakis, N. (2019) 'Nucleophagy: from homeostasis to disease', *Cell Death and Differentiation*, 26(4), pp. 630–639.

Papinski, D. *et al.* (2014) 'Early Steps in Autophagy Depend on Direct Phosphorylation of Atg9 by the Atg1 Kinase', *Molecular Cell*. The Authors, 53(3), pp. 471–483.

Park, E. S. *et al.* (2016) 'UbcD4, an ortholog of E2-25K/Ube2K, is essential for activation of the immune deficiency pathway in Drosophila', *Biochemical and Biophysical Research Communications*. Elsevier Ltd, 469(4), pp. 891–896.

Park SW, Jun YW, Jeon P, Lee YK, Park JH, Lee SH, Lee JA and Jang DJ (2019) LIR motifs and the membrane-targeting domain are complementary in the function of RavZ. BMB rep. 52(12): 700-705

Partridge L, Gems D and Withers DJ (2005) Sex and death: what is the connection? Cell. 120:461-472

Pastores, G. M. and Maegawa, G. H. B. (2013) 'Neuropathic Lysosomal Storage Disorders', *Neurologic Clinics*, 31(4), pp. 1051–1071.

Periyasamy-Thandavan, S. *et al.* (2009) 'Autophagy: molecular machinery, regulation, and implications for renal pathophysiology.', *American journal of physiology. Renal physiology*, 297(March 2009), pp. F244–F256.

Pickles, S., Vigié, P. and Youle, R. J. (2018) 'Mitophagy and Quality Control Mechanisms in Mitochondrial Maintenance', *Current Biology*, 28(4), pp. R170–R185.

Plaza-Zabala, A., Sierra-Torre, V. and Sierra, A. (2017) 'Autophagy and microglia: Novel partners in neurodegeneration and aging', *International Journal of Molecular Sciences*, 18(3).

Pohl, C. and Jentsch, S. (2009) ‘Midbody ring disposal by autophagy is a post-abscission event of cytokinesis’, *Nature Cell Biology*, 11(1), pp. 65–70.

Popovic, D. *et al.* (2012) ‘Rab GTPase-Activating Proteins in Autophagy: Regulation of Endocytic and Autophagy Pathways by Direct Binding to Human ATG8 Modifiers’, *Molecular and Cellular Biology*, 32(9), pp. 1733–1744.

Progida, C. and Bakke, O. (2016) ‘Bidirectional traffic between the Golgi and the endosomes – machineries and regulation’, *Journal of Cell Science*, p. jcs.185702.

Puri, C. *et al.* (2013) ‘Diverse autophagosome membrane sources coalesce in recycling endosomes’, *Cell*. Elsevier, 154(6), pp. 1285–1299.

Rabinovitch RC, Samborska B, Faubert B, Ma EH, Gravel SP, Andrzejewski S, Raissi TC, Pause A, St-Pierre J, Jones RG (2017) AMPK maintains cellular metabolic homeostasis through regulation of mitochondrial reactive oxygen species. Cell Rep 21:1-9

Randazzo PA, Nie Z, Miura K, Hsu VW (2000) Molecular aspects of the cellular activities of ADP-ribosylation factors. Sci STKE 1:1–15

Randow, F. and Youle, R. J. (2014) ‘Self and nonself: How autophagy targets mitochondria and bacteria’, *Cell Host and Microbe*, 15(4), pp. 403–411.

Ravikumar B, Berger Z, Vacher C, O’Kane CJ and Rubinsztein DC (2006) Rapamycin pre-treatment protects against apoptosis. Human Molecular Genetics. 15:1209-1216

Ravikumar, B. *et al.* (2010) ‘Plasma membrane contributes to the formation of pre-autophagosomal structures’, *Nature Cell Biology*, 12(8), pp. 747–757.

Reggiori, F. and Klumperman, J. (2016) *Lysosome Biogenesis and Autophagy*, *Lysosomes: Biology, Diseases, and Therapeutics*.

Reiter, L. T. *et al.* (2001) 'A systematic analysis of human disease-associated gene sequences in Drosophila melanogaster', *Genome Research*, 11(6), pp. 1114–1125.

Rekha Khandia, Maryam Dadar, Ashok Munjal, Kuldeep Dhama, Kumaragurubaran Karthik Ruchi Tiwari, Mohd. Iqbal Yatoo, Hafiz M.N. Iqbal , Karam Pal Singh, Sunil K. Joshi, andWanpen C. (2019) 'Various Roles in Infectious , Non-Infectious , and Lifestyle Diseases : Current Knowledge and Prospects for Disease Prevention , Novel Drug', *Cells*, 8(674), pp. 1-64

Renton AE, Chiò A, Traynor BJ (2014) State of play in amyotrophic lateral sclerosis genetics. Nat Neurosci 17:17-23.

Ricatti J, Acquasaliente, Ribaudo G, De Filippis V, Bellini M, Llovera RE, Barollo S, Pezzani R, Zagotto G, Persaud KC and Mucignat-Caretta C (2019) Effects of point mutations in the binding pocket of the mouse major urinary protein MUP20 on ligand. Scientific reports. 9(300):1-12

Rice AM and McLysaght A (2017) Dosage-sensitive genes in evolution and disease. BMC Biology 15:78

Rodrigues FF, Shao W and Harris TJC (2016) The Arf GAP Asap promotes Arf1 function at the Golgi for cleavage furrow biosynthesis in *Drosophila*. Molecular Biology of the Cell. 27(20):3005-3180

Rogov, V. *et al.* (2014) 'Interactions between Autophagy Receptors and Ubiquitin-like Proteins Form the Molecular Basis for Selective Autophagy', *Molecular Cell*, 53(2), pp. 167–178.

Rosa-Ferreira, C., Sweeney, S. T. and Munro, S. (2018) 'The small G protein Arl8 contributes to lysosomal function and long-range axonal transport in Drosophila', *Biology Open*, 7(9), pp. 1–10.

Del Roso, A. *et al.* (2003) 'Ageing-related changes in the in vivo function of rat liver macroautophagy and proteolysis', *Experimental Gerontology*, 38(5), pp. 519–527.

Le Roy, C. and Wrana, J. L. (2005a) 'Clathrin- and non-clathrin-mediated endocytic regulation of cell signalling', *Nature Reviews Molecular Cell Biology*, 6(2), pp. 112–126.

Le Roy, C. and Wrana, J. L. (2005b) 'Signaling and endocytosis: A team effort for cell migration', *Developmental Cell*, 9(2), pp. 167–168.

Rozenknop A, Rogov VV, Rogova NY, Lohr F, Guntert P and Dikic I (2011) Characterisation of the interaction of GABARAPL-1 with the LIR motif of NBR1. J mol Biol. 410: 477-487

Rubinsztein, D. C., Mariño, G. and Kroemer, G. (2011) 'Autophagy and aging', *Cell*, 146(5), pp. 682–695.

Rubinsztein, D. C., Shpilka, T. and Elazar, Z. (2012) 'Mechanisms of autophagosome biogenesis', *Current Biology*. Elsevier Ltd, 22(1), pp. R29–R34.

Rudolph KL, Chang S, Lee HW, Blasco M, Gottlieb GJ, Gre ider C, DePinho RA (1999) Longevity, stress response, and cancer in aging telomerase-deficient mice. Cell 96:701-712.

Ryoo, H. D. (2015) 'Drosophila as a model for unfolded protein response research', *BMB Reports*, 48(8), pp. 445–453.

Sahu, R. *et al.* (2011) 'Microautophagy of Cytosolic Proteins by Late Endosomes', *Developmental Cell*, 20(1), pp. 131–139.

Sarkar S, Ravikumar B, Floto RA, Rubinsztein DC (2009) Rapamycin and mTOR-independent autophagy inducers ameliorate toxicity of polyglutamine-expanded huntingtin and related proteinopathies. Cell Death Differentiation. 16:46-56

Schulze, R. J. *et al.* (2017) 'Hepatic lipophagy: New insights into autophagic catabolism of lipid droplets in the liver', *Hepatology Communications*, 1(5), pp. 359–369.

Schulze, R. J., Sathyanarayan, A. and Mashek, D. G. (2017) 'Breaking fat: The regulation and mechanisms of lipophagy', *Biochimica et Biophysica Acta - Molecular and Cell Biology of Lipids*, 1862(10), pp. 1178–1187.

Scott, R. C., Juhász, G. and Neufeld, T. P. (2007) 'Direct Induction of Autophagy by Atg1 Inhibits Cell Growth and Induces Apoptotic Cell Death', *Current Biology*, 17(1), pp. 1–11.

Scott, R. C., Schuldiner, O. and Neufeld, T. P. (2004) 'Role and regulation of starvation-induced autophagy in the Drosophila fat body', *Developmental Cell*, 7(2), pp. 167–178.

Scotter EL, Vance C, Nishimura AL, Lee YB, Chen HJ, Urwin H, Sardone V, Mitchell JC, Rogelj B, Rubinsztein DC, Shaw CE (2014) Differential roles of the ubiquitin proteasome system and autophagy in the clearance of soluble and aggregated TDP-43 species. J Cell Sci 127:1263-1278

Seluanov A, Mittelman D, Pereira-Smith OM, Wilson JH, Gorbunova V (2004) DNA end joining becomes less efficient and more error-prone during cellular senescence. Proc Natl Acad Sci U S A 101:7624-7629

Sentelle, R. D. *et al.* (2012) 'Ceramide targets autophagosomes to mitochondria and induces lethal mitophagy', *Nature Chemical Biology*, 8(10), pp. 831–838.

Sepe S, Milanese C, Gabriels S, Derks KW, Payan-Gomezvan IJcken WF, Rijksen YM, Nigg AL, Moreno S, Cerri S, Blandini F, Hoeijmakers JH, Mastroberardino PG (2016) Inefficient DNA repair is an aging-related modifier of Parkinson's disease. Cell Rep 15:1866-1875.

Shah P, Ding Y, Niemczyk M, Kudla G, Plotkin JB (2013) Rate-limiting steps in yeast protein translation. Cell 153:1589-1601

Sharma, V. *et al.* (2018) 'Selective autophagy and xenophagy in infection and

disease', *Frontiers in Cell and Developmental Biology*, 6(NOV), pp. 1–17.

Shi, J.-J., Liu, K.-Y. and Yang, Y.-P. (2009) 'Autophagy in the pathogenesis of Parkinson's disease.', *Sheng li ke xue jin zhan [Progress in physiology]*, 40(1), pp. 67–71.

Shiba, Y. *et al.* (2013) 'ArfGAP3 regulates the transport of cation-independent mannose 6-phosphate receptor in the post-golgi compartment', *Current Biology*. Elsevier Ltd, 23(19), pp. 1945–1951.

Shiba, Y. and Randazzo, P. A. (2014) 'ArfGAPs: key regulators for receptor sorting', *Receptors & Clinical Investigation*, 11158(10), pp. 158–158.

Shigenaga MK, Hagen TM, Ames BN (1994) Oxidative damage and mitochondrial decay in aging. Proc Natl Acad Sci U S A 91:10771-10778

Shpilka, T. *et al.* (2011) 'Atg8 : an autophagy-related ubiquitin-like protein family', *Genome Biology*, 12(226), pp. 1–11.

Shpilka, T. and Elazar, Z. (2015) 'Lipid droplets regulate autophagosome biogenesis', *Autophagy*, 11(11), pp. 2130–2131.

Siddiqi FH, Menzies FM, Lopez A, Stamatakou E, KarabiyikUreshino R, Ricketts T, Jimenez-Sanchez M, Esteban MA, Lai L, Tortorella MD, Luo Z, Liu H, Metzakopian E, Fernandes HJR,

Simonsen, A. *et al.* (2008) 'Promoting basal levels of autophagy in the nervous system enhances longevity and oxidant resistance in adult Drosophila', *Autophagy*, 4(2), pp. 176–184.

Simonsen, A. and Tooze, S. A. (2009) 'Coordination of membrane events during autophagy by multiple class III PI3-kinase complexes', *Journal of Cell Biology*, 186(6), pp. 773–782.

Singh, R. *et al.* (2009) 'Autophagy regulates lipid metabolism', *Nature*. Nature Publishing Group, 458(7242), pp. 1131–1135.

Singh, R. *et al.* (2010) 'NGAP_2020_Booklet', 458(7242), pp. 1131–1135.

Singh AK, Kashyap MP, Tripathi VK, Singh S, Garg G, Rizvi SI (2017) Neuroprotection through rapamycin-induced activation of autophagy and PI3K/Akt1/mTOR/CREB signaling against amyloid-β-induced oxidative stress, synaptic/neurotransmission dysfunction, and neurodegeneration in adult rats. Mol Neurobiol 54:5815-5828.

Sjödin, S. *et al.* (2019) 'Endo-lysosomal proteins and ubiquitin CSF concentrations in Alzheimer's and Parkinson's disease', *Alzheimer's Research & Therapy*. Alzheimer's Research & Therapy, 11(1), pp. 1–16.

Smith, M. D. *et al.* (2018) 'CCPG1 Is a Non-canonical Autophagy Cargo Receptor Essential for ER-Phagy and Pancreatic ER Proteostasis', *Developmental Cell*. Elsevier Inc., 44(2), pp. 217–232.

Søreng, K., Neufeld, T. P. and Simonsen, A. (2017) 'Membrane Trafficking in Autophagy', *International Review of Cell and Molecular Biology*, 336, pp. 1–92.

Sorensen JG, Kristensen TN, Kristensen KV and Loeschcke V (2007) Sex specific effects of heat induced hormesis in Hsf-deficient Drosophila melanogaster. Exp Gerontol. 42:1123-1129

Stenmark, H. (2009) 'Rab GTPases as coordinators of vesicle traffic', *Nature Reviews Molecular Cell Biology*. Nature Publishing Group, 10(8), pp. 513–525.

Stoebel DM, Dean AM, Dykhuizen DE (2008) The cost of expression of Escherichia coli lac operon proteins is in the process, not in the products. Genetics 178:1653-1660

Strappazzon, F. *et al.* (2015) 'AMBRA1 is able to induce mitophagy via LC3 binding, regardless of PARKIN and p62/SQSTM1', *Cell Death and Differentiation*. Nature

Publishing Group, 22(3), pp. 419–432.

Sun Y, Coppé JP, Lam EW (2018) Cellular senescence: the sought or the unwanted? Trends Mol Med 24:871-885.

Suzuki, K. *et al.* (2007) 'Hierarchy of Atg proteins in pre-autophagosomal structure organization', *Genes to Cells*, 12(2), pp. 209–218.

Swardfager W, Lanctôt K, Rothenburg L, Wong A, Cappell J, Herrmann N (2010) A meta-analysis of cytokines in Alzheimer's disease. Biol Psychiatry 68:930-941

Takats, S. *et al.* (2014) 'Interaction of the HOPS complex with Syntaxin 17 mediates autophagosome clearance in Drosophila', *Molecular Biology of the Cell*, 25(8), pp. 1338–1354.

Takáts, S. *et al.* (2013) 'Autophagosomal Syntaxin17-dependent lysosomal degradation maintains neuronal function in Drosophila', *Journal of Cell Biology*, 201(4), pp. 531–539.

Takáts, S. *et al.* (2018) 'Non-canonical role of the SNARE protein Ykt6 in autophagosome-lysosome fusion', *PLoS Genetics*, 14(4), pp. 1–23.

Takayama K, Kawakami Y, Lavasani M, Mu X, Cummins JH,Yurube T, Kuroda R, Kurosaka M, Fu FH, Robbins PD, Niedernhofer LJ, Huard J (2017) mTOR signaling plays a critical role in the defects observed in muscle-derived stem/progenitor cells isolated from a murine model of accelerated aging. J Orthop Res 35:1375-1382.

Takeshige, K. *et al.* (1992) 'Autophagy in yeast demonstrated with proteinase-deficient mutants and conditions for its induction', *Journal of Cell Biology*, 119(2), pp. 301–312.

Tan, C. C. *et al.* (2014) 'Autophagy in aging and neurodegenerative diseases: Implications for pathogenesis and therapy', *Neurobiology of Aging*. Elsevier Ltd,

35(5), pp. 941–957.

Terman, A., Gustafsson, B. and Brunk, U. (2007) ‘Autophagy, organelles and ageing A’, *Journal of Pathology*, 211, pp. 134–143.

Thumm, M. and Simons, M. (2015) ‘Myelinophagy: Schwann cells dine in’, *Journal of Cell Biology*, 210(1), pp. 9–10.

Thurston, T. L. M. *et al.* (2009) ‘The tbk1 adaptor and autophagy receptor NDP52 restricts the proliferation of ubiquitin-coated bacteria’, *Nature Immunology*. Nature Publishing Group, 10(11), pp. 1215–1222.

Thurston, T. L. M. *et al.* (2012) ‘Galectin 8 targets damaged vesicles for autophagy to defend cells against bacterial invasion’, *Nature*, 482(7385), pp. 414–418.

Tooze, S. A., Abada, A. and Elazar, Z. (2014) ‘Endocytosis and autophagy: Exploitation or cooperation?’, *Cold Spring Harbor Perspectives in Biology*, 6, pp. 1–15.

Tooze, S. A. and Yoshimori, T. (2010) ‘The origin of the autophagosomal membrane’, *Nature Cell Biology*. Nature Publishing Group, 12(9), pp. 831–835.

Tower J (2006) Sex-specific regulation of aging and apoptosis. Mech Ageing Dev. 127:705-718

Tower J and Arbeitman M (2009) The genetics of gender and life span. Journal of Biology. 8(38):1-3

Tsukada, M. and Ohsumi, Y. (1993) ‘Isolation and characterization of autophagy-defective mutants of Saccharomyces cerevisiae’, *Febs Letters*, 333(1), pp. 169–174.

Tsukamoto H, Senju S, Matsumura K, Swain SL, Nishimura Y (2015) IL-6-mediated environmental conditioning defective Th1 differentiation dampens antitumour immune responses in old age. Nat Commun 6:6702.

Tumbarello, D. A. *et al.* (2015) 'The Autophagy Receptor TAX1BP1 and the Molecular Motor Myosin VI Are Required for Clearance of Salmonella Typhimurium by Autophagy', *PLoS Pathogens*, 11(10), pp. 1–26.

Tusco, R. *et al.* (2017) 'Kenny mediates selective autophagic degradation of the IKK complex to control innate immune responses', *Nature Communications*. Springer US, 8(1), p. 1264.

van der Vaart, A., Griffith, J. and Reggiori, F. (2010) 'Exit from the Golgi Is Required for the Expansion of the Autophagosomal Phagophore in Yeast Saccharomyces cerevisiae Aniek', *Molecular Biology of the Cell*, 21, pp. 2270–2284.

Vermeulen, C. J., Bijlsma, R. and Loeschcke, V. (2008) 'A major QTL affects temperature sensitive adult lethality and inbreeding depression in life span in Drosophila melanogaster', *BMC Evolutionary Biology*, 8(1), pp. 1–11.

Vives-Bauza C, Zhou C, Huang Y, Cui M, de Vries RL, Kim J, May J, Tocilescu MA, Liu W, Ko HS, Magrané J, Moore DJ, Dawson VL, Grailhe R, Dawson TM, Li C, Tieu K, Przedborski S (2010) PINK1-dependent recruitment of Parkin to mitochondria in mitophagy. Proc Natl Acad Sci U S A 107:378-383.

Volpicelli-Daley LA, Gamble KL, Schultheiss CE, Riddle DM, West AB, Lee VM (2014) Formation of α-synuclein Lewy neurite-like aggregates in axons impedes the transport of distinct endosomes. Mol Biol Cell 25:4010-4023.

von Gaudecker, J. (1963) 'On variation in some cell organelles during formation of reserve substances in fatty bodies of drosophila larvae', *Z.Zellforsch.Mikrosk.Anat*, 61, 56-95.

Wallace, E. W. J. *et al.* (2015) 'Reversible, Specific, Active Aggregates of Endogenous Proteins Assemble upon Heat Stress', *Cell*. Elsevier Inc., 162(6), pp. 1286–1298.

Wang IF, Guo BS, Liu YC, Wu CC, Yang CH, Tsai KJ, Shen CK (2012) Autophagy activators rescue and alleviate pathogenesis of a mouse model with proteinopathies of the TAR DNA-binding protein 43. Proc Natl Acad Sci U S A 109:15024-15029.

Wang, C. *et al.* (2018) 'Endo-lysosomal dysfunction: a converging mechanism in neurodegenerative diseases', *Current Opinion in Neurobiology*. Elsevier Ltd, 48(Figure 1), pp. 52–58.

Wang WY, Tan MS, Yu JT, Tan L (2015) Role of pro-inflammatory cytokines released from microglia in Alzheimer's disease. Ann Transl Med 3:136.

Wang Y, Zhang N, Zhang L, Li R, Fu W, Ma K, Li X, Wang L, Wang J, Zhang H, Gu W, Zhu WG, Zhao Y (2016) Autophagy regulates chromatin ubiquitination in DNA damage response through elimination of SQSTM1/p62. Mol Cell 63:34-48.

Wang, Zheng *et al.* (2016) 'The Vici Syndrome Protein EPG5 Is a Rab7 Effector that Determines the Fusion Specificity of Autophagosomes with Late Endosomes/Lysosomes', *Molecular Cell*. Elsevier Inc., 63(5), pp. 781–795.

Ward, C. *et al.* (2016) 'Autophagy, lipophagy and lysosomal lipid storage disorders', *Biochimica et Biophysica Acta - Molecular and Cell Biology of Lipids*. The Authors, 1861(4), pp. 269–284.

Watson, P. J. *et al.* (2004) 'γ-COP appendage domain - Structure and function', *Traffic*, 5(2), pp. 79–88.

Wei, Y. *et al.* (2017) 'Prohibitin 2 Is an Inner Mitochondrial Membrane Mitophagy Receptor', *Cell*, 168, pp. 224–238.

Weidberg, H., Shvets, E. and Elazar, Z. (2011) 'Biogenesis and Cargo Selectivity of Autophagosomes', *Annual Review of Biochemistry*, 80(1), pp. 125–156.

Weimer, C. *et al.* (2008) 'Differential roles of ArfGAP1, ArfGAP2, and ArfGAP3 in COPI trafficking', *Journal of Cell Biology*, 183(4), pp. 725–735.

Weimer C, Beck R, Eckert P, Reckmann I, Moelleken J, Brugger B and Wieland F (2008) Differential roles of ArfGAP1, ArfGAP2, and ArfGAP3 in COPI trafficking. Journal of Cell Biology. 183(4):725-735

Wild, P., McEwan, D. G. and Dikic, I. (2014) 'The LC3 interactome at a glance', *Journal of Cell Science*, 127(1), pp. 3–9.

Winslow AR, Chen CW, Corrochano S, Acevedo-ArozenaGordon DE, Peden AA, Lichtenberg M, Menzies FM, Ravikumar B, Imarisio S, Brown S, O'Kane CJ, Rubinsztein DC (2010) α-Synuclein impairs macroautophagy: implications for Parkinson's disease. J Cell Biol 190:1023-1037.

Wirth, M. *et al.* (2019) 'Molecular determinants regulating selective binding of autophagy adapters and receptors to ATG8 proteins', *Nature Communications*, 10, pp. 1-18

Wu, Y. T. *et al.* (2010) 'Dual role of 3-methyladenine in modulation of autophagy via different temporal patterns of inhibition on class I and III phosphoinositide 3-kinase', *Journal of Biological Chemistry*, 285(14), pp. 10850–10861.

Wyant, G. A. *et al.* (2018) 'NUFIP1 is a ribosome receptor for starvation-induced ribophagy', *Science*, 360(6390), pp. 751–758.

Xie, Z., Nair, U. and Klionsky, D. J. (2008) 'Atg8 Controls Phagophore Expansion during Autophagosome Formation', *Molecular Biology of the Cell*, 19, pp. 3290–3298.

Xu, C. S. *et al.* (2020) 'A Connectome of the Adult Drosophila Central Brain', pp. 1–36.

Xu, H. and Ren, D. (2015) 'Lysosome Physiology', *Annual review of genetics*, 77, pp. 57–80.

Xu W, Fang F, Ding J and Wu C (2018) Dysregulation of Rab5-mediated endocytic pathways in Alzheimer's Disease. Traffic. 19(4):253-262

Yang, Z. and Klionsky, D. J. (2009) 'Autophagy in Infection and Immunity', *Current Topics in Microbiology and Immunology*, 335, pp. 1–32. doi: 10.1007/978-3-642-00302-8.

Yang, Z. and Klionsky, D. J. (2010) 'Eaten alive: A history of macroautophagy', *Nature Cell Biology*. Nature Publishing Group, 12(9), pp. 814–822.

Yao Y, Chinnici C, Tang H, Trojanowski JQ, Lee VM, Praticò D (2004) Brain inflammation and oxidative stress in a transgenic mouse model of Alzheimer-like brain amyloidosis. J Neuroinflammation 1:21.

Yim, W. W. Y. and Mizushima, N. (2020) 'Lysosome biology in autophagy', *Cell Discovery*. Springer US, 6(1).

Yin, Z., Pascual, C. and Klionsky, D. J. (2016) 'Autophagy: Machinery and regulation', *Microbial Cell*, 3(12), pp. 588–596.

Yoshii, S. R. and Mizushima, N. (2017) 'Monitoring and measuring autophagy', *International Journal of Molecular Sciences*, 18(9), pp. 1–13.

Youle, R. J. and Narendra, D. P. (2011) 'Mechanisms of mitophagy', *Nature Reviews Molecular Cell Biology*, 12(1), pp. 9–14.

Young AR, Narita M, Ferreira M, Kirschner K, Sadaie M, Darot JF, Tavaré S, Arakawa S, Shimizu S, Watt FM, Narita M (2009) Autophagy mediates the mitotic senescence transition. Genes Dev 23:798-803

Yuan, H. X., Russell, R. C. and Guan, K. L. (2013) 'Regulation of PIK3C3/VPS34 complexes by MTOR in nutrient stress-induced autophagy', *Autophagy*, 9(12), pp. 1983–1995.

Zatloukal, K. *et al.* (2002) 'P62 Is a Common Component of Cytoplasmic Inclusions in Protein Aggregation Diseases', *American Journal of Pathology*. American Society for Investigative Pathology, 160(1), pp. 255–263.

Yu L, McPhee MK, Zheng L, Mardones GA, Rong Y, Peng J, Mi N, Zhao Y, Liu Z, Wan F, Hailey DW, Oorschot V, Klumperman J, Baehrecke EH and Lenardo MJ (2010) Autophagy termination and lysosome reformation regulated by mTOR. Nature. 465(7300): 942-946.

Zhang, Y. *et al.* (2019) 'Listeria hijacks host mitophagy through a novel mitophagy receptor to evade killing', *Nature Immunology*. Springer US, 20(4), pp. 433–446.

Zhao, H. *et al.* (2018) 'Glycophagy: An emerging target in pathology', *Clinica Chimica Acta*, 484(June), pp. 298–303.

Zhao, Y. G. and Zhang, H. (2019) 'Autophagosome maturation: An epic journey from the ER to lysosomes', *Journal of Cell Biology*, 218(3), pp. 757–770.

Zheng, K. *et al.* (2019) 'Selective autophagy regulates cell cycle in cancer therapy', *Theranostics*, 9(1), pp. 104–125.

Zheng, Y. T. *et al.* (2009) 'The Adaptor Protein p62/SQSTM1 Targets Invading Bacteria to the Autophagy Pathway', *The Journal of Immunology*, 183(9), pp. 5909–5916.

Zhuang, X. and Jiang, L. (2019) 'Chloroplast degradation: Multiple routes into the vacuole', *Frontiers in Plant Science*, 10(March), pp. 1–8.

Zoppino, F. C. M. *et al.* (2010) 'Autophagosome formation depends on the small GTPase rab1 and functional ER exit sites', *Traffic*, 11(9), pp. 1246–1261.